NOTICE

THIS REPRODUCTION WAS MADE FROM THE BEST AVAILABLE COPY OF WHICH A NUMBER OF PAGES WERE OF POOR REPRODUCTION QUALITY.

NASA Conference Publication 2060

Fourteenth Annual Conference on Manual Control

April 25-27, 1978
University of Southern California
Los Angeles, California
and
Ames Research Center
Moffett Field, California

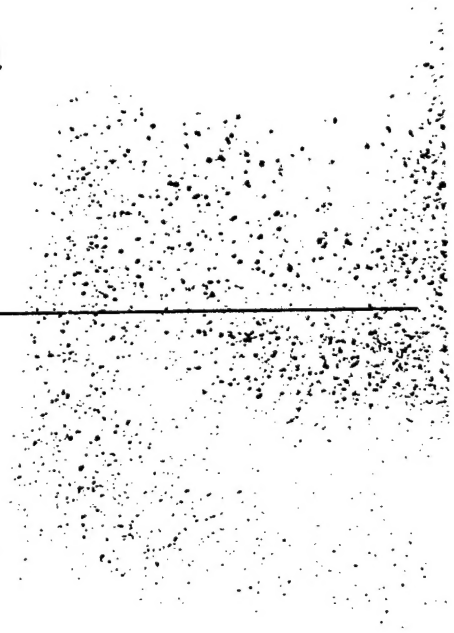

November 1978

National Aeronautics and
Space Administration

FOREWORD

This volume contains the proceedings of the Fourteenth Annual Conference on Manual Control held at the University of Southern California at Los Angeles from April 25 to 27, 1978. This report contains complete manuscripts of most of the papers presented at the meeting.

This was the fourteenth in a series of conferences dating back to December 1964. These earlier meetings and their proceedings are listed below:

First Annual NASA-University Conference on Manual Control, The University of Michigan, December 1964. (Proceedings not printed.)

Second Annual NASA-University Conference on Manual Control, MIT, February 28 to March 2, 1966, NASA SP-128.

Third Annual NASA-University Conference on Manual Control, University of Southern California, March 1-3, 1967, NASA SP-144.

Fourth Annual NASA-University Conference on Manual Control, The University of Michigan, March 21-23, 1968, NASA SP-192.

Fifth Annual NASA-University Conference on Manual Control, MIT, March 27-29, 1969, NASA SP-215.

Sixth Annual Conference on Manual Control, Wright-Patterson AFB, April 7-9, 1970.

Seventh Annual Conference on Manual Control, University of Southern California, June 2-4, 1971, NASA SP-281.

Eighth Annual Conference on Manual Control, University of Michigan, Ann Arbor, Michigan, May 17-19, 1972.

Ninth Annual Conference on Manual Control, Massachusetts Institute of Technology, May 23-25, 1973.

Tenth Annual Conference on Manual Control, Wright-Patterson AFB, April 9-11, 1974.

Eleventh Annual Conference on Manual Control, NASA-Ames Research Center, May 21-23, 1975, NASA TM X-62,464.

Twelfth Annual Conference on Manual Control, University of Illinois, May 25-27, 1976, NASA TM X-73,170

Thirteenth Annual Conference on Manual Control, Massachusetts Institute of Technology, June 15-17, 1977.

CONFERENCE CO-CHAIRMEN

George Bekey

University of Southern California

Duane McRuer

Systems Technology Incorporated

PUBLICATIONS COMMITTEE

Thomas Kempe

NASA-Ames Research Center

CONTENTS

CONTENTS (Continued)

CONTENTS (Continued)

CONTENTS (Concluded) Page

SESSION A: MANUAL TRACKING EXPERIMENTS

Chairman: D. Kleinman

DIRECTIONAL ERRORS OF MOVEMENTS AND THEIR CORRECTION IN A DISCRETE TRACKING TASK

Robert J. Jaeger
Gyan C. Agarwal
Gerald L. Gottlieb

College of Engineering
University of Illinois at Chicago Circle
Chicago, Illinois 60680

and

Rush Medical Center
Chicago, Illinois 60612

ABSTRACT

The human operator is prone to making errors in quick choice reaction time tasks. Many studies have shown that subjects can correct their own errors of movement more quickly than they can react to external stimuli. In the control of movements, three general categories of feedback have been defined as follows: 1) Knowledge of results, primarily visually mediated. 2) Proprioceptive or kinaesthetic such as from muscle spindles and joint receptors, and, 3) Corollary discharge or efference copy within the central nervous system.

Experiments were conducted on four normal human subjects to study the effects of these feedbacks on simple reaction time, choice reaction time, and error correction time. The movement used was plantarflexion and dorsiflexion of the ankle joint. The feedback loops were modified, 1) by changing the sign of the visual display to alter the subject's perception of results, and 2) by applying vibration at 100 Hz simultaneously to both the agonist and antagonist muscles of the ankle joint. The central processing was interfered with when the subjects were given moderate doses of alcohol (blood alcohol concentration levels of up to 0.07%).

Vibration and alcohol increase both the simple and choice reaction times. However, the error correction time is not influenced by either. This data reinforces the concept that there is a central pathway which can mediate error correcting responses.

INTRODUCTION

The human operator is prone to making errors in a quick choice reaction time (RT) task. The speed with which the operator can recognize errors and correct them is an important consideration in many industrial tasks. Many studies have shown that subjects can correct errors of movement more quickly

than they can react to external stimuli. (For a review of the literature see Schmidt, 1975, 1976; Angel, 1976; Schmidt & Gordon, 1977.)

In the control of movement by skeletal muscles, three general categories of feedback have been identified (Evarts, 1971). These feedbacks arise as follows: first, "knowledge of results" from the external environment is primarily visually mediated. Second, proprioception from internal receptors stimulated as a consequence of muscular contraction and joint rotation is primarily spindle and joint receptor mediated. Third, "efference copy" or "corollary discharge" (Von Holst, 1953) from structures and pathways within the central nervous system may operate before muscle contraction occurs.

Currently, the first and second categories of feedback are perhaps better understood than the third, although the role of efference copy in saccadic eye movements has received considerable attention (Robinson, 1971, 1976; Lehmann, 1971). These three categories of feedback may be anatomically interconnected, especially the proprioceptive and efference copy mechanisms (Oscarsson, 1970). It is postulated that the cerebellar anterior lobe is important for correcting errors in motor activity elicited from the cerebral cortex and carried out by command signals through pyramidal and extrapyramidal pathways.

Recent work of Angel and his colleagues (Angel & Higgins, 1969; Angel, 1976) has attempted to quantitatively approach efference copy by measuring RTs to correct movement errors and the accuracy of these corrections. It has also been noted (Poulton, 1974) that the many studies which have measured RTs for the correction of movements have found these times to range from essentially zero to in excess of 300 milliseconds.

Since a rather wide range of error correction times exists, it could be hypothesized that the three general categories of feedback each have their own range of operating times which together contribute to the overall wide range of these times. Under this hypothesis, if a sufficient number of measurements were made, a trimodal distribution might be found. The minimum duration for processing visual feedback from a movement appears to be over 190 msec (Keel & Posner, 1968). The kinaesthetic RT is of the order of 120 msec (Chernikoff & Taylor, 1952). This RT is of the same order as the time for "Functional Stretch Reflex" (Melville Jones & Watt, 1971; Evarts, 1973; Gottlieb & Agarwal, 1978). Dewhurst (1967) has reported values of kinaesthetic RT based on recordings of muscle activity in the biceps as short as 50 msec. However, he did not give any range for kinaesthetic RT or the mean value in his experiments.

The experiments of the present study were designed to enable comparison of correction times measured under normal conditions with those measured under conditions in which the proprioceptive mechanisms was interfered with. It was possible to do this by applying vibration to the tendons of the muscles involved. (Hagbarth & Eklund, 1966; Goodwin, McCloskey & Matthews, 1972; McCloskey, 1973; Craske, 1977). In some experiments, central processing was intertered with when the subjects were given moderate doses of alcohol (blood alcohol concentration (BAC) levels of up to 0.07%). Alcohol produces a depressive effect on the CNS much as a general anesthetic does and the degree of depression appears to be dose related (Wallgren & Barry, 1970.)

METHODS

Four subjects were used in the present study. Two of the subjects (GCA and GLG) had extensive previous experience with the experimental apparatus as subjects in other tracking type experiments, while the other two subjects had no such experience. Parts of these experiments were also done on several other subjects.

A schematic of the experimental apparatus is shown in Figure 1. (This apparatus has been used in several studies, for details see Agarwal & Gottlieb, 1977).

The subject sat in an adjustable height chair facing an oscilloscope display positioned at a slight angle in front of him. His right foot was strapped to a one degree of freedom foot pedal (rotation in plantar-dorsal directions) with velcro straps. Self adhesive surface electrodes were positioned over the soleus and anterior tibial muscles to record the electromyograms (EMGs) of these muscles. A ground electrode was placed on the thigh just proximal to the knee. The EMGs were full wave rectified and filtered before recording on the digital tape at a sampling rate of 500 per sec.

The oscilloscope display consisted of two dots. The first was the target dot which was under the control of the computer. It was defocussed to approximately 2 mm diameter. This dot assumed only one of three positions at any instant of time, either in the center of the screen or ±4.0 cm vertically away from the center. The second dot was the response dot which was under the control of the subject. It was focused to a sharp point approximately 0.5 mm in diameter. The subject could vary the position of the dot continuously along the vertical axis of the oscilloscope. The crucial part of the experiment was the "polarity" of the subjects' control of the response dot. This polarity was under the control of the computer. Normal or positive polarity meant that when the subject moved the pedal down (up) the response dot also moved down (up). Inverted or negative polarity meant that when the subject moved the pedal down (up), the response dot moved up (down). The purpose of this provision for polarity reversal was do decouple the proprioceptive feedback from the visual feedback and induce the subject to make errors in movement. The use of polarity reversal has been previously described by Gibbs (1965) and Angel and Higgins (1969).

The target dot was controlled by the computer as follows. The experiment began with the target dot in the center. After a random delay of 3 to 5 sec, the target dot stepped randomly up or down. The new position was maintained for a random period of 3 to 5 sec and then returned to center. Ten initial trials stepping out and returning to zero were performed at normal polarity. Following these ten initial trials, the computer reversed the polarity of the response dot. A random number (8 to 12) trials were performed at the reversed polarity, after which, the polarity again reversed for the next group of trials. The response immediately following a polarity reversal was always discarded, since it could be expected to contain a higher proportion of visually mediated error corrections than other responses.

This scheme of target dot movement also provided the opportunity to study simple and choice RTs, since the majority of responses were correct. When the target dot moved from the center, it moved randomly up or down, forcing the subject to choose before reacting. When the target dot next moved, it always

returned to zero, allowing the subject to make a simple reaction.

The subjects were instructed to make the response dot follow the movement of the target dot as quickly as possible with as much accuracy as possible, but to favor a fast response.

In the vibration experiments, two Hagbarth type vibrators (IVR vibrator - model #TMT-18, Heiwa Electronic Industrial Comp., Japan) were attached to the distal tendons of soleus and anterior tibial muscles (just above the ankle joint) with surgical tape. The vibrators were operated at 100 Hz continuously during the tracking task.

In the alcohol experiments, the subjects were given alcohol proportional to the body weight such that the ultimate BAC was in the range of 0.06 to 0.07%. The BAC was measured using a Mark II Intoximeter (Gas Chromatography Unit by Intoximeters, Inc.).

The measurement of the RTs were done off line by displaying the individual responses on a four channel oscilloscope using a cursor to indicate the time measurement after the input. The accuracy of these measurements is equal to the sampling interval, i.e., 2 msec. The RTs measured are indicated in Figures 2 and 3.

The statistical analysis included means and variances of the sample data and the t-test of equality of the means of two samples whose variances are assumed to be unequal (Sokal & Rohlf, 1969, Chapter 13).

RESULTS

Data were collected on separate days for each subject and for each experimental paradigm. The first day experiment was always under normal conditions. Typical responses are shown in Figure 2 for a correct response in a choice RT and for error response in Figure 3. The four traces are the angular rotation (θ), EMGs of the anterior tibial (AT) and gastrocnemius-soleus (GS) muscles and the angular velocity ($\dot{\theta}$). The angular velocity was obtained by digital differentiation of angular rotation. The simple and choice RTs (SRT & CRT), the error reaction time (ERT), and the error correction time (ECT) were measured using both the EMG and velocity data. In the following tables only the EMG related measurements are reported. The final conclusions would have been exactly the same using the velocity data.

Table I shows the simple and choice reaction times under normal conditions with positive and negative polarity movements. With the exception of subject GA, and GG's SRT, the RTs for the other three subjects with positive and negative polarity were not significantly different. In general there was a slight increase in the RTs with negative polarity. Since the RT differences with alcohol and vibration were more significant, the positive and negative polarity data was lumped together.

Table II shows SRTs for all subjects in three paradigm conditions. Note that in general, alcohol as well as vibration increased the SRT. This is also true for CRT shown in Table III. The t-test comparisons are made between the normal and altered conditions. In Table II, six out of eight t-test values are significant at $P < 0.01$ level. In Table III, seven out of eight t-test values are significant at $P < 0.01$ level.

Table IV shows the error reaction times in the three paradigm conditions.

Most errors occured in the choice reaction condition. There was a significantly larger number of errors with negative polarity than with positive polarity feedback. The error rates for the two conditions ranged between 16% and 33%. In these data, four out of eight t-test values show significant differences at $P < 0.01$ level.

Table V compares the data from Tables III and IV for choice RT and error RT under normal conditions. Note that error RTs are larger than the choice RTs and only one out of four t-test values show significant differences at $P < 0.01$ level.

Table VI shows the error correction times for the four subjects under our three paradigms. The error correction time is significantly less than the choice or error RT. None of the eight t-test values between normal and altered conditions show significance at $P < 0.01$ level.

Table VII shows the error rates for individual experiments as well as combined error rates for all subjects. The vibration input did not influence the error rates. Alcohol tended to increase the error rates in three out of four subjects but the t-test values do not indicate any significance. For $n = 4$ the t-test values are not very meaningful.

DISCUSSION

The paradigm of incompatible display has been used by Gibbs (1965), Angel & Higgins (1969), and Angel (1976). There is a clear increase in the SRT as well as CRT with negative polarity display (Table I). This increase was significant at $P < 0.01$ level for subjects GA and CG whose RTs were fastest. The significance of positive and negative polarity disappeared with increased RT of subject RJ and FM.

Vibration and alcohol increases both the SRT and CRT for correct movements as compared to the normal condition (Tables II and III). Carpenter (1962) has reviewed the literature on the effects of alcohol on psychological processes and concluded that in most studies, RT is lengthened at relatively low blood alcohol levels. Vibration of a tendon in humans causes a predictable increase in the contractile activity of the agonist, caused by autogenous reflex excitation of the alpha motoneuron (Hagbarth & Eklund, 1966). This leads to involuntary movements and illusion of movements (Goodwin et al 1972; McCloskey, 1973; Craske, 1977). In our experiments, vibrators were attached to both agonist-antagonist tendons and subjects reported numbness in the vibrated ankle joint. The significant increase in the SRT and CRT with vibration could indicate that large irrelevant position signals from the vibrated joint delays processing of visual information and command selection.

Tables IV and V show that the choice reaction time and the error reaction time (initial movement in the wrong direction) are not significantly different under normal conditions. This agrees with Gibbs (1965) findings that the response latencies of correct and incorrect responses were virtually equal on equiprobable steps. Although the response latencies for the four subjects are significantly different, there is no correlation between the response latencies and the errors of subjects (see Table VII), i.e., the subjects who responded most rapidly did not make the most errors (Gibbs, 1965). The ERT in most cases is longer than the CRT, suggesting that there was no temporal anticipa-

tion of the target (A paradigm which has been used by Schmidt and Gordon (1977) in their study).

The surprising result of this study is that whereas the SRT and CRT are influenced (increased) by vibration and alcohol, the error correction times are not significantly affected as given in Table VI. The average error correction time is shorter than the CRT for individual subjects. This is in agreement with findings by Gibbs (1965), Rabbitt (1966), and Angel and Higgins (1969), Megaw (1972), and Angel (1976).

The histograms of error correction times for the four subjects under three paradigm conditions are shown in Figure 4. For subjects GA and GG who had the most experience in tracking studies, most errors are corrected in less than 250 msec, i.e., less than their normal choice reaction times. For subject RJ a significant number of ECTs are larger than 250 msec. For subject FM, his RTs were the slowest and larger percentage of ECTs are above 250 msec.

The conclusion of Higgins & Angel (1970) and Angel (1976) that the origin of feedback from error responses is central rather than kinaesthetic is reinforced by the invariance of ECTs with vibration on the limb. The vibration increases the SRTs and CRTs which implies an influence of the peripheral input in motor command decision making.

Alcohol which is known to produce a depressive effect on the CNS also increases the SRTs and CRTs but does not significantly influence the ECTs with BAC levels of 0.07% or less used in these experiments.

ACKNOWLEDGEMENT

This work was supported by NSF grant ENG-7608754 and NIH grants NS-00196 and NS-12877. The alcohol experiments were supported by NIH grant AA02156 to Dr. Jeffrey Levett.

REFERENCES

Agarwal, G. C., & Gottlieb, G. L., Oscillation of the Human Ankle Joint in Response to Applied Sinusoidal Torque on the Foot. J. Physiology (London), vol. 268, pp. 151-176, 1977.

Angel, R. W., Efference Copy in the Control of Movement. Neurology, vol. 26, pp. 1164-1168, 1976.

Angel, R. W., & Higgins, J. R., Correction of False Moves in Pursuit Tracking. J. Expt. Psychology, vol. 82, pp. 185-187, 1969.

Carpenter, J. A., Effects of Alcohol on Some Psychological Processes. Quarterly J. Studies on Alcohol, vol. 23, pp. 274-314, 1962.

Chernikoff, R., & Taylor, F. V., Reaction Times to Kinaesthetic Stimulation Resulting from Sudden Arm Displacement. J. Experimental Psychology, vol. 43, pp. 1-8, 1952.

Craske, B., Perception of Impossible Limb Positions Induced by Tendon Vibration. Science, vol. 196, pp. 71-73, 1977.

Dewhurst, D. J., Neuromuscular Control System. IEEE Trans. Biomedical Eng., vol. BME-14, pp. 167-171, 1967.

Evarts, E. V., Central Control of Movement, Neuroscience Research Program, Bulletin, M.I.T. Press, vol. 9, 1971.

Evarts, E. V., Motor Cortex Reflexes Associated with Learned Movements. Science, vol. 179, pp. 501-503, 1973.

Gibbs, C. B., Probability Learning in Step-input Tracking. British ... Psychology, vol. 56, pp. 233-242, 1965.

Goodwin, G. M., McCloskey, D. I., & Matthews, P. B. C., The Contribution of Muscle Afferents to Kinaesthesia Shown by Vibration Induced Illusions of Movement and by the Effects of Paralysing Joint Afferents. Brain, vol. 95, pp. 705-748, 1972.

Gottlieb, G. L., & Agarwal, C. G., Stretch and Hoffmann Reflexes during Phasic Voluntary Contractions of the Human Soleus Muscle. Electroenceph. & Clinical Neurophysiology, 1978 (in press).

Hagbarth, K. E., & Eklund, G., Motor Effects of Vibratory Muscle Stimuli in Man. In Nobel Symposium I - Muscular Afferent and Motor Control, R. Granit (editor), Almquist and Wiksell, Stockholm, pp. 177-186, 1966.

Higgins, J. R., & Angel, R. W., Correction of Tracking Errors without Sensory Feedback. J. Experimental Psychology, vol. 84, pp. 412-416, 1970.

Keele, S. W., & Posner, M. J., Processing of Visual Feedback in Rapid Movements. J. Experimental Psychology, vol. 77, pp. 155-158, 1968.

Lehmann, D., EEG, Evoked Potentials, and Eye and Image Movements. In The Control of Eye Movements, P. Bach-y-rita (editor), Academic Press, N. Y., pp. 149-174, 1971.

McCloskey, D. I., Differences Between the Senses of Movement and Position Shown by the Effects of Loading and Vibration of Muscles in Man. Brain Research, vol. 63, pp. 119-131, 1973.

Megaw, E. D., Directional Errors and their Correction in a Discrete Tracking Task. Ergonomics, vol. 15, pp. 633-643, 1972.

Melville Jones, G., & Watt, D. G. D., Observations on the Control of Stepping and Hopping Movements in Man. J. Physiology (London), vol. 219, pp. 709-727, 1971.

Oscarsson, O., Functional Organization of Spinocerebellar Paths. In Handbook of Sensory Physiology, vol. II. Somatosensory System. A. Iggo (editor), Springer-Verlag, Berlin, pp. 121-127, 1970.

Poulton, E. C., Tracking Skill and Manual Control, Academic Press, N. Y., 1974.

Rabbit, P. M. A., Errors and Error Correction in Choice Response Tasks. J. Experimental Psychology, vol. 71, pp. 264-272, 1966.

Robinson, D. A., Models of Oculomotor Neural Organization. In The Control of Eye Movements, P. Bach-y-rita (editor), Academic Press, N. Y., pp. 519-538, 1971.

Robinson, D. L., & Wurtz, R. H., Use of an Extraretinal Signal by Monkey Superior Colliculus to Distinguish Real from Self-Induced Stimulus Movement. J. Neurophysiology, vol. 39, pp. 852-870, 1976.

Schmidt, R. A., A Schema Theory of Discrete Motor Skill Learning, Psychological Review, vol. 82, pp. 225-260, 1975.

Schmidt, R. A., The Schema as a Solution to Some Persistent Problems in Motor Learning Theory. In G. E. Stelmach (editor), Motor Control: Issues and Trends, Academic Press, N. Y., pp. 41-65, 1976.

Schmidt, R. A., & Gordon, G. B., Errors in Motor Responding, "Rapid" Corrections, and False Anticipations. J. Motor Behavior, vol. 9, pp. 101-111, 1977.

Von Holst, E., Relations Between the Central Nervous System and the Peripheral Organs. British J. Animal Beh., vol. 3, pp. 89-94, 1954.

Wallgren, H., & Barry, H., Actions of Alcohol, vol. 1 & 2, Elsevier Publishing Comp., 1974.

TABLE I: Effect of Display Polarity on Simple and Choice Reaction Times

SUBJ	Positive Polarity MEAN	SD	N	t	NEGATIVE POLARITY MEAN	SD	N
				Simple Reaction Times			
GA	216	32	113	-3.99*	248	78	110
GG	222	51	129	-2.52*	240	71	164
RJ	270	76	130	-1.42	283	78	156
FM	359	75	133	0.59	354	69	161
				Choice Reaction Times			
GA	235	57	98	-2.79*	272	102	73
GG	256	42	111	-2.00	271	70	122
RJ	268	80	83	-1.12	282	84	90
FM	338	76	112	-1.46	359	69	112

*P < 0.01

TABLE II: Simple Reaction Times

SUBJ	VIBRATION MEAN	SD	N	t	NORMAL MEAN	SD	N	t	ALCOHOL MEAN	SD	N
GA	246	45	150	-5.99*	219	39	233	-4.48*	235	42	297
RJ	316	92	156	-4.50*	277	77	286	-7.75*	333	96	269
FM	371	78	274	0.58	375	86	294	-5.68*	420	98	256
GG	311	84	164	-10.46*	232	64	293	-1.24	240	54	290

TABLE III: Choice Reaction Times

SUBJ	VIBRATION MEAN	SD	N	t	NORMAL MEAN	SD	N	t	ALCOHOL MEAN	SD	N
GA	317	111	131	-5.58*	253	80	171	-0.64	258	59	152
RJ	333	83	98	-5.27*	277	86	173	-8.25*	355	88	166
FM	409	96	211	-7.43*	348	73	224	-11.28*	443	100	212
GG	330	85	136	-6.9[illegible]	272	61	233	-3.34*	288	61	230

TABLE IV: Error Reaction Times

SUBJ	VIBRATION MEAN	SD	N	t	NORMAL MEAN	SD	N	t	ALCOHOL MEAN	SD	N
GA	274	60	19	-1.03	257	62	47	-0.56	263	59	104
RJ	342	65	55	-2.90*	311	55	80	-3.57*	343	69	111
FM	387	75	59	-1.83	363	72	68	-5.72*	443	70	41
GG	332	84	32	-2.42*	289	63	42	-0.08	290	60	45

TABLE V: Comparison of CRTS with ERTS under Normal Conditions

SUBJ	CHOICE REACTION TIMES MEAN	SD	N	t	ERROR REACTION TIMES MEAN	SD	N
GA	253	80	171	-0.37	257	62	47
RJ	277	86	173	-3.79*	311	55	80
FM	348	73	224	-1.50	363	72	68
GG	272	61	233	-1.62	289	63	42

TABLE VI: Error Correction Times

SUBJ	VIBRATION MEAN	SD	N	t	NORMAL MEAN	SD	N	t	ALCOHOL MEAN	SD	N
GA	137	69	19	0.32	143	72	47	0.67	135	59	104
RJ	194	101	55	-1.71	166	81	80	-1.62	186	88	111
FM	259	72	59	2.18	293	103	68	2.23	251	90	41
GG	170	84	32	-0.05	169	72	42	-0.68	150	74	45

TABLE VII: Rate of Errors in Percent

SUBJ	VIBRATION	NORMAL	ALCOHOL
GA	0.063	0.107	0.188
RJ	0.173	0.148	0.203
FM	0.110	0.116	0.081
GG	0.096	0.074	0.080

	VIBRATION	t	NORMAL	t	ALCOHOL
MEAN	0.112	-0.04	0.111	-0.74	0.138
SD	0.048		0.030		0.067
N	4		4		4

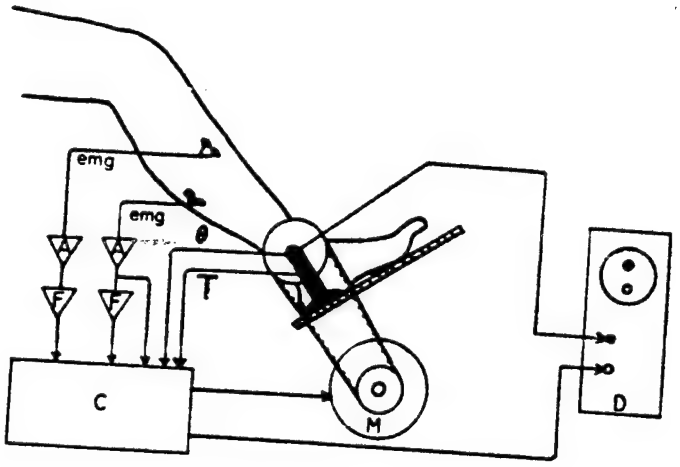

Figure 1

A schematic of the experimental apparatus. Electromyograms (EMGs) are measured using disk surface electrodes placed over the bellies of the gastrocnemius-soleus and anterior tibial muscles. EMG amplifiers (A) are differential amplifiers (bandwidth 60-600 Hz), filters (F) are third order averaging (10 msec averaging time), display oscilloscope (D) is a dual-beam Tektronix 502, digital computer (C) is a General Automation SPC016/65. The torque motor (M) and the torque measurements (τ) were not used in these experiments. The angular rotation (θ) is measured by a continuous transformer-type transducer, this signal is fed into the computer on an A/D input channel multiplied by +1 or -1 and outputed on D/A channel. This channel is operated independent of the data channels at a rate of 1 KHz.

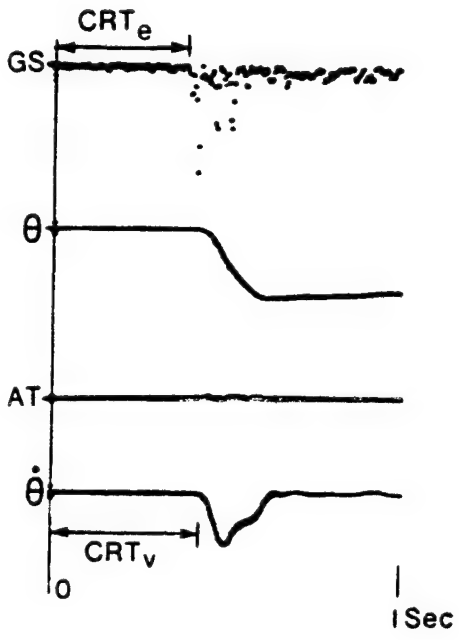

Figure 2

Typical response in a choice reaction with a display gain of +1 and a movement from central position to plantarflexion of the ankle joint. The choice reaction time (CRT) is measured from the jump of the target to the first EMG burst in gastrocnemius-soleus (GS) muscle. There is no EMG activity in the anterior tibial (AT) muscle. Total display time is 1 sec.

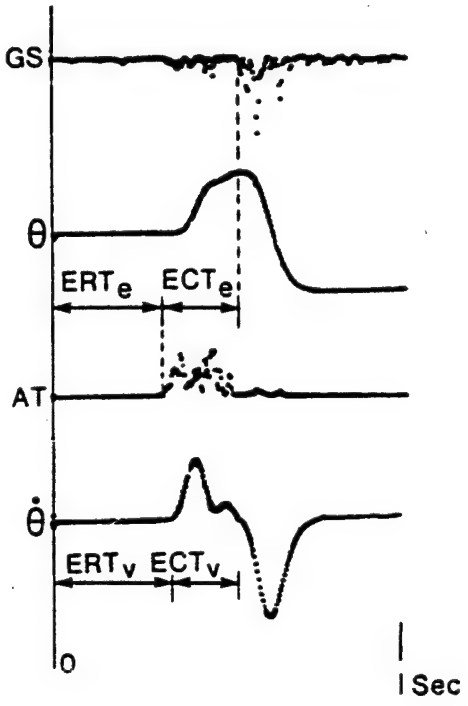

Figure 3

Typical response in error movement and subsequent correction. The display polarity is again +1. The error reaction time (ERT) and error correction time (ECT) are measured from the initial burst in the antagonist and agonist muscle EMGs. Total display time is 1 sec.

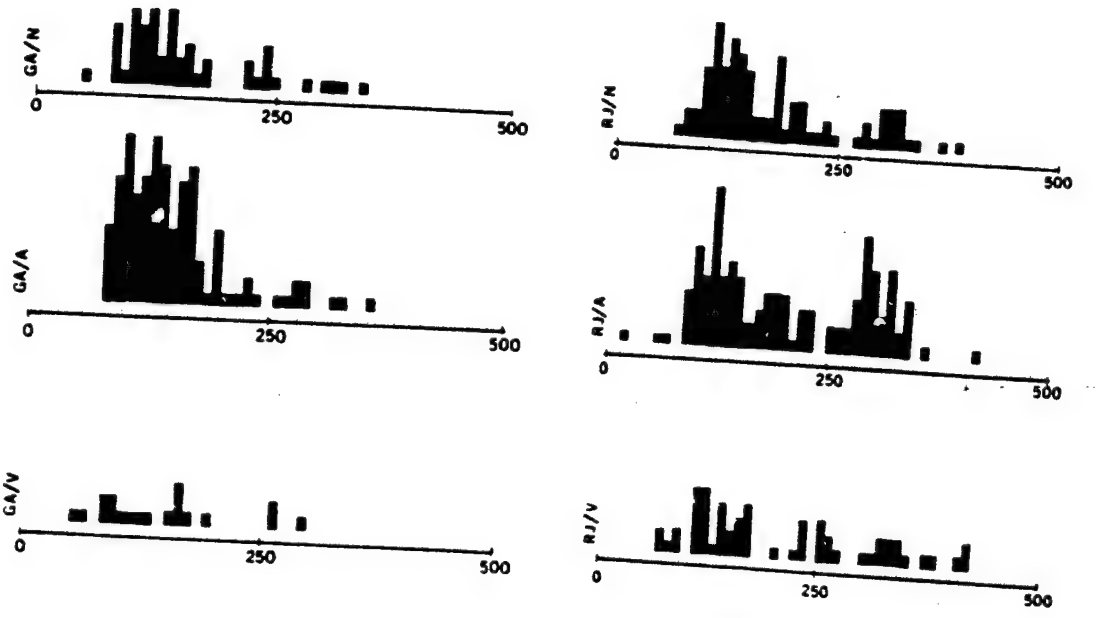

Figure 4

Histograms of the error correction times (ECTs) for the four subjects under normal (N), alcohol (A) and vibration (V) input paradigms. The time interval on abcissa is 500 msec. (continued on next page)

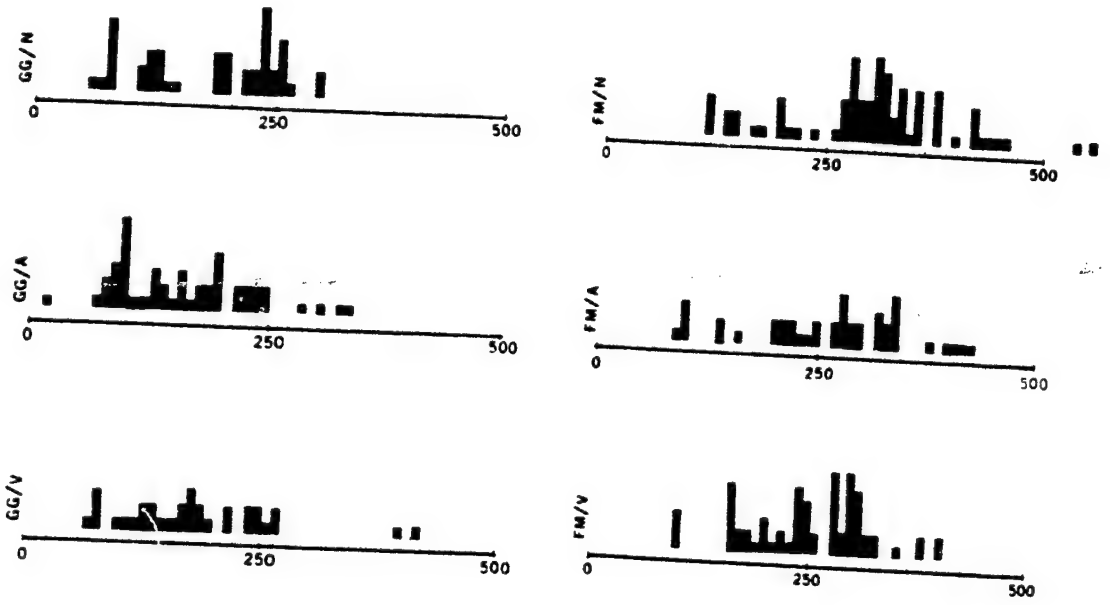

Figure 4 (continued)

N79-15590

A STUDY OF THE EFFECT OF FORCING FUNCTION CHARACTERISTICS ON HUMAN OPERATOR DYNAMICS IN MANUAL CONTROL

by Kyuichiro Washizu*, Keiji Tanaka** and Tatsuo Osawa*

*Department of Aeronautics, University of Tokyo, Tokyo,
**Instrumentation and Control Division, National Aerospace Laboratory, Chofu, Tokyo

SUMMARY

This paper deals with the effect of the spectrum of the forcing function on the human pilot dynamics in manual control. A simple compensatory tracking experiment was conducted, where the controlled element was of a second-order dynamics and the forcing function was a random noise having a dominant frequency. The dominant frequency and the power of the forcing function were two variable parameters during our experiment.

The results show that the human pilot describing functions are dependent not only on the dynamics of the controlled element, but also on the characteristics of the forcing function. This suggests that the human pilot behavior should be expressed by the transfer function taking into consideration his ability to sense and predict the forcing function.

SYMBOLS

$A_{ij}(k)$	element of k-th autoregressive coefficient matrix
B	backward shift operator
c(t), c(n)	human pilot output
dB	decibel
e(t), e(n)	displayed error
i(t), i(n)	forcing function
K_f	static gain of forcing function filter

M	order of autoregressive model
$m(t)$, $m(n)$	controlled element output
s	variable of Laplace transform
$Y_c(j\omega)$	controlled element
$Y_f(j\omega)$	forcing function filter
$Y_p(j\omega)$	human pilot describing function
Δ	sampling interval
ζ_f	damping of forcing function filter
ζ_n	damping of controlled element
σ_i^2	power of forcing function
ω_f	undamped natural frequency of forcing function
ω_n	undamped natural frequency of controlled element

INTRODUCTION

It is well known that when a human pilot controls the system, his control behavior depends on the characteristics of the forcing function to the system as well as of the controlled element itself. A great number of papers have been published on this problem.

Concerning the effect of the characteristics of the controlled element on pilot behavior, Washizu and Miyajima (reference 1), and Soto and Washizu (reference 2) pointed out in a series of study on manual control of a second-order system that the human pilot takes notice of the periodicity in the response of the controlled element, if any, and makes use of it to improve his control performance.

On the other hand, concerning the effect of the forcing function on pilot behavior, McRuer and Krendel (reference 3) pointed out that as the bandwidth of the forcing function increases, the effective time delay reduces probably due to the muscular reaction characteristics of the human pilot.

The purpose of the present paper is to investigate the effect of the forcing function spectrum on the human pilot dynamics in manual control. A simple compensatory tracking experiment was conducted, where the controlled element was of the second-order dynamics and the forcing function was a random noise having a dominant frequency. The dominant frequency and the power of the forcing function were two variable parameters during the experi-

ment. Pilot describing functions were derived from the autoregressive model coefficients identified using the Akaike's Final Prediction Error method.

EXPERIMENT

The system of our experiment was built up with an analogue computer, an oscilloscope and a control stick with a restoring spring. Its block diagram is as shown in figure 1. The error e(t) was displayed on the oscilloscope by a line segment moving vertically. The pilot was requested to minimize the error to the best of his ability. The controlled element had a second-order stable dynamics, and its transfer function was of the form;

$$Y_c(s) = \frac{\omega_n^2}{s^2 + 2\zeta_n\omega_n s + \omega_n^2} \quad . \tag{2}$$

The damping ζ_n and undamped natural frequency ω_n of the controlled element were held fixed throughout our experiment such as,

$$\zeta_n = 0.1 \quad ,$$
$$\omega_n = \sqrt{20} = 4.47 \text{ (rad/sec)} \quad .$$

The shaping filter of the forcing function also had a second-order stable dynamics as,

$$Y_f(s) = \frac{K_f\omega_f^2}{s^2 + 2\zeta_f\omega_f s + \omega_f^2} \quad , \tag{3}$$

where the damping ζ_f was held fixed to 0.1 and the static gain K_f and the undamped natural frequency ω_f were two variable parameters. Thus, the white noise was transformed into a forcing function having a dominant frequency after passing the filter. The dominant frequency was varied by selecting the values of ω_f as,

$$\omega_f = 3.16, 2.24, 1.58 \text{ (rad/sec)} \quad .$$

We chose four levels for the power of the forcing function σ_i^2 by adjusting K_f of the equation,

$$\sigma_i^2 = \frac{\omega_r K_f^2}{4 \zeta_r} \sigma_w^2 \qquad (3)$$

where σ_w^2 is the power of the noise source.

The experiment was of 12 cases, namely 3 kinds of frequencies and 4 power levels of the forcing function, and two runs of each case were performed. After sufficient excercise, the analog data of the length of 90 seconds for each runs were recorded. The data, i(t), e(t), c(t) and m(t) in figure 1 were transformed into digital data by use of the NOVA minicomputer system. The FACOM 230-75 computer was employed for numerical calculations of the following time series analysis.

ANALYSIS

By the use of the experimental data thus obtained, the human pilot describing functions were identified utilizing a time domain technique; that is, an autoregressive model was fitted to the data by using the Akaike's MFPE (Multiple Final Prediction Error) method. (reference 4)

In the first place, the data were sampled from the analog data of the pilot output c(t) and the error e(t) with the sampling interval Δ, which was set to be .1 sec. The sampled data are denoted by c(n) and e(n). Then, the autoregressive model of the form;

$$\begin{bmatrix} c(n) \\ e(n) \end{bmatrix} = \begin{bmatrix} A_{11}(B) & A_{12}(B) \\ A_{21}(B) & A_{22}(B) \end{bmatrix} \begin{bmatrix} c(n) \\ e(n) \end{bmatrix} + \begin{bmatrix} \sigma_{11} & \sigma_{12} \\ \sigma_{21} & \sigma_{22} \end{bmatrix} \begin{bmatrix} \xi_1(n) \\ \xi_2(n) \end{bmatrix} \qquad (4)$$

$$A_{ij}(B) = a_{ij}(1)B + a_{ij}(2)B^2 + \cdots\cdots + a_{ij}(M)B^M \qquad (5)$$

$$Bx(n) = x(n-1) \qquad (6)$$

was fitted to the given data. B is the backward shift operator as shown in equation (6), and $A_{ij}(B)$'s in equation (4) are the power series in B that are made up of the autoregressive model coefficients $a_{ij}(k)$ with k going from 1 through M. The order of the model M is determined by the MFPE method. $\xi_i(n)$'s in equation (4) are mutually independent white noises.

Once we have succeeded in fitting the model to the given data, namely, $\sigma_{11} = \sigma_{12} = \sigma_{21} = \sigma_{22} \neq 0$, we can compute the pilot describing function using

$$\hat{Y}_p(j\omega) = \frac{A_{12}(j\omega)}{1 - A_{11}(j\omega)} \quad , \qquad (7)$$

where $A_{11}(j\omega)$ and $A_{12}(j\omega)$ are obtained from $A_{11}(B)$ and $A_{12}(B)$ in equation (4) respectively, by replacing B with $\exp(-j\omega\Delta)$.

This method has recently been put into practical use, and our experience in using it has proved that it is quite efficient and powerful (reference 5). Application of this method to our data was also successful, as the estimated correlation coefficient of the noise sources, $\sigma_{12}/\sqrt{\sigma_{11}\sigma_{22}}$, was quite small.

RESULTS

Figures 2 and 3 are examples of the time histories of the records. Note that in figure 2, namely when the frequency of the forcing function ω_f was large, it is not evident that c(t) was affected by the forcing function periodicity. The pilot seemed to suppress only the controlled element periodicity.

On the other hand, figure 3 shows the time history of the case when ω_f was relatively small. In this case, it is evident that c(t) was made up of two main sinusoidals; one reflected the forcing function periodicity and the other reflected the pilot behavior which seemed to suppress the controlled element periodicity. This suggests that, when ω_f was relatively small, the human pilot behavior was affected by the forcing function.

Above tendencies can be seen more obviously in the power spectrum densities of the pilot output as shown in figure 4; namely in the vicinity of $\omega = \omega_n$, the power spectra were pulled up as σ_i^2 increased, and this phenomenon became more conspicuous when ω_f was relatively small.

Typical pilot describing functions are shown in figures 5 and 6. From these figures, the following tendencies have been observed;

1) If the power of the forcing function σ_i^2 is increased, while keeping the undamped natural frequency ω_f unchanged, the gain of the pilot describing function increases, but the phase lead becomes smaller in the frequency region below the undamped natural frequency of the controlled element ω_n.

2) If the frequency of the forcing function ω_f is decreased, while keeping the power σ_i^2 unchanged, the gain of the pilot describing function increases, but the phase lead becomes smaller in the low frequency range, especially in the neighbourhood of the undamped natural frequency of the forcing function.

Figure 7 shows the performance of the pilot control indicated by σ_e^2/σ_i^2. It is evident that the smaller the undamped natural frequency ω_f was, the better the performance became. This implies that when ω_f was small, the pilot could easily recognize the forcing function periodicity, and his task became easier.

These results lead to the following consideration concerning the forcing function effects on human pilot control behavior.

The effect of the forcing function bandwidth on the pilot describing function is reported in reference 3. It is pointed out in the report that the effective time delay of the human pilot decreases as the bandwidth of the forcing function increases.

On the other hand, the present study put emphasis on the effect of the frequency ω_f and K_f of the forcing function shaping filter. It has been suggested that the increase in the power of the forcing function is likely to work so as to make the pilot employ the control that takes into account the dominant periodicity in the forcing function. The attempt to suppress the dominant frequency component may lead to the reduction of the power of the error. It has also been suggested from the present study that if the response of the controlled element and the forcing function have periodicities, the human pilot would try to augment the system stability by making use of the periodicity in the response of the controlled element, and then, try to make the performance as good as possible by making use of the periodicity of the forcing function. Especially, if the power of the forcing function is large and the two natural frequencies are separated, it would be easy for the pilot to notice these frequencies and to make use of these frequencies in the control.

The present study has shown that the human pilot describing functions are dependent not only on the natural frequency of the controlled element, but also on the frequency and the power of the forcing function. These results seem to suggest that the human pilot control behavior couldn't be expressed by a simple transfer function compensating the controlled element delay only, but should be expressed by the transfer function taking into consideration his ability to sense and predict the forcing function.

CONCLUDING REMARKS

The results show the effects of the forcing function on the human pilot such as:

1) If the power of the forcing function σ_i^2 increases, the gain of the human describing function $|\hat{Y}_p|$ increases, but the phase lead of $\hat{Y}_p$ becomes smaller at $\omega < \omega_n$.
2) If the undamped natural frequency of the forcing function ω_f decreases, the gain $|\hat{Y}_p|$ increases but the phase lead of $\hat{Y}_p$ becomes smaller especially in the vicinity of $\omega = \omega_f$.

3) The human pilot seems to try to augment the system stability and make the performance better by use of ω_n and ω_p, especially when ω_i^2 is large, and ω_n and ω_p are separated.

ACKNOWLEDGEMENT

The authors are deeply indebted to Mr. M. Okabe, Chief of Human Engineering Section of NAL, for his support on conducting the experiment.

REFERENCES

1. Washizu,K.; and Miyajima,K.: Some Consideration on the Controllability Limit of a Human Pilot. AIAA J., Vol.5, No.1, 1967, pp.151-155.

2. Goto,N.; and Wahizu,K.: On the Dynamics of Human Pilots in Marginally Controllable Systmes. AIAA J., Vol.12, No.3, 1974, pp.310-315.

3. McRuer,D.T.; and Krendel,E.S.: Mathematical Models of Human Pilot Behavior. AGARD-AG-188, 1974.

4. Akaike,H.: Statistical Predictor Identification. Ann. Inst. Statist. Math., Vol.22, 1970, pp.203-217.

5. Tanaka,K.; Goto,N.; and Wahizu,K.: A Comparison of Techniques for Identifying Human Operator Dynamics Utilizing Time Series Analysis. 12th Ann. Conf. on Manual Control, NASA TM X-73,170, 1976, pp. 673-685.

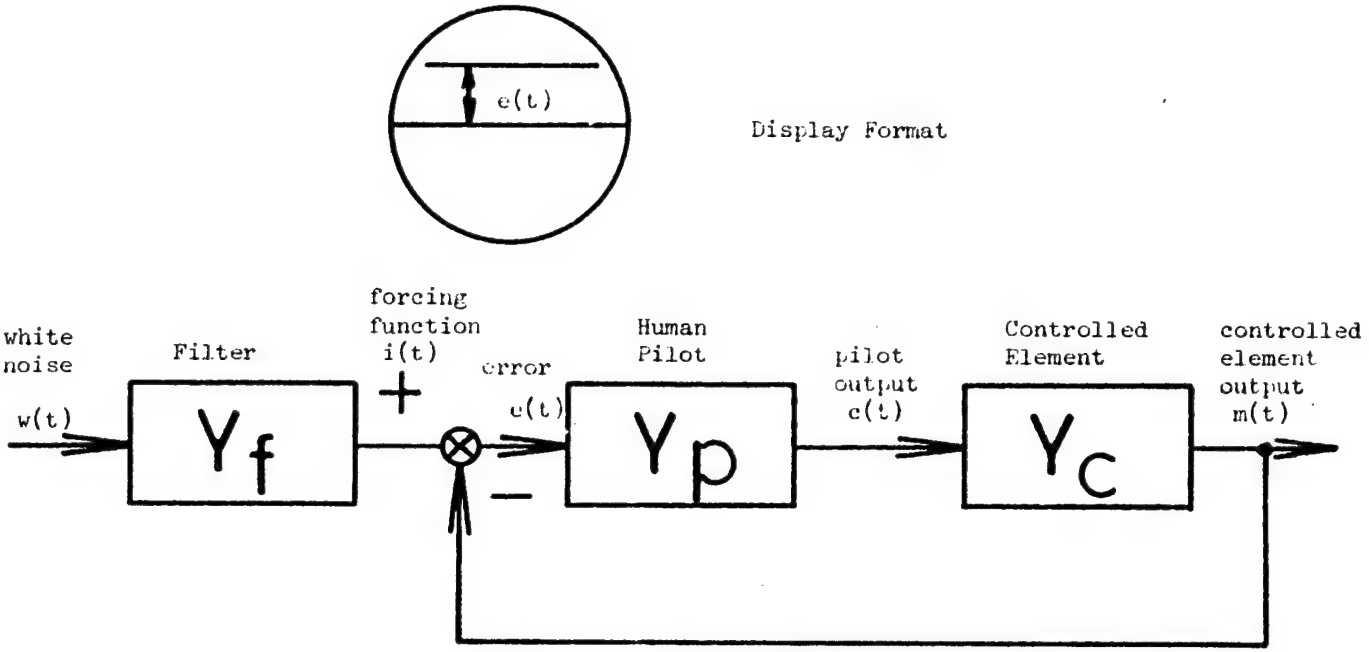

Figure 1. Block Diagram of the Experiment

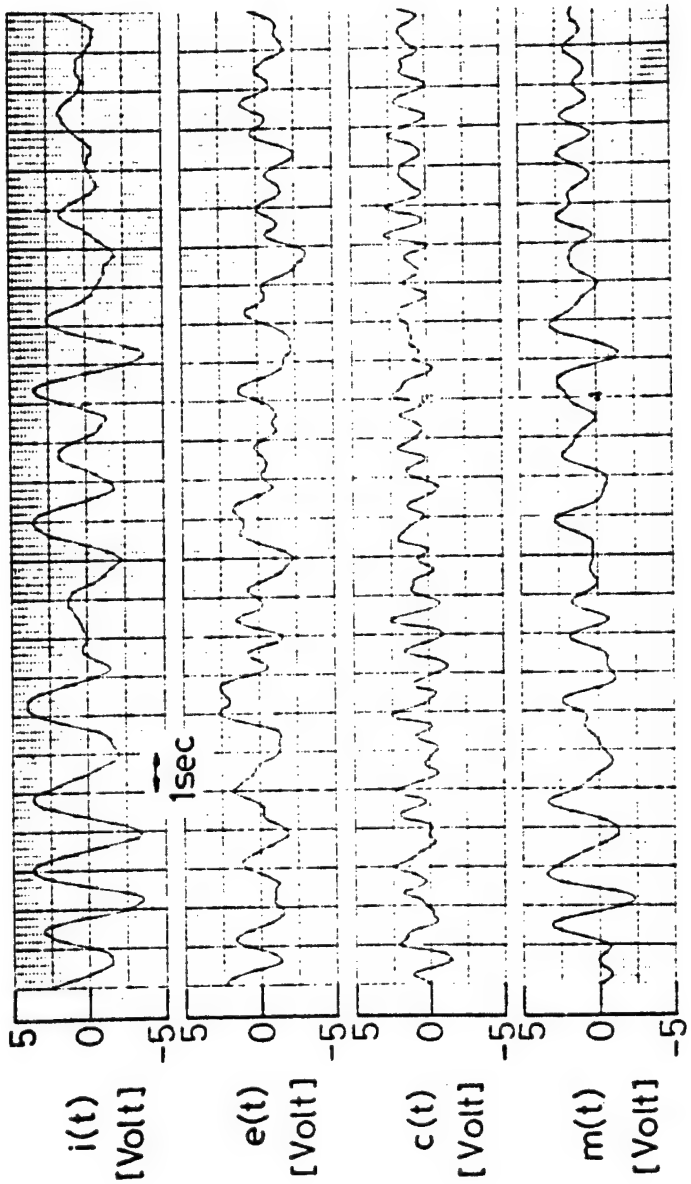

Forcing Function Periodic Time = $2\pi/\omega_f$ = 1.99 sec.
Controlled Element Periodic Time = $2\pi/\omega_n$ =1.40 sec.

Figure 2. An Example of the Time Histories of the Recorded Data
(ω_n = 3.16 rad/sec, and K_f = 1.41)

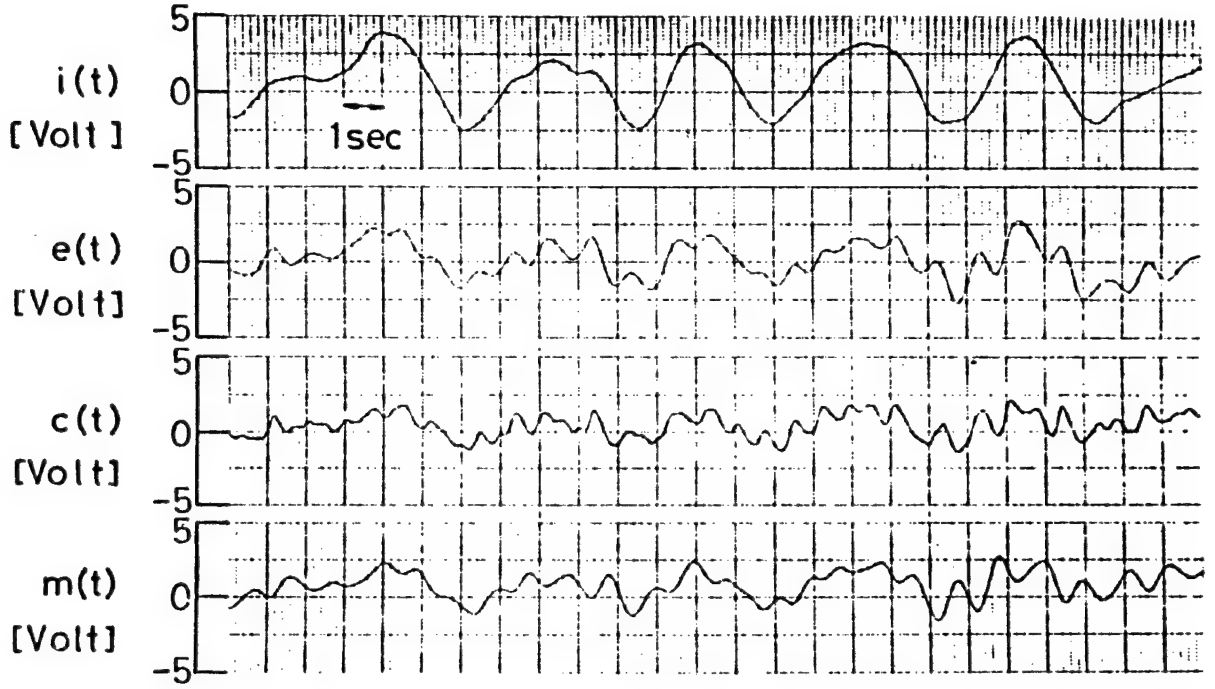

Forcing Function Periodic Time = $2\pi/\omega_f$ = 3.97 sec.
Controlled Element Periodic Time = $2\pi/\omega_n$ = 1.40 sec.

Figure 3. An Example of the Time Histories of the Recorded Data
(ω_f = 1.58 rad/sec, and K_f = 2.00)

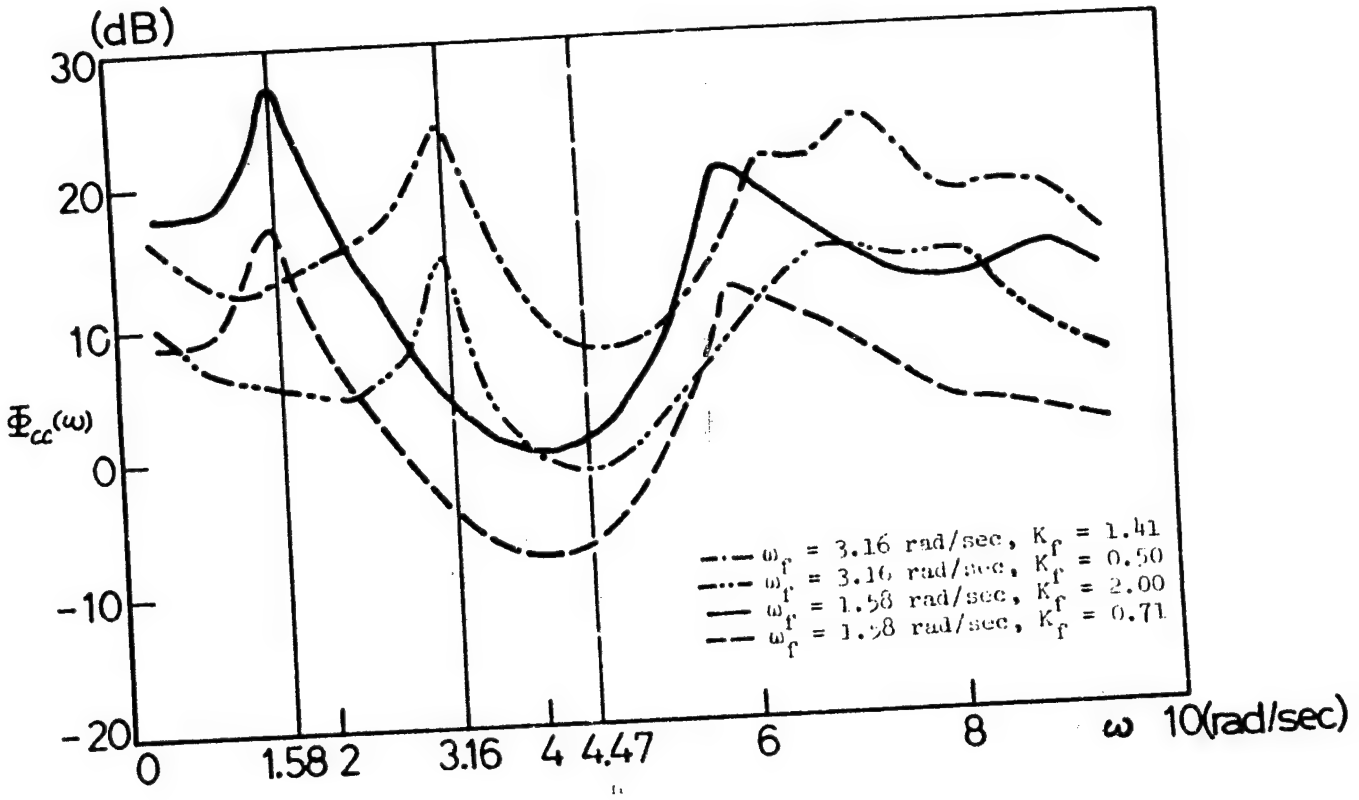

Figure 4. Examples of the Power Spectra of the Pilot Control Output

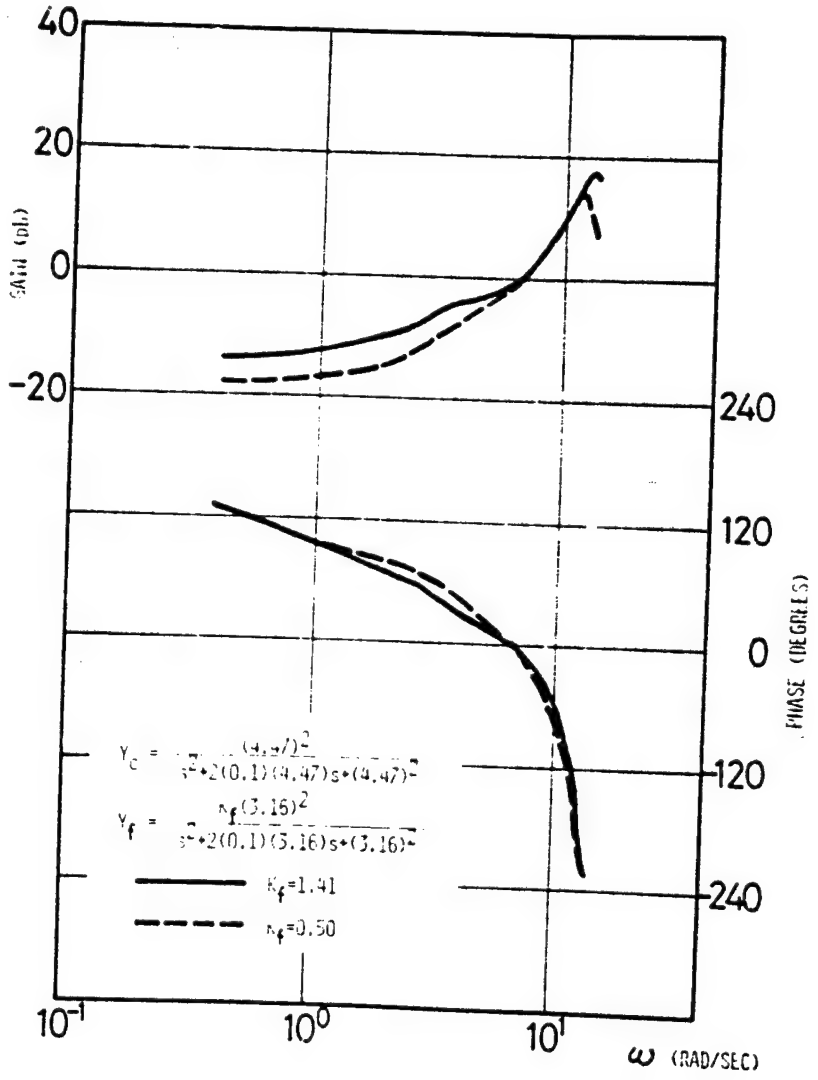

Figure 5. Comparison of Pilot Frequency Responses when ω_f=3.16 rad/sec.

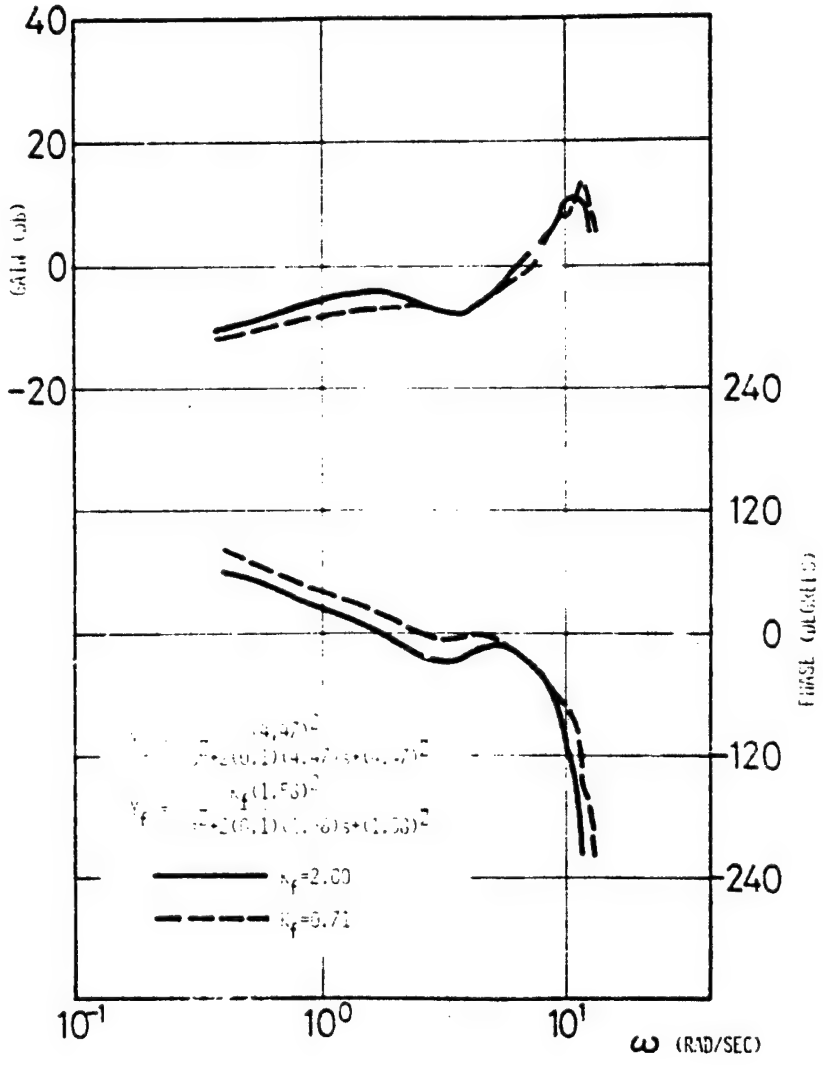

Figure 6. Comparison of Pilot Frequency Responses when ω_p=1.58 rad/sec.

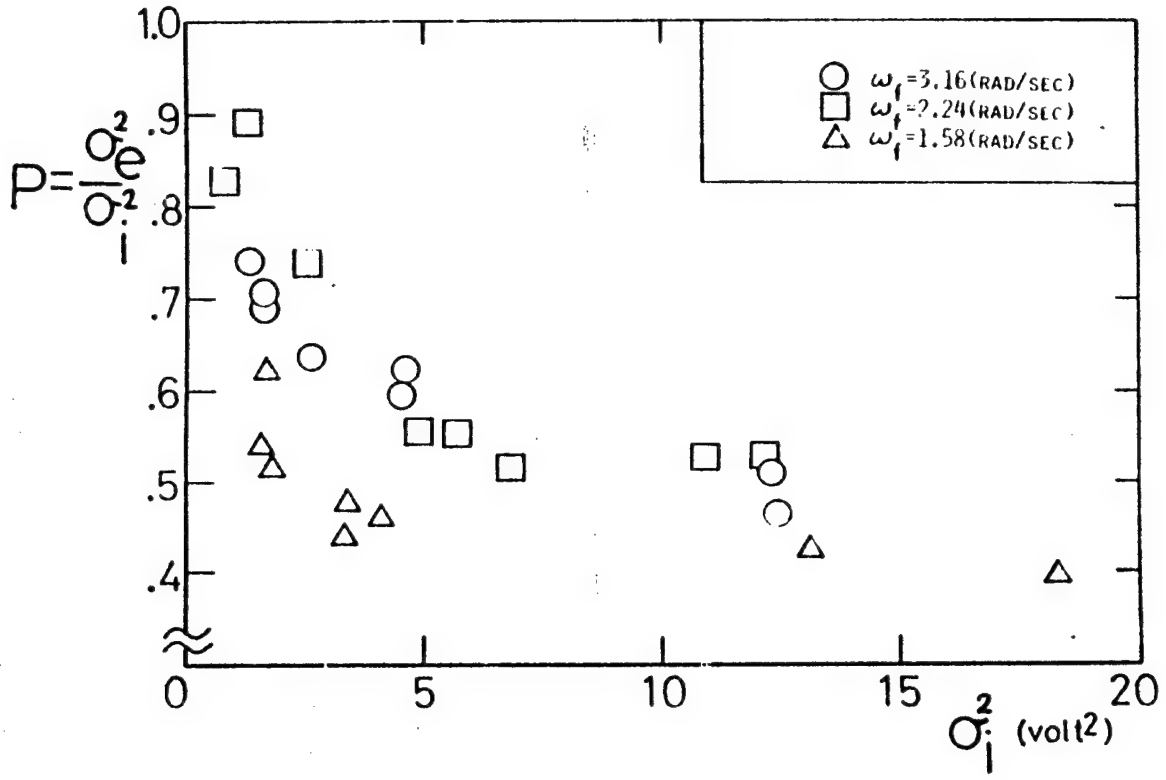

Figure 7. Effect of σ_i^2 and ω_f on Pilot Control Performance

AN EXTENSION OF THE QUICKENED DISPLAY FOR MANUAL CONTROL

By Masayoshi Tomizuka and Wai Ming Tam

Department of Mechanical Engineering
University of California, Berkeley

SUMMARY

It is very difficult (or even impossible) for a human to control plants of third order or more with little or no damping by just knowing the instantaneous error. It has been shown that adding first and/or higher order derivatives to the error signal and displaying the combined signal are effective in facilitating human control over such plants---signal quickening by Birmingham and Taylor. Their technique is further extended to incorporate the future trajectory variation into the displayed signal so as to minimize the tracking error. A method for tuning free parameters in ordinary and extended quickening is established by applying discrete-time optimal control. Experimental results for a triple integrator plant indicate the effectiveness of the proposed method to achieve high quality tracking.

INTRODUCTION

It is known to be very difficult for a human to control higher order plants with little or no damping with conventional compensatory or pursuit display (reference 1). To facilitate human control over such plants, Birmingham and Taylor (reference 2) proposed to incorporate the derivatives of the plant output into the displayed signal. The technique is called "signal quickening," and its effectiveness has been demonstrated. This can sometimes be done as shown in figure 1 for a triple integrator plant. When the reference trajectory, r(t), is constant, the quickened display makes it possible to achieve high quality regulation. However, if r(t) is time varying, it can not be expected that high quality tracking be achieved with the quickened display. This is because the human operator and plant introduce phase shifts between the reference trajectory and the plant output. To improve the tracking performance, more information on the reference trajectory, such as derivatives, future values, etc., is needed.

In many manual control situations, the reference trajectory is predetermined, or a portion of future reference trajectory can be detected in advance if not all future information is available. In such cases, the preview display in figure 2 has been shown to improve the tracking performance when the plant is relatively easy to control (references 3, 4 and 5). If the plant is higher order and weakly damped, preview information alone is not sufficient to achieve high quality tracking or even to stabilize the plant.

After noticing the limitations of quickened display and preview display, one may propose to combine those two and use a display as illustrated in figure 3. However, this scheme is not good for tracking since with such a dis-

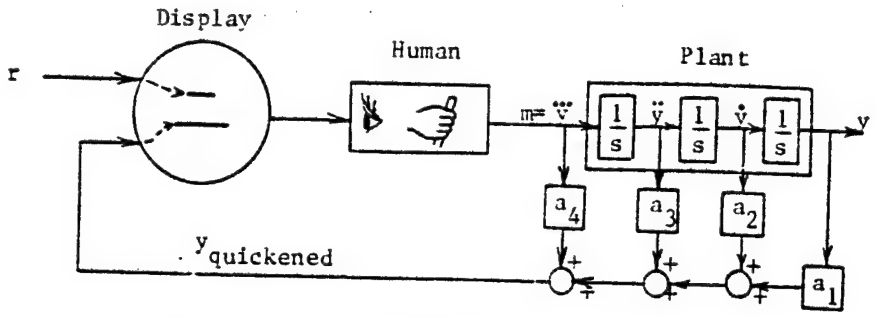

Fig. 1 Signal Quickening (Pursuit Type)

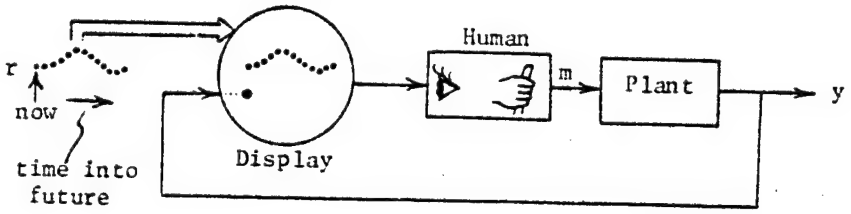

Fig. 2 Preview Tracking

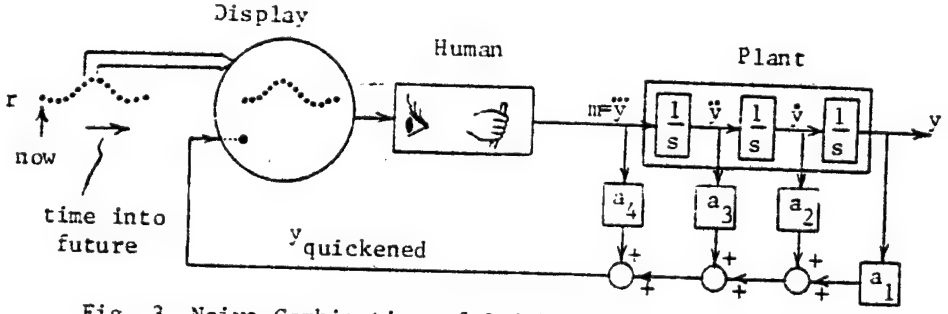

Fig. 3 Naive Combination of Quickened and Preview Displays

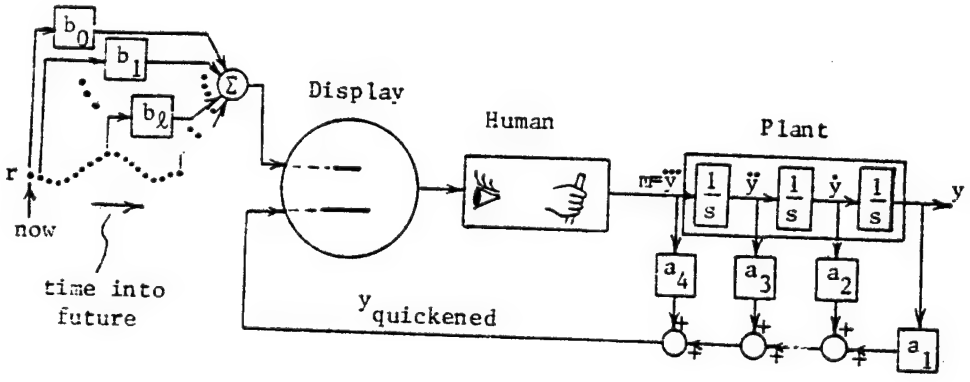

Fig. 4 Extended Quickening

play the human operator tries to match the distorted plant output with the reference trajectory. A better approach is to process future trajectory information by computer to generate a distorted reference signal which is compatible to the distorted plant output. This scheme is illustrated in figure 4 and is named "extended quickening". Due to innovations in microcomputer technology, this kind of digital data processing is not difficult nor expensive. The design of extended quickened displays involves the determination of the feedback (quickening) gains, a_i's, and feedforward or preview gains, b_i's, such that high quality tracking is assured. A design method based on discrete-time optimal control is presented in the next section.

DESIGN OF EXTENDED QUICKENED DISPLAY

To simplify treatment, the design method is described for a triple integrator plant. However, the method applies equally to other kinds of plants.

Controlled Plant

A triple integrator plant can be represented by the following state and output equations.

$$\frac{d\underline{x}_p}{dt} = \underline{A}_p\underline{x}_p + \underline{B}_p m \tag{1}$$

$$y = x_{p1} \tag{2}$$

where

$$\underline{x}_p = \begin{bmatrix} x_{p1} \\ x_{p2} \\ x_{p3} \end{bmatrix} = \begin{bmatrix} y \\ \dot{y} \\ \ddot{y} \end{bmatrix}, \quad \underline{A}_p = \begin{bmatrix} 0 & 1 & 0 \\ 0 & 0 & 1 \\ 0 & 0 & 0 \end{bmatrix}, \quad \underline{B}_p = \begin{bmatrix} 0 \\ 0 \\ 1 \end{bmatrix},$$

$\cdot$ denotes the time derivative, m is the controlling input adjusted by the human operator and y is the plant output. Since extended quickening assumes the use of digital computers, equation (1) is approximated by the discrete state equation,

$$\underline{x}_p(k+1) = \underline{A}'_p\underline{x}_p(k) + \underline{B}'_p m(k) \tag{3}$$

where

$$\underline{A}'_p = e^{\underline{A}_p \cdot \Delta t} = \begin{bmatrix} 1 & \Delta t & (\Delta t)^2/2 \\ 0 & 1 & \Delta t \\ 0 & 0 & 1 \end{bmatrix}, \quad \underline{B}'_p = \int_0^{\Delta t} e^{\underline{A}_p \cdot \sigma}\underline{B}'_p d\sigma = \begin{bmatrix} (\Delta t)^3/6 \\ (\Delta t)^2/2 \\ \Delta t \end{bmatrix},$$

Δt is the sampling period and the index k denotes k-th sampling instance or time $k \cdot \Delta t$. The sampling period is selected to be 0.025 sec which is short enough to maintain small approximation error and yet is long enough for most microcomputers to implement extended quickening.

Human Operator

For design purposes, the human operator is first approximated by a simple time delay, e^{-sL}, where the delay time, L, is typically 0.1~0.2 sec. With a sampling period of Δt, the discrete-time model is a simple delay chain, z^{-d}, where d can be determined from $(0.1\sim0.2)/\Delta t$. In the following development, d is selected to be 6 which corresponds to 0.15 sec time delay with the selected Δt of 0.025 sec. The input to the human, u(k), is the displayed signal and the output of the human is the plant input, m(k). A state space model for the human operator is

$$\underline{x}_h(k+1) = \underline{A}_h \underline{x}_h(k) + \underline{B}_h u(k) \tag{4}$$

$$m(k) = x_{h1}(k) \tag{5}$$

where

$$\underline{x}_h = \begin{bmatrix} x_{h1} \\ x_{h2} \\ x_{h3} \\ x_{h4} \\ x_{h5} \\ x_{h6} \end{bmatrix}, \quad \underline{A}_h = \begin{bmatrix} 0 & 1 & 0 & 0 & 0 & 0 \\ 0 & 0 & 1 & 0 & 0 & 0 \\ 0 & 0 & 0 & 1 & 0 & 0 \\ 0 & 0 & 0 & 0 & 1 & 0 \\ 0 & 0 & 0 & 0 & 0 & 1 \\ 0 & 0 & 0 & 0 & 0 & 0 \end{bmatrix} \quad \text{and} \quad \underline{B}_h = \begin{bmatrix} 0 \\ 0 \\ 0 \\ 0 \\ 0 \\ 1 \end{bmatrix}.$$

Equations (3), (4) and (5) characterize the open loop human-plant dynamics.

Optimal Control Problem

The parameters, a_i's and b_i's, in extended quickening can be found from the solution of an optimal control problem in which u(k) must be determined so as to minimize the cost functional given by

$$J = \sum_{i=k}^{\infty} \{(y(i) - r(i))^2 + w\cdot(\Delta u(i)/\Delta t)^2\} \tag{6}$$

where $\Delta u(i) = u(i) - u(i-1)$ $(=\Delta m(i+6))$, $\Delta u(i)/\Delta t \sim du/dt$, r is the reference trajectory and w is a positive constant. The first term in the cost functional penalizes the tracking error and the second term penalizes the jerky motion of the displayed signal.

The reference trajectory, r, is assumed to be previewable (by computer) in the sense that future information which includes the sampled values $\{r(k), r(k+1),\ldots,r(k+N_{\ell a})\}$ is avilable at time k where $N_{\ell a}$ is the preview (or look ahead) time. $N_{\ell a}$ is zero for conventional quickening. Preview information is not sufficient for finding the optimal control, u(k), since the cost functional includes r(i)'s from i=k to i=∞. Therefore, it is further assumed that the reference trajectory does not change from the time $i=k+N_{\ell a}$: i.e.

$$r(k+N_{\ell a}+i+1) = r(k+N_{\ell a}+i) \quad \text{for all } i>0 \tag{7}$$

Equation (7) applies for the determination of u(k) only. For determining u(k+1), updated preview information at time k+1 which includes the sampled value $r(k+1+N_{\ell a})$ is used, and the lower limit of the summation in the cost functional becomes k+1. If the statistical properties of the reference trajectory are known, they can be used in place of equation (7) (references 6,7). Figure 5 shows the assumptions made about the reference trajectory.

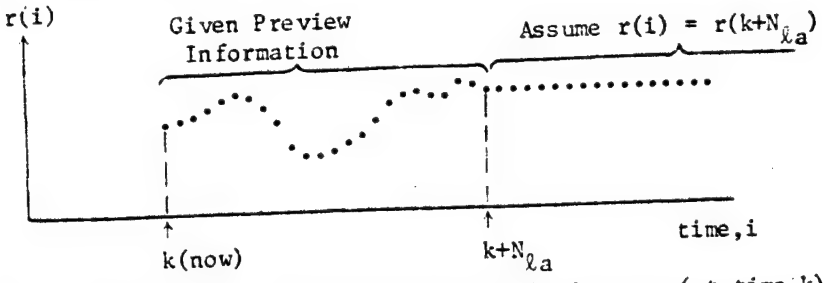

Fig. 5 Information ... Future Reference Trajectory (at time k)

Equations (2)-(7) define an optimal control problem or more specifically a discrete time optimal preview control problem. This problem can be solved by dynamic programming or applying the results of linear quadratic (LQ) optimal control (reference 8).

Solution of the Optimal Control Problem

The optimal control, $u^{opt}(k)$, is

$$u^{opt}(k) = -\sum_{i=1}^{3} g_{pi} x_{pi}(k) - \sum_{i=1}^{6} g_{hi} x_{hi}(k) + \sum_{\ell=0}^{N_{\ell a}} g_{r\ell} r(k+\ell) \tag{8}$$

where g_{pi}'s, g_{hi}'s and $g_{r\ell}$'s are all constant gains.
The feedback gains, g_{pi}'s and g_{hi}'s, are given by

$$\left[g_{p1}\ g_{p2}\ g_{p3}\ g_{h1}\ \cdots\ g_{h6}\right] = \left[R + \underline{B}^T \underline{K}\ \underline{B}\right]^{-1}\left[\underline{B}^T \underline{K}\ \underline{A} + \underline{P}\right] \tag{9}$$

where

$$\underline{A} = \begin{bmatrix} \underline{A}_p' & \underline{B}_p' \underline{0} \\ \underline{0} & \underline{A}_n \end{bmatrix}, \quad \underline{B} = \begin{bmatrix} \underline{0} \\ \underline{B}_n \end{bmatrix}, \quad R = w/(\Delta t)^2, \quad \underline{P} = \left[0\ 0\ 0\ 0\ 0\ 0\ 0\ 0\ -R\right],$$

$\underline{K}$ is the steady state solution of the matrix Riccati equation,

$$\underline{K}(i) = \underline{A}^T \underline{K}(i+1)\underline{A} + \underline{Q} - \left[\underline{B}^T \underline{K}(i+1)\underline{A} + \underline{P}\right]^T \left[R + \underline{B}^T \underline{K}(i+1)\underline{B}\right]^{-1}\left[\underline{B}^T \underline{K}(i+1)\underline{A} + \underline{P}\right] \tag{10}$$
$$(\underline{K}(\infty) = \underline{Q})$$

and $\underline{Q}$ is a 9X9 matrix whose 1-1 element is 1, 9-9 element is R and all other elements are 0. Since $\underline{A}$, $\underline{B}$, $\underline{Q}$ and $\underline{P}$ are sparse, the Riccati equation can be efficiently solved by simple recursions. For example, it can be easily seen that $\underline{B}^T \underline{K} = \left[k_{91}\ k_{92}\ k_{93}\ \cdots\ k_{99}\right]$ and $\underline{B}^T \underline{K}\ \underline{B} = k_{99}$.

The feedforward or preview gains, $g_{r\ell}$'s, are given as follows:
For $N_{\ell a} = 0$ (no preview),

$$g_{r0} = g_{p1} \tag{11}$$

For $N_{\ell a} > 0$,

$$\left.\begin{aligned} g_{r0} &= 0, \quad g_{r\ell} = -\left[R + \underline{B}^T \underline{K}\, \underline{B}\right]^{-1} \alpha_{\ell-1}, \quad 1 \le \ell \le N_{\ell a} - 1 \\ g_{rN_{\ell a}} &= g_{p1} - \sum_{\ell=0}^{N_{\ell a}-1} g_{r\ell} \end{aligned}\right\} \tag{12}$$

where α_ℓ is the 1-9 element of the matrix

$$(\underline{A}_{closed})^{\ell} = (\underline{A} - \underline{B}[g_{p1}\ g_{p2}\ g_{p3}\ g_{h1}\ \cdots\ g_{h6}])^{\ell}. \tag{13}$$

Notice that the matrix $\underline{A}_{closed}$ characterizes the closed loop dynamics of the human-plant model plus feedback control law, and is normally asymptotically stable. Equations (12) and (13) indicate that the future values of the reference trajectory must be used in a way compatible to the closed loop dynamics and that $g_{r\ell}$'s with increasing ℓ are closely related to the unit pulse response of the closed loop system. The second expression in (12) implies that the summation of $g_{r\ell}$'s with respect to ℓ must be equal to g_{p1}, which assures zero steady state error for the step reference trajectory. For asymptotically stable $\underline{A}_{closed}$, α_ℓ approaches zero as ℓ increases, which implies that the future is less important to determine $u^{opt}(k)$ as it becomes further apart from the present time. This point has also been found in preview tracking (references 3, 4, 5)

Sturcture of Extended Quickening

The structure of extended quickening based on the optimal control result is depicted in figure 6.

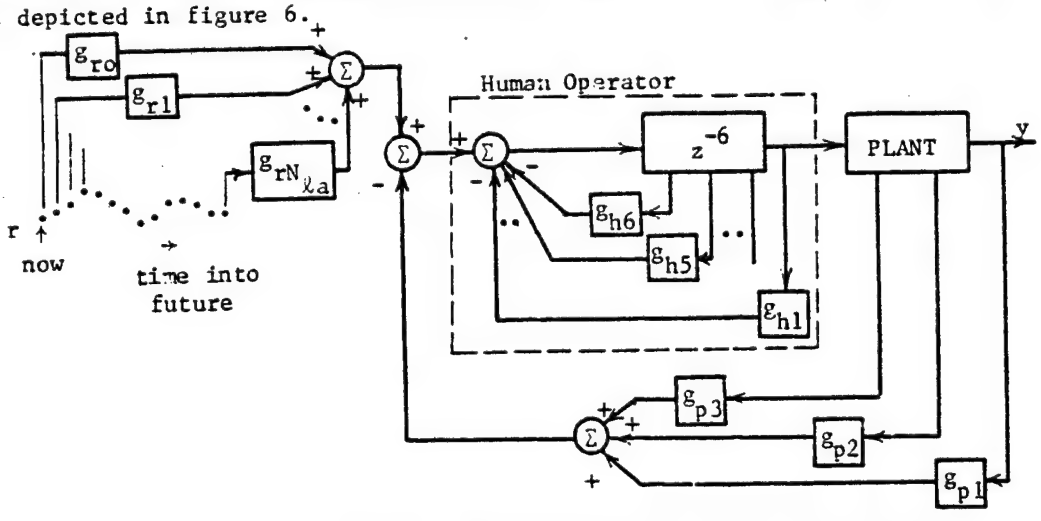

Fig. 6 Structure of Extended Quickening based on Optimal Control

The portion of the structure inside the dashed lines can be viewed as human operator. The reason for this will soon be explained.

For selected values of w over a wide range (w is defined in the cost functional (6)), the steady state solution of the Riccati equation (10) was computed and the feedback gains, g_{pi}'s and g_{hi}'s, were found. Results are summarized in the following table.

w	g_{p1}	g_{p2}	g_{p3}	g_{h1}	g_{h2}	g_{h3}	g_{h4}	g_{h5}	g_{h6}
1.0	0.0242	0.0669	0.0924	0.0023	0.0022	0.0022	0.0022	0.0021	-0.9347
0.1	0.0757	0.160	0.168	0.0042	0.0041	0.0040	0.0039	0.0038	-0.9129
0.01	0.236	0.382	0.309	0.0076	0.0074	0.0072	0.0069	0.0067	-0.884
0.001	0.730	0.914	0.573	0.014	0.013	0.013	0.012	0.012	-0.845
0.0001	2.255	2.20	1.076	0.026	0.025	0.024	0.022	0.021	-0.7935

Table 1 g_{pi}'s and g_{hi}'s for selected values of w

From Table 1, it is found that g_{h1}--g_{h5} are orders of magnitudes smaller than other feedback gains and that the values of g_{h6} is around -(0.8~0.9) regardless of the value of w. Hence it is possible to approximate the portion inside the dashed lines in figure 6 by

$$\frac{z^{-6}}{1 - (0.8\sim0.9)z^{-1}} . \qquad (14)$$

With our selection of Δt= 0.025 sec, the discrete transfer function (14) corresponds to

$$\frac{K\, e^{-0.15s}}{\tau_N s + 1} , \quad \tau_N = (0.125\sim0.25) \text{ sec} \qquad (15)$$

where the time constant, τ_N, was computed by $\tau_N \sim \Delta t/(1+ g_{h6})$. τ_N has a reasonable value as the human neromuscular lag constant (reference 1), which implies that the feedback effect via g_{h6} can be interpreted as a part of human dynamics. Therefore, the portion inside the dashed lines in figure 6 can be viewed as human operator, and the feedback gains to be externally furnished become g_{p1}, g_{p2} and g_{p3}. The feedforward and preview gains, $g_{r\ell}$'s, must also be externally furnished.

Determination of Parameters in Extended Quickening

In (extended) quickening (or more generally in manual tracking), the gain constants of the display and joystick are rather arbitrarily defined since their inputs and outputs are in different physical domains. It is also known that the human operator adjusts his gain so that the closed loop dynamics have reasonable response speed and adequate stability (reference 1). Therefore, for implementation of (extended) quickening the ratios among the feedback and feedforward gains (g_{pi}'s and $g_{r\ell}$'s) are more important than their values themselves. Based on this observation, we normalize the control gains with respect to g_{p1}. The normalized gains are the extended quickening parameters, a_i's and b_ℓ's, in figure 4, and they are

$$a_1 = 1,\ a_2 = g_{p2}/g_{p1},\ a_3 = g_{p3}/g_{p1},\ a_4 = 0 \text{ and } b_\ell = g_{r\ell}/g_{p1}. \qquad (16)$$

Using a_i's and b_ℓ's in (16), the signals to be displayed in extended quickening are, for pursuit type displays

$$s_p(k) = \sum_{i=1}^{3} a_i x_{pi}(k) \quad \text{and} \quad s_r(k) = \sum_{\ell=0}^{N_{\ell a}} b_\ell r(k+\ell) \tag{17}$$

and for compensatory type displays

$$s(k) = s_r(k) - s_p(k) \tag{18}$$

where s_p is the quickened plant output and s_r is the quickened reference trajectory. Final tuning of the parameters, a_i's and b_ℓ's, must be done by experiment.

EXPERIMENT

An experiment was conducted to examine the effect of different sets of feedback gains in Table 1 and to verify performance improvement that can be achieved by extended quickening. In the experiment, a triple integrator plant was implemented on an analog computer. An LSI-11 microcomputer was used for generating the reference trajectory, computing the extended quickening signals (s_p and s_r) and on-line data acquisition of experimental data. The display was of the pursuit type, and the two signals, s_p and s_r, were displayed by dots each with different intensity. Human subjects were asked to control the plant so that the quickened plant output, s_p, follow the quickened reference signal, s_r. Two kinds of reference trajectories were used in the experiment. One was a sequence of step changes with a 20 sec duration for each. The other was a Gauss-Markov random signal which was generated by a second order digital filter excited by a Gaussian white signal. The digital filter was an approximation of the continuous second order filter with the transfer function

$$G(s) = \frac{1}{s^2 + 2\zeta\omega_n s + \omega_n^2} \tag{19}$$

where ω_n and ζ were selected to be 1.5 rad/sec and 0.7. Selectable preview settings were provided which could be varied from $N_{\ell a} = 0$ (0 sec) to $N_{\ell a} = 200$ (5 sec). Evaluation of $s_r(k)$ with $N_{\ell a} = 200$ was not feasible in a 0.025 sec sampling period (cyclic time of computation). However, it was noted that the reference trajectory was smooth relative to a 0.025 sec sampling period (the approximate bandwidth of the filter (19) is 1.5 rad/sec ~ 0.25 Hz) and that a good approximation to $s_r(k)$ in (17) was

$$s_r(k) \simeq \sum_{\rho=0}^{N_{\ell a}/4} b'_\rho r(k+r\rho) \tag{20}$$

where $b'_\rho = b_{4\rho} + b_{4\rho+1} + b_{4\rho+2} + b_{4\rho+3}$. b'_ρ's were all precomputed, and (20) was used for on-line computation of $s_r(k)$.

Effect of Feedback Gains

The first set of experiment was conducted to examine the closed loop behavior with different combinations of feedback gains, g_{pi}'s (i.e. a_i's) in Table 1. In the experiment, the reference trajectory was a series of step changes and $N_{\ell a}$ was zero, i.e. conventional signal quickening. Time histories of the plant output (y's) for different values of w are shown in figure 7. It can be seen in the figure that the feedback gains obtained with the larger w make the closed loop relatively slow to respond while those obtained with the smaller w make the closed loop oscillatory and require more controlling effort of the human operator. It was concluded that the feedback gains obtained with w=0.01~0.1 were most suited for human control of the triple integrator plant.

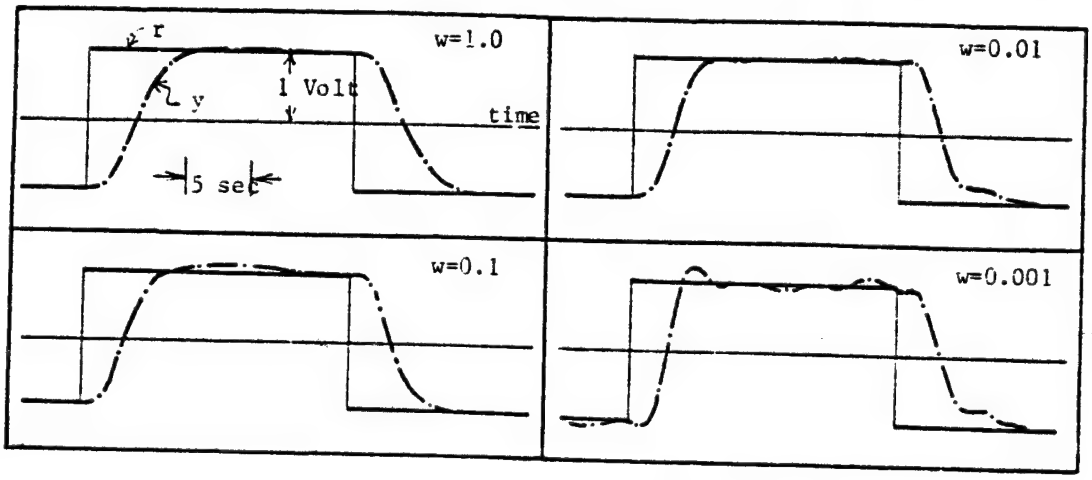

Fig. 7 Effect of Feedback Gains on Closed Loop Behavior

Extended Quickening

The extended quickening experiment was first conducted with the step reference trajectory. The parameters, a_i's and b_ℓ's, were selected to be those computed with w=0.1. This choice was based on the result of the first set of experiment, effect of feedback gains, described above. Time histories of the plant output for different values of preview time (or $N_{\ell a}$) are shown in figure 8. The inclusion of future values of the reference trajectory in the displayed signal, s_r, causes the plant output to respond prior to the step reference change. The maximum and RMS values of the tracking error were both improved by previewing the reference trajectory. A 4~5 second preview time ($N_{\ell a}$=160~200) was found to be sufficient to attain almost all the possible performance improvement relative

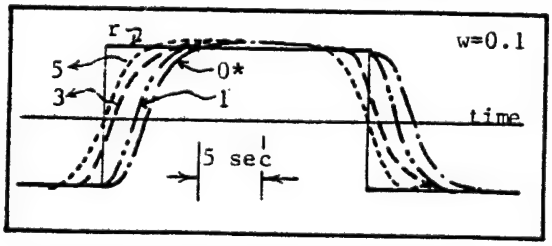

Fig. 8 Effect of Preview Time(* numbers indicate preview times in sec)

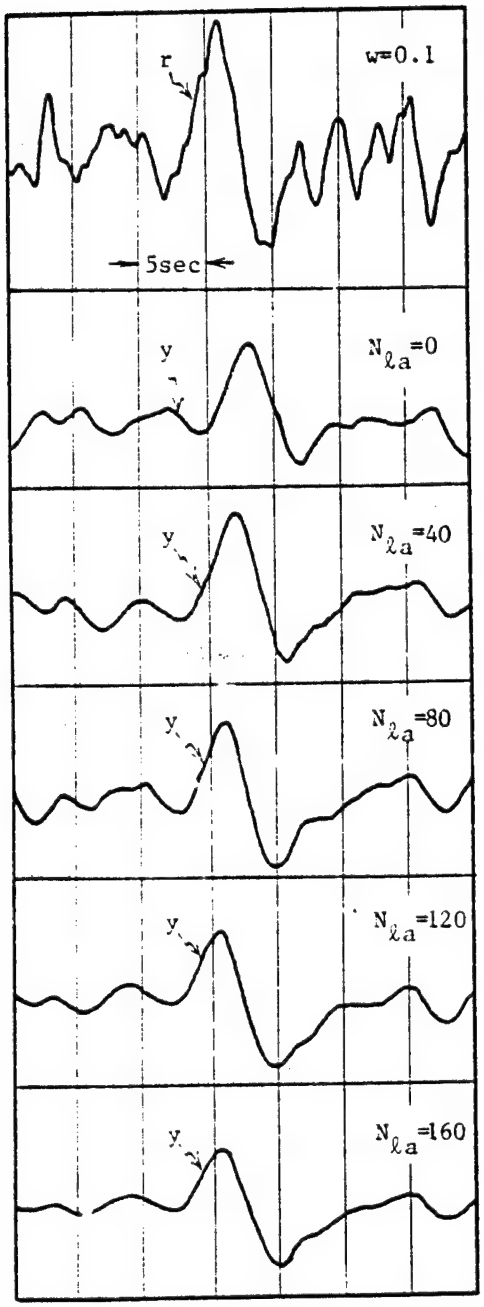

Fig. 9 Effect of Preview Time (random reference trajectory, Preview Time=0.025×$N_{\ell a}$ sec)

to the zero preview case which was about 50 % reduction of the maximum error (observed at the time of step reference change) and about 70 % reduction of the RMS error computed over 60 sec (i.e. 3 step changes of the reference trajectory). A similar improvement was also observed in the controlling input. Therefore, the difference among the four response curves in figure 8 is not simply a matter of translation.

The extended quickening experiment was also conducted with the random reference trajectory. Figure 9 shows the plant output for different values of $N_{\ell a}$. It can be seen in the figure that the phase shifts between the reference trajectory and the plant output gradually reduce as $N_{\ell a}$ increases. It was found that approximately a 2 second preview time ($N_{\ell a}$~80) was sufficient to achieve almost all the improvement in terms of the RMS tracking error, approximately 50 % reduction relative to the zero preview case. Further performance improvement beyond $N_{\ell a}$~80 was observed primarily in the controlling signal whose peak and RMS values were both continuously decreasing as $N_{\ell a}$ was increased from 80 to 200.

CONCLUSIONS

The signal quickening technique was extended to incorporate the future reference trajectory variation into the displayed signal so as to achieve high quality tracking in manual control of higher order plants with little or no damping. A design method for extended quickening systems was established based on the discrete time optimal control theory. The experiment for a triple integrator plant indicated that a drastic improvement of the closed loop performance can be obtained by extended quickening.

The extended quickening technique should be useful for various man-vehicle systems including airplane landing, maneuver, submarine control, etc. The main

motivation of (extended) quickening was to facilitate human control over high order plants with little or no damping. However, for the cases that plants are relatively easy to control, the technique should be still useful in various respects, e.g. for reducing the human work load.

The work reported in this paper is being continued to investigate the extended quickening technique in more realistic situations. Emphasis is placed on the following two points:

1. State Estimation: It was assumed that the derivatives of the plant output are directly measurable. Although the assumption holds in ideal situations such as the triple integrator plant on an analog computer in this paper, it is usually not possible to measure all derivatives directly. In such cases, one possibility is to include a Kalman filter or state observer in computer software.
2. Effect of Disturbance: In this paper, external disturbance inputs and/or noise were not considered. In practical situations, disturbance and noise can not be ignored, and their effect must be investigated.

REFERENCES

1. Sheridan, T. B. and Ferrell, W. R., Man-Machine Systems: Information, Control, and Decision Models of Human Performance, MIT Press, 1974.

2. Birmingham, H. P. and Taylor, F. V., "A Human Engineering Approach to the Design of Man-Operated Continuous Control Systems," Naval Res. Lab. Rep. 4333, April 1954.

3. Sheridan, T. B. et al., "Control Models of Creatures which Look Ahead," Proceedings of the 5th National Symposium on Human Factors in Electronics, 1964, pp. 229-240.

4. Reid, L. D. and Drewell, N. H., "A Pilot Model for Tracking with Preview," Proceedings of the 8th Annual Conference on Manual Control, AFFDL-TR-72-92, May 1972.

5. Tomizuka, M. and Whitney, D. E., "The Human Operator in Manual Preview Tracking (an Experiment and Its Modeling via Optimal Control)," Trans. of ASME, Journal of Dynamic Systems, Measurement, and Control, Vol. 98, No. 4, December 1976, pp. 407-413.

6. Tomizuka, M. and Whitney, D. E., "Optimal Discrete Finite Preview Problems (Why and How is Future Information Important?)," Trans. of ASME, Journal of Dynamic Systems, Measurement, and Control, Vol. 97, No. 4, Dec. 1975.

7. Tomizuka, M., "Optimum Linear Preview Control with Application to Vehicle-Suspension---Revisited," Trans. of ASME, Journal of Dynamic Systems, Measurement, and Control, Vol. 98, No. 3, September 1976.

8. Dorato, P. and Levis, A. H., "Optimal Linear Regulators: The Discrete-Time Case," IEEE Trans. on Automatic Control, Vol. AC-16, No. 6, Dec. 1971.

N79-15592

EFFECTS OF UNCERTAINTY ON MANUAL TRACKING PERFORMANCE

by Arye R. Ephrath & Barbara Chernoff

Department of Electrical Engineering & Computer Science
University of Connecticut
Storrs, Conn. 06268

SUMMARY

In this experimental study we investigated some transient phenomena and target acquisition modes associated with interrupted observations during ground-to-air AA tracking. Our subjects, using a two-axes control stick, tracked a computer-generated airplane image on a CRT display. The airplane image executed a low-level straight pass. At certain pseudo-random times during each 25-second run the screen was blanked for a period of one second (simulating a temporary loss of visual contact with the target due to clouds, fog or obstructions). When the target image reappeared the subjects reacquired it and continued tracking, attempting to minimize vector RMS error for the entire run (including the blanked period).

The results reveal an increase both in tracking error and in error variance during the blanked period, only when the target disappears while in the crossover region. Blanking at other times effected increased variance but had no effect on the mean error. Also, blanking before and after crossover had opposite effects: A blanking period just before crossover produced an increase lag while a blanking just after crossover resulted in a lead and thus made the error curve more symmetric.

INTRODUCTION

The problem of manual tracking performance with sampled observations has been studied before [e.g., Refs. 1, 2] from a "macroscopic" point of view. In these studies the overall control performance was investigated when the human was assumed to have access to periodic, frequent observations of the system outputs.

In the study reported here we intended to concentrate on the microscopic aspects of the tracking behavior. We were not interested in the operator's performance as a whole; rather, we set out to examine the details of the tracking behavior during periods when observations of the system outputs were not available to the human. Understanding the operator's behavior during such essentially open-loop tracking is of interest as these situations occur quite frequently in practice. Examples of operators subjected to this type of manual tracking may be the driver of a high-speed automobile during the first few seconds after entering a dark tunnel; a radar operator attempting to track a target with the aid of noisy position

data; or an anti-aircraft battery operating in an environment of electronic counter-measures, optical counter-measure or simple topographical and meteorelogical obstructions masking the target's image. Indeed, our experimental set-up simulated the situation of the latter, i.e., the AAA paradigm.

THE EXPERIMENT

Our experimental facility consisted of a PDP 11/20 computer, a CRT screen, and a two-axes control stick. The PDP 11/20 generated a delta-shaped airplane image used in the compensatory tracking, with the image displayed on the CRT screen (see Fig. 1).

Our subjects were instructed to manually track the delta-shaped image, both in elevation and in azimuth, as it passed across the CRT screen. Each target pass was a 25.6-seconds straight-and-level flyby. At predetermined times during the run the target disappeared from the screen for a period of one-second. This blanking simulated the temporary loss of visual contact with the target. Five experimental conditions were implemented.

Condition A: No blanking

Condition D: Blankings at -5 sec. and at +9 sec. (0. sec. = crossover)

Condition E: Blanking at -3 sec.

Condition F: Blanking at +1 sec.

Condition G: Blanking at +3 sec. and at +9 sec.

The purpose of two blanking periods (Conditions D and G) was twofold: In an attempt to prevent the subjects from relaxing their tracking effort after the first blank occured, the second blanking at +9 seconds was introduced. Also, this set of blanking periods enabled us to compare the transient tracking behavior of subjects during periods of good tracking (where the target angular velocity is small and the tracking error is also small) with the transient phenomena in the crossover region. Condition A - no blanking served as the control for the subjects' baseline tracking ability.

Six University of Connecitcut students, members of the University Air Force ROTC program, participated in thes experiment. They were trained extensively in this task by tracking a variety of flybys; however, they were not exposed to blankings until the formal experimentation commenced.

Each subject was presented with each of the five experimental conditions in randomized order and there were 7 replications, for a total of 35 runs per subject. The subjects were not informed as to the number of blanking periods in each run, nor were they told how many experimental conditions were to be presented. They were told, however, the total number of runs to be presented. The subjects were instructed to minimize their RMS tracking error for the entire run, including the blanked periods. Following each

run, each subject was informed of his RMS error score and was encouraged to keep it as low as possible.

Tracking errors in azimuth and elevation, and the control inputs in these axes were sampled by the PDP-11/20 at a rate of 40 Hz. Each 25.6-second run thus yielded 1024 datum points for each of these four dependent variables. The data were stored in real-time or secondary devices (discs and magtapes) for subsequent, off-line processing and analysis.

RESULTS AND DISCUSSION

Some results of this experiment are presented in Figures 2-6. Each figure is the summary azimuth data of the (6 subjects x 7 replications =) 42 runs per experimental condition. (In the interest of brevity, elevation data, which are completely analogous, were omitted here.) Figures 2a and 2b are the mean and standard deviation, respectively, of the angular tracking error under the baseline condition, Condition A (no blanking). Figure 2a exhibits the asymmetry (large lag just before crossover and smaller lead immediately after) characteristic of this tracking task [3]. Also, the tracking errors are quite small in the so-called "areas of good tracking" outside the crossover region.

Comparison of Figure 3 (standard deviation, Condition D) with Figure 2b reveals the two blanking periods which manifest themselves as spikes in Fig. 3. As expected, a blanking period just before crossover produces an increased lag (Fig. 5), while a blanking period just after crossover effects a lead and thus makes the error curve more symmetric (Fig. 6a).

These deviations from the baseline error curve were tested using a point-by-point t-test and were found to be significant, under Condition E and F, at the $P < 0.01$ level. During periods of good tracking, however, blanking had no effect on the tracking error mean. This was true not only with respect to the blanking period at +9 seconds but also with respect to the blankings at -5 seconds and at +3 seconds.

CONCLUSIONS

Increasing the operator's uncertainty of the target's position for short periods increases the lagging tendency before crossover and the leading tendency - when the instance of uncertainty occurs after crossover. Uncertainty on the operator's part of the target's motion always results in increased error variance; the error mean, however, is sensitive to uncertainty only when the tracking task is difficult. In periods of good tracking (and hence, small tracking error) uncertainty has little effect on the error mean.

REFERENCES

1. Senders, J.W., Ward, J.L., and Carbonell: Human Visual Sampling Processes. NASA CR-1258, 1969.

2. Senders, J.W. et al.: An Investigation of the Visual Sampling Behavior of Human Observers. NASA CR-434, 1966.

3. Kleinman, D.L. and Ephrath, A.R.: Effects of Target Motion and Image on AAA Tracking. Decision and Control Conference, New Orleans, La., Dec. 1977.

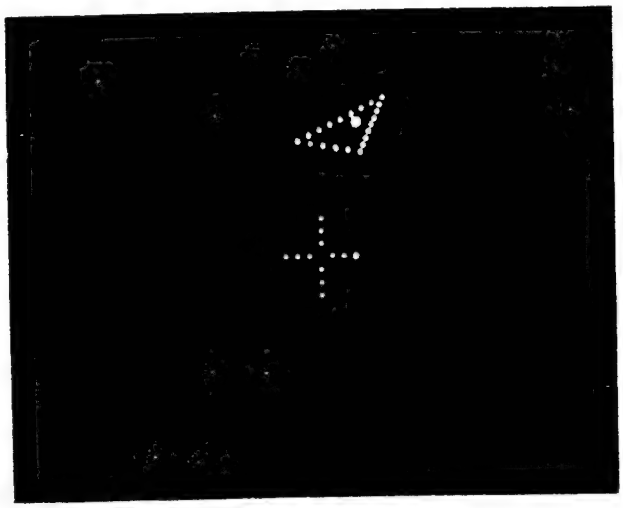

FIG. 1: CRT DISPLAY

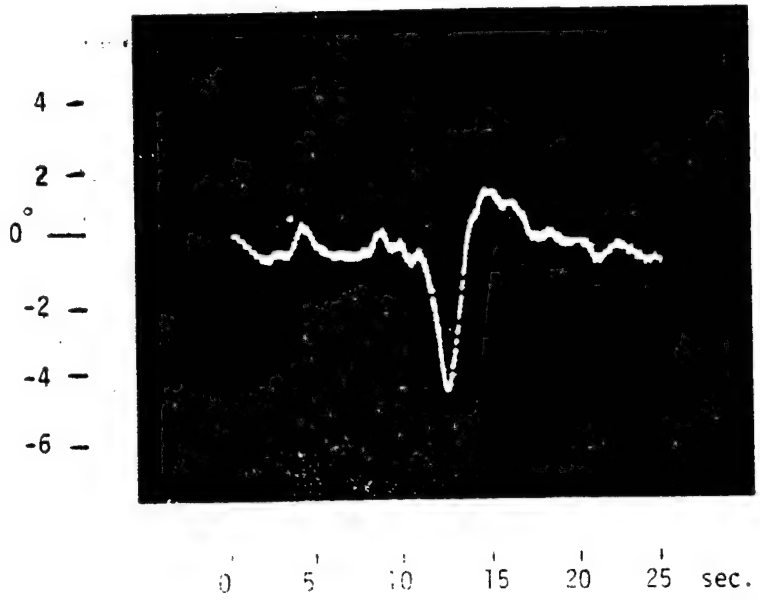

FIG. 2a: Azimuth Error Mean, No Blanking

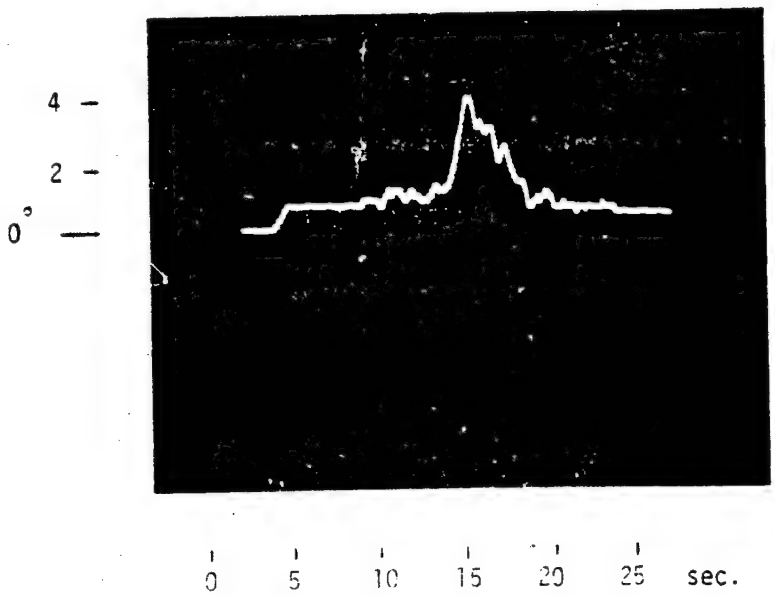

FIG. 2b: Azimuth Error S.D., No Blanking

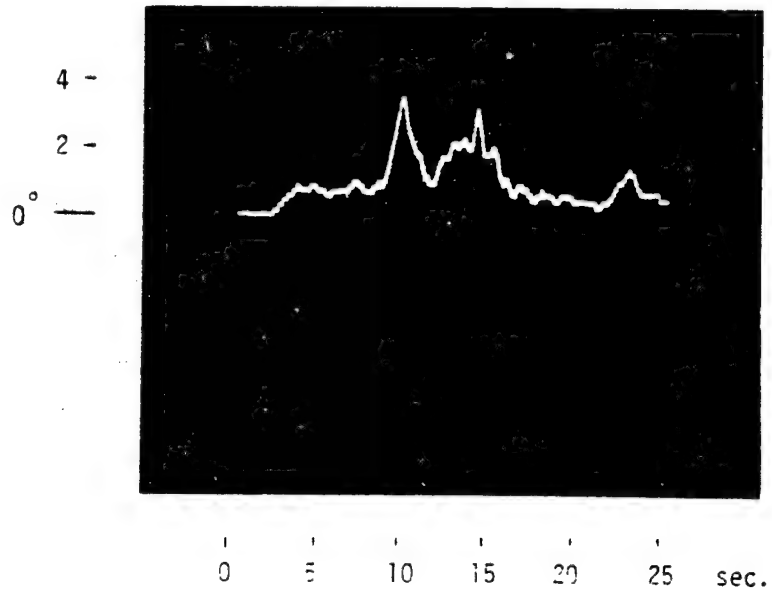

FIG. 3: Azimuth Error S.D., Blankings @ -5 & +9 sec

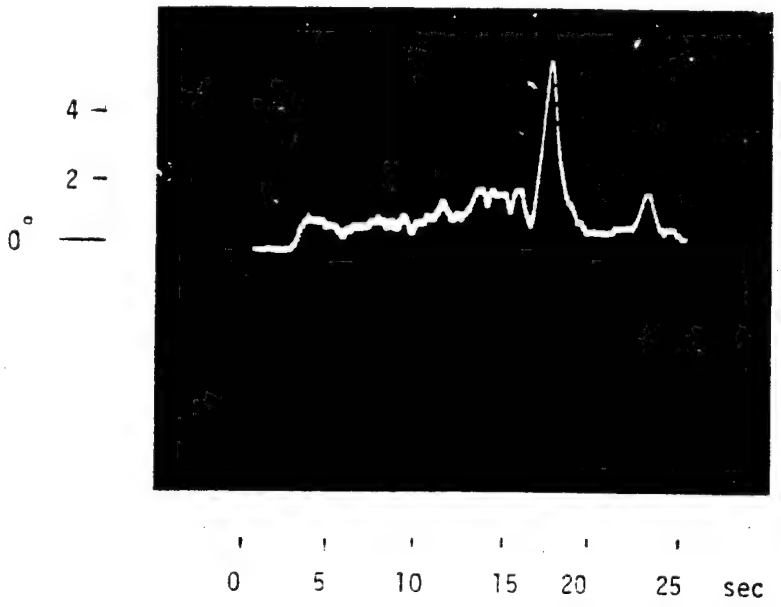

FIG. 4: Azimuth Error S.D., Blankings @ +3 & +9 sec.

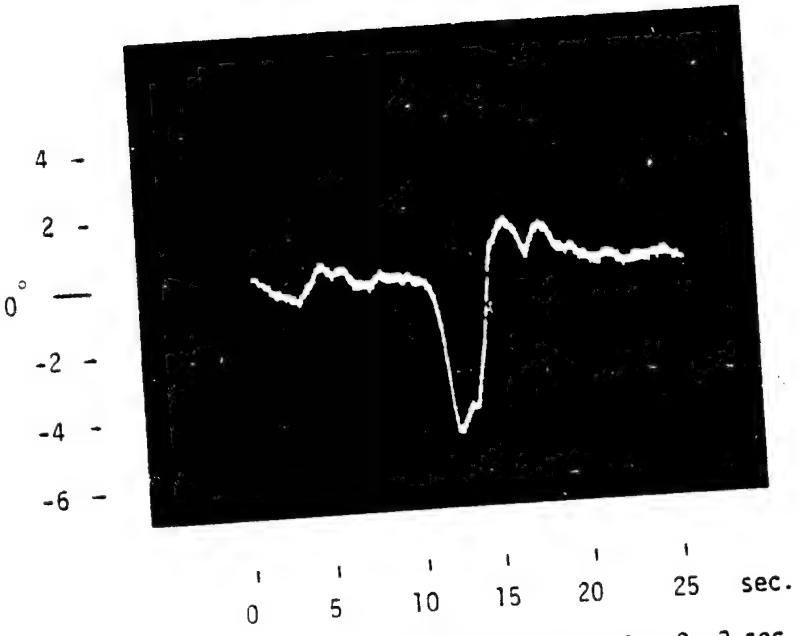

FIG. 5: Azimuth Error Mean, Blanking @ -3 sec.

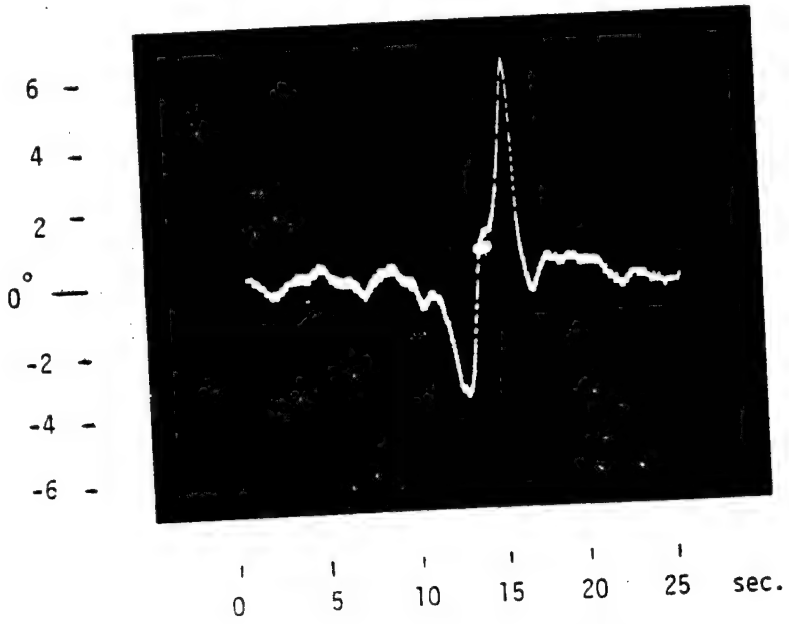

FIG. 6a: Azimuth Error Mean, Blanking @ +1 sec.

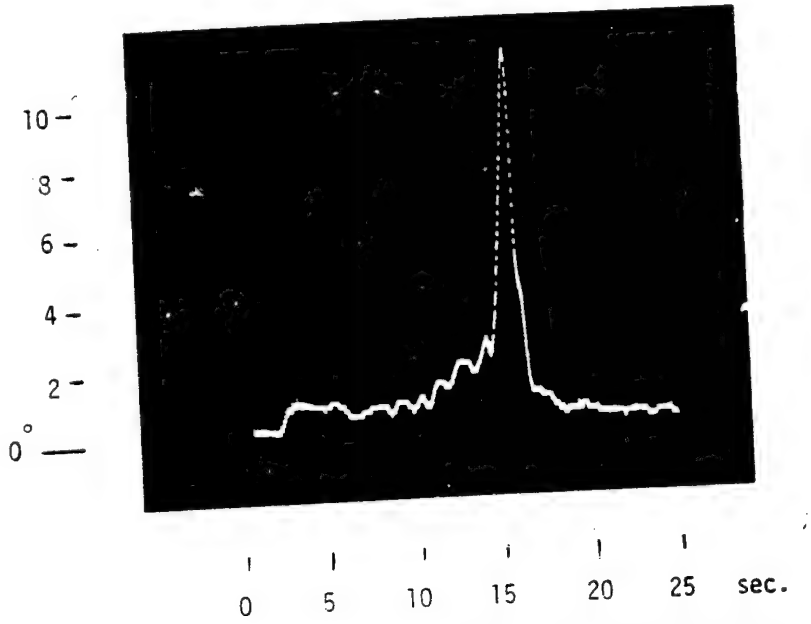

FIG. 6b: Azimuth Error S.D., Blanking @ +1 sec.

SESSION B: HUMAN OPERATOR MODELS: IDENTIFICATION AND CONJECTURE

Chairman: S. Baron

MODELING THE EFFECTS OF HIGH-G STRESS ON PILOTS IN A TRACKING TASK

by Jonathan Korn and David L. Kleinman

Department of Electrical Engineering & Computer Science
University of Connecticut
Storrs, Conn. 06268

SUMMARY

Air-to-Air tracking experiments have been conducted at the Aerospace Medical Research Laboratories (AMRL) using both fixed and moving base (Dynamic Environment Simulator-DES) simulators. The obtained data, which includes longitudinal error of a simulated air-to-air tracking task as well as other auxiliary variables, was analyzed using an ensemble averaging method.

In conjunction with these experiments, the Optimal Control Model (OCM) is applied to model a human operator under high-G stress.

INTRODUCTION

Recent efforts at Aerospace Medical Research Laboratories, WPAFB, have demonstrated initial feasibilities of applying the Optimal Control Model [1] of human response to the air-to-air tracking problem. The model has been able to generate predictions of ensemble mean and standard deviations of longitudinal tracking error, aircraft state variables and attained G_z forces corresponding to arbitrary target profiles. The preliminary modeling efforts were focused on two subproblems. First, effects that related cost functional weightings and internal model parameter changes to G-stress were considered. Second, a structural change of the model was suggested. The data for this model development and validation has been generated on the centrifuge (DES) facility at AMRL. The most recent data vs. model comparisons have shown excellent correspondance for tracking error ensemble statistics. Further model refinement efforts are now under investigation.

ENGAGEMENT SCENARIO

Figure 1 shows the geometry of the air-to-air tracking in the longitudinal plane [2]. In our modeling efforts we assumed no gunsight dynamics, i.e. the sight is fixed and aligned with the aircraft body axis. An additional simplification has been added by assuming that pitch angle equals the flight path angle.

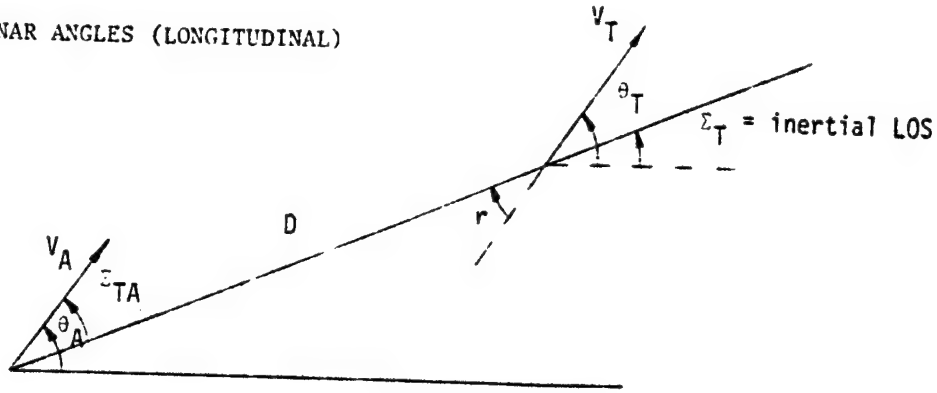

FIG. 1: TRACKING GEOMETRY

θ_A = pursuer fp angle θ_T = evader fp angle

Σ_T = inertial line of sight

$\Sigma_{TA} = \Sigma_A - \Sigma_T$ = relative line of sight

$r = \theta_T - \Sigma_T$ = aspect angle

OPTIMAL CONTROL MODEL FOR AIR-TO-AIR TRACKING

The OCM, modified to treat deterministic target motion assumes the system dynamics

$$\dot{\underline{x}}(t) = A_o \underline{x}(t) + \underline{b}_o u(t) + F_o z(t) \tag{1}$$

$$\underline{y}(t) = C_o \underline{x}(t) \tag{2}$$

where $u(t) \triangleq \delta_A$ is the elevator deflection and $z(t)$ is a function of the target motion. The state vector is

$$\underline{x}' = [q_T, q_A, \alpha_A, \theta_A - \theta_T, e]'$$

where $q_T(q_A)$ is the target (attacker) pitch rate, α_A is the attacker angle of attack and e is the tracking error. The observations are

$$\underline{y}' = [e, \dot{e}, r, \dot{r}]'$$

with correspondance to the OCM assumtion on observations. The human perceives only a delayed and noisy signal

$$\underline{y}_p(t) = \underline{y}(t-\tau) + \underline{v}_y(t) \tag{3}$$

where $\underline{v}_y(t)$ is a white observation noise with covariance

$$V_{y_i}(t) = \frac{\rho_y^\circ}{f_i(t)} \cdot \frac{(\bar{y}_i^2 + \sigma_i^2)}{N^2(a_i)} \qquad i = 1, \ldots, 4 \tag{4}$$

τ = operator time delay

ρ_y° = nominal noise to signal ratio

$f_i(t)$ = fractional attention allocation to the i-th observed variable

$N(a_i)$ = equivalent gain of the visual/indifference threshold a_i

$\bar{y}_i$ = mean of y_i

σ_i = standard deviation of y_i

The control input corresponds to the differential equation

$$\dot{u}(t) = -L_c \begin{bmatrix} \hat{\underline{x}}(t) \\ u(t) \end{bmatrix} + \frac{1}{\tau_N} v_u(t) \tag{5}$$

where L_c is the feedback gains vector, $\hat{\underline{x}}(t)$ is the estimated state, τ_N is the neuro-motor time constant and $v_u(t)$ is a white motor noise with covariance proportional to the covariance of u(t)

$$V_u(t) = \rho_u \, \mathrm{cov}[u(t)], \tag{6}$$

ρ_u being the motor noise ratio coefficient. The system matrices are

$$A_o = \begin{bmatrix} 0 & 0 & 0 & 0 & 0 \\ 0 & M_q & M_\alpha & 0 & 0 \\ 0 & 1 & Z_\alpha & 0 & 0 \\ -1 & 1 & 0 & 0 & 0 \\ 0 & 1 & 0 & V/D & 0 \end{bmatrix} \qquad \underline{b}_o = \begin{bmatrix} 0 \\ M_\delta \\ 0 \\ 0 \\ 0 \end{bmatrix}$$

$$C_o = \begin{bmatrix} 0 & 0 & 0 & 0 & 1 \\ 0 & 1 & 0 & V/D & 0 \\ 0 & 0 & 0 & -1 & 1 \\ 1 & 0 & 0 & V/D & 0 \end{bmatrix}$$

The vertical accelerations of the target, and those commanded by the attacker are respectively

$$G_T(t) = \frac{V}{g} \cdot x_1(t) + 1 \qquad (7a)$$

$$G_A(t) = \frac{V}{g} \cdot x_2(t) + 1 \qquad (7b)$$

The constants are

$M_\delta = 11$

$V = 1000$ ft/sec $D = 1000$ ft.

$g = 32.2$ ft/sec^2

$M_q = -7.63$ sec^{-1}

$M_\alpha = -20.66$ sec^{-1}

$Z_\alpha = -2.27$ sec^{-1}

A typical G_T time history, used in the present AMRL studies is shown in Fig. 2.

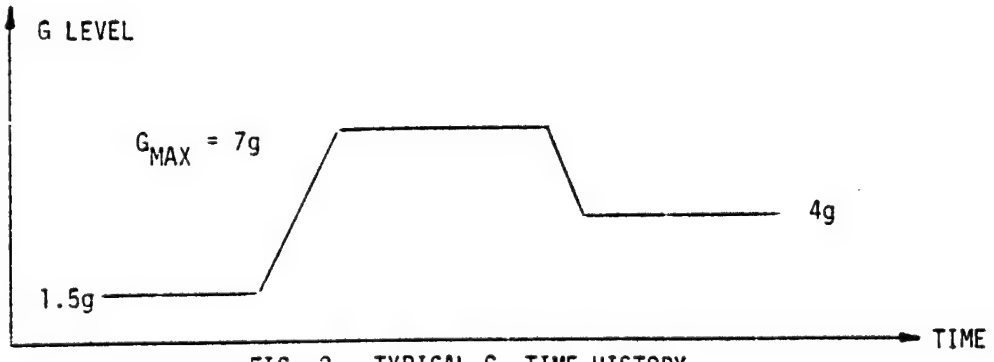

FIG. 2: TYPICAL G_T TIME-HISTORY

The internal model parameters were set to their nominal values $\tau = .2$ sec, $\rho_u = -20$ dB, $\rho_y = -14$ dB, $\tau_N = .1$ sec. Usually, the nominal value of ρ_y ($=\rho_y^\circ$) for a single observation channel would be -20 dB. In our case there are 4 observation channels which increase the nominal ρ_y to -14 dB.

PILOT MODEL REVISION AND RESULTS

Motivated by recent results in modeling AAA tracking under high uncertainty [3], we write the human's internal characterization of target motion ($x_1 = q_T$) as

$$\dot{x}_1(t) = -a(t)\, x_1(t) + z_1(t) \tag{8}$$

rather than

$$\dot{x}_1(t) = z(t). \tag{9}$$

Now,

$$z_1(t) = z(t) + a(t)\, x_1(t) = \frac{g}{V}\,[\dot{G}_T(t) + a(t)\, G_T(t)] \tag{10}$$

Using this approach we note the following facts:

1. $a(t)$ does not affect the system model.
2. $a(t)$ does affect the Kalman filter submodel equation associated with this state,

$$\dot{x}_1(t) = -a(t)\, x_1(t) + \xi(t)\ ;\ \xi(t) \text{ - white noise} \tag{11}$$

The target motion is perceived by the human operator as a Markov process as opposed to a random walk ($a=0$). It reflects the pursuer's uncertainty in perceiving the target's motion. $a(t)$ is chosen according to

$$\tau_L\, \dot{a}(t) + a(t) = \mathcal{N}(G_T) \cdot \sqrt{\Sigma_{11}} \tag{12}$$

where

$$\mathcal{N}(G_T) = 3 \cdot \left(\frac{G_T}{4}\right)^4 \tag{13}$$

The resulting model-vs-data comparisons for ensemble mean error ($\bar{e}(t)$) for dynamic and static-G cases (G-stress and no G-stress) are shown in Figures 3-4, respectively. The agreements are excellent through the transient G peak to recovery. Nominal parameters have been used for the basic OCM response parameters; the only change between static and dynamic cases is

$$\tau_L = \begin{cases} .53 & \text{static} \\ .97 & \text{dynamic} \end{cases} \tag{14}$$

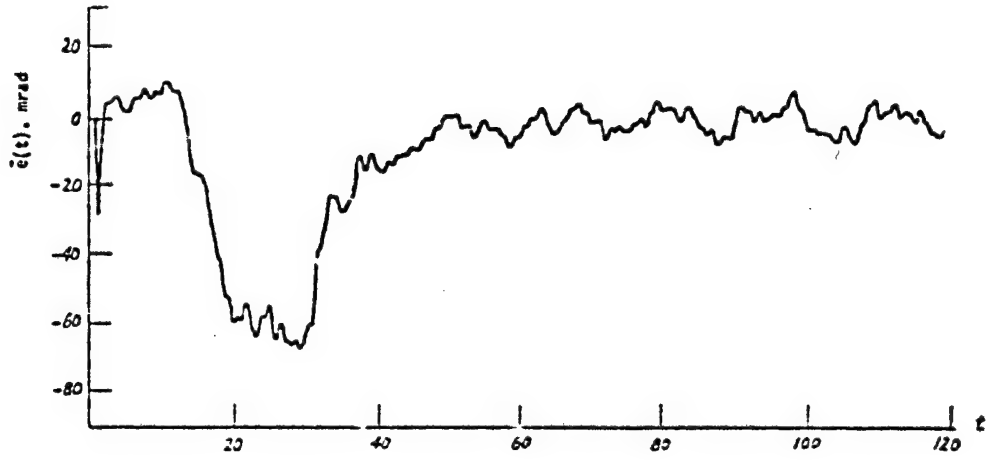

a) Experimental Data

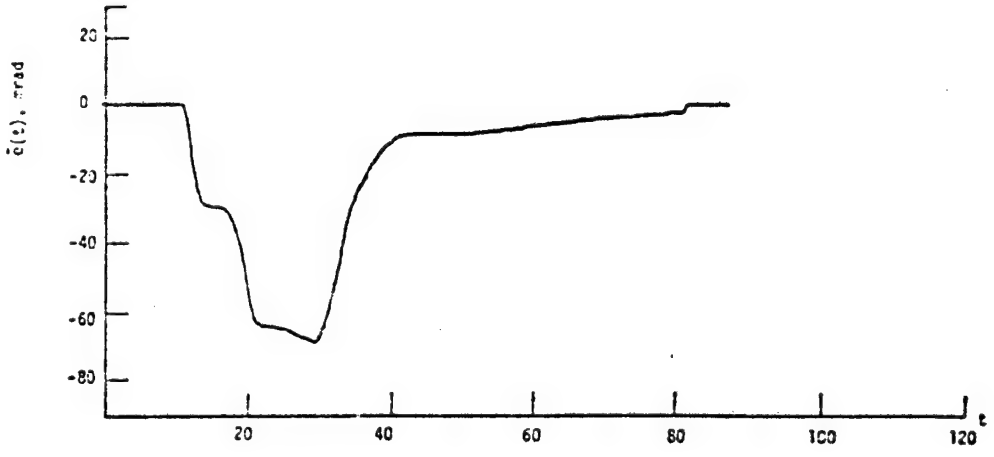

b) Model Predictions

FIG. 3: MEAN PITCH TRACKING ERROR, 1 PEAK, G STRESS

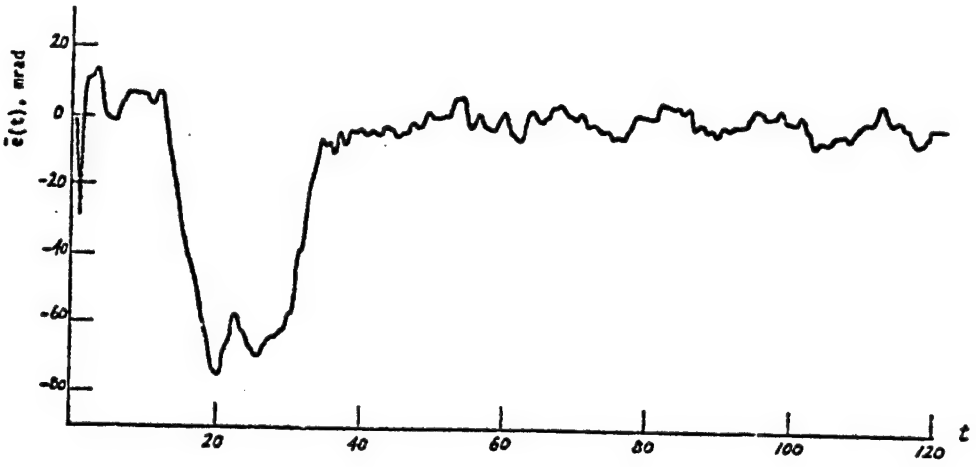

a) Experimental Data

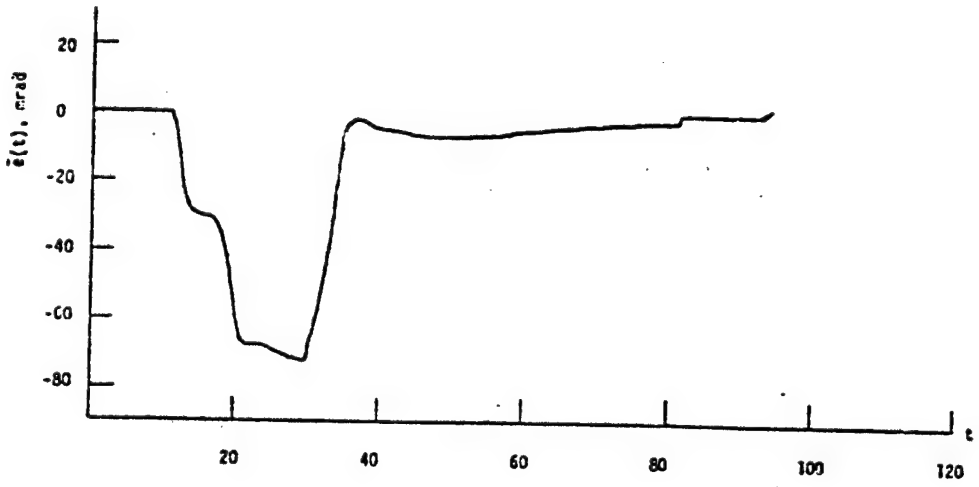

b) Model Predictions

FIG. 4: MEAN PITCH TRACKING ERROR, 1 PEAK, STATIC G

CONCLUDING REMARKS

A preliminary modeling work in the area of air-to-air tracking task has been conducted and the initial results have been extremely encouraging. However, further research is needed, and is presently continuing, to interpret these results and to match the standard deviation data.

For modeling work, a major concern is involved with the OCM internal parameters and their dependence on G_z and $\dot{G}_z$ levels. A set of new experiments will be conducted in the near future to enhance the observations of this dependence.

Also, the present model formulation does not include any motion-derived cues as G_z or $\dot{G}_z$; it merely regards these quantities as external stressors, and neglects any useful motion cues that they may provide. It is the feeling of the authors that this aspect of modeling work need to be considered in any future modeling efforts.

REFERENCES

1. Kleinman, D.L., Baron, S. and Levison, W.H.: A Control Theoretic Approach to Manned-Vehicle Systems Analysis. IEEE Trans. Autom. Control, Vol. AC-16, No. 6, 1971.

2. Harvey, T.R. and Dillow, J.D.: Application of an Optimal Control Pilot Model to Air-to-Air Combat. AIAA Guidance and Control Conference, August 1974.

3. Kleinman, D.L., Ephrath, A.R., and Rao, P. Krishna: Effects of Target Motion and Image on AAA Tracking. Univ. of Conn., Dept. of EECS, Tech. Report TR-77-7, Nov. 1977.

N79-15594

AAA GUNNER MODEL BASED ON OBSERVER THEORY

By R. S. Kou*, B. C. Glass*, C. N. Day** and M. M. Vikmanis*

*Systems Research Laboratories, Inc.
Dayton, Ohio 45440

**Aerospace Medical Research Laboratory
Wright-Patterson Air Force Base, Ohio 45433

SUMMARY

The Luenberger observer theory is used to develop a predictive model of a gunner's tracking response in antiaircraft artillery (AAA) systems. This model is composed of an observer, a feedback controller and a remnant element. An important feature of the model is that the structure is simple, hence a computer simulation requires only a short execution time. A parameter identification program based on the least squares curve fitting method and the Gauss Newton gradient algorithm is developed to determine the parameter values of the gunner model. Thus, a systematic procedure exists for identifying model parameters for a given antiaircraft tracking task. Model predictions of tracking errors are compared with human tracking data obtained from manned AAA simulation experiments conducted at the Aerospace Medical Research Laboratory, Wright-Patterson AFB, Ohio. Model predictions are in excellent agreement with the empirical data for several flyby and maneuvering target trajectories.

INTRODUCTION

A systematic study of threat effectiveness for antiaircraft artillery (AAA) systems requires the development of a mathematical model for the gunner's tracking response. The gunner model is then incorporated into computer simulation programs as shown in reference 1 for predicting aircraft attrition with respect to specific antiaircraft weapon systems. Two of the fundamental design requirements of a gunner model are simplicity in model structure and accuracy in the tracking error predictions. A simple gunner model structure will shorten computer simulation execution time. Obviously, accurate predictions of tracking error implies model fidelity with respect to describing the gunner's tracking performance. Then, the manned threat quantification in the threat analysis will be reliable.

An antiaircraft gunner model based on the Luenberger observer theory in references 2, 3 and 4, is developed in this paper. It satisfies both the design requirements mentioned above. The structure of the model is simple and its predictions of tracking errors are accurate. It is composed of three main parts - an observer, a feedback controller, and a remnant element. An observer is itself a dynamic system whose output can be used as an estimate of the state of a given system. The simplicity of the observer design makes the observer an attractive design method. The estimated state is then used to implement a linear state variable feedback controller which represents the gunner's control function in the compensatory tracking task. The effects of all the randomness sources due to human psychophysical limitations and of modelling errors are lumped into one random remnant element in this model design. Another important feature of this model is that its parameters can be determined systematically instead of by trial-and-error. A parameter identification program based on the least squares curve-fitting method in reference 5 and the Gauss-Newton gradient algorithm in reference 6 is developed for this purpose. This program iteratively adjusts the parameter values to minimize the least squares error between the model prediction of tracking error and actual human tracking data obtained from manned AAA simulation experiments conducted at the Aerospace Medical Research Laboratory, WPAFB, Ohio. Thus, it provides a convenient procedure for model validation. In addition, a computer simulation program is developed with the designed model describing the gunner's response for a given AAA tracking task. The program provides time functions of the ensemble mean and standard deviation for the model's tracking error predictions (azimuth and elevation). Computer simulation results are in excellent agreement with the empirical data for several aircraft flyby and maneuvering trajectories. This verifies that the model can predict tracking errors accurately and thus is a reliable description of the gunner's compensatory tracking characteristics.

A comparison between this model and the optimal control model in references 7, 8 and 9 (by Kleinman, Baron, Levison) is also given. It can be shown that the model based on observer theory is as accurate as the optimal control model in predicting tracking errors. In addition, the computer execution time of the AAA closed loop system simulation utilizing this model is less than 15% of that using the optimal control model. This is a primary advantage of a model with simple structure.

DESCRIPTION OF AN AAA GUN SYSTEM

The tracking task of an antiaircraft artillery (AAA) gun system can be described by a closed loop (single axis tracking loop) block diagram as shown in figure 1. Two gunners, one each for azimuth and

elevation axes, play the role of controller in this man-machine feedback control system. From his visual display, each gunner observes the tracking error, e_T (one for azimuth error and the other for elevation error), which is the difference between the target position angle θ_T and the gunsight line angle θ_g. Independently, the gunners operated the hand crank to control the gunsight system in order to align the gunsight line angle (output) with the target position angle (input). Therefore, the azimuth tracking task is decoupled from the elevation tracking task in this AAA system.

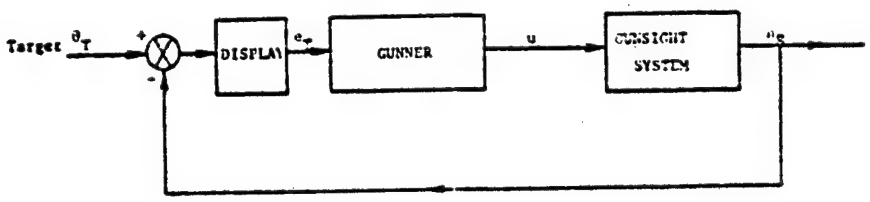

FIGURE 1: BLOCK DIAGRAM OF THE AAA CLOSED LOOP SYSTEM

The purpose of this paper is to develop a mathematical model of the response characteristics of a gunner in a compensatory tracking task. Therefore, in the following, we first describe the mathematical representation of the gunsight and rate-aided control dynamics (the gunsight system) and the target trajectories. In this paper the transfer function of the gunsight system considered is:

$$\frac{\Theta_g(s)}{U(s)} = \frac{1}{s} \tag{1}$$

for the azimuth angle tracking as well as the elevation angle tracking. ($\Theta_g(s)$ and U(s) are the Laplace transforms of $\theta_g(t)$ and u(t) respectively.) It can be shown that this transfer function is a valid representation of many practical gunsight systems. Several flyby and maneuvering trajectories in reference 10 of the target aircraft of 45 seconds duration were selected as input to the AAA system of figure 1. These trajectories are deterministic functions of time. (But their dynamic properties $\dot{\theta}_T$, $\ddot{\theta}_T$, etc., are not known precisely to trackers. The state space equation of the gunsight system and the target motion can be derived as follows.

$$\dot{\underline{x}} = A\underline{x} + Bu + F\ddot{\theta}_T \tag{2}$$

where $\underline{x}$ denotes the state vector having two components,

$$\underline{x} = \begin{bmatrix} x_1 \\ x_2 \end{bmatrix} = \begin{bmatrix} \theta_T - \theta_g \\ \dot{\theta}_T \end{bmatrix}$$

and A, B, and F matrices are

$$A = \begin{bmatrix} a_{11} & a_{12} \\ a_{21} & a_{22} \end{bmatrix} = \begin{bmatrix} 0 & 1 \\ 0 & 0 \end{bmatrix},$$

$$B = \begin{bmatrix} b_1 \\ b_2 \end{bmatrix} = \begin{bmatrix} -1 \\ 0 \end{bmatrix}, \quad F = \begin{bmatrix} f_1 \\ f_2 \end{bmatrix} = \begin{bmatrix} 0 \\ 1 \end{bmatrix},$$

and the scalars u and $\ddot{\theta}_T$ denote the control from the AAA gunner and the target acceleration. The tracking error e_T on the visual display is observed by the gunner and is expressed in the measurement equation:

$$y = C\underline{x} \tag{3}$$

where y is the observed tracking error and C is a row vector [1 0]. Equations (2) and (3) will be used in the next section to develop an AAA gunner model.

AAA GUNNER MODEL

This section presents a mathematical model of an antiaircraft gunner in the compensatory tracking task. The main design requirements for developing this model are:

- accurate model prediction of tracking errors
- simple model structure
- systematic determination of model parameters

In this paper, the Luenberger reduced order observer theory has been applied to design the gunner model which satisfies the above design requirements. Figure 2 shows the block diagram of this model consisting

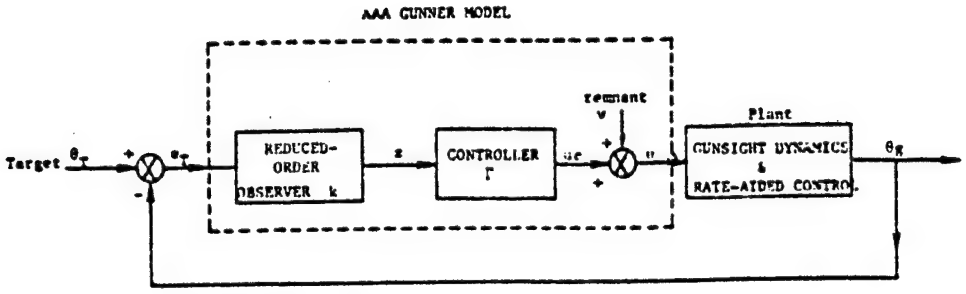

FIGURE 2: BLOCK DIAGRAM OF THE STRUCTURE OF THE AAA GUNNER MODEL

of three main elements: observer, controller, and remnant. The first element is a reduced-order observer which processes the gunner's observation from the visual display to provide an estimate of the states of the AAA system. It will be shown that the system equation (2) is a 2nd order system, but the reduced-order observer is only of the first order. Since some components of the state as given by the system outputs are already available by direct measurement. The estimation of these components of the state is not necessary and will cause a certain degree of redundancy. The use of a reduced-order observer eliminates this redundancy and still provides sufficient information to reconstruct (or estimate) the state of the observed system. The controller represents the gunner's tracking function by an estimated-state linear feedback control law. The observer and the controller consists of the deterministic part of the gunner model. The effects of the various randomness sources in the AAA man-machine closed loop system and of the modelling errors are lumped into one element called remnant which is the stochastic part of the gunner model. These randomness sources include the modelling error, the observation error, the neuromotor noise, etc. Mathematical equations of this model are given below.

Model Equations

System equations (2) and (3) are used in the design of the gunner model. However, the gunner doesn't have the precise information about the target dynamics, so the term representing target acceleration, θ_T, in Eq. (2) will not be included in the design of the observer equation. The effect on the tracking error due to the modelling error of the gunner's uncertainty about target dynamics will be included in the remnant element. Now from Eq. (3),

$$y = Cx = x_1$$

the tracking error is available from direct observation. Thus, it is only necessary to estimate the second component x_2 of the state vector $\underline{x}$ in order to implement a state variable feedback control law. By the

reduced-order Luenberger observer theory in reference 4, an estimate $\hat{x}_2$ of the state variable x_2 can be obtained by

$$\dot{\hat{x}}_2 = (a_{22} - ka_{12})\,\hat{x}_2 + k\dot{y} + (a_{21} - ka_{11})\,y + (b_2 - kb_1)\,u_c \tag{4}$$

where a_{ij} and b_k are the elements of matrices A and B in Eq. (2), the scalar k is the observer gain, y and $\dot{y}$ are the observed tracking error and error rate respectively, and u_c is the linear feedback control law (the controller) with the form:

$$u_c = -[\gamma_1 \ \gamma_2] \begin{bmatrix} y \\ \hat{x}_2 \end{bmatrix}$$

where the feedback control gains γ_1 and γ_2 are two constants determined in reference 10. Note that the state feedback is composed of y (the observed variable which is x_1) and $\hat{x}_2$ (the estimated state of x_2). It can be shown that the system (2) and (3) is completely observable. (The definition of observability and the conditions of a system to be observable can be found in reference 11). Then, by the observer theory, there always exists an observer gain k to make the eigenvalue of the observer (Eq. (4)) negative. Thus, the output of the observer will be a good estimation to the state of the observed system. This shows the existence of proper observer gain k in Eq. (4). Actually, the value of observer gain k is determined by a curve-fitting identification program. The required differentiation of y in Equation (4) can be avoided by introducing the following variable:

$$z(t) = \hat{x}_2 - ky(t) \tag{5}$$

Hence the observer dynamics can be represented by

$$\dot{z} = (a_{22} - ka_{12})z + (a_{22} - ka_{12})ky + (a_{21} - ka_{11})y + (b_2 - kb_1)u_c \tag{6}$$

Next, the actual output of this model is expressed as the sum of the output u_c of the controller and the remnant element v.

$$\begin{aligned} u &= u_c + v \\ &= -[\gamma_1 \gamma_2] \begin{bmatrix} y \\ \hat{x}_2 \end{bmatrix} + v \end{aligned} \tag{7}$$

where the remnant term v(t) is modeled as a white noise and its statistical properties are selected to be

$$\begin{aligned} &E\,[v(t)] = 0 \qquad \text{for all } t \\ &E\,[v(t)\,v(\tau)\,] = q(t)\,\delta(t - \tau) \qquad \text{for all } t \text{ and } \tau \text{ where} \end{aligned} \tag{8}$$

E is the expectation operator, $\delta(t)$ is the Dirac delta function and the

covariance function q(t) is assumed as a function of estimated target dynamics,

$$q(t)= \alpha_1 + \alpha_2 \dot{\hat{\theta}}_T^2(t) + \alpha_3 \ddot{\hat{\theta}}_T^2 (t) \tag{9}$$

where α_1, α_2, and α_3 are three nonnegative constants to be determined, and $\dot{\hat{\theta}}_T$ and $\ddot{\hat{\theta}}_T$ are estimated target angle rate and acceleration respectively.

Equations of the Closed-loop AAA System

In the previous section, the gunner model equations of the observer, the controller, and the remnant have been derived. These equations are combined with system equations (2) and (3) to obtain the mathematical model of the closed loop AAA system. Since $x_1 = y$, Eqs. (2) and (6) can be rewritten as follows:

$$\begin{aligned}
\dot{y} &= a_{11}y + a_{12}x_2 + b_1 u + f_1 \ddot{\theta}_T \\
\dot{x}_2 &= a_{21}y + a_{22}x_2 + b_2 u + f_2 \ddot{\theta}_T \\
\dot{z} &= (a_{22} - ka_{12})z + (a_{22} - ka_{12})ky + (a_{21} - ka_{11})y + (b_2 - kb_1)\, u_c \\
u &= u_c + v \\
u_c &= -[\gamma_1 \ \gamma_2] \begin{bmatrix} y \\ \hat{x}_2 \end{bmatrix}
\end{aligned} \tag{10}$$

By introducing new variables:

$$x_3 = x_2 - ky$$

and

$$e = x_3 - z \tag{11}$$

Eq. (10) can be rewritten as

$$\dot{X} = A_1 X + F_1 \ddot{\theta}_T + D_1 v \tag{12}$$

where X is the state vector of the overall system with components:

$$X = \begin{bmatrix} y \\ x_3 \\ e \end{bmatrix} = \begin{bmatrix} y \\ x_2 - ky \\ x_3 - z \end{bmatrix}$$

and A_1, F_1, and D_1 are matrices defined as follows:

$$A_1 = \begin{bmatrix} a_{11} + a_{12}k - b_1(\gamma_1 + k\gamma_2) & a_{12} - b_1\gamma_2 & b_1\gamma_2 \\ (a_{22}-ka_{12})k+a_{21}-ka_{11} & a_{22}-ka_{12}-(b_2-kb_1)\gamma_2 & (b_2-kb_1)\gamma_2 \\ -(b_2-kb_1)(\gamma_1+k\gamma_2) & & \\ 0 & 0 & a_{22} - ka_{12} \end{bmatrix}$$

$$F_1 = \begin{bmatrix} f_1 \\ f_2 - kf_1 \\ f_2 - kf_1 \end{bmatrix}, \qquad D_1 = \begin{bmatrix} b_1 \\ b_2 - kb_1 \\ b_2 - kb_1 \end{bmatrix}$$

Once the structure of the model is designed, the next step is to determine the parameters associated with this model (i.e. k, γ_1, γ_2, α_1, α_2, α_3 in Eqs. (6), (7) and (9)). It is important to have a systematic method to determine these parameters for a given AAA system. A parameter identification program based on the least squares curve-fitting method and the Gauss Newton gradient algorithm has been developed by the authors. This program can easily determine the parameters of the gunner model by minimizing the difference between the model prediction of the tracking error and the corresponding empirical data. The following equations (mean equation and covariance equation) are used in the curve-fitting program. Letting the expectation value of X be $\bar{X}$, then we have,

$$\dot{\bar{X}} = A_1\bar{X} + F_1\ddot{\theta}_T \tag{13}$$

and the covariance matrix of X (t) is $P(t) = E[(X(t) - \bar{X}(t))(X(t)-\bar{X}(t))^T]$; then it can be shown in reference 11 that the covariance matrix is governed by

$$\dot{P} = A_1P + PA_1^T + D_1\, q(t)\, D_1^T \tag{14}$$

Equations (13) and (14) are used in the paremeter identification program to fit the empirical data obtained from the manned AAA simulation experiments conducted at the Aerospace Medical Research Laboratory, Wright-Patterson AFB, Ohio. The detail of the identification program and the curve-fitting procedure can be found in reference 10. The results

of curve-fitting parameter identification program are shown in the following table:

	k	γ_1	γ_2	α_1	α_2	α_3
Azimuth Tracking	2.94	-2.87	-1.00	.0496	.0024	.103
Elevation Tracking	3.02	-3.01	-1.00	.0032	.00047	.259

SIMULATION RESULTS AND DISCUSSION

The numerical values of the parameters of this gunner model were determined in the previous section with respect to the gunsight dynamic system (Eq. (2)) and a specific target trajectory. The gunner model is now ready to be used for computer simulation. A computer simulation program of the AAA system with this model representing the gunner response was developed. The input to this program is the target motion trajectory. The outputs are the model predictions of the ensemble mean and standard deviation of the tracking error. A typical result is plotted in fig. 3 for a specific target trajectory. The solid line in fig. 3 denotes the

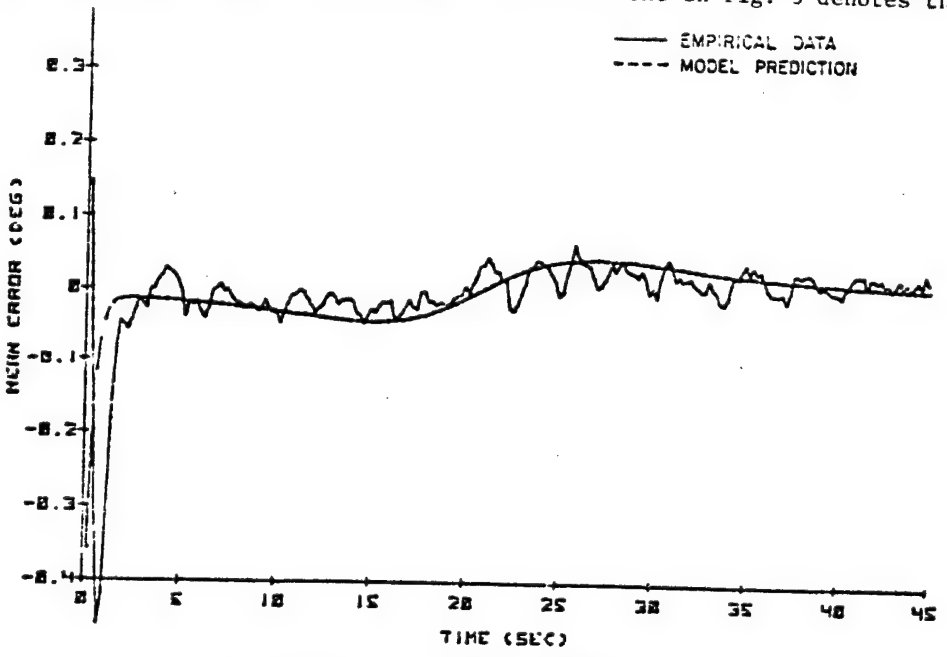

FIGURE 3. MEAN TRACKING ERROR

empirical data of the sample ensemble mean for azimuth tracking errors. The corresponding model prediction is denoted by the dotted line in fig 3. There is an excellent match between these two curves. Similar comparison between model predictions and empirical data for several other flyby and maneuvering target trajectories can be found in reference 10. All the simulation results show that this gunner model with the same parameter values can predict accurately the tracking errors for various target trajectories with similar frequency band widths. Therefore, it is a predictive model. The values of the model paremeters depends on the gun-sight dynamic system. Furthermore, this model is adaptive with respect to the target motion and this adaptive property is considered in the structure of the covariance function (Eq. (9)) of the remnant element.

A comparison of the model prediction accuracy between this model and the optimal control model in reference 7 has been done for several target trajectories. All the results show that both models give accurate predictions of tracking errors. A typical result is shown in fig. 4 for a flyby trajectory. It is obvious that the gunner model developed in

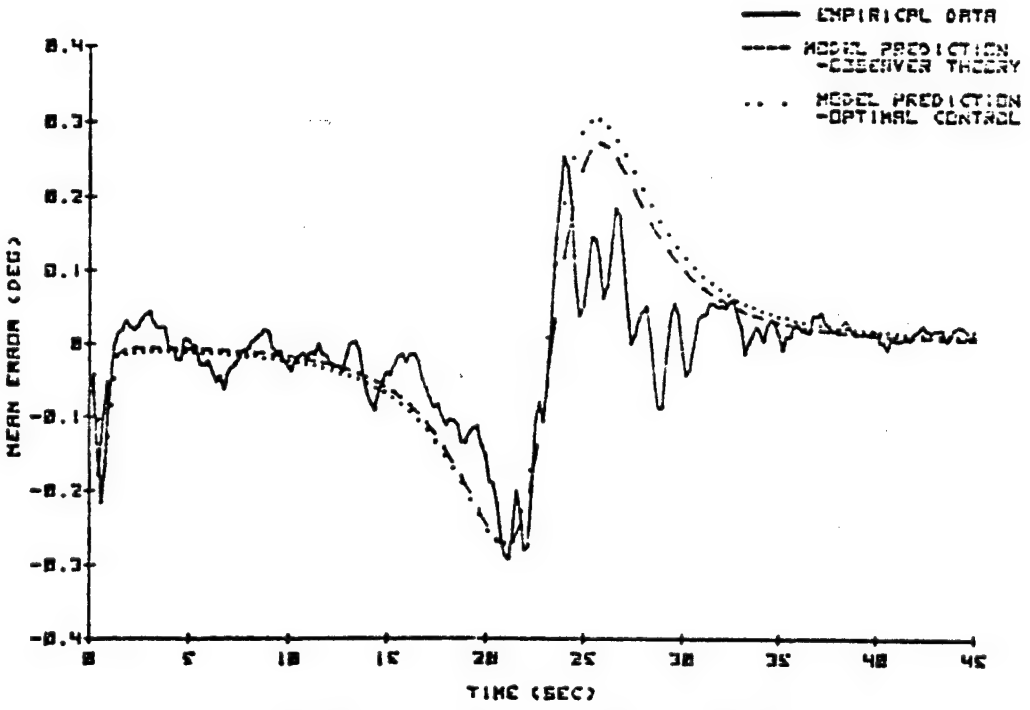

FIGURE 4. MEAN TRACKING ERROR
AZIMUTH

this paper can predict the tracking errors as accurately as those obtained by the optimal control model. However the computer execution time of simulating the AAA gun system using the gunner model is less than 15% of that by the optimal control model. It is a primary advantage of a model with simple structure. It can be concluded that the gunner model based on observer theory is very useful in the analysis of the performance of the AAA gun system.

CONCLUSION

The Luenberger observer theory has been applied to design an antiaircraft gunner model which is composed of a reduced-order observer, a state variable feedback controller and a remnant element. The highlights of this model are simple in the structure and accurate in the model prediction of tracking errors. The key design requirement is to make the model structure simple so that it can shorten computer simulation time. It has also been shown in figures 3 and 4 that this model can predict the tracking errors accurately. In addition, a parameter identification program based on the least squares curve-fitting method and the Gauss Newton algorithm has been used to systematically determine the numerical values of the model parameters. This gunner model has been used to study the AAA effectiveness of several air defense weapon systems at the Aerospace Medical Research Laboratory, Wright-Patterson AFB. All the results show that it is an accurate and efficient antiaircraft gunner model.

REFERENCES

1. J. Severson and T. McMurchie, "Antiaircraft Artillery Simulation Computer Program - AFATL Program P001 - Vol I, User Manual", Developed by Air Force Armament Laboratory, Eglin AFB, Florida; Published under the auspices of the Joint Aircraft Attrition Program, Advanced Planning Group.

2. D. G. Luenberger, "Observing The State Of A Linear System", IEEE Transactions On Military Electronics, Vol. MIL-8, pp. 74-80, April 1964.

3. D. G. Luenberger, "Observers For Multivariable Systems," IEEE Transactions on Automatic Control, Vol. AC-11, pp. 190-197, April, 1966.

4. D. G. Luenberger, "An Introduction To Observers", IEEE Transactions On Automatic Control, Vol. AC-16, pp. 596-602, December 1971.

5. A. P. Sage and J. L. Melsa, System Identification, New York, Academic Press, 1971.

6. P. Eykhoff, System Identification. New York: John Wiley & Sons, 1974, p. 161.

7. D. L. Kleinman, S. Baron, and W. H. Levison, "A Control Theoretic Approach To Manned-Vehicle Systems Analysis", IEEE Transactions on Automatic Control, Vol. AC-16, No. 6, December 1971, pp. 824-832.

8. D. L. Kleinman and T. R. Perkins, "Modeling Human Performance in a Time-Varying Anti-Aircraft Tracking Loop", IEEE Trans. AC, Vol. AC19, No. 4, Aug. 1974.

9. D. L. Kleinman and B. Glass, "Modeling AAA Tracking Data Using The Optimal Control Model", 13th Annual Conference on Manual Control, MIT, June 1977.

10. R. S. Kou and B. C. Glass, "Development of Observer Model for AAA Tracker Response", Systems Research Laboratories, Inc., Report No. 6872-4. December 1977.

11. J. S. Meditch, Stochastic Optimal Linear Estimation and Control. New York: McGraw-Hill Book Company, 1969. P. 258.

MODELING THE HUMAN AS A CONTROLLER IN A MULTITASK ENVIRONMENT*

T. Govindaraj and William B. House

Department of Mechanical and Industrial Engineering
Coordinated Science Laboratory
University of Illinois
Urbana, Illinois

SUMMARY

Modeling the human as a controller of slowly responding systems with preview is considered. Along with control tasks, discrete non-control tasks occur at irregular intervals. In multitask situations such as these, it has been observed that humans tend to apply piecewise constant controls. It is believed that the magnitude of controls and the durations for which they remain constant are dependent directly on the system bandwidth, preview distance, complexity of the trajectory to be followed, and nature of the non-control tasks. A simple heuristic model of human control behavior in this situation is presented. The results of a simulation study, whose purpose was determination of the sensitivity of the model to its parameters, are discussed.

INTRODUCTION

Although successful operation of an airliner is now possible from take-off to touchdown with minimum involvement of the human pilot [1] he must still perform various routine checks in the course of a normal flight. In addition, even when flying on autopilot, constant monitoring of various instruments is necessary to detect any out of tolerance signals and abnormal occurences of any events. Further, malfunctions or changes in atmospheric conditions, for example, might require that the pilot take over control and make course changes that are different from the preplanned trajectory. Thus, despite advances in automation, human control of aircraft is certainly still of interest.

When the human is controlling a plant, it has been observed that the controls applied are not always continuous. Continuous controls are necessary and are observed when the time constants involved are rather small and the deviations from some reference trajectory must be kept within some close tolerance. But when the time constants are relatively large, it is unnecessary and also difficult to apply the right amount of continuous control. For slowly responding processes it is often sufficient and desirable to apply step-like controls intermittently. This gives an opportunity to observe the actual behavior of the system, compare it with the

* This research was supported by the National Aeronautics and Space Administration under NASA-Ames Grant NSG-2119.

predicted behavior, and take corrective action. This usually prevails in a tracking situation where a certain length of the future command trajectory is available, along with the present required position. Further, applying the step-like controls also frees the human to engage in non-control tasks. In fact, this kind of behavior is common in process control situations and also has been observed in simulations of a flight management situation [2], [3].

When preview of the command trajectory for a certain distance into the future is available, it is likely that the human would apply step-like controls so as to minimize the future trajectory deviations rather than instantaneous deviations. A model which appears reasonable is one which updates the expected deviations of the cost over the length of the previewed trajectory and uses this information along with the knowledge that it "costs" to change control values. The cost to change control reflects the fact that non-control tasks must be attended to, though they may not be of primary importance. The "cost" is thus due to the feeling that the non-control tasks would "suffer" if attention is focused away from them and on the primary task alone. This cost may manifest itself as a tolerance threshold for error below which no action is taken. A measure for the cost of not attending to the subsystem tasks is available as a function of various probabilities and costs for delay of subsystem tasks [4].

BACKGROUND

Of the available models for manual control, the optimal control model would appear to be a suitable candidate. However, this model assumes that control remains non-zero at all times whereas in an intermittent control situation, control is zero for a significant portion of the time. Hence the mean fraction of time devoted solely to control, corresponding to non-zero control intervals, cannot be calculated with the optimal control model. For a given fraction of attention, the conventional optimal control model predicts only RMS errors and RMS control actions. While recent versions of the model do yield a measure of attention that should optimally be used for monitoring subsystems that dynamically relate to the control task, subsystem tasks that only remotely relate to the aircraft's dynamic response cannot be considered. Further, in multitask situations the optimal control model's performance criterion, which minimizes mean squared deviations, may not be appropriate. Finally, these approaches do not yield any predictions of the split of attention between control and non-control tasks or about the probability that the human is involved in the control of a continuous system at any particular instant.

The human in multitask situations has been modeled by Walden and Rouse [3] as a 'server' in a queue where 'customers' are the control and non-control tasks. The customers are assumed to arrive for service with exponentially distributed inter-arrival times (Poisson arrivals.) Service times are Erlang-k distributed. Some customers have a higher priority over others (e.g., control tasks over non-control tasks.) There are a total of N customers in the population (total number of possible tasks the human may be

called upon to attend), and N spaces are available in the queue (i.e., at worst all the N systems may require service simultaneously.) This situation can be modeled as a ($M/E_k/1$:PRP/N/N) queue. (See references [5] or [6] for details about the notation.) The queueing model predicts the fraction of time spent in each type of task (i.e., server utilization). The emphasis in this model is on the subsystem task performance. The control task is modeled in the sense that performing it consumes time. However, measures characterizing control performance (i.e., RMS errors) are not available.

AN INITIAL MODEL

Some success has been achieved using a heuristic model to describe control of an aircraft (with simplified dynamics) in a horizontal plane. Initial computer simulations indicate that this could be a fruitful approach. A piece-wise straight line map was created using uniformly distributed random variables for the length of straight line segments. The magnitudes for angle of turn between segments were chosen from nine values ($10°$-$90°$) with equal probability. The direction was chosen randomly. This type of map was designed because of the flexibility in determining the parameters. It is a simple matter to change the probability distributions of various parameters of the path, so that different conditions could be easily tested. It was assumed that the aircraft would be moving forward with constant speed. A point moved along the map corresponding to the desired aircraft position. A distance equivalent to two time constants ahead of the desired position on the map was shown as preview. Only lateral motion was considered. Control in the horizontal plane was achieved through use of the aileron to change the bank angle. The dynamics are shown in Figure 1.

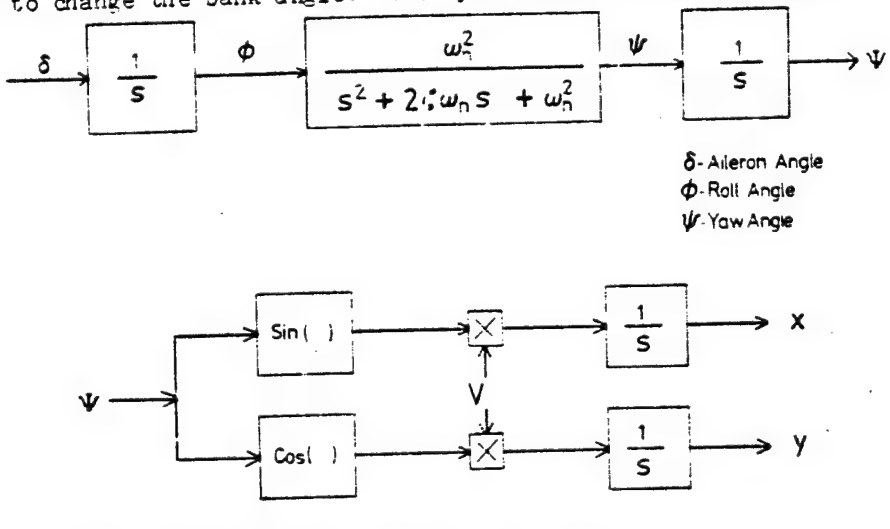

Fig 1 Simplified Lateral Dynamics

The deviation from the desired position was constantly monitored. A perfect internal model of the aircraft was assumed. At every time instant, the model calculated the future positions for the entire preview length assuming that the roll angle would be zero. At any point, the error was calculated as the deviation from the commanded position, instead of the perpendicular distance to the map

It appears reasonable to expect that the importance given by the human operator to deviations from the desired trajectory will vary along the length of the trajectory. Deviations at the current time cannot be corrected or changed significantly due to the slow response of the system. Also, the expected deviations near the end of the previewed command trajectory need not be considered immediately, since enough time will be available in the future to correct these. Further, any changes "beyond the horizon" that would come into view soon can reasonably be ignored. Accordingly, the human might weight the mid-portion of the previewed command more than either end. So the weighting function for errors would increase to a maximum (from zero), about one time constant from the current position, and decrease again to a near zero value at the end of the trajectory.

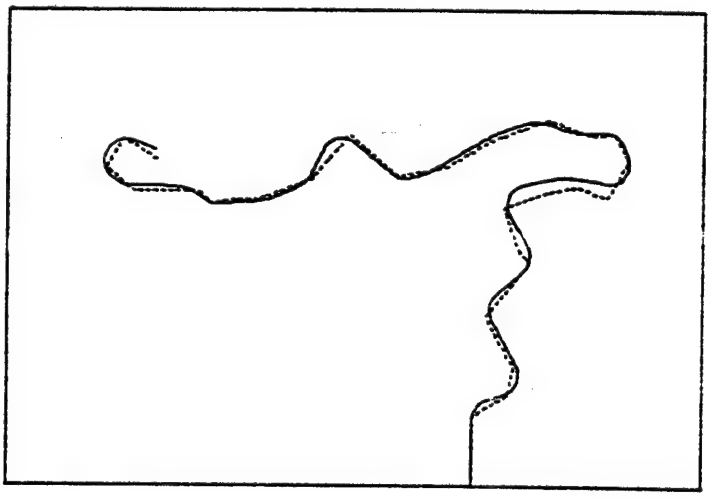

Fig 2 Simulation Results : Heuristic Model

Weighted error is squared and summed over the preview length. If this predicted error function exceeds a certain threshold, 'aileron' is held at a maximum value until maximum bank angle is reached. If the error is within the threshold, the bank angle is made zero. Constant weights on errors were used for the simulation. The results are shown in Figures 2 and 3 and appear reasonable. The time intervals corresponding to non-zero

aileron action give a direct measure of fraction of time required for control which is proposed as a correlate of workload. Although the human must continuously monitor for cumulative error, workload due to this is assumed negligible compared to the workload involved in control where he must watch the effect of his actions more carefully.

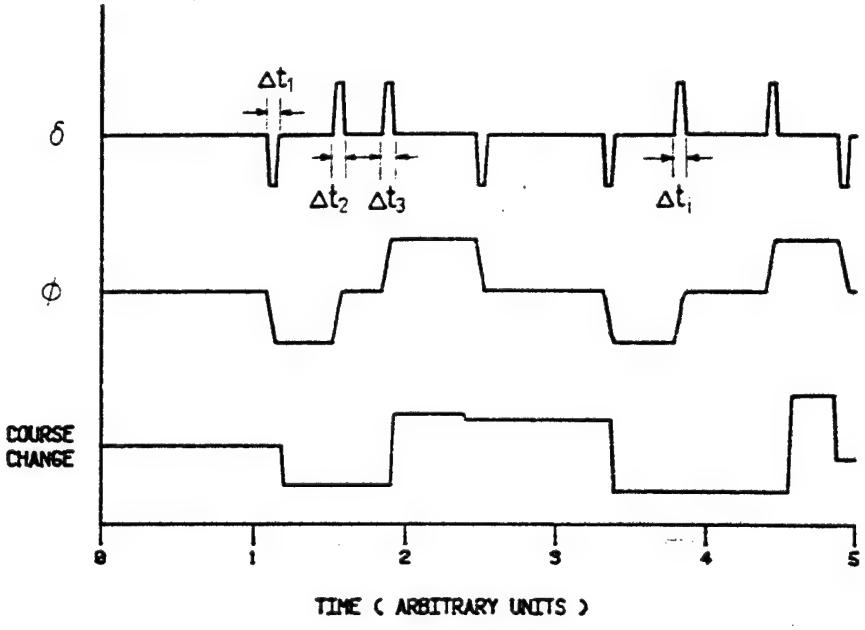

Fig.3 Control and Roll Angle History for a Given Course Change

Simulation experiments were conducted using a fractional factorial design to find out the sensitive/relevant parameters. A resolution VI design was used so that no main effect or two factor interaction is confounded with any other main effect, two factor interaction, or three factor interactions. The following parameters were assumed to affect performance:

1. Dynamics (τ of the process),	τ = 1.5
2 Average arrival rate of turns,	$1/\mu = 3\tau, 6\tau$
3 Standard deviation of course changes	σ = 10°, 30°
4. Amount of preview	$T_p = 2\tau, 4\tau$
5. Weighting function,	Rect. Triang.
6 Threshold on cumulative weighted error.	Low High

RMS errors and the fraction of time spent on control were used as performance measures. A constant function (rectangular) and a triangular function were used for weighting on errors. For other parameters, two extreme values were chosen, to obtain a total of 32 different conditions. Exponentially

distributed segment lengths and normally distributed angles of turn were used for the map. For each condition, two replications were run. The results are shown in Tables I and II.

Table I

Analysis for RMS Error

Factor	Effect	Sum of Squares	DOF	F Ratio	
1	4.433	314.409	1	131.037	P < 0.001
2	-0.671	7.206	1	3.003	
3	1.477	34.887	1	14.540	P < 0.001
4	4.087	267.247	1	111.381	P < 0.001
5	-1.397	31.219	1	13.011	P < 0.001
6	0.622	6.188	1	2.579	
12	-0.268	1.145	1	0.477	
13	1.108	19.653	1	8.191	P < 0.01
14	4.174	278.726	1	116.165	P < 0.001
15	-0.386	12.557	1	5.233	P < 0.05
16	-0.250	1.004	1	0.418	
23	-0.288	1.325	1	0.552	
24	0.049	0.038	1	0.016	
25	0.335	1.794	1	0.748	
26	1.315	27.676	1	11.535	P < 0.005
34	0.563	2.350	1	0.979	
35	1.295	26.822	1	11.179	P < 0.005
36	0.197	0.619	1	0.258	
45	-0.914	13.364	1	5.570	P < 0.025
46	0.256	1.052	1	0.443	
56	0.124	0.246	1	0.102	
Average Error	4.192				
Total		100.774	42		
		1150.313	63		

(1-Period, 2-Segment Length, 3-Angle of Turn,
4-Preview Length, 5-Weight, 6-Threshold)

Table II

Analysis for Fraction of Attention

Factor	Effect	Sum of Squares	DOF	F Ratio	
1	0·231	0.856	1	33·221	P < 0.001
2	-0.057	0·051	1	1.999	
3	0.017	0.005	1	0.181	
4	0.144	0.331	1	12.837	P < 0.001
5	-0.117	0.218	1	8.468	P < 0.01
6	-0.139	0·311	1	12.084	P < 0.005
12	0·004	0.000	1	0.011	
13	-0.018	0.005	1	0.206	
14	0.269	1.158	1	44.963	P < 0.001
15	0.000	0·000	1	0.000	
16	0.004	0.000	1	0.006	
23	0.067	0·072	1	2.783	
24	0.030	0.014	1	0·541	
25	0·005	0·000	1	0.017	
26	0 060	0.058	1	2·234	
34	-0.074	0·087	1	3·359	
35	0.047	0.035	1	1.374	
36	-0.043	0.030	1	1.155	
45	0·005	0 000	1	0·014	
46	0.048	0.037	1	1·435	
56	0.090	0.129	1	5.011	P < 0·05
Average	0·256				
Error		1.082	42		
Total		4·479	63		

(1-Period, 2-Segment Length, 3-Angle of Turn,
4-Preview Length 5-Weight. 6-Threshold)

It can be seen that period, preview length and their interaction have the largest effect on performance. Different weighting functions also affect performance. In addition, RMS error is affected by the magnitude of turns and various interactions. Fraction of time spent on control is affected by the threshold. Higher threshold values reduce this fraction.

Though the interaction of mean segment length and threshold affects the RMS error, segment length alone does not affect either of the performance measures. This could be due to the constant forward speed in all cases, whereas the mean segment length is scaled by the time constant. For slower process, for a given threshold any error that may result takes a longer time to reduce to zero. Since the 'vehicle' would stay away from the

trajectory for a longer time, higher RMS error results.

Relatively high workload as well as higher RMS error is observed for the slower process with longer preview. Once the threshold is exceeded, the model applies an appropriate amount of control. However, due to the slow response, the magnitude of error remains near the threshold for some time. But, the error could change sign as new points come into view, and might call for a different control action. Due to longer preview the error changes sign quite frequently resulting in increased control action. This again results in the error remaining near the threshold. Thus, behavior similar to a limit cycle results which, interestingly, has been observed when naive subjects control slow processes. This could possibly be avoided by having one threshold above which control is actuated, and a lower threshold below which control is made zero.

CONCLUSIONS

The next phase of this work will involve development of an experimental situation for use with human subjects. Non-control tasks will be included to simulate a multitask environment. Simple arithmetic tasks may be used. Multiplication tasks with keyboard entry of results are a possibility. Complexity and the rate at which these are presented could be varied, so control task error criterion (i.e. the threshold) may perhaps be manipulated.

The possibility of developing analytical models using the min-max approach [7],[8],[9],[10], satisfaction approach [11], and fuzzy sets [12] will be pursued. An attempt will be made to cast our problem in a form suitable for analysis using the above methods, with possible modifications where necessary. Especially interesting in this regard is the satisfaction approach. It may be possible to formulate our problem in this framework, and obtain a heuristic-based solution with the addition of a few conditions related to the problem structure. With these models available, a more realistic experiment will be developed using the General Aviation Trainer II (GAT II). Along with the control task, the non-control tasks will be made more realistic.

In summary, a simple heuristic model for the control task was presented. Simulation results for a set of conditions describing various trajectories were given. The controller part assumes perfect internal model. Only the threshold must be determined to yield intermittent control. The period and the preview length were found to be the most important parameters affecting performance. This will form the basis for proposed experiments with humans. The model will be refined to take into account the results of these experiments and then, will be used along with a queueing model for non-control tasks, to model the overall multitask situation.

REFERENCES

1. Ropelewski, R. R.: "Air Inter's A-300 Autolandings Routine", Aviation Week and Space Technology, April 24,1978, pp.45-57.

2. Kok, J. J.; and van Wijk, R. A.: "A Model of the Human Supervisor", Proceedings of the Thirteenth Annual Conference on Manual Control, MIT, June 15-17, 1977.

3. Walden, R. S.; Rouse, W. B.: "A Queueing Model of Pilot Decision Making in a Multi-Task Flight Management Situation", Proceedings of the Thirteenth Annual Conference on Manual Control, MIT, June 15-17, 1977.

4 Rouse W. B.; and Greenstein, J. S.: "A Model of Human Decision Making in Multi-Task Situations: Implications for Computer Aiding", presented at the International Conference on Cybernetics and Society, Washington, D.C., 1976.

5. Allen, A. O.: "Elements of Queueing Theory for Systems Design", IBM Systems Journal, vol.14 no. 2. 1975, pp 161-187.

6. White, J. A.; Schmitt, J. W.; and Bennet, G. K.: ANALYSIS OF QUEUEING SYSTEMS, New York: Academic, 1975.

7. Witsenhausen, H. S.: "A Minimax Control Problem for Sampled Linear Systems", IEEE Trans. on Automatic Control. vol. AC-13, no. 1 February 1968.

8. Delfour, M. C.; and Mitter, S. K.: "Reachability of Perturbed Systems and Min Sup Problems", SIAM J. Control, vol. 7, no. 4, November 1969.

9. Bertsekas, D. P.; and Rhodes I. B.: "On the Minimax Reachability of Target Sets and Target Tubes", Automatica, vol. 7, 1971, pp. 233-247.

10. Milanese M.; and Negro, A.: "Min-max Control of Systems Approximated by Simple Models: L_1-Type Cost Functionals", Journal of Optimization Theory and Applications. vol 16. nos. 5/6, 1975, pp. 519-537.

11 Mesarovic M. D.: "Satisfaction Approach to the Synthesis and Control of Systems", Proceedings of the Third Allerton Conference, 1965, pp. 930-942.

12 King P. J.; and Mamdani, E. H.: "The Application of Fuzzy Control Systems to Industrial Processes", Automatica, vol. 13, 1977, pp 235-242.

N79-15596

THE INTERNAL MODEL: A STUDY OF THE RELATIVE CONTRIBUTION OF PROPRIOCEPTION AND VISUAL INFORMATION TO FAILURE DETECTION IN DYNAMIC SYSTEMS*

By Colin Kessel and Christopher D. Wickens

Department of Psychology, University of Illinois

SUMMARY

The development of the internal model as it pertains to the detection of step changes in the order of control dynamics is investigated for two modes of participation: whether the subjects are actively controlling those dynamics or are monitoring an autopilot controlling them. A transfer of training design was used to evaluate the relative contribution of proprioception and visual information to the overall accuracy of the internal model. Sixteen subjects either tracked or monitored the system dynamics as a 2-dimensional pursuit display under single task conditions and concurrently with a "sub-critical" tracking task at two difficulty levels. Detection performance was faster and more accurate in the manual as opposed to the autopilot mode. The concurrent tracking task produced a decrement in detection performance for all conditions though this was more marked for the manual mode. The development of an internal model in the manual mode transferred positively to the automatic mode producing enhanced detection performance. There was no transfer from the internal model developed in the automatic mode to the manual mode.

INTRODUCTION

Over the past few years there has been a great deal of research directed at the problem of determining the differences between operators and monitors of dynamic systems (References 1-7). While the conclusions reached by these authors do not always coincide, there is a general consensus that a greater understanding of the different processes operating in the two modes of participation is necessary for the successful integration of automated systems in the workplace.

We have provided a detailed theoretical analysis of the processes involved in the two modes of participation (Reference 7). Briefly, this analysis has argued that one way in which the differences between modes of participation can be studied is by determining the relative sensitivity of operators versus monitors in a failure detection task.

*This research was funded by the Life Sciences Program, Air Force Office of Scientific Research, Contract Number F44620-76-C-0009. Dr. Alfred Fregly was the scientific monitor of the contract.

Three attributes were identified that would seemingly facilitate failure detection in the contro'ling mode: (i) a smaller variability of the internal model of the system; (ii) the options of testing hypotheses about the nature of the dynamics by introducing signals into the system; and (iii) a greater number of information channels available upon which to base failure detection decisions. It was recognised however, that this latter advantage may be mitigated to the extent that: a) adaptation takes place reducing the strength of visual error information and, b) proprioceptive sensitivity is less than visual.

In comparison the monitoring mode was also characterised by two attributes that could facilitate detections: a greater "strength" of the visual signal (if adaptation by the autopilot does not take place) and a lower level of operator workload.

The study conducted (Reference 7) to test the above theoretical analysis found that detection performance in the manual mode was faster and only slightly less accurate than the autopilot mode. Furthermore the observed manual superiority was attributed to the additional proprioceptive information resulting from operator control adaptation to the system change. It is possible that some contribution to manual mode superiority in our prior study resulted from the greater internal model consistency in that mode. However this hypothesis was assumed to be doubtful because a within subjects design was employed, so that the same subjects participated in both automatic and manual conditions. Thus the internal model developed in manual conditions would presumably be available to facilitate detection in the automatic conditions as well.

In order to generate a greater distinction between the internal model employed in the two modes, the present study employed a between subject design using a transfer of training technique. This procedure enables an examination of the development of internal models, in the two modes of participation, and subsequently measures their impact upon transfer to the other mode.

It was hypothesized that this technique would increase the differential performance in detection between the two modes of participation while at the same time demonstrating that the internal model developed in the manual mode can subsequently be utilized to facilitate automatic mode failure detection performance.

METHOD

Subjects:

The subjects were 18 right-handed male university students. Subjects were paid a base rate of $2.50 per hour but could increase their average pay by maintaining a high level of detection performance.

Apparatus:

The basic experimental equipment included a 7.5 x 10 cm Hewlett Packard Model 1300 CRT display, a spring-centered, dual-axis tracking hand control with an index-finger trigger operated with the right hand, and a spring loaded finger controller operated with the left. A Raytheon 704 16-bit digital computer with 24k memory and A/D, D/A interfacing was used both to generate inputs to the tracking display and to process responses of the subject. The subject was seated on a chair with two arm rests, one for the tracking hand controller and one for the side-task finger controller. The subject's eyes were approximately 112 centimeters from the CRT display so that the display subtended a visual angle of 1.5°.

Tracking tasks. The primary pursuit-tracking task required the subject to match the position of a cursor with that of a target which followed a semi-predictable two-dimensional path across the display. The target's path was determined by the summation of two non-harmonically related sinusoids (.05 and .08 Hz) along each axis with a phase offset between the axes. The position of the following cursor was controlled jointly by the subject's control response and by a band-limited forcing function with a cutoff frequency of .32 Hz for both axes. Thus the two inputs to the system were well differentiated in terms of predictability, bandwidth, and locus of effect (target vs. cursor). The control dynamics of the tracking task were of the form $Y_c = \frac{1-\alpha}{s} + \frac{\alpha}{s^2}$ for each axis, where α was the variable parameter used to introduce changes in the system dynamics. These changes, or simulated failures, were introduced by step changes in the acceleration constant α from a normal value of .3, a mixed velocity and acceleration system, to $\alpha = .9$, a system that approximates pure second order dynamics that requires the operator to generate considerable lead in order to maintain stable performance.

As the loading task, the Critical Task (Reference 8) was employed. This was displayed horizontally in the center of the screen and required the subject to apply force to the finger control in a left-right direction to maintain the unstable error cursor centered on the display. The value of the instability constant λ in the dynamics $Y_c = \frac{k\lambda}{s - \lambda}$ was set at a constant subcritical value. Two values ($\lambda = 0.5$ and $\lambda = 1.0$) were employed on different dual task trials.

Experimental Design and Task:

Three groups were used in the transfer of training design (see Figure 1). Group one transferred from manual (MA_I) on session one to automatic (AU_{II}) on session two; group two transferred from automatic (AU_I) to manual (MA_{II}) while group three was the control group for the automatic condition and monitored in the automatic mode in both sessions ($AU_{I(C)}$ and $AU_{II(C)}$). The control group for the manual group (MA_{II}) was MA_I. The various group comparisons are represented in Figure 1 by arrows and will be referred to at greater length in the results section.

Each group participated in six consecutive days of data collection. These were divided into two sessions; 3 days in each session with each session comprising 1 training day and two experimental days. Subjects in group one for example participated in 3 manual (MA_I) sessions and then transferred to 3 automatic (AU_{II}) sessions.

In the manual (MA) condition the subject performed the tracking manually while in the autopilot (AU) condition, his role in the control loop was replaced by simulated autopilot control dynamics consisting of pure gain, effective time delay, and a small added remnant. Each trial, MA or AU, lasted 150 seconds.

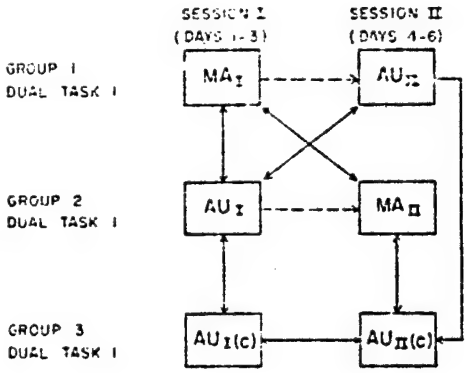

Figure 1: Experimental design and group comparisons

Training Day: The training day was designed to give the subject maximum experience and practice with the system. Subjects therefore received extensive practice tracking (or monitoring) with both prefailure and postfailure dynamics. Following this, they observed and then detected the step changes in dynamics. Practice with the critical side task was also included.

The presentation of the failure was generated by an algorithm that assured random intervals between presentations and allowed the subject sufficient time to establish baseline tracking performance before the onset of the next change. Task logic also ensured that changes would only be introduced when system error was below a criterion value. In the absence of this precaution, changes would sometimes introduce obvious "jumps" in cursor position.

During the detection trials, the detection decision was recorded by pressing the trigger on the control stick. This response presented a "T" on the screen and returned the system to normal operating conditions of the prefailure dynamics. If the subject failed to detect the change, the system returned to normal after six seconds via a 4 second ramp. On the basis of pretest data, it was assumed that six seconds was the interval within which overt responses would correspond to detected failures and not false alarms. The subjects were told to detect as many changes as possible as quickly as possible.

Experimental Days: The training day was followed by two consecutive experimental days. After four refresher trials in the AU or MA modes (depending upon the condition) with the side task, and a number of demonstrated failures, the subjects performed 15 experimental trials: 5 single task, tracking (or monitoring) only; 5 tracking with the easy critical task ($\lambda = 0.5$); and 5 tracking with the difficult critical task ($\lambda = 1.0$). The

order of presentation was randomized. Each trial contained an average of 5 failures per trial with a range of 4 to 6.

The subject was instructed to "do the side task as efficiently and accurately as possible," and told to maintain that task at a standard level of performance. After each trial the subject received feedback about both his side task and detection performance. The instructions, feedback and payoff schedule, therefore, clearly defined the side task as the loading task while allowing the tracking and detection tasks to fluctuate in response to covert changes in available attentional resources (Reference 9).

ANALYSIS

Detection performance was assessed in terms of the accuracy and latency of responses. In computing the accuracy measure, signal detection theory analysis based upon the method of free response was employed (Reference 10). This technique accounts for the presence of hits and false alarms in the data; and the semi random occurance of failures within a trial. The area under the ROC curve (A[ROC]) was employed as the final accuracy measure (Reference 11). Further details of this analysis procedure may be found in Wickens and Kessel (Reference 7, 12).

The A(ROC) measure and the latency measure were then plotted in the form of a joint speed-accuracy measure depicted in Figure 2. "Good" performance is represented by points lying on the upper left, in the region of fast accurate response. Performance was quantified by projecting the point locus obtained onto the positive diagonal performance axis. The performance scale is computed as (10 times A[ROC] - LATENCY) and will be called the "derived performance score." This procedure produces a performance index that ranges from 0 for chance level of accuracy with a latency of 5" to 10.0 for perfect detection with 0 second reaction time. The units assigned to this performance index are somewhat arbitrary but are based on the observation that the overall variability (standard deviation) of the raw latency scores were found to be roughly 10 times the variability of the A(ROC) measure.

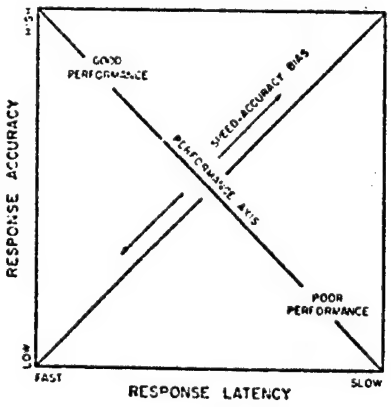

Figure 2: Speed-accuracy representation of detection performance

RESULTS

Averages and standard deviations were computed for the accuracy (A[ROC]), the latency and the derived performance measures following the rational and the procedures outlined in the preceding section.

The group averages for all three measures are presented graphically in Figures 3 and 4. Figure 3 represents the results for the single task condition while Figure 4 represents the dual task, workload condition collapsed over both levels of dual task difficulty (the rationale for this procedure is discussed below). The symbols in Figures 3 and 4 represent the group results in the speed-accuracy space, while the arrows and labels depict the derived performance scores for the various groups along the performance axis. In figures 5, 6, and 7 the experimental groups are plotted with the average derived performance score on the Y-axis.

The presentation of the results of the detection of failures will be divided into three sections. The first presents the results for each mode of participation, and represents a replication of the Wickens and Kessel (Reference 7) study with the between subjects design, the second examines the results of the loading task, while the third reports the results of the transfer of training experiment. Group differences were analyzed by means of a 3-way Analysis of Variance-ANOVA (groups x dual task x experimental days).

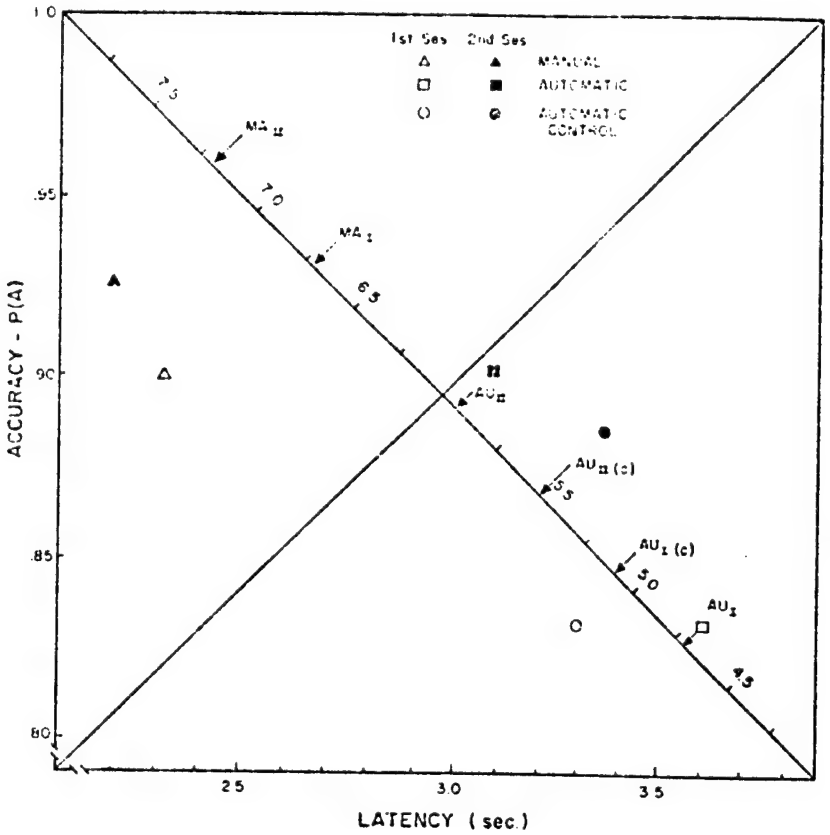

ORIGINAL PAGE IS OF POOR QUALITY

Figure 3: Effect of participatory mode and experimental condition on detection performance-Single Task

(a) Mode of Participation

The most pronounced effect in the experimental data is the consistent superiority of MA over AU detection. This statistically reliable effect is clearly evident in the derived performance score shown in Figures 5 and 6 and was tested by contrasting group AU_I with MA_I ($F_{1,10} = 18.4$ $p < .001$). Examination of Figures 3 and 4 reveals that the MA superiority is reflected in detection latency ($F_{1,10} = 13,66$, $p < .01$), as well as accuracy ($F_{1,10} = 15.55$, $p < .01$).

While these findings essentially replicate the Wickens and Kessel (Reference 7) study, it is important to note that the extent of MA superiority observed in the present results is greatly enhanced. In fact the magnitude of the MA-AU difference in the desired performance score is roughly five times its value obtained in the previous within-subject design. Contrasting the two studies, one finds that AU performance is unchanged, but MA performance in the present results is reliably superior to its level in the previous study ($t_9 = 2.18$, $p < .05$). These findings add strength to the argument

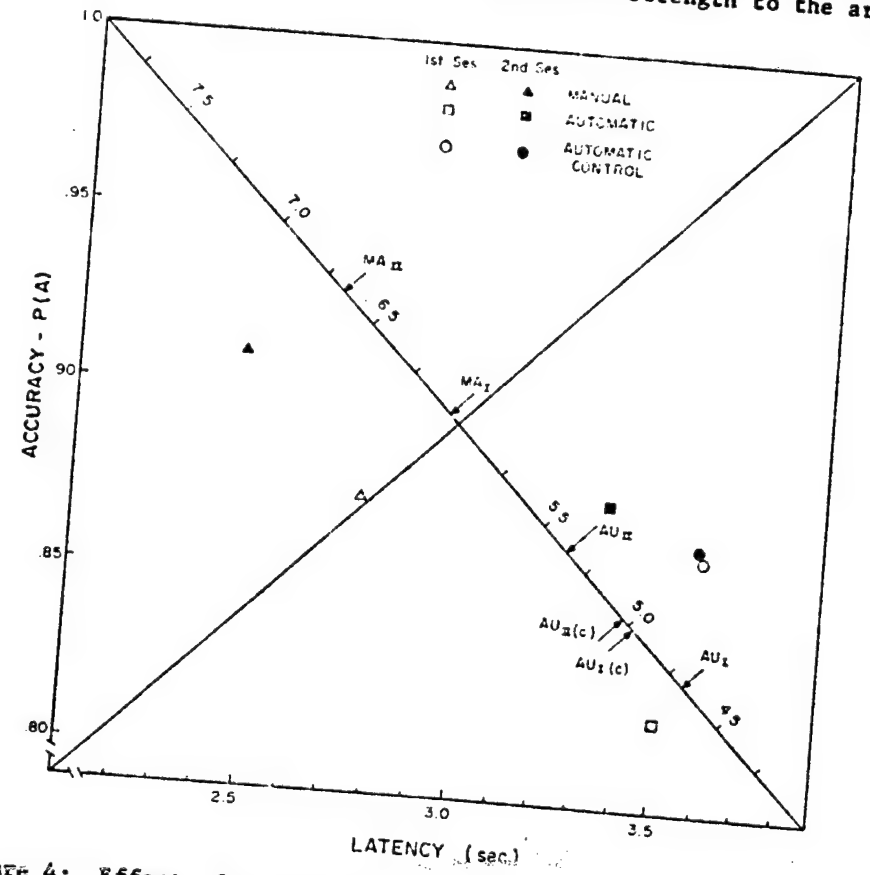

Figure 4: Effect of participatory mode and experimental condition on detection performance_Dual Task

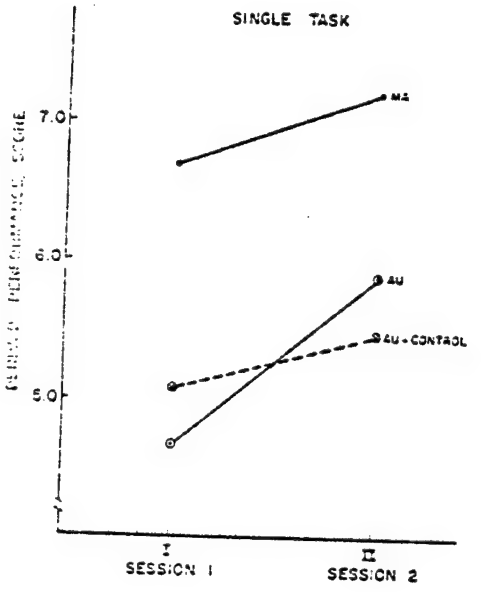

Figure 5

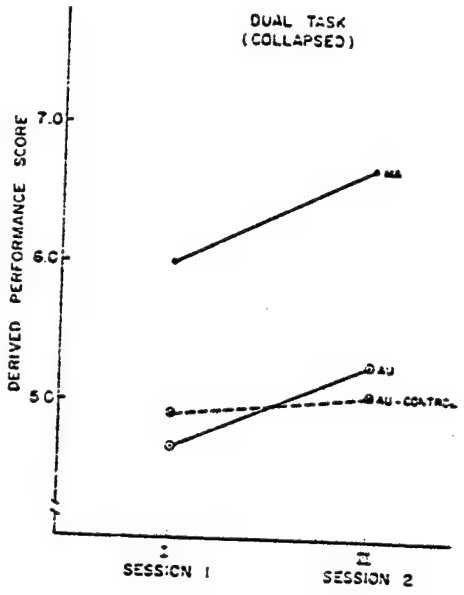

Figure 6

Detection performance as a function of experimental condition

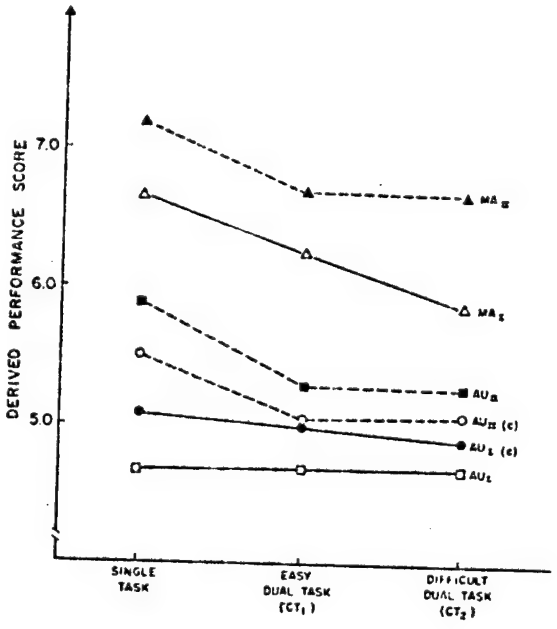

Figure 7: Effect of dual task on detection performance

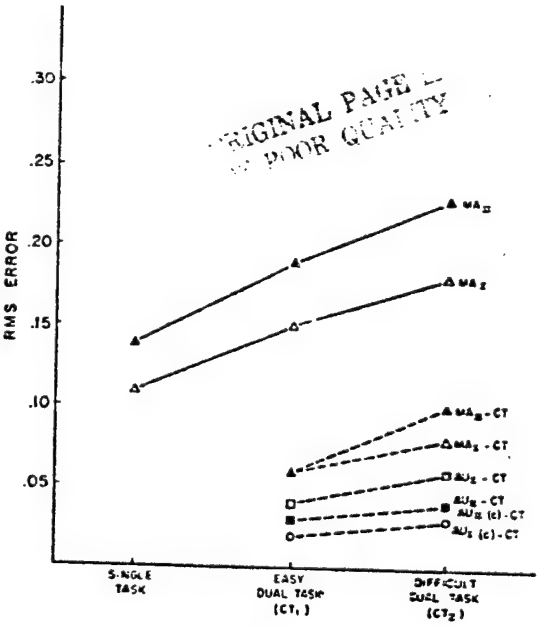

Figure 8: Effects of dual task on manual tracking and critical task performance

that internal models developed separately tend to be more consistent, less variable and more sensitive to system changes.

By comparing the single task performance in MA_{II} with AU_{II} (see Figures 3 and 5) it is possible to determine whether MA superiority is maintained after prior training in the other mode of participation. From Figures 3 and 5 we can see that while this difference has been reduced somewhat, the overall MA superiority remains intact. This MA_{II}-AU_{II} group difference is also statistically reliable ($F_{1,10} = 6.76$, $p < .05$).

(b) Critical Task

The impact of the critical tracking task may be evaluated both as it affected detection performance (Figure 7) and, in the MA mode, as it affects performance of the primary tracking task (Figure 8). From Figure 7, it is evident that the introduction of the CT produced a decrement in detection. As might be expected, the decrement in the MA mode was somewhat more pronounced. While there was no decrement for the AU_I groups there is a substantial decrement for the AU_{II} groups, equivalent to the decrement of both the MA groups. For both the MA_I-AU_I and the MA_{II}-AU_{II} analyses, task loading showed a statistically reliable effect ($F_{2,20} = 3.60$, $p < .05$; $F_{2,20} = 5.45$, $p < .025$ respectively). It should be noted however that the primary impact of this effect is localized in the introduction of the critical task, and not with the increase in its difficulty level, a point born out by further statistical analysis. (The near equivalence of the two dual task conditions was the justification for collapsing detection performance over the two conditions in further analysis.)

Figure 8 reveals that the critical task had a clear influence on MA tracking performance, both with its introduction, and with the increasing difficulty. Analysis performed on the MA_I and MA_{II} data alone[1] indicated that the effect was statistically reliable ($F_{2,20} = 45.97$, $p < .001$).

Finally, Figure 8 reveals slight, but consistent, decreases in critical tracking performance that occur as a result of increasing λ. These increases were found to be statistically reliable for all the groups. Since the subjects were all treating the critical task as a loading task it can be concluded that the increase in λ fact did serve to divert attentional resources from the primary tracking/detection process.

(c) Transfer of Training

Manual Mode. In determining the relative amount of transfer to the manual mode resulting from prior automatic training, the MA_{II} group is compared with its control group MA_I (Figure 1) which essentially had no prior experience in the failure detection task.

[1] Naturally AU "tracking" performance remains unaffected by critical task difficulty level.

From Figures 3 through 7 it can be seen that in general there is an overall MA_{II} superiority over MA_{I} for both single and dual task conditions. However the ANOVA failed to reveal these differences to be statistically reliable. Examination of the data on a day by day basis reveals that the overall MA_{I}-MA_{II} difference is due to large differences that exist on day 1 which appear to dissipate completely when the two groups are compared on day 2 performance. This finding can be seen as support for the basic hypothesis that exposure to prior AU tracking and the development of an internal model based on visual cues only, produces only a small and transient facilitation of subsequent development of the internal model based on MA tracking.

Automatic Mode. The degree of transfer resulting from prior MA training to the AU mode is reflected in the performance of subjects in condition AU_{II}, and the comparison of this performance with that of the control group ($AU_{I(C)}$-$AU_{II(C)}$). In Figures 5 and 6, it is evident that the latter group failed to benefit at all from prior AU training, an observation supported by the lack of statistical reliability of the main effect when $AU_{I(C)}$ and $AU_{II(C)}$ are compared. In marked contrast, Figures 5 and 6 suggest that the AU_{II} group in fact showed considerable benefit from their prior MA training when their performance is contrasted with that of the AU_{I} group. In Figure 5, the magnitude of this effect is seen to be considerably larger than the effect for the control group or for the MA_{I}-MA_{II} contrast discussed in the preceding section.

The statistical reliability of this improvement on the single task data was assessed by a groups (AU_{I} vs. AU_{II})x days (Day 1 vs. Day 2) 2 x 2 ANOVA.

Both main effects were statistically reliable. This indicates that (a) both groups improved with practice (over two days) in their respective AU conditions ($F_{1,10} = 14.77$, $p < .001$). (b) More crucially, from the viewpoint of the hypothesis under investigation, the AU_{II} group performed reliably better than did the AU_{I} group ($F_{1,10} = 5.19$, $p < .05$). It is of course possible to argue that this effect resulted from greater exposure to and familiarity with the overall experimental environment experienced by the AU_{II} group and not to transfer of the internal model. However this interpretation appears unlikely because the control group failed to show any such "generalized" transfer.

We can conclude that there is a transfer from MA to AU. The AU_{I}-AU_{II} differences are very large and statistically reliable and as such support the basic hypothesis that while there are different sets of cues operating, the MA condition produces an internal model of the system that can be utilized to advantage in subsequent automatic monitoring.

SUMMARY AND CONCLUSIONS

The major results can be summarized as follows:

1) Detection of step increases in system order when the operator remains in the control loop (MA mode) is considerably faster and more accurate than

when he is removed (AU mode). This finding is consistent with both the findings of Young (Reference 2) and of Wickens and Kessel (Reference 7).

2) The manual mode superiority was found to be more pronounced in this between subject design than the previous within subject study (Reference 7). This difference can be attributed to the fact that the subjects were allowed to develop separate internal models for either the manual or the automatic mode, thereby producing models that were always appropriate for the mode of participation employed.

What is interesting in contrasting the two studies is the fact that AU performance is virtually identical. The effect of the between-subjects manipulation instead seems to have been to produce a large improvement in MA detection.

This result suggests that in the previous experiment the AU internal model was developed unhindered by the concurrent development of the MA internal model while the reverse situation did not hold. It would appear that the development of the MA internal model in the previous experiment was somehow subject to interference from the AU model development, suggesting that subjects were paying attention to non-relevant, visual cues. It has been argued (Reference 7) that the sensitivity to proprioceptive information is reduced relative to visual information particularly when the two sources are available at the same time and are conveying conflicting information (References 13, 14, 15). In the AU mode the subjects have only visual cues as information while in the MA mode both visual and proprioceptive information is available. Thus in the previous study, during the development of the MA internal models there were times when these cues might be in conflict and subjects tended to fall back on the visual cues learned in the AU mode. This produced an over-emphasis on the visual cues and a subsequent degrading of the crucial proprioceptive information. The introduction of the between subject design forced subjects to develop separate internal models based upon the relevant cues available within each condition--a situation that has enhanced the MA-AU differences found in the previous experiment.

3) The overall MA superiority is evident in both single and dual task conditions. The effect of adding the Critical Task was to reduce the overall detection performance via a reduction in the accuracy of detections and an increase in response latencies. The impact of the second task was more marked for the MA condition than the AU condition. This result is consistent with the fact that the critical tracking task, placing heavy demands upon the subject's response mechanism, produced an increase in interference at the structural, motor level of performance in the MA mode that was not present in the AU mode of operation. Increasing the difficulty of the subcritical loading task appeared to have little effect on detection performance in either mode, although it did serve to disrupt tracking performance.

4) An analysis of the transfer of training experiment shows that there is very little transfer from the automatic mode to the manual mode. This fact adds further weight to the argument that the development of the internal model for the manual mode cannot utilize to advantage the internal model developed

for the automatic mode. The addition of the proprioceptive channels and the interactive describing function in the manual mode appears to require the development of a separate and unique internal model.

5) There does appear to be positive transfer from the manual mode to the automatic, a finding that supports the basic hypothesis outlined above that while there are different sets of cues operating, the MA mode produces an internal model of the system that can be utilized to advantage in subsequent automatic monitoring.

6) Finally, the successful transfer from manual to automatic and the lack of transfer from the automatic to the manual modes tends to add weight to the basic hypothesis outlined above. This hypothesis states that the internal models developed in different modes of participation are relatively independent and therefore care must be exercised in extrapolating expected results in one mode of participation from performance in the other.

REFERENCES

1. Vreuls, D., et al. Pilot Failure Detection Performance with Three Levels of Fault Warning Information. Bunker-Ramo Corp., Report No. SRDS-RD-68-9, 1968.

2. Young, L.R. On Adaptive Manual Control. IEEE Transactions on Man-Machine Systems, Vol. MMS-10, pp. 292-331, 1969.

3. Ephrath, A.R. Detection of System Failures in Multi-axes Tasks. Proceedings of the 11th Annual NASA-University Conference on Manual Control. NASA TMX, 1975, 62, 464.

4. Curry, R.E. and Ephrath, A.R. Monitoring and Control of Unreliable Systems. T.B. Sheridan and G. Johannsen, Eds., Monitoring Behavior and Supervisory Control, New York: Plenum Press, 1976.

5. Johannsen, G., Pfendler, C. and Stein, W. Human Performance and Workload in Simulated Landing-approaches with Autopilot-failures. In T.B. Sheridan and G. Johannsen, Eds., Monitoring Behavior and Supervisory Control, New York: Plenum Press, 1976.

6. Ephrath, A.R. and Curry, R.E. Detection by Pilots of System Failures During Instrument Landings. IEEE Transactions on Systems Man & Cybernetics. Vol. SMC-7, No. 12, pp. 841-848, 1977.

7. Wickens, C.D. and Kessel, C. The Effects of Participatory Mode and Task Workload on the Detection of Dynamic System Failures. 13th NASA Conference on Manual Control, NASA, TMX-73, 170, 1977.

8. Jex, R., McDonnell, J.D. and Phatak, A.V. A 'Critical" Tracking Task for Manual Control Research. IEEE Transactions on Human Factors in Electronics, Vol. HFE-7, pp. 138-144, 1966.

9. Wickens, C.D. In N. Moray, Ed., Mental Workload: Theory and Measurement. New York, Plenum Press, 1978, (in press).

10. Watson, C.S. and Nichols, T.L. Detectability of Auditory Signals Presented without Defined Observation Intervals. Journal of Acoustic Society of America, Vol. 59, pp. 655-668, 1976.

11. Green, D.M., and Swets, J.A. Signal Detection Theory and Psychophysics. New York: John Wiley and Sons, Inc., 1966.

12. Wickens, C.W. and Kessel, C. The Effects of Participatory Mode and Task Workload on the Detection of Dynamic System Failures. Institute of Aviation Tech. Report ARL-77-8/AFOSR-1977.

13. Posner, M.I. et al. Visual Dominance: An Information-processing Account of its Origins and Significance. Psychological Review, 1976, 83, No. 2, 157-171.

14. Klein, R.M. and Posner, M.I. Attention to Visual and Kinesthetic Components of Skills. Brain Research, Vol. 71, pp. 401-411, 1974.

15. Jordan, T.C. Characteristics of Visual and Proprioceptive Response Times in the Learning of a Motor Skill. Quarterly Journal of Experimental Psychology, Vol. 24, pp. 536-543, 1972.

SESSION C: NOVEL MODELING CONCEPTS

Chairman: R. Hess

A COMPARISON OF MOTOR SUBMODELS IN THE OPTIMAL CONTROL MODEL

by Roy E. Lancraft and David L. Kleinman

Department of Electrical Engineering & Computer Science
University of Connecticut
Storrs, Conn. 06268

ABSTRACT

Recent interest in the areas of modeling the effects of motion on human operators, and manual control of low bandwidth systems has led to the need for accurate submodels of the low frequency characteristics of the Human Operator (HO). Unfortunately, matching low frequency human response data has been a problem with almost all HO models, the well known Optimal Control Model (OCM) being no exception. This research is an attempt to better understand and hopefully eliminate these problems.

In this paper, properties of several structural variations in the neuromotor interface portion of the OCM are investigated. For example, it is known [1-2] that commanding control-rate introduces an open-loop pole at S=0 and will generate low frequency phase and magnitude characteristics similar to experimental data. However this gives rise to unusually high sensitivities with respect to motor and sensor noise-ratios, thereby reducing the models' predictive capabilities. Relationships for different motor submodels are discussed to show sources of these sensitivities. The models investigated include both pseudo motor-noise and actual (system driving) motor-noise characterizations. The effects of explicit priprioceptive feedback in the OCM is also examined. To show graphically the effects of each submodel on system outputs, sensitivity studies are included, and compared to data obtained from [1-2].

INTRODUCTION

Recently, motion studies [2,3] have shown the major effects of motion to be on low frequency ($\omega < 1$ rad/sec) HO magnitude and phase characteristics. This means that low frequency modeling errors present in the baseline implementation of the OCM must be minimized if the effects of including motion variables are to be felt. It is known [1,2] that changing the structure of the neuro-motor interface portion of the OCM will give the desired low frequency effects. Specifically if the HO commands control rate rather than control, the low frequency phase drooping occurs. However, in order to match human response data over simple vehicle dynamics, large deviations in the motor noise ratios were needed [2]. This clearly degrades the predictive

power of the model. In this paper sub-models developed in [1,2] will be compared from a sensitivity point of view, in an attempt to better understand the limitations of each approach.

Problem Formulation

In this section structural changes will be made to the baseline OCM (for a more detailed description see Levison [2]). A general form will be developed first, with specific models introduced as special cases to it. In the development which follows, the time delay will be ignored since it has little bearing on our discussion.

The system being controlled is described by the state-space equation

$$\dot{x} = Ax + Bu + Ew \tag{1}$$

where:

x = "true" system state
u = "true" control input

and where displayed system variables are given by

$$y = Cx + Du \tag{2}$$

The system is assumed to be controlled to minimize (in steady-state) a quadratic cost functional

$$J = E\{y' Q_y y + q \dot{u}^2\} \tag{3}$$

based on the (delayed and) noisy information perceived by the HO. This information is assumed to consist of both displayed and proprioceptive variables, i.e.,

$$y_p = Cx + Du + v_y \tag{4a}$$

$$u_p = u + v_u \tag{4b}$$

where:

$$\text{cov}\{v_y\} = V_y + \rho_y E\{y^2\} \tag{5a}$$

$$\text{cov}\{v_u\} = V_u + \rho_u E\{u^2\} \tag{5b}$$

The control law that minimizes J is given by

$$\dot{u} = -[L_x \; L_u] \begin{bmatrix} \hat{x} \\ \hat{u} \end{bmatrix} \triangleq \dot{u}_c \tag{6}$$

where:

$\hat{x}$ = human's best internal estimate of x
$\hat{u}$ = " " " " u

To model any actual noise at the motor end, a driving motor noise is added to (6). Notice control rate is generated rather than control. Thus,

$$\dot{u} = \dot{u}_c + v_{\dot{u}} \tag{7}$$

where:

$$\mathrm{cov}\{v_{\dot{u}}\} = V_{\dot{u}} + \beta_{\dot{u}} E\{\dot{u}_c^2\} \tag{8}$$

However the human's internal representation of the neuromotor interface, Eq. (7), is:

$$\dot{u} = \dot{u}_c + v_p \tag{9}$$

where:

$$\mathrm{cov}\{v_p\} = V_p + \beta_p E\{\dot{u}_c^2\} \tag{10}$$

and typically $\mathrm{cov}\{v_p\} \neq \mathrm{cov}\{v_{\dot{u}}\}$.

The pseudo motor noise v_p does not act as a driving noise to the system, but instead degrades performance by making estimation sub-optimal [2].

Implementing these changes gives rise to the structure shown in Fig. 1.

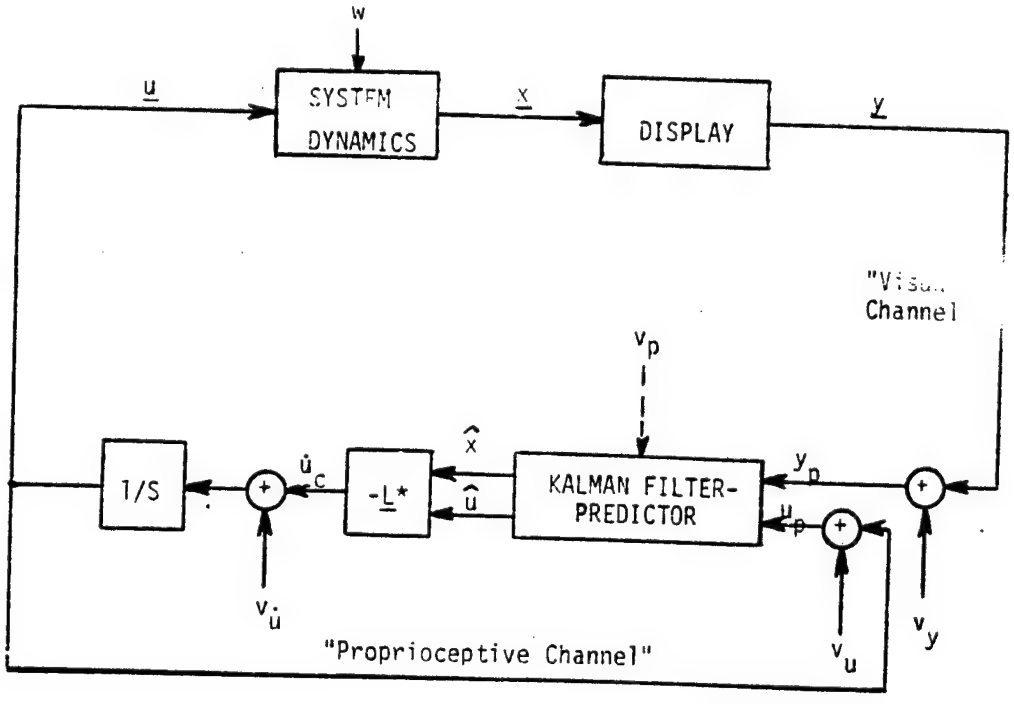

FIG.1 REVISED OPTIMAL CONTROL MODEL.

The particular submodels considered in this study are as follows:

Driving Noise Models:

1) $cov[v_p] = cov[v_u]$, i.e., optimal estimation occurs, driving motor noise equal to v_u
   - proprioceptive information available

2) Same as model (1), except no proprioceptive information available

Pseudo noise models:

3) $v_u = 0$, i.e., sub-optimal estimation occurs, only pseudo noise present
   - proprioceptive information available

4) Same as model (3) except no proprioceptive information available

SENSITIVITY RESULTS

Data from [1,2] was matched using each of the aforementioned models. Only K/S and K/S**2 dynamics were considered. The reader is referred to the sensitivity studies included in [1] so a comparison can be made to the baseline model.

K/S Dynamics

The following nominal parameters were found to give reasonable matches to the data, and will be used as a basis for the K/S sensitivity work. Notice that proprioceptive feedback is not needed for K/S dynamics; this agrees with findings in [1,2]. Therefore, for K/S dynamics we need only consider two models, driving noise and pseudo noise.

Model	SNR	SNR-u	MNR	TD	TN
1 & 3	-20	-∞	-40	.17	.08
2 & 4	-20	--	-40	.17	.08

$SNR = \sigma_{v_c}$

$SNR - u = \sigma_u$

$MNR = \sigma_u$ or σ_p

$TD = \tau$, $TN = L_u^{-1}$

It was found that the trends discussed in [1] for SNR, TD and TN were the same for all the models considered. The only exception to this was for the driving noise models, where the low frequency remnant curves were slightly higher.

Effects of MNR

From Fig. 2 it is clear that motor noise mainly affects the low fre-

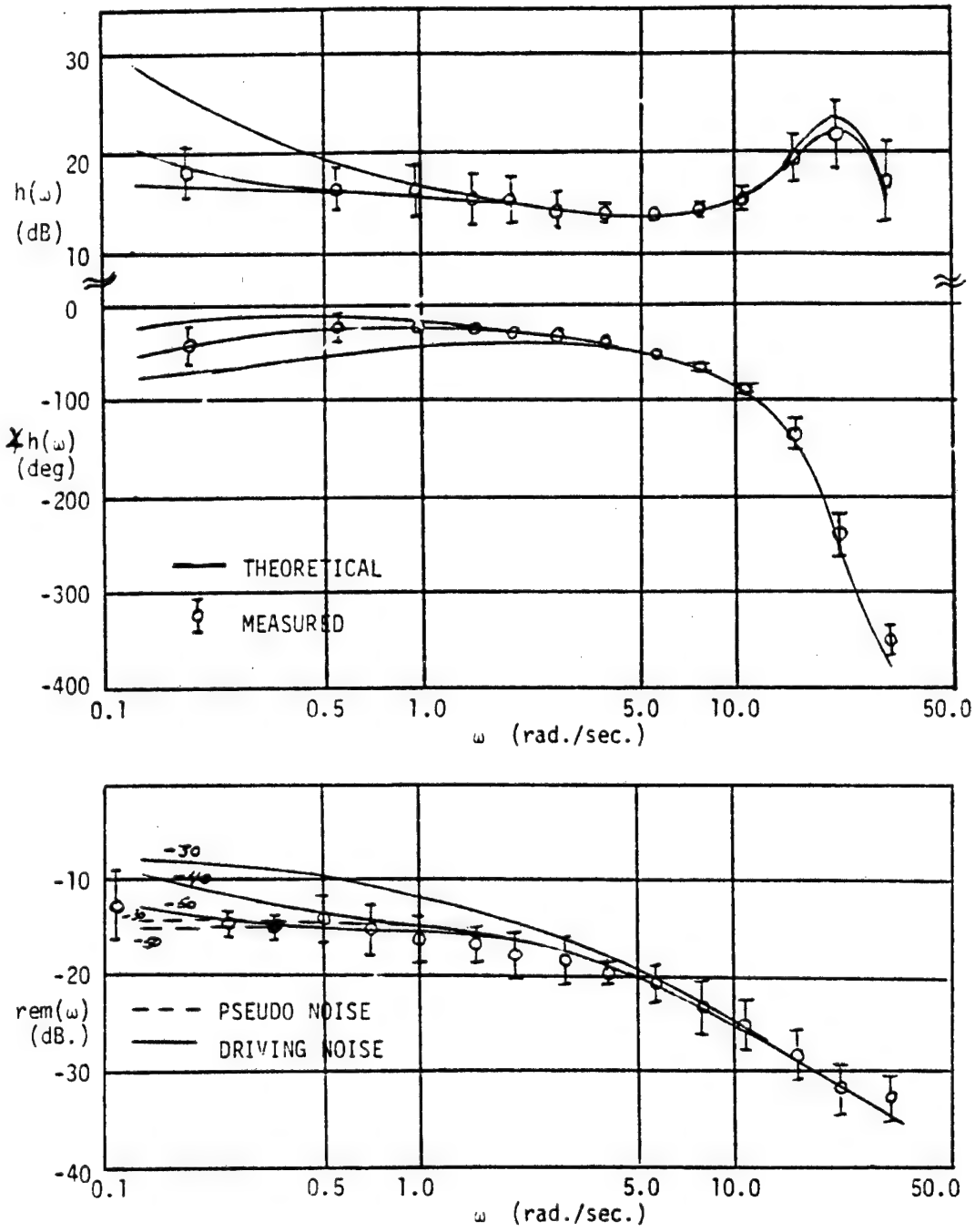

FIG.2 EFFECTS OF MNR ON K/S DYNAMICS.

quency portion of the magnitude, phase and remnant curves. There are basically two reasons for this. First, the shape of the low frequency portion is due to the integrator at the motor end (where in the baseline OCM, $1/(T_N S+1)$ was present). Secondly, the sensitivity is due to the degradation of estimation performance as the motor noise is increased. Because the level of the driving noise is so low, the linear part of the HO model (Bode plot) is the same whether pseudo noises or driving noises are used. Notice that the driving noise has a dominant affect only on the low frequency remnant.

All scores increase with increasing motor noise. Scores using the pseudo model are fairly insensitive to motor noise, since it is the degraded estimation which causes them to change. Scores using the driving model are much more sensitive to motor noise, since increasing the motor noise increases the remnant in the system.

K/S**2 Dynamics

The following is the nominal parameter set found for K/S**2 dynamics.

Model	SNR	SNR-u	MNR	TD	TN
1 & 3	-20	-25	-40	.21	.1
2 & 4	-20	---	-54	.21	.1

Here, as in K/S dynamics, trends discussed in [1] for SNR, TD, and TN also hold for our revised models. Below we discuss only the effects of MNR & SNR on control.

Effects of MNR

No Proprioceptive Information (models 2 & 4)

Looking at Figure 3 it is clear that the motor noise affects the low frequency Bode plots in a manner similar to that found for K/S dynamics. Again, more remnant power is shifted to the low frequencies for model 2 than for model 4.

Notice that model 4 matches the low frequency remnant very poorly (this could be improved slightly by increasing the noise on displayed error) and may be interpreted as a major shortcoming of this model since we desire a nominal set of parameters.

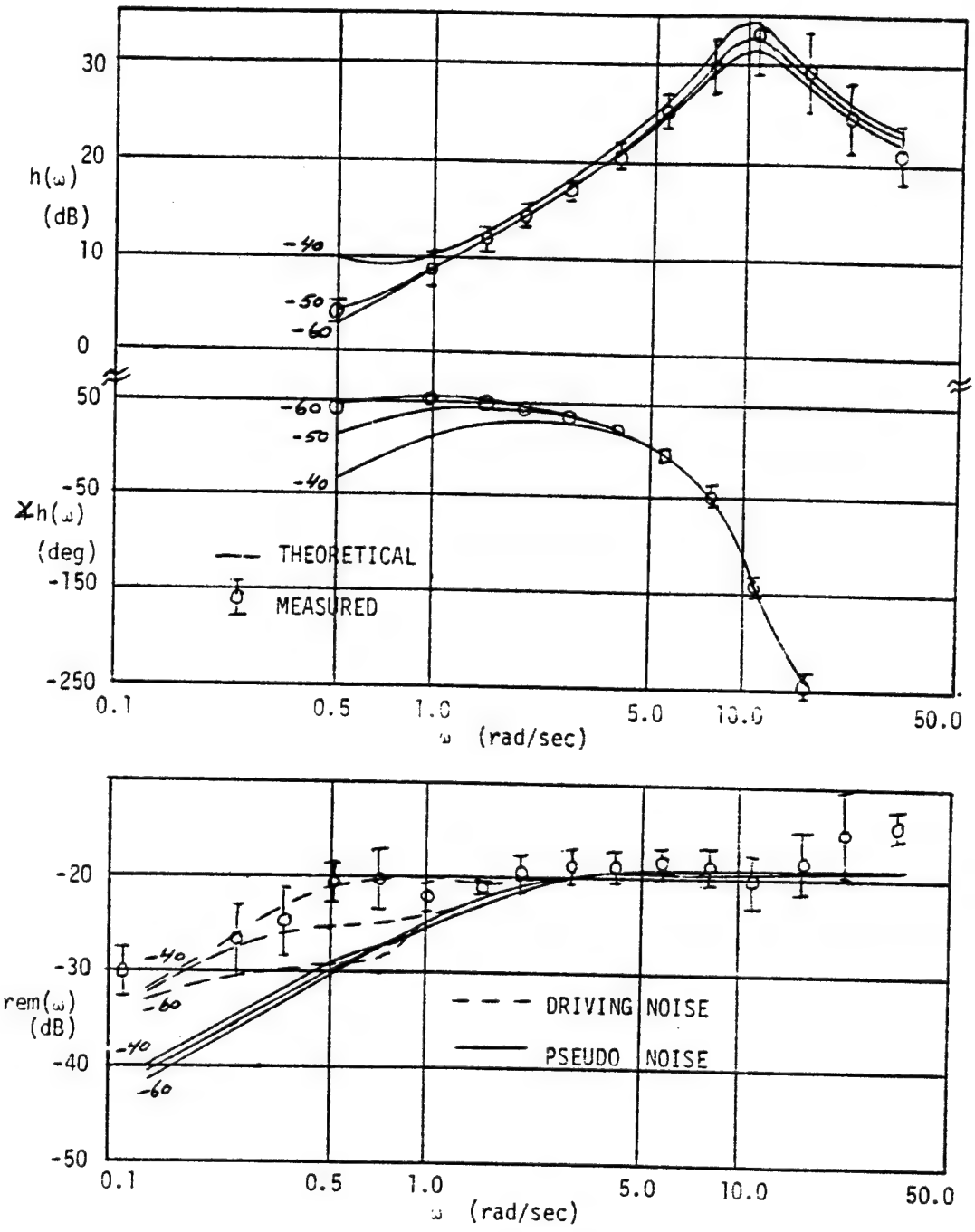

FIG.3 EFFECTS OF MNR ON K/S**2 DYNAMICS (MODELS 2 & 4).

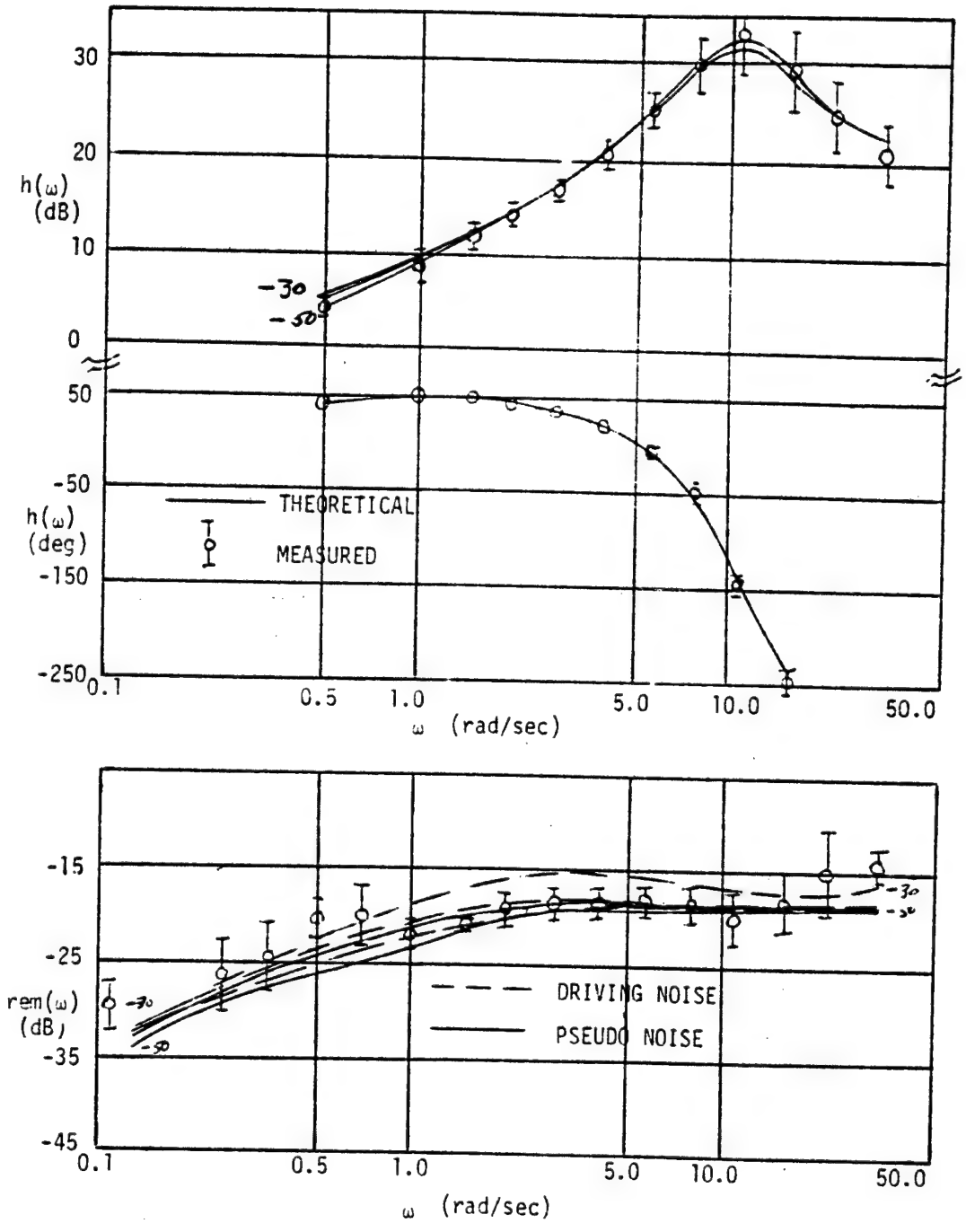

FIG.4 EFFECTS OF MNR ON K/S**2 DYNAMICS (MODELS 1 & 3).

With Propioceptive Information (Models 2 & 4)

The effects of including proprioceptive feedback can be seen by comparing Figs. 3 & 4. Again remnant is higher for driving motor noises, but it is spread out over a wider band of frequencies. This may be due to the circulation of remnant in the feedback loop. Although not shown, the scores for model 1 were always higher and more sensitive than those for model 3, and seemed to match the data better.

Notice that the sensitivity of the model to changes in the motor noise has been reduced dramatically by including proprioceptive feedback. Because the model now has observations of control and control rate to use in forming an estimate of control, estimation stabilizes and improves.

Effects of SNR (Models 1 & 3)

Figure 5 shows the low frequency remnant for model 3 much closer to that of model 1. Notice if the sensor noise is too large (>-15dB), the model ignores this observation and models 1 & 3 effectively become models 2 & 4. Since knowledge of the control signal is important in this task, it is clear that the model should be, and is, sensitive to the quality of this information. The low frequency effects result primarily from the movement of the estimator poles.

Sensitivity of Scores

Relative RMS error is plotted in Fig. 6 as a function of MNR. Because RMS error is the most sensitive score, Fig. 6 shows that including proprioceptive feedback reduces the sensitivity of all the scores.

Review

From the sensitivities studies it was seen that in general:

- All predicted scores were lower than measured ones for pseudo noise
- All system measures were more sensitive to driving motor noise than to pseudo noise
- This sensitivity can be reduced by including an observation of control
- The level of sensor noise on control induces the low frequency effects
- The integrator at the motor end confines the remnant power to the low frequencies

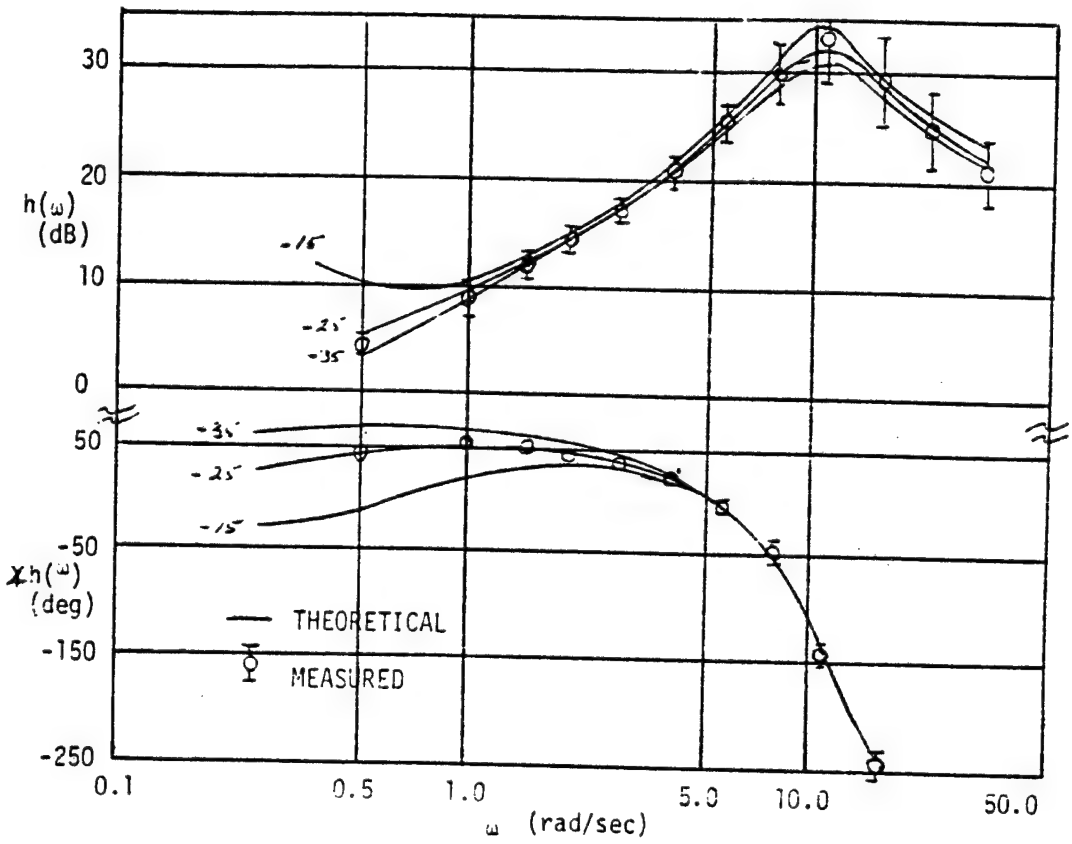

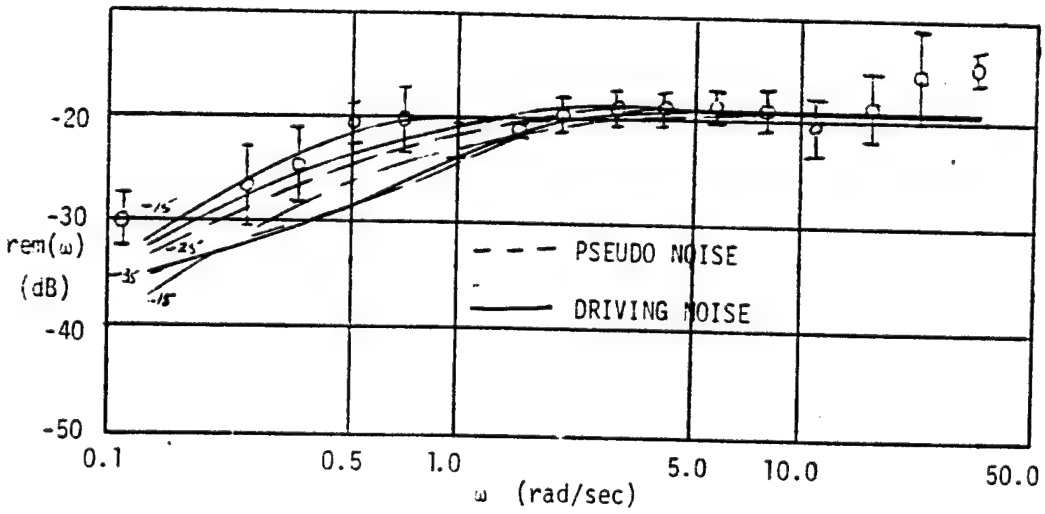

FIG.5 EFFECTS OF SNR-U ON K/S**2 DYNAMICS (MODEL 1 & 3).

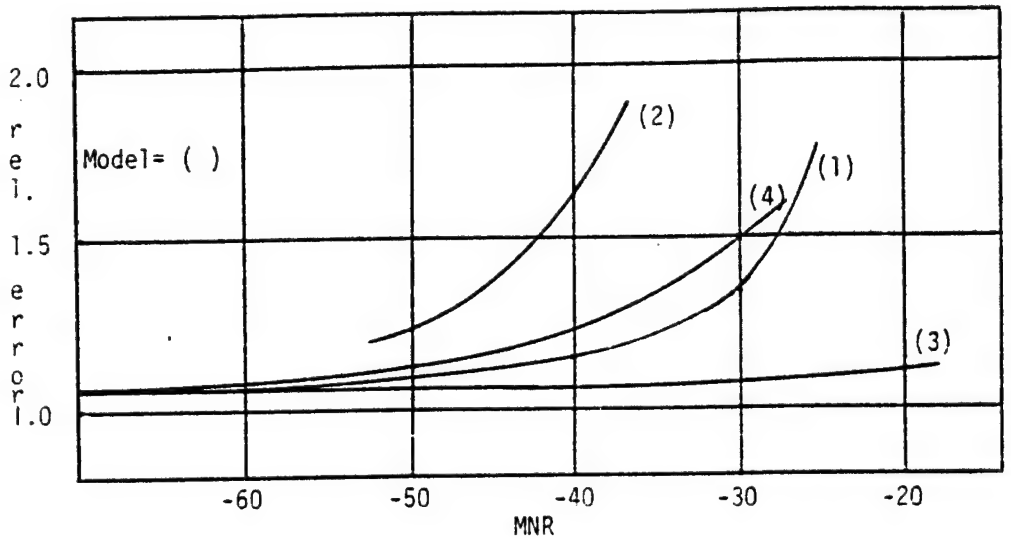

FIG. 6: SENSITIVITY OF RMS ERROR (K/S**2 TASK)

- It is difficult to match K/S**2 data, with a nominal set of parameters, using models 2 & 4

FINAL COMMENTS

Sensitivity studies have shown that including observations on control can reduce model sensitivity to driving motor noises. Also it was shown that a sensor noise added to control does not greatly affect the uncorrelated part of the model. Nominal parameters were found that could match K/S & K/S**2 dynamics, provided that observations on control are included for K/S**2 but not for K/S. If the model is allowed to allocate attention freely among all observed variables, this may provide a scheme for determining the sensor noises. One hypothesis is that this essentially forms a decision step (perhaps as part of the learning process) in the HO model, where it must evaluate the benefits of all the cues it has available to it and then decide on a subset which will be useful for control purposes.

More work needs to be done in order to find a good rule for picking the sensor noises. Testing models 1 and 3 over a wider set of system dynamics is also important to see if our findings are true in general or just a special case.

REFERENCES

1. Kleinman, D.L. & Baron, S.: Manned Vehicle Systems Analysis by Means of Modern Control Theory. NASA CR-1753, June 1971.

2. Levison, W.H., Baron, S., Junker, A.M.: Modeling the Effects of Environmental Factors on Human Control and Information Processing, AMRL-TR-75-74, Aug. 1976.

3. Levison, W.H. & Junker, A.M.: A Model for the Pilots Use of Motion Cues in Roll-Axis Tracking Tasks. AMRL-TR-77-40, June 1977.

N79-15598

CLOSED LOOP MODELS FOR ANALYZING THE EFFECTS OF SIMULATOR CHARACTERISTICS*

by

Sheldon Baron, Ramal Muralidharan, David Kleinman
Bolt Beranek and Newman Inc., Cambridge, MA

ABSTRACT

The optimal control model (OCM) of the human operator is used to develop closed-loop models for analyzing the effects of (digital) simulator characteristics on predicted performance and/or workload. Two approaches are considered: the first utilizes a continuous approximation to the discrete simulation in conjunction with the standard optimal control model; the second involves a more exact discrete description of the simulator in a closed-loop multi-rate simulation in which the optimal control model "simulates" the pilot. Both models predict that simulator characteristics can have significant effects on performance and workload.

1. INTRODUCTION

The development of engineering requirements for man-in-the-loop digital simulation is a complex task involving numerous trade-offs between simulation fidelity and costs, accuracy and speed, etc. The principal issues confronting the developer of a simulation involve the design of the cue (motion and visual) environment so as to meet simulation objectives and the design of the digital simulation model to fulfill the real-time requirements with adequate accuracy.

The design of the simulation model has become increasingly important and difficult as digital computers play a more central role in the simulations. For real-time digital simulation with a pilot in the loop the design problem involves specification of conversion equipment (A-D and D-A) as well as of the discrete model of the system dynamics. The design of an adequate discrete simulation is also related closely to the cue generation problem inasmuch as the errors and, in particular, the delays introduced by the simulation will be present in the information cues utilized by the pilot. The significance of this problem has been amply demonstrated.[1,2] Of course, human pilots can compensate for model shortcomings as well as for those of cue generation, with possible effects on the subjective evaluation of the simulation.

The objective of the work reported here was to develop a closed loop analytic model, incorporating a model for the human pilot (namely, the optimal control model), that would allow certain simulation design tradeoffs to be evaluated quantitatively and to apply this model to analyze a realistic flight control problem. The effort concentrated on the dynamic, closed loop aspects of

*The work described herein was performed under Contract No. NSA1-14449 for NASA - Langley Research Center. Mr. Russell Parrish was the Technical Monitor and contributed many helpful suggestions.

the simulation. Problems associated with perceptual issues in cue generation were not considered. However, the limitations imposed by the dynamics of visual cue generation equipment are considered and the model can be readily extended to incorporate the dynamics associated with motion simulation.

The optimal control model of the human operator[3,4] is central to the closed loop analysis techniques that have been employed. This model has been validated and applied extensively and has a structure that is well-suited to analysis of the simulation problems of interest. The model can be used to generate predictions of attentional workload as well as of closed-loop performance. This is significant because, as noted earlier, pilots may compensate for simulation shortcomings but with a workload penalty; such simulation-induced operator tradeoffs need to be explored.

Two approaches to closed-loop modelling are considered. The first employs a continuous approximation to the open-loop dynamics of the digital simulation in conjunction with the standard OCM. The second model attempts to represent the discrete simulation dynamics more exactly. It utilizes a simulation version of the OCM. This latter model is referred to as the hybrid model.

In the remainder of this paper, the closed loop models are described and some results of applying the models are presented and discussed. More extensive discussion and additional results may be found in Reference 5.

2. CONTINUOUS CLOSED LOOP MODEL

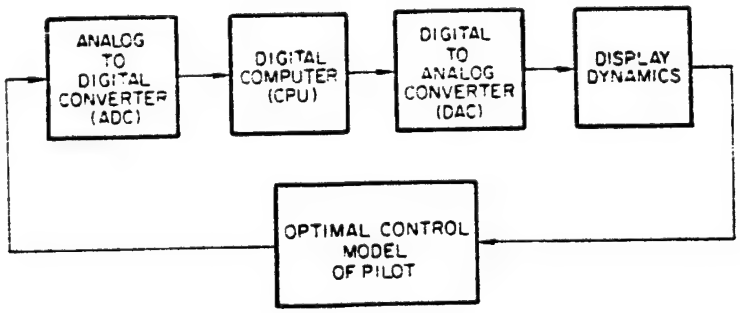

Figure 1. Simplified Model for Closed Loop Analysis of Digital Simulation

Figure 1 is a block diagram of a simplified closed-loop model for analyzing problems in digital, piloted simulation. The pilot model in Figure 1 is the OCM.[3,4] The elements corresponding to the simulator are an analog-to-digital converter (ADC), a digital computer (CPU), a digital-to-analog converter (DAC) and a visual display system. Briefly, the ADC is a sampler preceded by a

low-pass filter included to minimize aliasing effects, the CPU implements difference equations so as to simulate the vehicle's response to the pilot's (sampled) input, the DAC is a data-hold (either zero-order or first-order), and the visual display system is a servo-driven projector that continuously displays target position (relative to the aircraft) to the pilot. These elements will be discussed in more detail below.

2.1 Optimal Control Model for Pilot

Some of the features of the OCM that are particularly relevant to subsequent discussions are reviewed briefly here. Figure 2 illustrates the

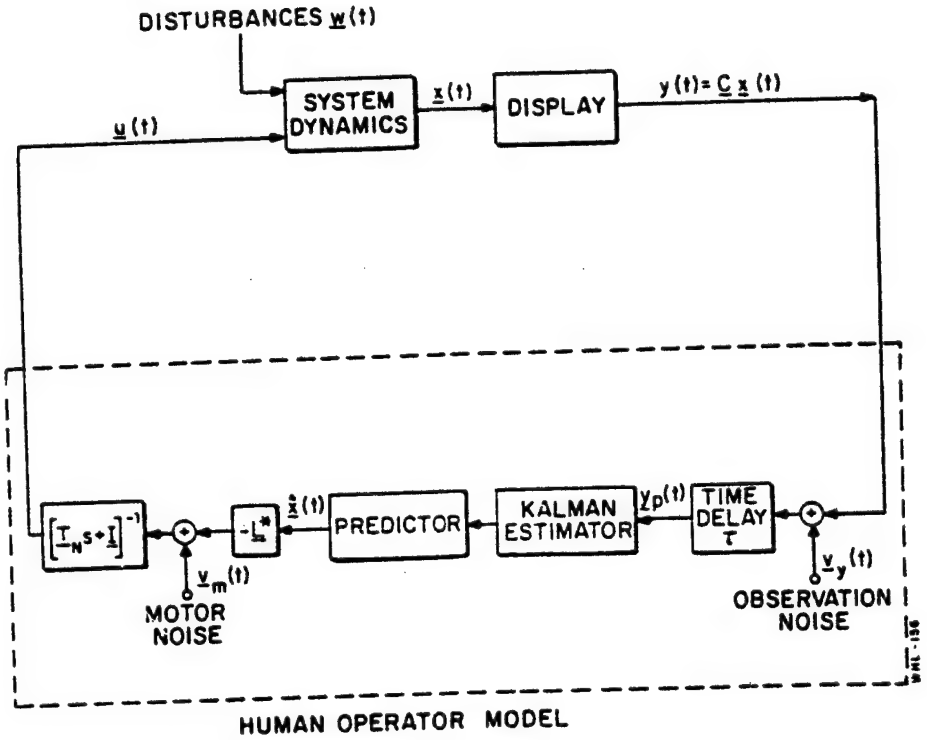

Figure 2. Structure of Optimal Control Model

structure of the OCM.

The OCM as originally conceived and developed presupposes that the system dynamics, corresponding to the element to be controlled, may be expressed in state variable format

$$\dot{\mathbf{x}}(t) = \mathbf{A}_c\mathbf{x}(t) + \mathbf{B}_c\mathbf{u}(t) + \mathbf{E}_c\,\mathbf{w}(t)$$
$$\mathbf{y}(t) = \mathbf{C}_c\mathbf{x}(t) + \mathbf{D}_c\mathbf{u}(t) \qquad (1)$$

where $\mathbf{x}$ is the n-dimensional state-vector, $\mathbf{y}$ is an m-dimensional vector of displayed outputs, $\mathbf{u}$ is the r-dimensional control input vector and $\mathbf{w}$ is a vector of disturbance and/or command inputs. The system matrices ($\mathbf{A}_c$, $\mathbf{B}_c$, $\mathbf{C}_c$, $\mathbf{D}_c$, $\mathbf{E}_c$) are generally assumed to be time-invariant, although this restriction can be relaxed. The above system dynamics include the linearized dynamics of the aircraft (or other controlled element) and any dynamics associated with measurement, control and display systems. The subscript c on the system matrices is included to emphasize that the dynamics are assumed to represent a continuous system.

For purposes of discussion it is convenient to consider the model for the pilot as being comprised of the following: (i) an "equivalent" perceptual model that translates displayed variables into noisy, delayed perceived variables denoted by $\mathbf{y}_p(t)$; (ii) an information processing model that attempts to estimate the system state from the perceived data. The information processor consists of an optimal (Kalman) estimator and predictor and it generates the minimum-variance estimate $\hat{\mathbf{x}}(t)$ of $\mathbf{x}(t)$; (iii) a set of "optimal gains", $\mathbf{L}^*$, chosen to minimize a quadratic cost functional that expresses task requirements; and (iv) an equivalent "motor" or output model that accounts for "bandwidth" limitations (frequently associated with neuromotor dynamics) of the human and an inability to generate noise-free control inputs.

The time delay or transport lag is intended to model delays associated with the human. All displayed variables are assumed to be delayed by the same amount, viz. τ seconds. However, delays introduced by the simulation can be added to the human's delay without any problem, so long as all outputs are delayed by the same amount. If such is not the case, then all outputs can be delayed by τ, where τ is now the sum of the minimal delay introduced by the simulation and the operator's delay, and additional delays for the outputs requiring them can be modeled via inclusion of Pade approximations in the output path.

The observation and motor noises model human controller remnant and involve injection of wide-band noise into the system. This noise is "filtered" by the other processes in the pilot model and by the system dynamics. It should be emphasized that the injected remnant is a legitimate (if unwanted) part of the pilot's input to the system and, therefore, significant amounts of remnant power should not be filtered out in the de-aliasing process of a valid simulation.

The neuro-motor lag matrix limits the bandwidth of the model response. Typically, for wide-band control tasks, involving a single control variable, a bandwidth limitation of about 10-12 rad/sec gives a good match to experimental results (i.e., a neuro-motor time constant of T_N = .08 - .10). For many

aircraft control tasks there is no significant gain (i.e., reduction in error) to be obtained by operating at this bandwidth, and there can be some penalty in unnecessary control activity. For such tasks larger time constants (lower bandwidths) have been observed. In these cases, if the neuro-motor time constant is arbitrarily set at the human's limit (say $T_N = .1$) good predictions of tracking or regulation performance are usually obtained; but the control activity and pilot bandwidth tend to be overestimated. Inasmuch as it may be useful to have more accurate estimates of pilot bandwidth for making decisions concerning approximations to the discrete simulations, T_N was chosen in this study on the basis of a model analysis of the tradeoff between error and control-rate scores. Essentially, this involves using the model to sweep out a curve of error-score versus control-rate score to find the value of T_n where marginal improvements in performance require substantial increases in rms control-rate (the "knee" of the curve). A value of approximately .15 sec (an operator bandwidth of about 1 Hz) was determined on the basis of this analysis.[5]

The optimal estimator, predictor and gain matrix represent the set of "adjustments" or "adaptations" by which the human attempts to optimize performance. The general expressions for these model elements depend on the system and task and are determined by solving an appropriate optimization problem according to well-defined rules. Of special interest here is that, in the basic continuous OCM, the estimator and predictor contain "internal models" of the system to be controlled and the control gains are computed based on knowledge of system dynamics. The assumption is that the operator learns these dynamics during training.*

The question arises as to the appropriate internal model when the human controls a discrete simulation of a nominally continuous system. It would appear that if the operator is trained on the simulation, then the appropriate model corresponds to the simulation model.** This will be the assumption employed with the continuous model.

Finally, it should be mentioned that the solution to the aforementioned optimization problem yields predictions of the complete closed-loop performance statistics of the system. Predictions of pilot describing functions and control and error spectra are also available. All statistical computations are performed using covariance propagation methods, thus avoiding costly Monte Carlo simulations. This is not the case for the hybrid model described later.

---

*This is generally more convenient than assuming that the external model differs from the true model and also leads to good performance prediction.[6]

**If the simulation model is poor, a control strategy that is inappropriate for the actual system could be learned with negative results in, say, transfer of training. This issue can be addressed with the hybrid model described later.

2.2 Open-Loop Simulator Dynamics

The application of the standard OCM to closed-loop analysis requires a continuous state representation of the complete controlled element. Since the human pilot in closed loop control will operate on essentially continuous outputs to generate continuous control inputs even when digital computers are used in the aircraft simulation, it is meaningful to consider a continuous transfer function approximation to the open loop simulation dynamics. Such an approximation is developed here. It consists of a rational transfer function multiplied by a transportation lag. The rational transfer function approximates the amplitude distortions introduced by discrete integration of the flight dynamics. The delay accounts for all the phase lags introduced by the simulator components. These phase lags are the major source of degraded performance and increased workload in closed loop tasks. However, the amplitude distortions can be significant for open-loop responses.

System Function From Stick Input to Displayed Output

Figure 3 is an elaborated diagram of the simulator portion of Figure 1.

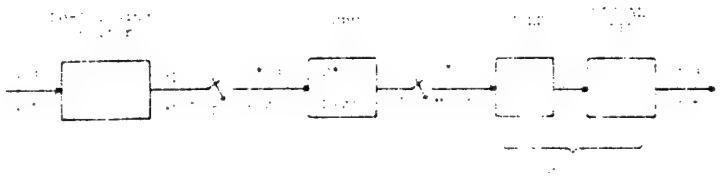

Figure 3. Open Loop Simulator Dynamics

Note that the output of the visual servo, y(t), is a continuous signal as is the input, u(t), to the A-D dealiasing pre-filter.* For analysis purposes we use the notation implied in Figure 3. Variables or functions with argument s represent Laplace transforms and those with argument z correspond to z-transforms. The starred quantities correspond to Laplace transforms of impulse sampled signals or of functions of z and are defined, e.g., by[7]

$$u_1^*(s) \triangleq u_1(z)\Big|_{z=e^{sT}} = \frac{1}{T}\sum_{n=-\infty}^{\infty} u_1(s+jn\Omega) \qquad (2)$$

or

*For simplicity, we consider single-input, single-output systems. The results obtained here can be generalized to more complex situations.

$$D^*(s) = D(z)\Big|_{z=e^{sT}} \tag{3}$$

where T is the sample period and

$$\Omega = \frac{2\pi}{T} = \text{sampling frequency} \tag{4}$$

From Figure 3, we obtain

$$y(s) = F_2(s)y_1^*(s) = F_2(s)D^*(s)u_1^*(s)$$

$$= F_2(s)D^*(s)\ \frac{1}{T}\sum_{n=-\infty}^{\infty} F_1(s+jn\Omega)u(s+jn\Omega) \tag{5}$$

Equation (5) gives the exact transfer relation between u(s) and y(s). However, it is not a useful expression from the standpoint of closed-loop modeling because of the infinite summation.

The system function for a linear system (such as the simulation system under analysis) may be obtained by computing the steady-state response of the system to an input of the form exp(st). It is shown in Reference 5 that the system function from u(s) to y(s) (in steady-state) is periodic in time with a period equal to the sampling period. However, if the output y(t) is considered only at sampling instants, which amounts to introducing a "fictitious" sampler at the output[7] then the following time-independent transfer function is obtained.

$$G(s;t)\Big|_{\substack{\text{sample}\\ \text{times}}} = G(s) = F_2^*(s)D^*(s)F_1(s) \tag{6}$$

We shall consider G(s) defined in (6) to be the "exact" transfer function for the simulation. Note that $F_2^*(s) = (VH_1)^*(s)$.

Equation (6) is intractable for use with the continuous OCM. Therefore, it will be necessary to approximate (6) for closed-loop analysis. A straightforward approximation is to ignore all but the n=0 term in the expression for F_2^* which results in

$$G(s) \approx \frac{F_2(s)D^*(s)F_1(s)}{T} = \frac{V(s)H_i(s)D^*(s)F_1(s)}{T} \tag{7}$$

In utilizing (7) it will be necessary to approximate $D^*(s)$; the procedure for doing this will be discussed subsequently.

For the simulator of interest here,[8] the transfer functions for the de-aliasing filter and servo are, respectively,

$$F_1(s) = \frac{\omega_c^3}{s^3 + 2\omega_c s^2 + 2\omega_c^2 s + \omega_c^3} \tag{8}$$

$$V(s) = \frac{\omega_n^2}{s^2 + 2\zeta\omega_n s + \omega_n^2} \tag{9}$$

The hold transfer function is either

$$H_o(s) = \frac{1-e^{-sT}}{s} \tag{10}$$

or

$$H(s) = T(1+Ts)\left(\frac{1-e^{-Ts}}{Ts}\right)^2 \tag{11}$$

Sample periods, T, of 1/32, 1/16, 1/10 will be considered as these cover the likely range of interest for piloted simulation. Therefore, if the cutoff of the de-aliasing filter is chosen on the basis of the sampling theorem, $\omega_c >$ 5Hz. The visual servo dynamics of interest are characterized by ω_n = 25 rad/sec and ζ = .707.[8]

With these parameter values, each of the transfer functions of (8) - (11) may be approximated reasonably well by a pure transport lag in the frequency region of interest for manual control ($\omega <$ 10 rad/sec). That is,

$$
\begin{aligned}
F_1(s) &\approx e^{-\tau_F s} \\
V(s) &\approx e^{-\tau_V s} \\
H_o(s) &\approx e^{-\tau_o s} \\
H_1(s) &\approx e^{-\tau_1 s}
\end{aligned}
\tag{12}
$$

where

$$
\begin{aligned}
\tau_F &\approx \frac{2}{\omega_c} = \frac{2T}{\pi} & \tau_o &= T/2 \\
\tau_V &\approx (\zeta\omega_n)^{-1} = .057 \text{ sec} & \tau_1 &= T
\end{aligned}
\tag{13}
$$

Substitution of (12) into (7) yields

$$
F_1(s)D^*(s)F_2(s) \approx D^*(s) \exp\left[-(\tau_F + \tau_V + \tau_i)s\right] \tag{14}
$$

where i = 0 or 1 for the zero-order or first-order hold, respectively.

2.3 Effects of Discrete Integration

In the previous section the transfer function D*(s) was left unspecified as was the manner in which it was to be approximated for continuous closed-loop analysis with the OCM. In general, D*(s) will be a "distorted" version of the continuous system dynamics that are to be simulated. Some general features of the distortions introduced by various integration schemes are analyzed and presented in Reference 5 along with results pertinent to the F-8 dynamics that are to be analyzed later. Here, we present a brief discussion of the general effects of discrete integration followed by a description of the method that will be used to approximate D*(s) in the continuous closed-loop analysis.

Consider the continuous vehicle-dynamics as described in the state-variable form of Equation (1). For constant system matrices, the transfer matrix between system outputs and control inputs is given by

$$
\begin{aligned}
\mathbf{y}(s) &= \boldsymbol{\Phi}_c(s)\, \mathbf{u}(s) \\
\boldsymbol{\Phi}_c(s) &= \mathbf{C}_c(s\mathbf{I}-\mathbf{A}_c)^{-1}\mathbf{B}_c + \mathbf{D}_c
\end{aligned}
\tag{15}
$$

When equations (1) are "integrated" digitally, they lead to a discrete approximation with the following transfer matrix[5]

$$
D^*(s) = \left\{C_d[zI-A_d]^{-1} B_d + D_d\right\}\Big|_{z=e^{sT}} \tag{16}
$$

where the matrices in (16) depend on the particular integration scheme and sample period as well as on the corresponding continuous system matrices. Several points concerning Equation (16) are noteworthy. First, the elements of the discrete transfer matrix $D^*(s)$, cannot, in general, be expressed as the ratio of two polynomials in s of finite degree. Second, the Bode responses corresponding to (16) will differ from the continuous responses in both amplitude and phase; and, further, the responses for the discrete system are periodic in frequency with period equal to $2\pi/T$. Third, the poles and zeros of Equation (16) are infinite in number and are given by, for example,

$$p_i = \sigma_i + j(\omega_i + 2\pi k);\ k = 0, \pm 1, \pm 2, \ldots$$

Moreover, the principal values for the poles and zeros, i.e., those with $k = 0$, are not, in general, equal to the corresponding poles and zeros of the continuous system. Finally, simple integration schemes, such as Euler, will have the same number of principal poles as the continuous system, whereas multi-step integration schemes, like (Adams-Bashforth), will introduce principal roots that are spurious.

We now turn to the problem of approximating $D^*(s)$ so that the continuous representation of the simulator dynamics may be completed. Because of the restrictions imposed by the OCM, we restrict the possible approximations to the following form:

$$\frac{Y_i}{u_j} = D^*_{ij}(s) \approx \tilde{D}_{ij}(s)e^{-\tau_c s}$$

where $\tilde{D}(s)$ is a ratio of finite polynomials in s with numerator degree less than or equal to the degree of the denominator. Note that the same "computation" delay, τ_c is associated with each transfer function. This turns out to be a good approximation for the dynamics considered in Section 4. If different delays were needed, they would be included in $\tilde{D}$ via a rational Pade approximation.[5]

The simplest approach to selecting $\tilde{D}$ is to use (15) and let

$$\tilde{D}_{ij}(s) = \Phi_{c_{ij}}(s) \tag{17}$$

From the standpoint of the OCM, this means that the state equations for the original dynamics are used and discrete integration is modeled by adding a delay determined from the phase distortion. As has been stated earlier, such an approximation probably accounts for the major source of difficulty of discrete integration in closed-loop control. However, to employ it exclusively is to leave us somewhat uncertain as to the closed-loop significance of the amplitude distortions.

It was found[5] that very good approximations to discrete Bode responses could be obtained for the longitudinal control tasks that are to be analyzed later. These approximations involved perturbation of aircraft stability derivatives and CAS parameters to yield continuous modes that agreed with the discrete modes. In the case of A-B integration, it was also necessary to introduce a zero in the continuous vehicle transfer in order to reproduce the amplitude distortion introduced by this integration scheme.

When Equation (17) is substituted in (14), the basic result is that for the frequency range likely to be of interest in continuous aircraft control problems, the simulator transfer function can be modelled as

$$\frac{Y(s)}{u(s)} = \tilde{D}(s)e^{-\tau_s s} \tag{18}$$

where D(s) is an "approximation" to the Bode response for digital integration of the vehicle dynamics. The simulator delay, is given by

$$\tau_s = \tau_F + \tau_H + \tau_V + \tau_C \tag{19}$$

where τ_F, τ_H, τ_V and τ_C respectively, are the delays introduced by the de-aliasing filter, hold, visual servo and CPU (discrete integration).

The approximation of Equation (18) readily lends itself to efficient application of the OCM. The system matrices corresponding to a state representation of $\tilde{D}$ and the values for τ_s are easily obtained for different sample periods, etc. For each condition, a single run of the OCM is sufficient to predict the corresponding performance. Adjustment of pilot parameters, specifically observation noise levels, allows the sensitivity to pilot attention to be examined.[9]

3. THE HYBRID MODEL

There are shortcomings in the continuous model. For example, the effects of aliasing are not considered. Thus, the degrading effects of the de-aliasing filter are included in the continuous model but not its benefits. This means that decreasing the bandwidth, ω_c, of that filter can only lead to negative results, a situation that is not obviously true, in general. Similarly, because only the delays inherent in the data holds are considered, zero-order holds will always show less degradation than first-order holds. But, in some instances, the first order hold may provide advantages that outweigh the additional delay penalty. This type of trade-off cannot be explored with the continuous OCM without more sophisticated approximation to the simulator dynamics. Because of these and other potential shortcomings, it was decided to develop a hybrid model.

The approach to developing the hybrid model is to "simulate" the closed-loop simulation. A discrete simulation version of the OCM[10] was used in a closed-loop digital Monte Carlo type computation* in which "continuous" elements of the loop are updated at a rate significantly greater than discrete elements. In other words, the hybrid model is a multi-rate sampling system, rather than a true hybrid system. (Informal experimentation indicates that a sample rate five times that of the discrete elements is adequate to simulate continuity for the cases considered here.) In addition, to different sample rates for continuous and discrete elements, the updating of the discrete equations of the hybrid model is different for the two kinds of elements. In particular, discrete elements are updated by means of the integration scheme and time-step specified for the "true" simulation. The equations for continuous elements are updated at the faster rate via transition matrix methods.

The equations describing the hybrid model are quite complex and are described in detail in Reference 5. Here, we simply note two features of the model that are interesting and useful in subsequent analyses. First, the hybrid model was implemented so that the prediction time in the predictor of the OCM (See Figure 2) could be selected arbitrarily. This contrasts with the standard OCM in which the prediction time is always equal to the time delay. This additional freedom allows us to "sweep out" curves of performance versus prediction time. Theoretically, best performance should be obtained when the prediction time is equal to the sum of the human's delay and the simulator's delay, i.e. when the operator compensates optimally for both delays. Since the human's delay is an assumed parameter, the compensation time for best performance yields an independent measure of the simulator delay.

A second feature of the hybrid model is that the internal model for the OCM need not be the same as the system model.* This flexibility provides the hybrid model with a capability for examining transfer-of-training questions. In addition, since optimal performance should correspond to the operator's model being equivalent to the system model, the hybrid model can be used to evaluate different (internal) approximations to the discrete simulation.

A final point concerning the hybrid model is worth noting. Because it is a Monte Carlo model, it normally will require many computer solutions to obtain meaningful statistics. In the analyses to be performed here, however, we are interested in the steady-state response of stationary systems. Rather than average over many Monte Carlo solutions, we have assumed ergodicity of the processes and utilized time-averaging of a single response. Even with this simplification, it is fairly expensive computationally to obtain valid statistical results.[5]

---

*A truly hybrid (analog/digital) model is possible but would require a hybrid computer (which was not available).

*Indeed, the system model can even be nonlinear.

4. AN EXAMPLE

The models for closed-loop analysis of simulator effects have been applied to an "example" simulation involving air-to-air target tracking. Results have been obtained for both longitudinal and lateral control tasks, for augmented and unaugmented dynamics and for different target motions. In addition, the effects of changes in design parameters of each simulation component have been explored. The full range of results may be found in Reference 5. Here, a sample of the results is presented to show the extent of the simulation effects and the capabilities of the closed-loop models.

4.1 The Tracking Problem

Figure 4 shows the geometry of the air-to-air tracking in the longitudinal plane. The gunsight is assumed to be fixed and aligned with the aircraft body axis. For longitudinal tracking, we will assume that no information concerning the target's pitch angle, ϕ nor the relative aspect angle is available. The pilot's task is assumed to be that of minimizing the mean-squared, line-of-sight

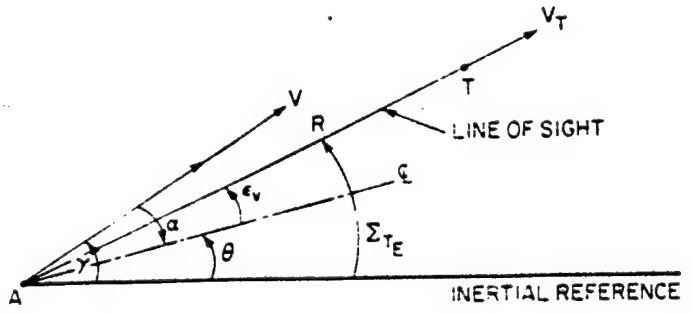

Σ_{T_E} = INERTIAL LINE-OF-SIGHT ANGLE (ELEVATION)
R = TARGET RANGE
ϵ_v = ELEVATION TRACKING ERROR = $\Sigma_{T_E} - \theta$

Figure 4. Target Geometry

tracking error ϵ_v.

The target is assumed to execute random vertical evasive maneuvers. In particular, target altitude variations are generated by passing white, gaussian noise through a third order filter as illustrated below.

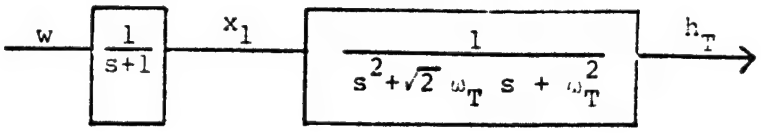

By selecting the covariance of the white noise and the cutoff frequency of the Butterworth filter, rms altitude variations and normal accelerations may be specified. Here, a cutoff frequency of $_t$ = .5 rad/sec was used and the noise covariance was chosen to give an rms altitude variation of 267 ft. and an rms acceleration of 3.1 g. Of course, the linearity of the problem allows us to scale the results to correspond to higher or lower accelerations.

The longitudinal short-period dynamics of the F8 without gmentation will be the baseline dynamics. The relevant equations may be found in Reference 5. The short period dynamics have a natural frequency of 2.28 rad/sec and a damping coefficient of .29; this represents poor short period handling qualities.[2] Because of this, and because we are interested in the effects of simulation parameters as a function aircraft dynamics, a set of augmented longitudinal dynamics will also be considered. A pitch command augmentation system (CAS) is used to modify the base airframe characteristics. The CAS design is a modified version of the design proposed in Reference 11.

The equations for the augmented dynamics are given in Reference 5. The F8 with the pitch CAS has short period roots with a natural frequency of 2.78 rad/sec and a damping coefficient of .64; this constitutes a significant improvement in the short period handling qualities.[2]

5. MODEL RESULTS

5.1 Continuous Model

The continuous model was used to analyze the effects of both simulation parameters and problem variables. With respect to the simulation, the effects of sample period and integration scheme are presented for the longitudinal CAS-OFF dynamics. Problem dependent effects are illustrated by comparing CAS-OFF and CAS-ON results.

We define a basic simulation configuration, corresponding to Figure 3, in which the cutoff of the de-aliacing filter is set at half the sample frequency, the visual servo has the DMS characteristics (ζ = .707, ω_n = 25 rad/sec), and a zero-order hold is used in data reconstruction.

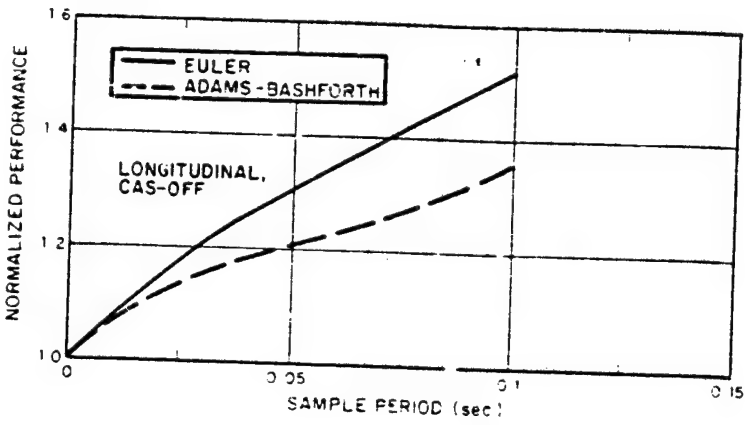

Figure 5. Effect of Discrete Simulation on Normalized Performance

Figure 5 gives normalized performance for the basic configuration as a function of sample period and integration scheme. Normalized performance is defined as the tracking error obtained for the simulation configuration divided by the tracking error that would be obtained in a continuous simulation with **no delays** (or in flight).* The normalization is determined by computing the performance utilizing the original, continuous state equations and assuming the only delay is that of the operator (.2 seconds).

Figure 5 shows substantial effects are introduced by the simulation, particularly at low sample rates. Even for the highest sample rate (T = .03125), there is a 16-20 percent performance degradation. A change of this magnitude exceeds the normal intra- and inter-subject variability in manual tracking tasks and would, therefore, be expected to be significant. For the lowest sample rates the performance degradation ranges from 35-50 percent, numbers that are clearly consequential. It is clear that, from a closed-loop tracking standpoint, A-B integration is superior to Euler integration.

The results in Figure 5 assume that the only adjustments in pilot strategy resulting from the simulation are an increase in prediction time to compensate for simulator delays and the adoption of an internal model that accounts for the amplitude distortions (and pole perturbations) introduced by the CPU. The results are based on the assumption of a fixed level of attention throughout. However, the pilot may choose to devote more attention to the task (work harder) and, thereby, reduce tracking error. A reasonable question to ask, then, is "How much more attention to the task would be required to achieve performance levels comparable to those that could be obtained in a continuous simulation?" This question can be addressed using the model for workload associated with the OCM.[9] The result of this analysis is shown in Figure 6.

*As might be the case in an all analog simulation with analog displays providing undelayed visual information.

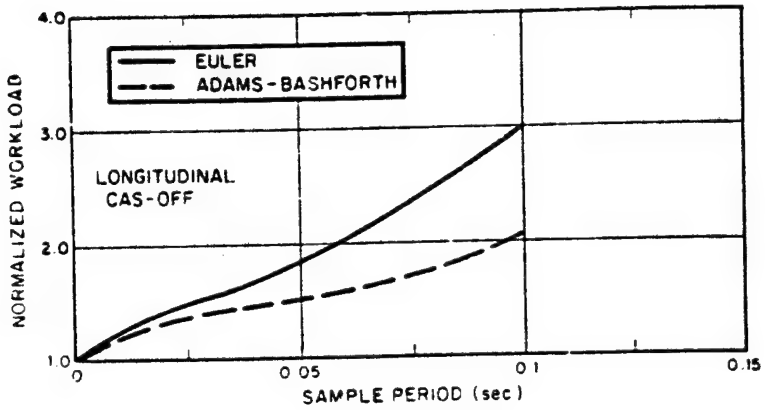

Figure 6. Simulation Workload Penalty

It can be seen from Figure 6 that to achieve the performance equivalent to that for continuous simulation, the pilot would have to increase his attentional workload by factors up to three for the conditions considered. There is a substantial workload penalty and it might be expected that a compromise between performance degradation and increased workload might evolve. This would be the case, especially if the pilot had not flown the vehicle or a continuous simulator in the same task so that there would be no basis for setting a criterion level of performance.

Before leaving the workload question, a further point is worth noting. In the describing function literature, it has been common practice to associate workload with the generation of lead. However, there has been no quantitative connection between the amount of lead and the increase in workload. In the present context, one can think of the increased prediction time necessary to compensate for simulator delays as imposing a (processing) workload analogous to that of lead generation. The measure of attentional workload given previously may then be thought of as an alternative means of quantifying the workload imposed by the requirement for additional prediction.

It was anticipated that there would be an interaction between the effects of simulation parameters and problem variables such as vehicle handling qualities. Thus, the above tracking task was analyzed for the CAS/ON configuration.

Figure 7 compares normalized longitudinal CAS-ON and CAS-OFF performance for the basic simulation. It can be seen that the CAS-ON performance is degraded more by the discrete simulation than the CAS-OFF performance. These results are explained by the fact that the delays introduced by digital integration are larger for CAS-ON dynamics than they are for CAS-OFF dynamics. The effects of longitudinal dynamics when viewed in terms of absolute performance are interesting and are also shown in Figure 7. The absolute performance for continuous simulation is better for CAS-ON than CAS-OFF (by about 3.5 percent) and the sensitivity to incremental computation delay is about

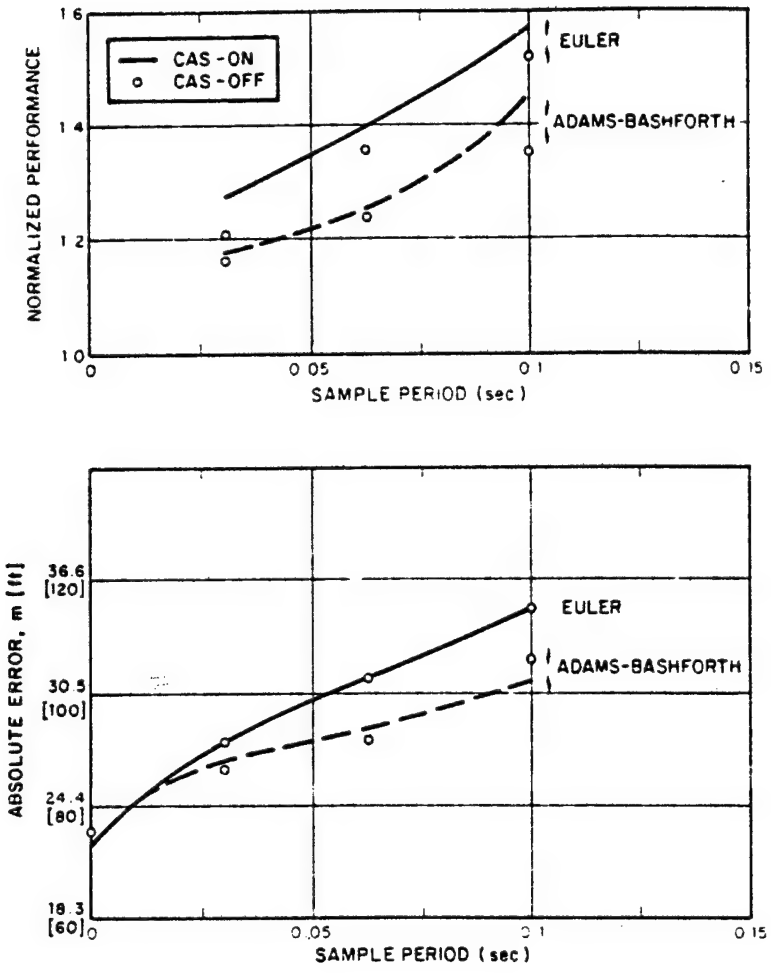

Figure 7. Effect of Vehicle Dynamics

the same for the two configurations. Thus, for a given simulation configuration, absolute performance for CAS-ON and CAS-OFF configurations will be about the same if Euler integration is used and the CAS-OFF configuration can give better performance if A-B integration is used. In other words, the discrete simulation washes out any improvement due to the CAS!

5.2 Hybrid Model

The hybrid model was used to investigate several issues that could not be examined readily in the continuous model context. Results were limited to the longitudinal unaugmented dynamics because of cost and time considerations

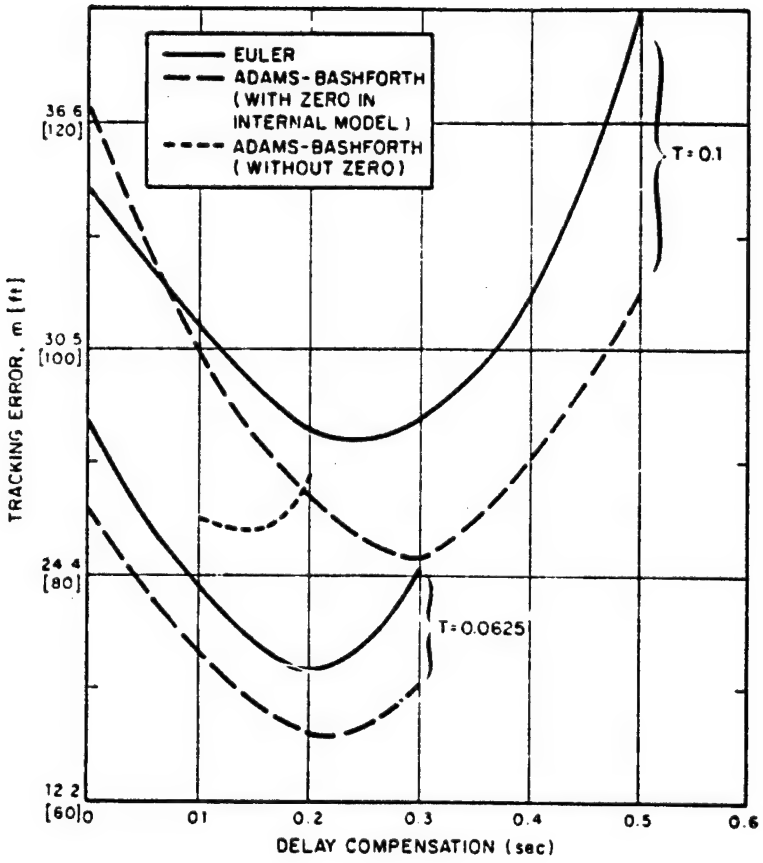

Figure 8. Effect of Operator Prediction Time

Figure 8 shows the sensitivity of performance to delay compensation time* for the basic simulation configurations with both Euler and A-B integration and

*The prediction time in excess of that needed to compensate for the operator's intrinsic delay of .2 sec.

for T = .1 and T = .0625. The "internal" models for the OCM in these cases are the continuous approximations to the discrete transfers that incorporate amplitude distortion effects; however, no delay is added to the human's delay of .2 seconds to account for the simulations delays. Thus, we expect the optimal prediction times to be approximately equal to the delay introduced by the simulation. This is indeed the case as can be seen in Figure 8. For Euler integration the minima occur at ~.26 sec and ~.2 sec. for T = .1 and .0625, respectively; the corresponding simulation delays are .27 and .19 .

For A-B integration the minima are at larger compensation times than for Euler. This is a result of the method used to account for amplitude distortion. (Recall that a zero was introduced in the transfer function and this necessitated an increased transport delay to match the phase lag at mid-frequencies.) With T = .1, the optimal prediction time is around .3 seconds and the simulation delay is ~.32 seconds. For T = .0625, performance does not appear to be very sensitive to prediction time in the neighborhood of the optimum. The simulation delay is ~.21 seconds and performance for this prediction time is indistinguishable from optimal performance. Figure 8 also shows a curve for the case where the operator's internal model does not include a zero to match the amplitude distortion of A-B integration. It can be seen that for this case a delay compensation of only ~.17 seconds is required. This corresponds to the delays introduced by the servo, pre-filter and zero-order hold. The optimal performance is marginally poorer than for the case with amplitude distortion included in the internal model. These results suggest that although including the zero provides a better model of the effect of A-B integration, the increased delay compensation needed to offset the extra lead should not be viewed here as a workload penalty.

These results confirm the estimates of simulation delay used in the continuous model. They also demonstrate implicitly how operators may adapt their behavior to compensate for simulator inadequacy. The added prediction required may impose a workload penalty as noted earlier.

Another form of adaptation to the simulation involves the pilots internal model. Two questions are of interest: 1.) What model will the trained operator adopt when "flying" the simulator?; and 2.) What is the "transfer" effect of a wrong model when transitioning from discrete simulator to continuous simulator (flight)? At least partial answers to these questions for the longitudinal dynamics and Euler integration are provided by the results shown in Figure 9.

Figure 9 gives performance vs. delay compensation for T = .1 and two internal models. One internal model is that derived to match the corresponding discrete transfer function while the other is the basic continuous model. It can be seen that better performance is obtained when the internal model corresponds to the approximate discrete model implying that this is a better model of the discrete simulation than is the original continuous model. Figure 9 also shows the effect of using the model corresponding to T = .1 seconds in a simulation where the actual sample period is .03125 seconds (i.e., nearly continuous) as compared to using the model for T = .03125 seconds (i.e., the correct one). If the operator optimizes delay compensation, performance will be degraded by about 10%. If, on the other hand, the delay compensation appropriate to T = .1 is used, a performance penalty of about 19% will be incurred. The effect is not substantial here but it might be in other tasks.

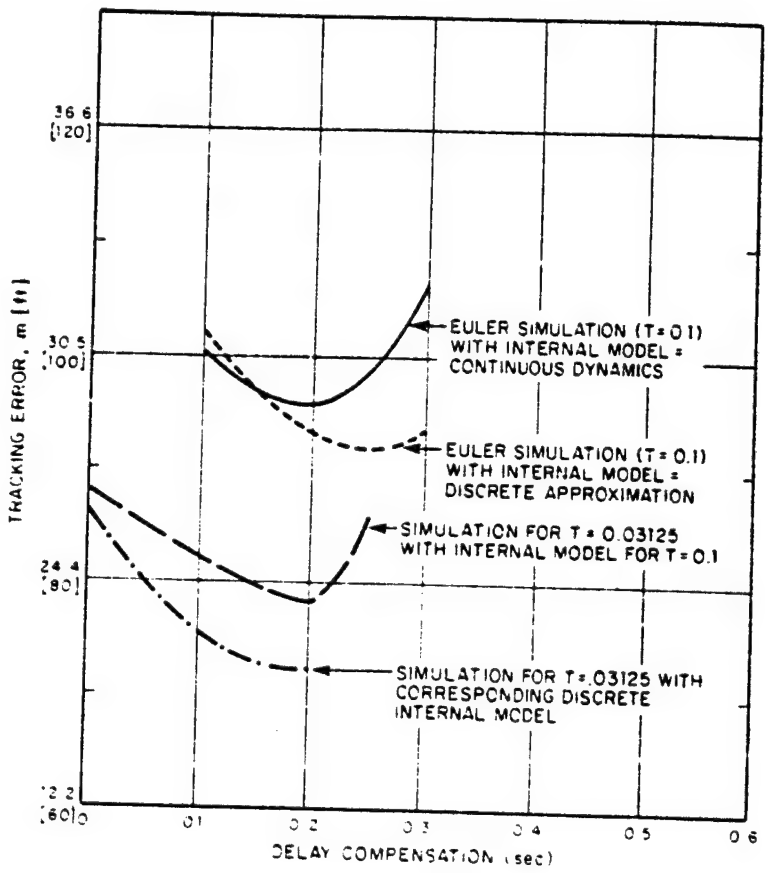

Figure 9. Effect of Internal Model

The effect of the cutoff frequency of the de-aliasing filter on performance is shown in Figure 10. Euler integration of the vehicle equations is used and other simulation parameters correspond to the basic configuration. The results are for a sample frequency of 10 Hz (T = .1) so a cutoff frequency of ω_c = 5 Hz satisfies the Nyquist requirement. Results are obtained for ω_c = 1, 5 and 20 Hz, respectively. The lowest value of ω_c = 20 Hz is based on the assumption that there is not significant signal power beyond 5 Hz so there is no need to set the filter break-point at that frequency and incur the delay penalty. The results in Figure 10 favor using the higher cutoff frequency, ω_c = 20 Hz, for this problem. Furthermore, there is a substantial penalty for using the low frequency cutoff. These two results imply that aliasing is not a problem here. We also note that the performance minima for ω_c = 20 Hz and 5 Hz occur at about the correct value of prediction time; the optimum prediction time for ω_c = 1 Hz

is much larger but not quite so large as the estimated total simulation delay of

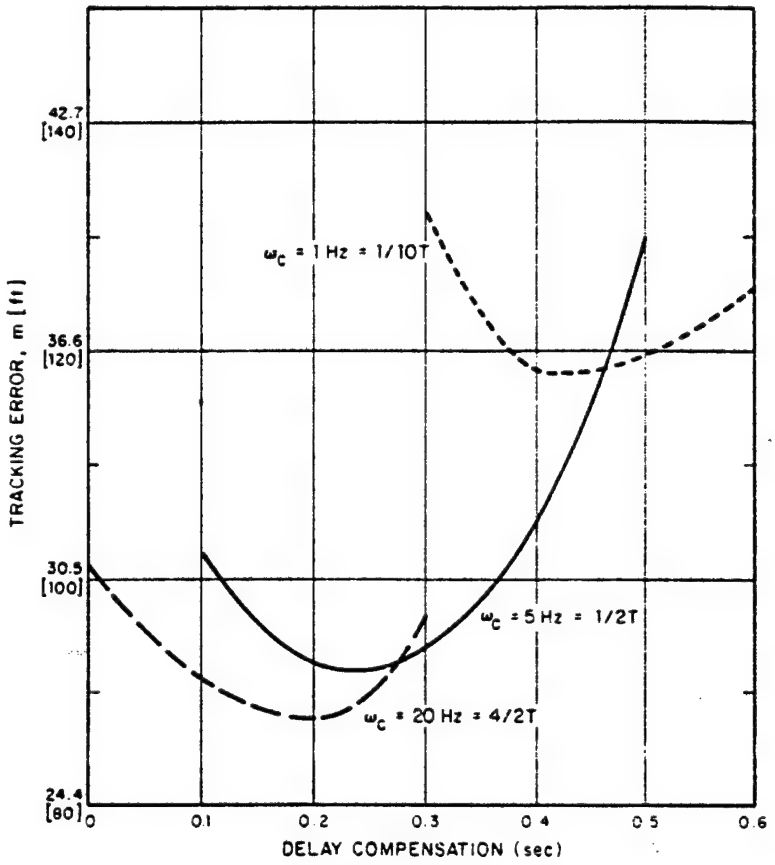

Figure 10. Effect of Dealiasing Filter Cutoff Frequency

.53 seconds.

The effects of using a first order hold instead of a zero order hold are shown in Figure 11 for both Euler and A-B integration at T = .1 and for Euler integration at T = .0625. The corresponding best zero order hold performance values are also shown for comparison purposes. At a sample period of .1 seconds, slightly lower tracking errors are obtained for Euler integration with a first order hold than with a zero order hold; in addition, the minimum performance is obtained with less delay compensation. The situation for A-B integration and a .1 second sample period is the reverse of that for Euler. That is, for A-B integration the first order hold degrades performance.

A possible explanation for these results is as follows. The first order hold uses intersample information which provides some lead. For long sample

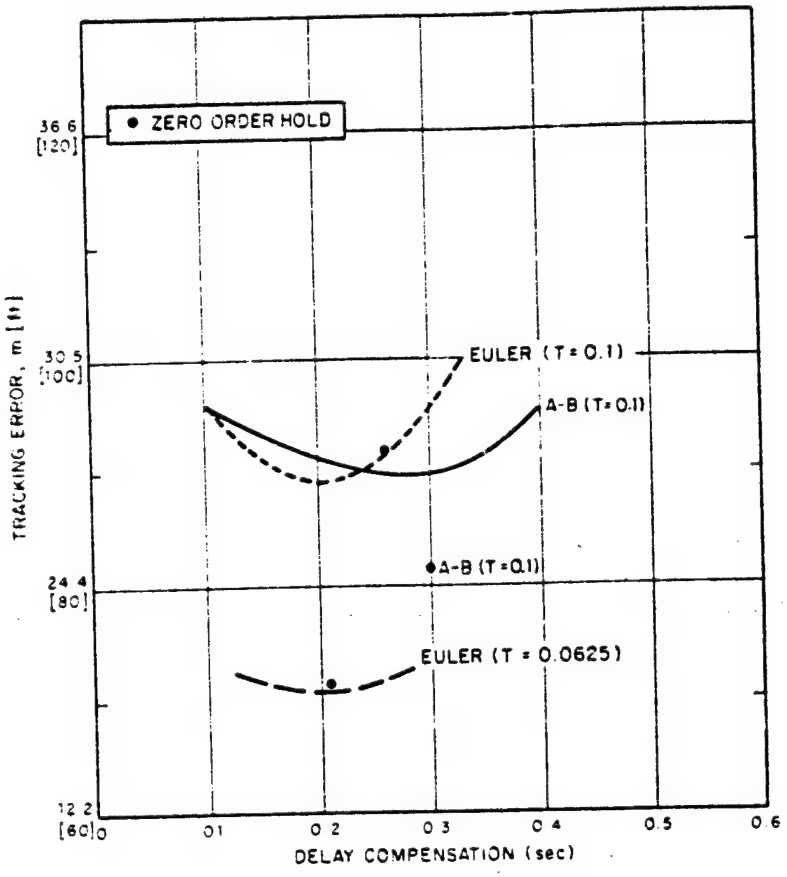

Figure 11. Effect of First Order Hold

periods and Euler integration, the effective lead provided is apparently more beneficial than the lag penalty associated with the higher order hold. The beneficial effects of a first order hold should decrease as the sample period decreases. This is supported by the results for T = .0625 which show no difference between the two holds. In the case of A-B integration the added delay of the first order hold dominates. This may be due to A-B integration having an implicit first order hold at the input, thereby reducing any advantage in adding such a hold at the output.

6. SUMMARY AND CONCLUSIONS

In this paper we have examined the effects of simulation parameters and components on simulator fidelity, particularly with regard to predicting operator performance and workload. Our focus has been on the dynamical aspects of simulator primarily as they relate to closed loop control. We have generally ignored questions that would necessitate inclusion of detailed models for cue perception leaving these to future study.

An approximate continuous model of the discrete simulation was incorporated in the standard optimal control model for the human operator. The resulting continuous closed-loop model was used to analyze both overall simulation effects and the effects of individual elements. The results showed that, as compared to an ideal continuous simulation, the discrete simulation could result in significant performance and/or workload penalties. The magnitude of the effects depended strongly on sample period as expected. From a closed-loop standpoint it seemed clear that A-B integration was much to be preferred. With respect to the other simulation components it can be said that any reduction in delay is desirable. Such reductions inevitably involve increased costs (hardware or software) which must be balanced against the expected improvements.

In addition to the continuous model, a hybrid model was developed to allow investigation of situations that could not be treated adequately with the continuous model. Several interesting results were obtained with this model. It was shown that for this (fairly typical) aircraft control problem signal bandwidths were such that the de-aliasing filter cutoff frequency could be set at a value greater than half the sample frequency. Also, there appeared to be a potential under certain conditions for improved simulator performance with a first order hold (rather than a zero order hold). The model was also used to show demonstrable effects for adopting the simulator dynamics as an internal model. The need to compensate for simulator delays via added prediction was also shown.

We believe the models developed here can be very useful in developing engineering requirements for flight simulators. These requirements will be problem dependent which is one reason why models are needed. As we see it now, the process for using the models would involve the following steps:

i) Use standard OCM to analyze ideal continuous simulation to develop baseline performance and to determine expected signal bandwidths.

ii) Analyze distortion introduced by discrete integration schemes and develop continuous models for discrete dynamics valid over the band of interest.

iii) Analyze effects of integration, cue dynamics etc. using continuous model.

iv) Use hybrid model to examine effects of data reconstruction, de-aliasing cutoff frequency etc.

Before this procedure could be used with complete confidence the models described herein need further validation and extension. It is especially important to collect data in a carefully controlled experiment to verify the individual simulation effects.

REFERENCES

1. Gum, D. R. and W. B. Albury, "Time-Delay Problems Encountered in Integrating the Advanced Simulator for Undergraduate Pilot Training," **Journal of Aircraft**, Vol. 14, No. 4, April 1977.

2. Queijo, M. J. and D. R. Riley, "Fixed-Base Simulator Study of the Effect of Time Delays in Visual Cues on Pilot Tracking Performance," NASA TN D-8001, October 1975.

3. Kleinman, D. L., S. Baron and W. H. Levison, "An Optimal Control Model of Human Response," **Automatica**, Vol. 6, No. 3, pp. 367-384, May 1970.

4. Baron, S., "A Model for Human control and Monitoring Based on Modern Control Theory", **Journal of Cybernetics and Information Science**, Vol. 1, No. 1, Spring 1976.

5. Baron, S., R. Muralidharan and D. L. Kleinman, "Closed Loop Models for Analyzing Engineering Requirements for Simulators", Bolt Beranek and Newman Inc., Report No. 3718, May 1978.

6. Baron, S. and J. Berliner, "The Effects of Deviate Internal Representations in the Optimal Model of the Human Operator," **Proceedings of Thirteenth Annual Conference on Manual Control**, M.I.T., Cambridge, Mass., June 1977.

7. Rosko, J.S., "Digital Simulation of Physical Systems" Addison-Wesley Publishing Co., Reading, Mass., 1972.

8. Ashworth, B.R. and W. M. Kahlbaum, Jr., "Description and Performance of the Langley Differential Maneuvering Simulator," NASA TN D-7304, NASA, Langley Research Center, June 1973.

9. Levison, W. H., J. I. Elkind and J. L. Ward, "Studies of Multi-Variable Manual Control Systems: A Model for Task Interference," NASA CR-1746, May 1971.

10. Kleinman, D. L., S. Baron and J. Berliner, "MCARLO: A Computer Program for Generating Monte-Carlo Trajectories in a Time-Varying Man-Machine Control Task," U.S. Army Missile Research and Development Command, Tech. Report TD-CR-77-2, Redstone Arsenal, Ala., June 1977.

11. Hartmann, G. L., J. A. Hauge and R. C. Hendrick, "F-8C Digital CCV Flight Control Laws," NASA CR-2629, February 1976.

N79-15599

PROSPECTS OF A MATHEMATICAL THEORY OF HUMAN BEHAVIOR IN COMPLEX MAN-MACHINE SYSTEMS TASKS*

Gunnar Johannsen** and William B. Rouse

Department of Mechanical and Industrial Engineering
Coordinated Science Laboratory
University of Illinois
Urbana, Illinois 61801

SUMMARY

Many useful mathematical models for manual control monitoring and decision-making tasks in man-machine systems have been designed and successfully applied. However, critical comments have occasionally been made, mainly by practitioners concerned with the design of complex man-machine systems. They blame especially models which seem to explain only data from abstract subtask experiments designed particularly for these models.

In this paper, an initial approach to bridging the gap between these two points of view is presented. From the manifold of possible human tasks, a very popular baseline scenario has been chosen, namely car driving. A hierarchy of human activities is derived by analyzing this task in general terms. A structural description leads to a block diagram and a time-sharing computer analogy.

The range of applicability of existing mathematical models is considered with respect to the hierarchy of human activities in real complex tasks. Also, other mathematical tools so far not often applied to man-machine systems are discussed. The mathematical descriptions at least briefly considered here include utility, estimation, control, queueing, and fuzzy set theory as well as artificial intelligence techniques. Some thoughts are given as to how these methods might be integrated and how further work might be pursued.

* This research was supported by the National Aeronautics and Space Administration under NASA-Ames Grant NSG-2119.

**Permanent address: Research Institute for Human Engineering (FAT) D-5309 Meckenheim, F.R. Germany

INTRODUCTION

When designing such systems as automobiles, aircraft, power plants, and management information systems, it is very important to understand the human's role in the system and design the man-machine interface appropriately. The engineering approach, which leads one to represent the machine in terms of differential equations, networks, etc. suggests that the human can also be represented as a set of mathematical equations for the purpose of systems analysis and design. Thus, considerable effort has been devoted to developing mathematical models of human behavior.

Despite the criticisms of those who find the analogy between humans and equations unpalatable, many models have been reasonably successful within the limited domains that they addressed. In fact, if we accept the premise that human behavior mainly reflects the external environment [1], then it is not surprising that man and machine can be described in similar terms. Quite simply, since the human adapts his behavior to the machine, his actions become somewhat machine-like. (Of course, from a design point of view, one tries to avoid requiring the human to adapt to the machine to any extreme extent.)

On the other hand, the success of models in limited domains has not had substantial impact in realistically complex domains. For example, manual control models are not everyday tools for the aircraft designer. Further, as the reader will see manual control models capture only a small portion of the <u>total</u> task of driving an automobile. For these reasons, designers have been known to claim that mathematical models of human behavior are not particularly useful. While the authors only partially agree with this opinion, even as it relates to currently available models, such statements have motivated the work upon which this paper is based.

Within this paper, the authors present a realistically complex task (i.e., automobile driving) and illustrate the various aspects of the task by using written protocols of subjects' behavior. A hierarchy of human activities is derived by analyzing this task in general terms. A time-sharing computer analogy and block diagram are presented. Numerous mathematical methodologies appropriate to representing such a model are discussed. Finally the state-of-the-art is summarized and the prospects are considered.

A REALISTIC TASK

In considering alternative realistic task domains, the authors discussed a variety of domains including aircraft piloting, industrial process monitoring, and automobile driving. After substantial discussion, it became quite clear that the domain to which both the authors and potential readers could most relate was automobile driving.

The "experiment" involved a hypothetical trip from the driveway of one author's house (GJ) to the home of the other author (WR). Two subjects participated (GJ and WR). Their task was to explain in detail what they would be doing throughout the hypothetical trip. Each subject independently generated a written protocol of the trip. The two resulting protocols were merged to produce Figure 1.

The activities in this figure can be categorized into several levels of behavior:

1. Reaching, twisting, and listening
2. Steering, accelerating, and braking
3. Looking around and estimating
4. Updating and evaluating
5. Planning
6. Reflecting and daydreaming

The authors would like to suggest that a theory of human behavior in realistic tasks should be able to model levels 1 through 5. In pursuit of this possibility, this list was somewhat compacted to yield the following aspects of behavior to be modeled:

1. Sensing and interpreting inputs
2. Planning
3. Implementing plans

To consider these three topics, an overall framework will be discussed in the next section and then, specific approaches to modeling will be considered in the subsequent section.

STRUCTURAL DESCRIPTION

Looking at the hierarchy of human activities discussed above as information processing activities, a time-sharing computer analogy seems to be a very appealing approach to understanding the structural interrelationships.

Figure 2 shows a sketch of such a time-sharing computer analogy. There are several possibilities for the central nervous system (CNS) to interact with the peripheral input and output devices (i.e., the sensory and the motor systems including speech generation). The CNS is viewed as being divided into an operating system and four classes of "jobs," i.e., program/data files (see, e.g., [2], [3]). Hereby, a multi-processor system allowing a mixture of parallel and serial information processing is most likely to be a reasonable assumption for the human operator [4].

The operating system is responsible for scheduling the programs in a time-shared manner by using a priority interrupt policy. Conflicting criteria with respect to priority have to also be evaluated by the operating system. This might be a crucial task, especially in urgent situations.

Figure 1: Protocol for Typical City Trip

INSERT KEY IN IGNITION

PUT ON SEAT BELT

PRESS GAS PEDAL TO FLOOR AND ALMOST TOTALLY RELEASE

TURN KEY

LISTEN FOR ENGINE SOUND

IF SO, THEN GIVE GAS

ELSE, STOP AND GO BACK TO TURN KEY

WAIT FOR CAR TO WARM UP - DAYDREAM

LOOK AROUND - SEE IF I CAN BACK UP OKAY - INCLUDES USING MIRRORS

IF SO, THEN PUT CAR IN REVERSE

ELSE, WAIT FOR ALL CLEAR

PUT RIGHT ARM ON SEAT BACK SO AS TO SEE BETTER

STEER WITH LEFT ARM, ACCELERATE AND BACK ONTO STREET

DETERMINE WHEN CLEAR TO GO FORWARD - STOP BACKING UP - PRESS BRAKE

PUT CAR IN DRIVE

LOOK AROUND - SEE IF I CAN PROCEED

IF SO, ACCELERATE

ELSE, WAIT FOR ALL CLEAR

LIMIT SPEED SINCE STOP SIGN COMING UP - CONTINUE LOOKING AROUND

STEER SO AS TO STAY "SORT OF" IN LANE

ESTIMATE DISTANCE TO STOP SIGN - CHECK FOR TIME TO DECELERATE

IF SO, REMOVE FOOT FROM GAS AND OVER TO BRAKE

ELSE, UPDATE ESTIMATE OF DISTANCE - CONTINUE LOOKING AROUND/STEERING

TURN ON LEFT DIRECTIONAL

WHEN FAIRLY CLOSE TO STOP SIGN, PUSH BRAKE HARDER AND STOP

LOOK LEFT AND RIGHT FOR TRAFFIC

IF NONE TOO CLOSE (ESTIMATE IF I CAN MAKE IT) ACCELERATE TURN LEFT

ELSE, WAIT FOR ALL CLEAR AND CONTINUE UPDATING ESTIMATES

STRAIGHTEN OUT SO AS TO KEEP "SORT OF" IN LANE

ACCELERATE, BUT NOT TOO MUCH BECAUSE STOP SIGN COMING UP

LOOK AROUND AT TRAFFIC - ALSO AT HOUSES AND YARDS - DAYDREAM

EXECUTE STOP SIGN ROUTINE - ONE FOR STOPPING - ONE FOR STARTING

- USE FOUR-WAY STOP SIGN ROUTINE

EXECUTE ENROUTE ROUTINE - INCLUDING TALKING, SIGHTSEEING, ETC.

.

.

PLAN ROUTE - WHAT STREETS TO TAKE

.

.

EXECUTE STOP SIGN/STOP LIGHT/TURNING/PASSING/LANE CHANGING ROUTINES

LOOK AROUND FOR APPROPRIATE PARKING SPACE

IF ONE FOUND, DETERMINE PLAN FOR GETTING INTO IT

ELSE, CONTINUE LOOKING - CONTINUE LOOKING AROUND AND STEERING

EXECUTE PLAN OPEN-LOOP, WITH FINAL UPDATES AS ERRORS CAN BE ESTIMATED

PUT CAR IN PARK

TURN OFF RADIO HEATER, ETC., IF APPROPRIATE

TURN OFF KEY

REMOVE KEY

The four classes of program/data files relate to a central-nervous representation of tasks the human operator has to perform. Each of these program classes is structured into main programs and interrelated subroutines.

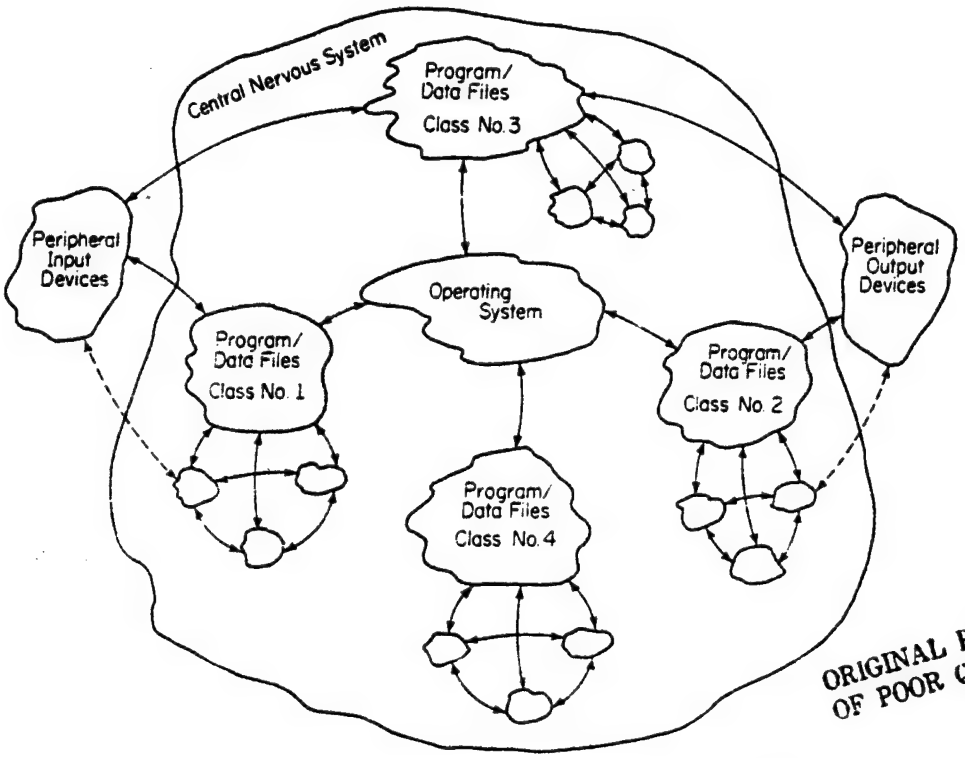

Figure 2: Sketch of a Time-Sharing Computer Model of the Human Operator

Class No. 1 comprises input-related programs, e.g., human monitoring tasks and looking around procedures. Class No. 2 is similarly related to output activites, e.g., the structural organization of motion patterns (e.g., in reaching) and speech. Class No. 3 programs describe strict input-output relationships as in tracking-type control and choice-reaction tasks. All three classes contain programs with a high level of autonomy, perhaps carried out by peripheral processors. The operating system has to initiate and supervise these autonomous processes. Additionally, the adaptive control of the sampling process in parallel tasks has to be accomplished by the operating system.

Class No. 4 represents the long-term memory of the human which includes a knowledge base of facts, models, and procedures. The programs of class No. 4 are concerned with internal processes such as reflecting and planning which have access to the knowledge base, thereby occasionally

modifying it. The operating system is responsible for searching through the knowledge base (see, e.g., [5], [3]).

The time-sharing computer analogy outlined here is mainly assumed as a possible framework for future thinking about complex man-machine systems. To further illustrate the hierarchical multi-level structure of human activities within this framework, a block diagram is shown in Figure 3. Only the most important information flows between the different levels are outlined.

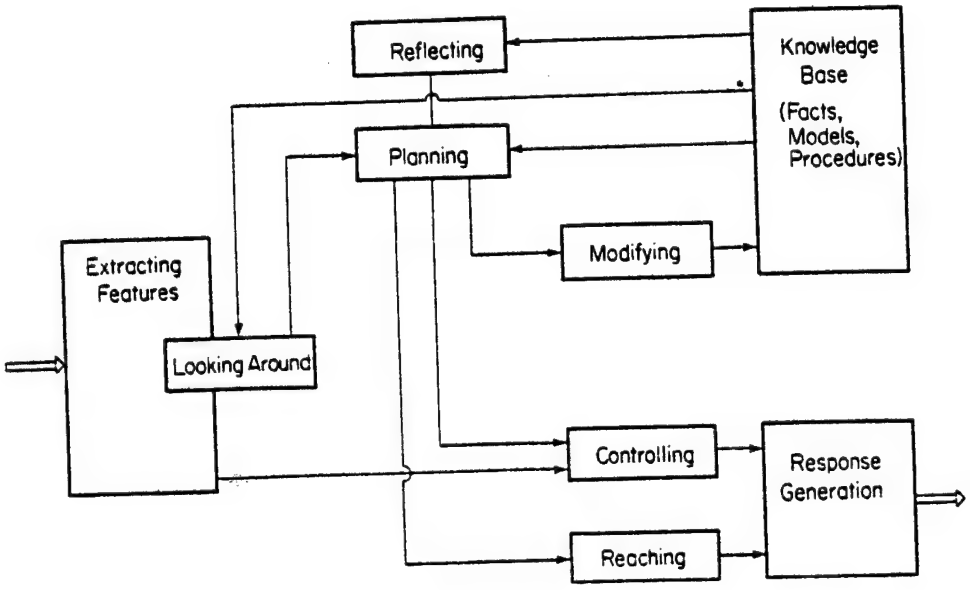

Figure 3: Hierarchical Multi-Level Structure of Human Activities

Lower level processes (bottom of Figure 3) are normally characterized by events occurring at a high frequency as compared to higher level processes (top of Figure 3). This refers to different time scales for different levels. However, because lower level processes may be autonomous, the difference in time scales does not mean that these processes have to be considered by the operating system more frequently.

In Figure 3, planning is denoted as a major activity. With data from the knowledge base and those from lower-level looking around procedures, sometimes influenced by higher-level reflecting, planning is the development of procedures to achieve overall goals and subgoals for lower-level processes. Modifying the knowledge base as well as goal-setting for controlling and reaching are shown as examples. Controlling itself is also best described as a multi-level structure, being a subset of the overall multi-level structure of Figure 3. Controlling and

reaching procedures result in output actions of the human operator via response generation which refers to the peripheral output devices in Figure 2. Correspondingly, the peripheral input devices of Figure 2 extract task-relevant features from sensory input information. This process is very closely linked with looking around procedures which are also indicated in Figure 3.

MATHEMATICAL MODELS

Sensing and Interpreting Inputs

Reconsidering the task analysis of car driving, how does the driver recognize stop signs, other cars, children, etc? Could one, at least in theory, develop an algorithm that successfully performs these aspects of driving?

To pursue this question, the literature of pattern recognition and artificial intelligence was considered. Fortunately, the literature in these areas has recently been summarized in the Systems, Man, and Cybernetics Review [6], by Sklansky [7], and in books by Winston [8], [9] for pattern recognition and artificial intelligence respectively.

Two approaches to pattern recognition have received particular attention: statistical methods and syntactical methods. The statistical methods use discriminant functions to classify patterns. This involves extracting a set of features from the pattern and statistically determining how close this feature set is to the a priori known features of candidate classes of patterns. The class whose features most closely match the measured features is chosen as the match to the pattern of interest, with of course some consideration given to the a priori probabilities of each class and the costs of errors.

The syntactic methods partition each pattern into subpatterns or pattern primitives. It is assumed that a known set of rules (a grammar) is used to compose primitives into a pattern. One approach to recognizing primitives is to use the statistical approach noted above.

Another aspect of pattern recognition involves image processing. Here, each picture point (pixel) is classified according to gray level. Then, thresholds are used to segment the picture. More elaborate approaches use multi-dimensional classification of each pixel and then use an appropriate multi-dimensional clustering of similar pixels.

Artificial intelligence researchers have devoted considerable effort to scene analysis. With emphasis on understanding scenes composed of somewhat arbitrary collections of blocks, methods have been developed to pick particular blocks out of scenes, even if the desired block is partially hidden.

Most of the methods discussed above have worked reasonably well within limited domains. When the context within which one is working is well-understood, it is often possible to successfully sense and interpret

inputs, although considerable computational power may be needed.

While the advent of inexpensive microelectronics might allow one to utilize large amounts of computational power in a model of human sensing and interpretation of data, there are bigger problems to be solved. Namely, it is difficult to deal with realistic contexts in a static manner. What a human sees depends on what he is looking for, what he expects to see, and the costs of not seeing it. These aspects of seeing cannot be considered out of context and without reference to the specific individual involved.

Several investigators have considered the issue of how the human allocates his attention among multiple displays [10], [11], [12], [13], [14]. However, these models have only been tested in fairly well-structured situations and thus, are as yet unproven in realistically complex tasks. Further, it is by no means obvious that these models will ever be able to handle looking around in the sense it appears in the driving scenario.

Thus, a general mathematical theory of human sensing and interpreting of inputs is far from available, especially if one would like to program this theory to drive a car. On the other hand, the disciplines of pattern recognition and artificial intelligence are beginning to succeed in specific applied domains such as industrial inspection [15], [16] and medical diagnosis [17]. Perhaps a concatenation of specific successes will lead to new insights into the problems of context and individual differences.

Planning

Studying the task analysis of car driving, it is readily apparent that much of the subjects' conscious activities were devoted to developing, initiating, and monitoring plans. This observation agrees with analyses of verbal protocols in several other task domains [1]. In fact, one might expect this result within any purposeful activity for which there are goals as yet unfulfilled.

To discuss planning, one first must emphasize the distinction between the process of developing plans and the process of executing plans [18]. Within this section only plan development will be considered, while the following section will discuss plan execution. One way to illustrate the difference between these two activities is to characterize plan development as a problem solving activity, while plan execution is looked at as a program execution activity [1].

One develops a plan in hopes that its execution will achieve some goals. While one usually accepts the overall goal as given (e.g., land the aircraft), the process of developing subgoals is often left to the human. The partitioning of goals into subgoals and then subgoals into lesser subgoals, etc. reflects a hierarchical mode of planning that has received considerable attention [19], [20].

The hierarchical approach allows one to develop plans that are broad and sketchy as opposed to detailed and concise. Thus, low level subgoals can be temporarily ignored until their immediacy demands attention. Similarly, future actions which require preconditions that are not as yet assured can perhaps be temporarily ignored if one feels that the environment is hospitable to one's goals [20].

On the other hand, low level subgoals must eventually be dealt with. Then, a concise system dynamics model such as Carbonell's probably provides a reasonable description of human behavior [21]. This model assumes that the human is dealing with a system describable by quantitative state transitions and amenable to quantitative control actions.

Such low level planning is probably unconscious. From the perspective of a computer analogy, one might say that high level conscious planning is like executing an interpreted program. (An interpreted program is one where the computer consciously has to interpret the meaning of each statement as it is executed.) On the other hand, low level unconscious planning is similar to executing a compiled program [1]. In fact, it might be claimed that low level planning cannot really be called planning. Instead, such activities are only the details of implementation, which are discussed later in this paper.

Planning appears to include the following aspects:

1. Generation of alternative plans,
2. Imagining of consequences,
3. Valuing of consequences,
4. Choosing and initiating plan,
5. Monitoring plan execution,
6. Debugging and updating plan,

where the latter three aspects deal with observing plan execution and subsequent replanning, but <u>not</u> with actual implementation.

How might one model the generation of alternative plans? One can look at a plan as a linked set of subplans [20]. However, at some level, subplans must be specific. In many tasks, the alternatives are clearly defined at the outset. On the other hand, there are many interesting tasks (e.g., engineering design) where the human must create alternatives. In such cases, humans usually first consider alternatives that have been successful in previous situations.

One might use Newell's pattern-evoked production systems as a model of how the human accomplishes this search for alternatives [1]. A production is a rule consisting of a situation recognition part that is a list of things to watch for, and an action part that is a list of things to do. (The word "production", as it is used here, has absolutely nothing to do with the manufacturing connotation of the word.)

As an alternative to production systems, the idea of scripts might provide a reasonable model, "A script is a structure that describes appropriate sequences of events in a particular context" [22].

The ideas of production systems and scripts are both related to the idea of the human having an internal model. However, as the reader will see, it is very different from the type of model assumed in the system dynamics domain. Namely, productions and scripts provide forecasts of typical consequences rather than models of internal state transitions.

Sometimes a <u>new</u> alternative is needed and it is very difficult to say how a totally new idea is generated. Linking the idea of associative memory [23], [24] with the idea of production systems or scripts, one can conjecture that new ideas are generated when the criterion for matching the new subgoal with past experiences is relaxed and/or non-standard features of the situation are emphasized.

Long-term plans that will not be immediately implemented are probably developed at the highest level in the goal hierarchy with only major goals considered. Such a plan might be a somewhat vague verbal statement or perhaps a sketch of activities and relationships. It is interesting to speculate upon (and perhaps research) what plans look like in the "mind's eye." For example, are plans list-like or are they more spatial, such as Warfield's interpretive structural models [25].

Short-term plans that will require immediate implementation cannot be quite so sketchy. In this case, the human has to consider specific actions. One would probably be reasonably successful in modeling this type of plan using production systems. In this case, specific features of the environment would automatically evoke particular responses. This type of behavior falls into the category of class No. 3 programs as defined in the time-sharing computer analogy introduced earlier. Realistic examples of application of this idea include aircraft attitude instrument flying [26] and air traffic control [27].

Given a set of candidate plans, the human must forecast or imagine the consequences of implementing each plan. One might assume that the human performs some type of mental simulation of the plan. For example, the human might use his current perception of the system dynamics to extrapolate the system's state as a function of planned control strategy. Rouse has developed a model that describes this type of behavior. Succinctly, the model assumes that the human has both a long-term and short-term model of the system with which he is dealing and, that he uses a compromise between the two state predictions obtained from these models as a basis for decision making [28].

However, when plans are sketchy, at least in terms of intermediate preconditions, the human probably does not actually calculate consequences but instead simply maps plan features to previously experienced consequences. Then, until evidence forces him to reject the assumption, he assumes these previously experienced consequences will prevail. This type of behavior is represented quite nicely by the scripts concept [22].

Imagined consequences are then compared to goals. For low level plans, the comparison might be based on a well-defined criterion function. However, this is probably not the case for high level plans. Since high level goals and imagined consequences may be verbal and rather vague, it is likely that the human only tries to satisfice rather than optimize. One might represent this phenomenon using multi-attribute utility functions [29] that have broad optima. Alternatively, concepts from fuzzy set theory [30], [31] might be used to consider the membership of a set of consequences in the fuzzy set of acceptable consequences. The utility function approach is probably appropriate if one assumes that the human has a fairly precise knowledge of the possible consequences, and subsequently values some more than others. On the other hand, the fuzzy set approach would seem to be applicable to situations where the human's perception of the consequences is actually fuzzy.

The human chooses the most satisfactory plan and initiates its execution. If none of the available plans meets an acceptable level of satisfaction, the human either tries to debug the set of plans under consideration or perhaps tries to develop new plans. Debugging of partially failed plans may initially involve local experimentation to determine the cause of plan failure rather than a global reevaluation and complete replanning [32]. One approach to modeling debugging or trouble-shooting of plans is with fuzzy set theory [33].

Assuming that a plan has been initiated, the human monitors its execution and only becomes involved (in the sense of planning) if the unanticipated occurs or execution reaches the point that some phase of the plan must be more concisely defined. Monitoring for the unexpected might be modeled using production systems that trigger when the preconditions are not satisfied. Other approaches, based on filter theory [34] or pattern recognition methods [35], are also available but beyond the scope of the discussion here.

Once the unexpected has been detected, planning might shift into the above mentioned debugging mode. On the other hand, the need to shift from sketchy to concise planning may involve abandoning, for the moment, the broad hierarchical mode and shifting to a detailed partially pre-programmed mode.

How do all these bits and pieces fit into an overall model of planning? While it does seem that the hierarchical approach to planning combined with the production system and script ideas provide a reasonable framework, the state-of-the-art certainly does not allow one to construct a context-free planning model in the form of an executable computer program. This may be an inherent limitation if one accepts the premise that much of human behavior is merely a reflection of the task environment [1]. If this premise is true, then one should be very careful that laboratory abstractions capture a sufficient portion of the real world environment and thereby allow results to actually be transferable. Otherwise, one is only developing a theory of human behavior in laboratory games.

As a final comment on planning, a very important issue concerns the level at which one's study of planning behavior should be addressed. While an approach at the neuron level [36] may eventually lead to a successful model of human planning behavior, such an approach is unlikely to lead to success in the near future. Alternatively, one might try to develop models that explain or predict whether or not a plan will be successful. However, this type of model would yield little information about the planning process. It seems that one must approach studies on the conscious planning level using either verbal protocols [1], [37], [38] or at least methods that require plans to be explicitly measurable. Then, the variety of approaches to modeling discussed in this section can be applied to describing the planning process.

IMPLEMENTING PLANS

Implementing plans refers to human action, mainly controlling and reaching in the multi-level structure of Figure 3. Two basic approaches for mathematically describing these actions can be distinguished. The first approach includes time-line analysis, queueing theory, and simulation techniques, whereas the second includes the control theoretic approach in a more general sense.

In time-line analyses, the execution times of all particular task elements of a certain multi-task situation are assessed as well as the total task time needed [39], [40], [41], [42]. Available time margins or expected time pressure of the human operator can be calculated in order to estimate total task system performance and human operator workload. This method has been applied to evaluating rather complex man-machine systems by taking these apart in very much detail, e.g., to the level of reaching times for single switches.

A related but more analytical approach is the queueing theoretic one [11], [12], [43], [44], [45], [46], [47]. It is suitable not only for analysis but also for design purposes. The different tasks of a multi-task situation are considered as customers in a queue waiting to be serviced. Arrival and service rates as well as the waiting time for the tasks are characteristic measures. Service with a priority policy is possible. Also several servers (e.g., the human operator and a computer) may share responsibility for the total task.

Both approaches, time-line analysis and queueing theory, look at the implementation of actions in terms of time expenditure. If the accuracy of the actions is also to be taken into account, these methods have to be combined with others. Simulation techniques seem to be a reasonable approach where micro-subroutines simulate dynamically such human operator behaviors as short-term memory recall and movement of hands and feet [48]. This leads back to the time-sharing computer analogy. A goal-oriented priority interrupt structure for handling all tasks appropriately in a multi-task situation is most promising. However, this results in a more artificial-intelligence oriented simulation, using heuristics and data handling algorithms, rather than an analytical description.

A different approach for the description of human actions in man-machine systems applies control theory. Models for continuous manual control are well established. Numerous summaries in the forms of reports and books exist (e.g., [49], [50], [51]). Most popular are the quasi-linear and the optimal control models. The quasi-linear models describe the human control behavior by some task-specific modification of a generalized transfer function which is best satisfied in the crossover frequency region for many controlled element dynamics. In addition, an internal human noise source (the remnant) summarizes the portion of the human's output which cannot be explained linearly.

The optimal control model [52] includes two noise sources and also has a time delay and a neuromuscular lag term with a time constant similar to that of the quasi-linear model. A Kalman filter estimates the states of the controlled element, whereas a predictor compensates for the time delay. The optimal gains are calculated with respect to a criterion function which is a weighted sum of mean squared values of state and control variables.

The control theory models have been applied in several domains including aircraft piloting, automobile driving, ship piloting, and anti-aircraft artillery. Further, several display design methodologies have been developed. A recent special issue of Human Factors reviews many applications of control theory models [53].

With both the crossover model and the optimal control model, a stochastic reference input, either forcing function or disturbance, has been assumed. Therefore, these models are mostly applicable to the inner loops of manual vehicle guidance and control tasks. In the case of the optimal control model, key elements of this have also been applied to monitoring and decision-making tasks.

Many realistic tasks exist, however, in which deterministic inputs are dominant. Taking the baseline car driving scenario as an example, a more complicated deterministic input exists, i.e., the course of the street. For this task, a two-level model has been proposed which has a closed-loop stabilization controller and an anticipatory open-loop guidance controller working in parallel [54], [55]. The perceptual aspects of the anticipation of changes in the course of the street have been explained. However, it has been assumed that the driver tries to eliminate all deviations from the middle line of the street.

To overcome this simplification, the street might be viewed as a target tube in which the driver is allowed to move his car. Interestingly enough, many other human control tasks in vehicle guidance and industrial process control also require controlling the state of the system within a target tube rather than along a single reference line. Such a criterion makes these tasks much more relaxed than one often assumes in man-machine systems experiments.

Reviewing the control theory literature, some applicable methods for controlling within a target tube were found. They have never been used with man-machine systems problems. One approach assumes a criterion

function which puts less weight on small errors by taking the fourth power of the error instead of the second power as in the optimal control model [56]. The other approach is called unknown-but-bounded control [57], [58], [59]. Figure 4 illustrates how the controller tries to keep the state (X) of the system always in an effective target tube to assure that it will never cross the boundaries of the outer target tube under all expected disturbances.

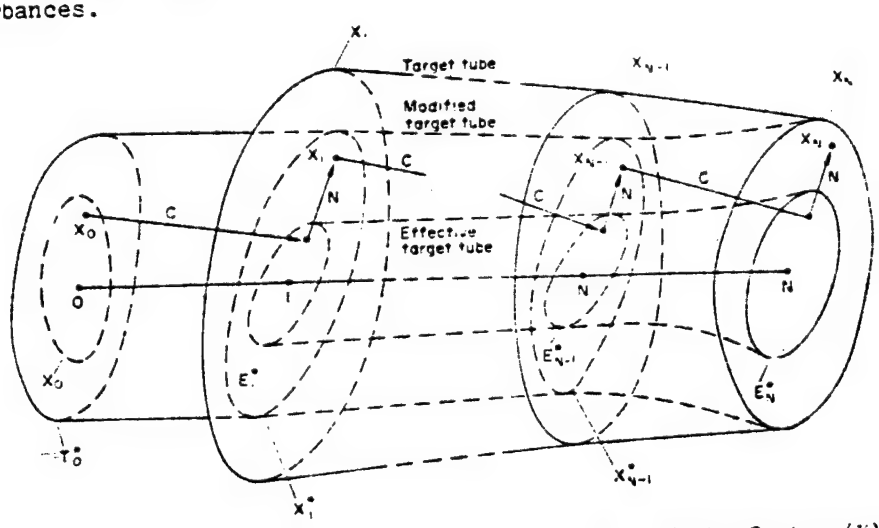

Figure 4: Schematic Presentation of the State of the System (X) as Affected by the Action of the Controller (C) to Counteract Disturbances (N) for Reachability of a Target Tube (from [57])

The unknown-but-bounded control approach combines state variable with set theoretic descriptions. Due to the higher mathematical effort, this approach has infrequently been applied in automatic control situations. However, it seems worthwhile to consider this approach in modeling biological or sociological systems. Human behavior in general is goal-oriented and the goal is very often defined as bringing or keeping some state variables within a certain target set or target tube.

In the baseline scenario, the target tube of Figure 4 would be the width of the street or one of its lanes. The effective target tube is planned by the driver as an area inside of which no control actions are necessary (see linear-plus-dead-band control laws in Glover and Schweppe [58]). Planning the effective target tube might also include some fuzziness. Whether the unknown-but-bounded control approach can be combined with fuzzy set theory which has recently been applied in industrial process control [60] has not as yet been investigated.

Another interesting issue is the notion of the internal model which has been considered to some extent in the discussion of the planning process. In modeling how the human chooses among alternative courses of action, an important issue concerns whether the human possesses a correct

internal model of his environment or, whether the model is incorrect as in learning situations or, very approximative as in large-scale systems (see, e.g., [61]). The process of building up an internal model during learning and how to use it by changing control laws or choosing among different kinds of control laws in time-varying systems, should be further investigated. The literature on adaptive manual control shows, for example, that the models assume a set of predetermined control laws matched with a set of different system dynamics (see e.g., [62]).

This leads to the idea of a memory for motor patterns. Instead of having an input-output transfer behavior, the human operator initializes predetermined motor patterns in many situations. These patterns are slightly corrected during their actual execution (see,e.g., [63]). Good examples are walking, bicycle riding, and piano playing. Also, the coordination and timing of a series of discrete manual control actions, e.g., in trouble-shooting tasks or in checking procedures of aircraft pilots or process operators, can be explained by predetermined motor patterns.

DISCUSSION AND CONCLUSIONS

In considering various approaches to tying all of the discussions in this paper together, the authors found the diagram in Figure 5 to be most useful. This diagram is a variation of a diagram discussed by Johannsen [64] for vehicle control tasks and Sheridan [1976] for human control of vehicles, chemical plants, and industrial robots.

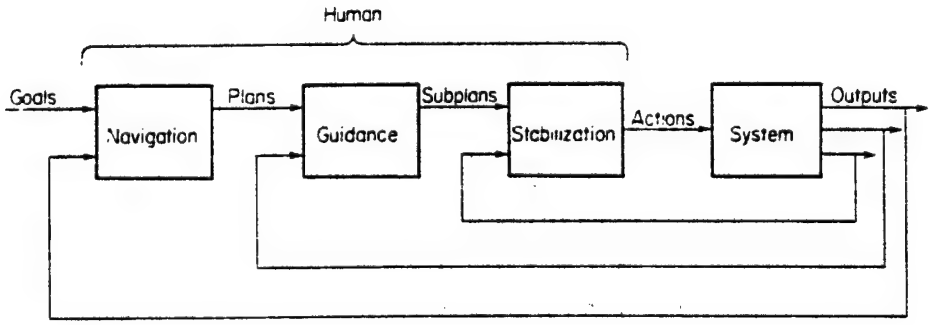

Figure 5: Hierarchy of Human Behavior

This diagram can be used to represent well-defined man-machine systems tasks such as those discussed by Johannsen [64] and Sheridan [65] as well as less well-structured tasks. For example, goals could mean success in life, plans could mean a career outline, subplans could mean a scheme to succeed in a specific job, and actions could mean one's daily activities. Thus, the diagram has broad applicability.

How can one analytically deal with such a general description? If one looks at control theory with a very general perspective that includes control with respect to continuous events as well as discrete events, then one can subsume most analytical methods (e.g., linear systems theory and queueing theory) within the category of control theory. This generalization, and willingness to expand the set of tools one utilizes, enables quantitative analysis of a larger portion of the hierarchy of behavior.

However, there are limits to context-free analytical modeling. First, there is the very important idea that human behavior mainly reflects the task environment. Thus, searching for a specific analytical model of general human behavior may only be fruitful to the extent that all task environments are common. Perhaps then, one should first search for commonality among environments rather than intrinsic human characteristics. In other words, a good model of the demands of the environment may allow a reasonable initial prediction of human performance. Thus, it is reasonable to initially assume that the human will adapt to the demands of the task and perform accordingly.

A second limitation to analytical modeling is due to the human's lack of analytical thinking, especially at upper levels of the hierarchy. First of all, the human is more of a satisficer than an optimizer. Thus, ideas such as a target tube within control tasks, fuzzy set theory, and some concepts from utility theory deserve more study and application within man-machine systems. What this means is that one should look at optimization with respect to broad criteria that allow multiple satisfactory solutions. An alternative approach to this issue is to discard optimization, but this would leave the modeler stripped of one of his most important tools and without a viable alternative.

Beyond the idea of satisficing, another important limitation to analytical modeling is that humans simply do not worry about details until it becomes necessary to do so. Thus, planning can be sketchy, perhaps in the form of scripts. Such sketchy planning can mean a drastic reduction in mental workload and also, that the human has the resources left to deal with more tasks as well as the flexibility to react to unforeseen events. These characteristics are precisely the reasons why humans are often included in systems.

However, the scripts idea presents a problem. While everyone might agree that humans use scripts to expedite performance of many tasks, knowledge of their existence is not sufficient to predict performance. One must know what the script specifically is. Thus, in complex tasks, one must measure not only performance (e.g., RMS error) but also the script.

This suggests that verbal protocols (perhaps analyzed by a computer that understands natural language) may be increasingly important research tools.

To conclude, this paper has presented a fairly general, but mainly verbal, model of human behavior in complex tasks. The ideas discussed have been based on analysis of a specific complex task (car driving) as well as a thorough review of the literature. Three very specific ideas have emerged. First, control should be looked at in a broad sense, incorporating a wide range of analytical methodologies. Second, the human satisfices rather than optimizes and criteria should reflect this. Third, higher-level activities such as planning require approaches that allow incompleteness, and approaches that capture the process of these activities and not just the results.

REFERENCES

1. Newell, A. and Simon, H.A., Human Problem Solving, Englewood Cliffs, N.J.: Prentice-Hall, 1972.

2. Tsichritzis, D.C. and Bernstein, P.A., Operating Systems. New York: Academic Press, 1974.

3. Habermann, A.N., Introduction to Operating System Design, Chicago: Science Research Associates, Inc., 1976.

4. Sanders, A.F., "Some Remarks on Mental Load," Moray, N. (Ed.). Mental Workload, New York: Plenum Press, 1978.

5. Atkinson, R.C. and Juola, J.F., "Search and Decision Processes in Recognition Memory," in: D.H. Krantz et al. (eds.): Contemporary Developments in Mathematical Psychology, Vol. I. San Francisco: W.H.Freeman and Company, 1974, pp. 243-293.

6. IEEE, "Current Perspectives in Pattern Recognition," Systems, Man, and Cybernetics Review, Vol. 6, No. 4, August 1977.

7. Sklansky J., "Image Segmentation and Feature Extraction," IEEE Transactions on Systems, Man. and Cybernetics, Vol. SMC-8, No. 4, April 1978, pp. 237-247.

8. Winston P.H. (Ed.), The Psychology of Computer Vision, New York: McGraw-Hill, 1975.

9. Winston, P.H., Artificial Intelligence. Reading, Mass.: Addison-Wesley, 1977.

10. Senders, J.W., "The Human Operator as a Monitor and Controller of Multidegree of Freedom Systems," IEEE Transactions on Human Factors in Electronics, Vol. HFE-5, No. 1, September 1964, pp. 2-5.

11. Carbonell, J.R., "A Queueing Model of Many-Instrument Visual Sampling," IEEE Transactions on Human Factors in Electronics, Vol. HFE-4, No. 4, December 1966 pp. 157-164.

12. Carbonell, J.R.; Ward, J.L.; and Senders, J.W., "A Queueing Model of Visual Sampling: Experimental Validation," IEEE Transactions on Man-Machine Systems, Vol. MMS-9, No. 3. September 1968, pp. 82-87.

13. Rouse, W.B. and Greenstein, J.S., "A Model of Human Decision Making in Multi-Task Situations: Implications for Computer Aiding," Proceedings of the 1976 International Conference on Cybernetics and Society, Washington, November 1976, pp. 425-433.

14. Sheridan, T.B. and Tulga, M.K., "A Model for Dynamic Allocation of Human Attention Among Multiple Tasks," to appear in the Proceedings of the Fourteenth Annual Conference on Manual Control. University of Southern California, April 1978.

15. Chien, R.T. and Snyder, W., "Visual Understanding of Hybrid Circuits via Procedural Models," Proceedings of the Fourth International Joint Conference on Artificial Intelligence, Tbilisi, USSR, September 1975 pp. 742-745.

16. Perkins W.A., "Model-Based Vision System for Scenes Containing Multiple Parts," Proceedings of the Fifth International Joint Conference on Artificial Intelligence, MIT, August 1977, pp. 678-684.

17. Wechsler, H. and Sklansky, J., "Automatic Detection of Rib Contours in Chest Radiographs," Proceedings of the Fourth International Joint Conference on Artificial Intelligence, Tbilisi, USSR, September 1975, pp. 688-694.

18. Martino, J.P., Technological Forecasting for Decision Making, New York: American Elsevier, 1972, Chap 10.

19 Sacerdoti, E.D , A Structure for Plans and Behavior, Ph.D. Dissertation, Stanford University, 1975.

20. Weissman, S.J., On a Computer System for Planning and Execution in Incompletely Specified Environments, Ph.D. Dissertation, University of Illinois at Urbana-Champaign, 1976.

21. Carbonell, J.R., "On Man-Computer Interaction: A Model and Some Related Issues," IEEE Transactions on Systems Science and Cybernetics Vol. SSC-5, No. 1, January 1969, pp. 16-26.

22. Schank, R.C. and Abelson R.P., Scripts, Plans, Goals, and Understanding, Hillsdale, N.J.: Lawrence Erlbaum, 1977.

23. Anderson, J.R. and Bower, G.H., Human Associative Memory, New York: Wiley, 1973.

24. Kohonen, T., Associative Memory, New York: Springer-Verlag, 1977.

25. Warfield, J.N., Societal Systems: Planning, Policy, and Complexity, New York: John Wiley, 1976.

26 Goldstein, I.P. and Grimson, E.. "Annotated Production Systems: A Model for Skill Acquisition," Proceedings of the Fifth International Joint Conference on Artificial Intelligence, MIT, August 1977, pp. 311-317.

27. Wesson, R.B., "Planning in the World of the Air Traffic Controller," Proceedings of the Fifth International Joint Conference on Artificial Intelligence, MIT. August 1977 pp. 473-479.

28. Rouse, W.B., "A Theory of Human Decision Making in Stochastic Estimation Tasks," IEEE Transactions on Systems, Man, and Cybernetics. Vol. SMC-7. No. 4, April 1977, pp. 274-283.

29. Keeney, R.L. and Raiffa, H., Decision with Multiple Objectives, New York: Wiley, 1976.

30. Zadeh, L.A.; Fu, K.S.; Tanaka, K; and Shimura, M. (Eds.), Fuzzy Sets and Their Applications to Cognitive and Decision Processes, New York: Academic Press, 1975.

31. Kaufman A., Introduction to the Theory of Fuzzy Subsets, New York: Academic Press, 1975.

32. Davis, P.R., Using and Re-Using Partial Plans, Ph.D. Dissertation, University of Illinois at Urbana-Champaign, 1977.

33. Rouse, W.B., "A Model of Human Decision Making in a Fault Diagnosis Task," IEEE Transactions on Systems. Man, and Cybernetics Vol. SMC-8, No. 5, May 1978. pp. 357-361.

34. Gai E. and Curry, R.E., "A Model of the Human Observer in Failure Detection Tasks," IEEE Transactions on Systems. Man, and Cybernetics. Vol. SMC-6, No. 2. February 1976. pp. 85-94.

35 Greenstein, J.S. and Rouse, W.B.,"A Model of Human Event Detection in Multiple Process Monitoring Situations," to appear in the Proceedings of the Fourteenth Annual Conference on Manual Control, University of Southern California, April 1978.

36. Scott, A.C., Neurophysics, New York: Wiley, 1977.

37. Rasmussen, J. and Jensen, A., "Mental Procedures in Real-Life Tasks: A Case Study of Electronic Trouble Shooting," Ergonomics Vol. 17, No. 3, May 1974, pp.293-307.

38. Rasmussen, J., "Outlines of a Hybrid Model of the Process Plant Operator," in Sheridan, T.B. and Johannsen, G. (Eds.), Monitoring Behavior and Supervisory Control. New York: Plenum Press 1976, pp. 371-383.

39. Siegel, A.J. and Wolf, J.J., Man-Machine Simulation Models, New York: Wiley, 1969.

40 Linton, P.M.; Jahns, D.W.; and Chatelier, P.R., "Operator Workload Assessment Model: An Evaluation of a VF/VA-V/STOL System," Methods to Assess Workload, AGARD-CPP-216,1977.

41 Pew, R.W.; Baron, S; Feehrer, C.E.; and Miller, D.C., Critical Review and Analysis of Performance Models Applicable to Man-Machine Systems Evaluation, Bolt Beranek and Newman, Inc., Cambridge, Mass.: Rept. No. 3446, 1977.

42. Moray, N. (ed.), Mental Workload, New York: Plenum Press. 1978.

43. Senders, J.W. and Posner, M.J.M., "A Queueing Model of Monitoring and Supervisory Behavior," in T B. Sheridan and G. Johannsen, (Eds.), Monitoring Behavior and Supervisory Control, New York: Plenum Press 1976.

44. Rouse, W.B., "Human-Computer Interaction in Multi-Task Situations." IEEE Transactions on Systems, Man and Cybernetics, Vol. SMC-7. No. 5, May 1977, pp. 384-392.

45. Walden, R.S. and Rouse, W.B., "A Queueing Model of Pilot Decision Making in a Multi-Task Flight Management Situation," Proceedings of the Thirteenth Annual Conference on Manual Control. MIT, June 1977, pp. 222-236.

46. Chu, Y.Y. and Rouse, W.B., "Optimal Adaptive Allocation of Decision Making Responsibility Between Human and Computer in Multi-Task Situations," Proceedings of the 1977 International Conference on Cybernetics and Society, Washington, September 1977, pp. 168-185.

47. Chu, Y.Y. and Rouse, W.B., "Pilot Decision Making in a Computer-Aided Flight Management Situation," to appear in the Proceedings of the Fourteenth Annual Conference on Manual Control, University of Southern California, April 1978.

48. Wherry, R.J., Jr., "The Human Operator Simulator - HOS," Sheridan. T.B. and Johannsen, G. (Eds.) 1976, Monitoring Behavior and Supervisory Control. New York: Plenum Press, 1976, pp. 283-293.

49. McRuer, D.T. and Krendel, E.S., "Mathematical Models of Human Pilot Behavior," Advisory Group Aerospace Research Development, Neuilly sur Seine, France: AGARDograph No. 188, 1974.

50. Sheridan T.B. and Ferrell, W.R., Man-Machine Systems: Information, Control, and Decision Models of Human Performance, Cambridge, Mass.: MIT Press, 1974.

51. Johannsen, G., Poller H.E., Donges, E., and Stein, W., Der Mensch im Regelkreis, Lineare Modelle, Munchen: Oldenbourg, 1977.

52. Kleinman, D.L.; Baron, S.; and Levison, W.H., "An Optimal Control Model of Human Response. Part I: Theory and Validation," Automatica, Vol. 6, 1970, pp. 357-369.

53. Rouse, W.B. (Ed.), Special Issue on Applications of Control Theory in human Factors, Human Factors, Vol. 19, Nos. 4 and 5, August and October 1977.

54. Donges, E., "Experimentelle Untersuchung des menschlichen Lenkverhaltens bei simulierter Strassenfahrt," Automobiltechnische Zeitschrift, Vol. 77, 1975 pp.141-146, 195-190.

55. Donges, E. "A Control Theoretic Model of Driver Steering Behavior," Proceedings of the 13th Annual Conference on Manual Control. MIT. Cambridge, Mass, 1977, pp. 165-171.

56. Galiana, F.D. and Glavitsch, H., "State Adaptation in Power Systems Control," Proceedings of the IEEE Power Engineering Society, Winter Meeting, New York, 1973.

57. Bertsekas, D.P. and Rhodes, I.B , "On the Minimax Reachability of Target Sets and Target Tubes," Automatica, Vol. 7, 1971, pp. 233-247.

58. Glover, J.D. and Schweppe, F.C., "Control of Linear Dynamic Systems with Set Constrained Disturbances." IEEE Transactions on Automatic Control Vol. AC-16, 1971, pp. 411-423.

59. Schweppe, F.C., Uncertain Dynamic Systems, Englewood Cliffs, N.J.: Prentice-Hall, 1973.

60. King, P.J. and Mamdani, E.H., "The Application of Fuzzy Control Systems to Industrial Processes," Automatica, Vol. 13, 1977, pp. 235-242.

61. Sheridan, T.B. and Johannsen, G. (Eds.), Monitoring Behavior and Supervisory Control, New York: Plenum Press, 1976.

62. Young, L.R , "On Adaptive Manual Control " Ergonomics, Vol. 12, 1969, pp.635-674.

63. Adams, J.A., "A Closed-Loop Theory of Motor Learning," J. Motor Behavior, Vol. 3, 1971, pp. 111-150.

64. Johannsen, G., "Preview of Man-Vehicle Control Session," in: Sheridan, T.B. and Johannsen, G. (eds), Monitoring Behavior and Supervisory Control, New York: Plenum Press, 1976, pp. 3-12

65. Sheridan, T.B., "Review of the International Symposium on Monitoring Behavior and Supervisory Control," Proceedings of the Twelfth Annual Conference on Manual Control. University of Illinois at Urbana-Champaign, May 1976. pp. 3-13.

N79-15600

PETRI NETS AS A MODELING TOOL FOR DISCRETE CONCURRENT TASKS OF THE HUMAN OPERATOR

By W. Schumacher, G. Geiser

Fraunhofer-Gesellschaft e. V., Institut für Informationsverarbeitung in Technik und Biologie (IITB), Karlsruhe, F. R. of Germany

SUMMARY

Petri nets have been developed as a fundamental model of technical systems with concurrent discrete events. The major use of Petri nets has been the modeling of hardware systems and software concepts of computers. After a very brief introduction to their basic concepts, the use of Petri nets is proposed for modeling the human operator dealing with concurrent discrete tasks. Their properties useful in modeling the human operator are discussed and practical examples are given. By means of an experimental investigation of binary concurrent tasks which are presented in a serial manner it is shown how human behavior may be represented by Petri nets.

INTRODUCTION

In different application areas the human operator's role in man-machine systems is changing from that of a continuous controller to that of a monitor. This change is happening in control rooms of industrial plants and in aircraft piloting, where dispatching of concurrent demands becomes an essential feature of the human operator's task. Furthermore the multiple task situation is also given in automobile driving. Especially in high density traffic situations the driver has to deal with many concurrent demands originating from other road users, from traffic regulation, and from his own vehicle.

In general, concurrent tasks are imposed on the human operator by displays or by real events, their service requires a response from the human operator which is specified by the task. There are continuous demands like the control error of a continuous control loop or there are discrete events, which require continuous or discrete actions respectively. These demands compete for the human operator's attention, if they arrive in such an intensity, that the human operator's capacity is at least temporarily exceeded. In this case demands which cannot be dispatched immediately have to be stored in his memory, otherwise they are lost.

For the design of such man-machine systems, i. e. of their dynamic properties, displays, and controls, the human strategies in dispatching concurrent demands have to be described by means of experimental investigations and resulting quantitative models. Notions of queueing theory are suitable for the formulation of this task of the human operator (refs. 1, 2, 3), however instead of analytical solutions human behavior is often studied by simulation.

In this paper Petri nets are discussed as a modeling tool for the human operator dealing with concurrent demands. As a practical example the apolication of Petri nets for modeling human strategies is shown. These strategies have been evaluated by means of an experimental investigation of binary concurrent tasks displayed in a serial manner.

PETRI NETS

In the following a brief introduction to the Petri net is given; a more detailed presentation is contained in ref. 4.

A Petri net is an abstract, formal model of the information flow in systems with discrete sequential or parallel events. Its pictorial representation is a directed graph, for which an example is shown in Fig. 1. The graph consists of two types of nodes: places p_i (represented by circles) and transitions t_j (represented by bars). These nodes are connected by directed arcs from places to transitions and from transitions to places. If an arc is directed from node i to node j, then i is an input to j, and j is an output of i. In Fig. 1, e. g., place p_1 is an input to transition t_2, while places p_3 and p_4 are outputs of transition t_3. The nodes and arcs describe the static properties of a Petri net, its dynamic characteristics are represented by the movement of tokens (represented by black dots within the places). The distribution of tokens in a Petri net defines the state of the net and is called marking μ. For each marking μ a new marking μ' is defined by the following rules:

1. A transition is called enabled, if each of its input places has at least one token in it (e. g. transition t_2 in Fig. 1 is enabled).

2. Each transition which is enabled may fire.

3. A transition fires by removing one token from each of its input places and by adding one token to each of its output places (e. g. in Fig. 1, firing of transition t_2 results in two tokens in place p_1, zero tokens in p_4, and one token in place p_2).

The formal description of a Petri net is defined as a four-tupel of sets

$$C = (P, T, I, O) ,$$

with P as a set of places, T as a set of transitions, I as the input function, and O as the output function. The input function I defines for each transition t_j the set of input places $I(t_j)$. The output function $O(t_j)$ is defined correspondingly. For the example shown in Fig. 1 there are the following sets

$$P = \{p_1, p_2, p_3, p_4\} ,$$

$$T = \{t_1, t_2, t_3, t_4\} ,$$

$$I(t_2) = \{p_1, p_4\} ,$$

$$I(t_3) = \{p_2\} ,$$

$$I(t_4) = \{p_3\} ,$$

$$O(t_1) = \{p_1\} ,$$

$$O(t_2) = \{p_2\} ,$$

$$O(t_3) = \{p_3, p_4\} .$$

The vector $\mu = (\mu_1, \mu_2, \ldots, \mu_n)$ gives, for each of the n places in the net, the number of tokens in that place. A Petri net $C = (P, T, I, O)$ with the marking μ becomes the marked Petri net $C^* = (P, T, I, O, \mu)$.

An important tool for analysis of systems modelled by a Petri net is the reachability tree. It consists of a tree, whose nodes represent markings of the Petri net, and whose arcs represent the transitions which are enabled. The Petri net shown in Fig. 1 has the following degenerated reachability tree:

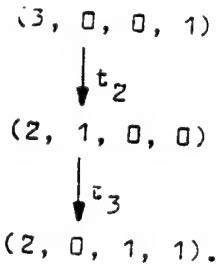

PROPERTIES OF PETRI NETS WITH REGARD TO THE DESCRIPTION OF THE HUMAN OPERATOR

In the following the properties of Petri nets are summarized with regard to the description of the human operator dealing with discrete concurrent demands (Table 1).

- Description of sequential and parallel processes
- Description of interactions between parallel processes
- Interpreted and uninterpreted modeling
- Hierarchical modeling
- Description of temporal order
- Description of deterministic and stochastic processes
- Modeling of priority systems
- Formal and graphic description

Table 1: Properties of Petri Nets with regard to the Modeling of the Human Operator

Petri nets are suitable for the description of sequential and parallel concurrent demands of the human operator as well. A net having only one token at the same time is describing a sequential process. The position of the token represents the state of the 'sequence control register' of the process. The graphic representation of such a net containing only transitions with one input and one output corresponds to the usual flow-chart. Fig. 2 shows as an example the observation of a traffic light represented by a flow-chart and by a Petri net.

A net having more than one token at any time describes a non-sequential process. Several tokens may result from a transition with several output places or they are an initial marking. Fig. 1 shows a Petri net with an initial marking of four tokens. Therefore it describes a system of partially parallel activities. It may be interpreted as a general model of the dispatching of concurrent demands, presented in a serial manner to the human operator. Concurrency is given by the fact, that during the service of one demand other demands are waiting or arriving. Then places p_1 to p_4 of Fig. 1 have the following interpretations:

p_1: number of demands waiting for service (represented by the corresponding number of tokens),

p_2: one demand is being served,

p_3: one demand has been served,

p_4: the human operator is ready for the next service.

The description of parallel activities by Petri nets can be applied to the modeling of interactions between different stages of human information processing and between the tasks of several operators as well. Fig. 3 shows as an example the crossing of two automobile drivers where two conflicting transitions without indication of priority exist. Modeling of priority systems is considered later on.

The interpretation of the Petri net shown in Fig. 1 may be specified with regard to practical applications. E. g. the demands may represent traffic signs which have to be observed by the driver or they are alarms of an industrial plant presented on displays in the control room. On the other hand Petri nets exist as uninterpreted models of which the abstract properties may be investigated.

Another valuable feature of Petri nets is their ability to model a system hierarchically. This means that parts of the human information processing may be represented by a single place or transition in order to have a more abstract model. Conversely places and transitions may be specified by subnets in order to get a more detailed description. The example of Fig. 1 is an extremely abstract model of the human operator, which will be specified by means of experimental results in chapter 4.

Petri nets describe the possible sequences of events, they do not reflect the variable amounts of time required by the different events. Because of this property Petri nets give no information about the duration of information processing of the human operator.

Petri nets are suitable for the modeling of deterministic and of stochastic sequences of events. Deterministic sequences ever have one transition being enabled, while stochastic sequences lead to situations in which more than one transition is enabled. The choice of the next transition to be fired occurs randomly. Fig. 4 shows two types of stochastic firing of transitions. Concurrent transitions may fire in either order whereas in conflicting transitions the firing of one will disable the other.

In order to model priority systems Petri nets were extended by inhibition arcs represented by an arc with a small circle instead of an arrowhead. An inhibition arc from place p_i to transition t_j enables the transition only to fire if the place p_i has zero token in it. Fig. 5 shows as an example the crossing of two drivers (compare Fig. 3) with priority of driver 1, described by an inhibition arc.

Furthermore Petri nets may be described in a formal as well as in a graphic manner. Especially the graphic representation seems to be a useful tool in describing complex information processing of the human operator.

MODELING OF HUMAN STRATEGIES IN DISPATCHING CONCURRENT DEMANDS BY PETRI NETS

Experimental Set-up

In order to investigate the human behavior in dispatching concurrent demands a simulator for the generation of the demands and for their service has been established. Fig. 6 shows the block diagram of the experimental set-up. There are 8 streams of binary demands presented by the numbers 1 to 8 on a common numeric display to the operator. The arrival pattern of each stream is given by the Poisson distribution. The service of each demand consists in pressing a corresponding push-button during a fixed lapse of time which is indicated by a service time lamp. The traffic intensity ρ, i. e. the ratio of the service time and the mean interarrival time of the demands, varied in the range $0.8 \leq \rho \leq 1.6$. The service of the demands had to be done in the order of arrival. The experimental sessions consisted of five trials of 200 s duration each. After each trial the traffic intensity was increased by an amount of 0.2, beginning with the value of $\rho = 0.8$. For $\rho \geq 1$ the human operator is unable to deal with the demands as fast as they arrive. Consequently the demands have to queue up in the operator's short term memory. Because of its limited capacity demands may be lost. By recording the service activities of the subjects the strategies in dealing with concurrent demands could be evaluated.

In the following the results from one experiment are presented, further investigations with this experimental set-up are described in ref. 5.

Experimental Results

In order to analyse the human strategies the contents of

the memory were evaluated; it is called waiting-room diagram. Fig. 7 shows a typical waiting-room diagram, where the number of demands in waiting-room 1, i. e. the length of the queue, is plotted as a function of time. At the arrival of a demand the length of the queue increases by one, at the beginning of a service the plot decreases by one. The upper plot shows the ideal waiting-room diagram, which is based on the assumption that there is an infinite waiting-room. All arriving demands are waiting for service, no demand is lost. The lower plot shows the minimal waiting-room diagram, with the assumption that lost demands did never enter the waiting-room. Demands which are not served are marked by a "N". By asking the subjects to communicate the contents of their memory at certain time instants, it could be shown that the real waiting-room diagram corresponds largely to the minimal waiting-room diagram.

By the analysis of the waiting-room diagram and supported by statements of the subjects two strategies for the service of the concurrent demands can be specified:

- Waiting-room with permanent access
  The demands enter into the waiting-room and queue up until a maximum length of the queue ($l_{max} \approx 3$) is reached. Then if one demand is served another may enter.

- Waiting-room with intermittent access
  The demands enter the waiting-room and queue up. By certain triggering events all arriving demands are rejected until the length of the queue is reduced to a low value. Triggering events are the reaching of a maximum length of the queue or the arrival of several demands with short interarrival times. In this case the maximum length of the queue is higher ($l_{max} \approx 5$) than with the strategy of permanent access.

The described strategies are extreme forms of behavior, in reality they occur in an approximate and mixed form. The strategy with intermittent access can be observed more often (factor 1.5) than the strategy with permanent access. Fig. 7 shows the waiting-room diagram in the case of intermittent access. This strategy is less efficient, because with permanent access there is a higher utilization of the waiting-room, i. e. the mean length of the queue is increased.

Modeling of the Human Strategies by Petri Nets

The human operator's activities in dealing with concurrent tasks are the input of information, the storage of information in his memory (waiting-room), and the service of demands by reactions. Fig. 8 shows the Petri net of the strategy with permanent access divided into these three parts. For simplicity the waiting-

room is assumed to have a capacity of three demands.

Complementary places are labelled by p and p'. For example the interpretation of place p_2 is "information input is idle" and of place p_2' "information input is busy". At the arrival of a demand it depends on the state of the information input whether the demand is lost (place p_2' marked) or not (place p_2 marked). In the latter case transition t_1 is fired and the demand is stored in that position of the waiting-room (p_4 ... p_6), which is free and has the lowest number. By the entrance of the demand into the waiting-room (firing of transition t_4, t_5 or t_6) the information input is reset by firing transition t_{11}. Demands arriving when the input is busy are lost by firing of transition t_2. Also if the waiting-room is completely occupied, i. e. the place p_6 is marked, the arriving demand is rejected and lost by firing of transition t_3.

If the waiting-room is empty, the arriving demand is stored in the first place of the waiting-room (marking of p_4'). If the service mechanism is idle (place p_7' marked), then the service of this demand may be carried out by firing of transition t_7 and by setting free the waiting-room place. If there are further demands in the waiting-room they advance one step by means of the transitions t_8 and t_9.

Fig. 9 shows the Petri net of the strategy with intermittent access. Compared with permanent access there are modifications especially in the input part of the model. The states of the places p_{12} and p_{12}' determine whether arriving demands are rejected or not. The rejection state (p_{12}' is marked) is triggered if the waiting-room is completely occupied, i. e. p_6' is marked. Then all demands are rejected and lost until the waiting-room is empty and the transition t_{12} is fired. Then arriving demands again have access to the waiting-room.

The strategies described have been simulated by means of a digital computer. Simulation data showed close agreement with experimental results. The description of the human strategies by means of Petri nets turned out to be a valuable tool for the analysis of human information processing.

This report was supported by the German Federal Ministry of Defense.

REFERENCES

1. Carbonell, J.R.: A Queueing Model of Many-Instrument Visual Sampling. IEEE Trans. on HFE-7 (1966), 157-164.

2. Chu, Y.Y.; Rouse, W.B.: Optimal Allocation of Decision Making Responsibility between Human and Computer in Multi-Task Situations. Proc. of the International Conference on Cybernetics and Society, Sept. 19-21, 1977, Washington, 168-175.

3. Tulga, M.K.; Sheridan, T.B.: Modeling human decision making behavior in supervisory control. Proc. of the International Conference on Cybernetics and Society, Sept. 19-21, 1977, Washington, 201-206.

4. Peterson, J.L.: Petri Nets. Computing Surveys, 9 (1977), 223-252.

5. Schumacher, W.: Human operator strategies in dispatching concurrent binary demands in man-machine systems. IITB-Mitteilungen 1978, Institut für Informationsverarbeitung in Technik und Biologie der Fraunhofer-Gesellschaft e. V., Karlsruhe, F.R. of Germany.

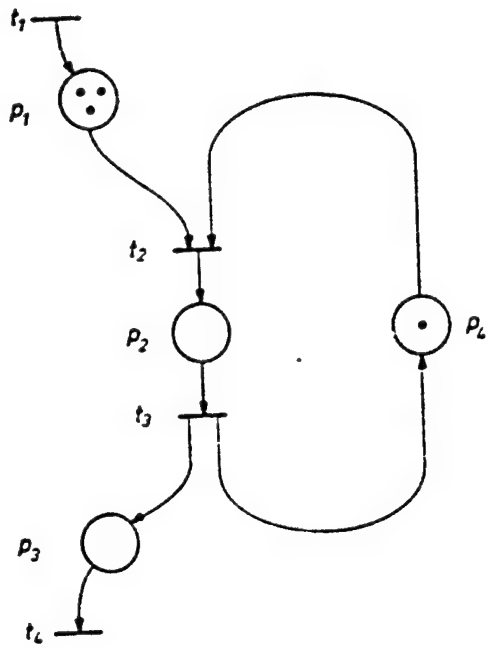

Fig. 1: A Petri net graph

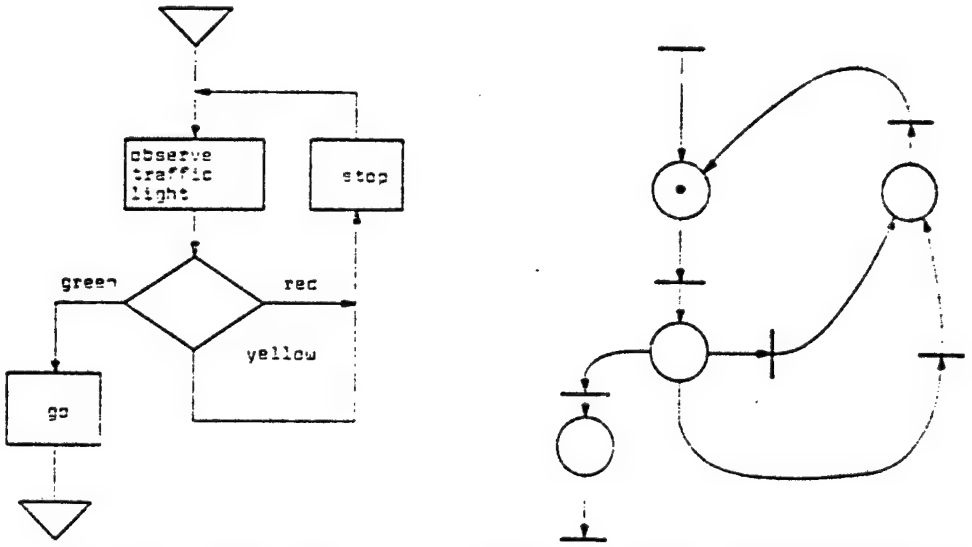

Fig. 2: Observation of a traffic light represented by a flow-chart and a Petri net

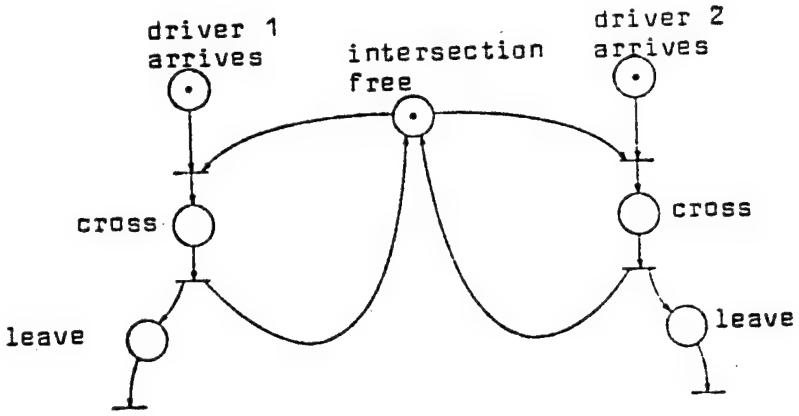

Fig. 3: Petri net of the crossing of two drivers

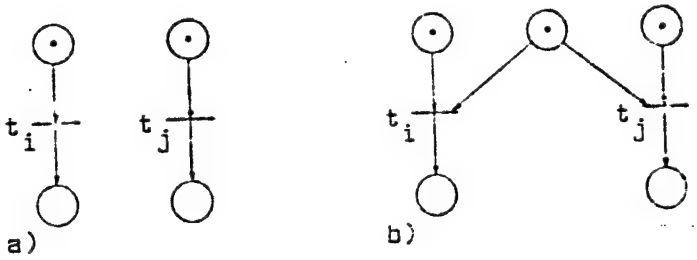

Fig. 4: a) Concurrent and b) conflicting transitions t_i and t_j

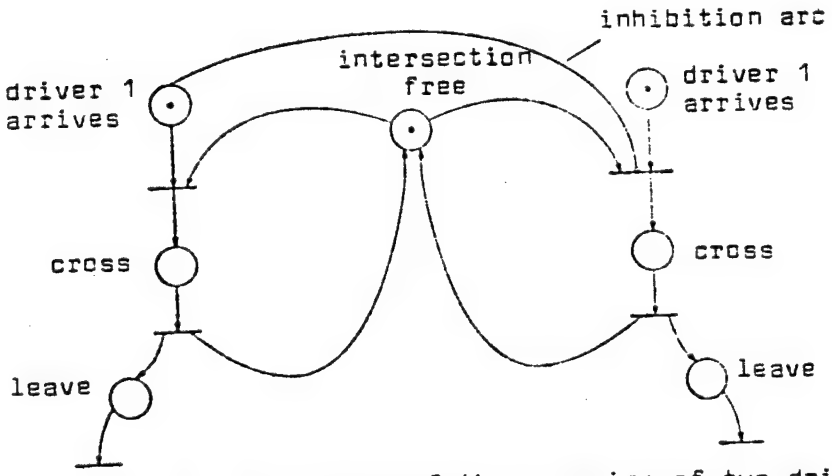

Fig. 5: Petri net of the crossing of two drivers with priority of driver 1

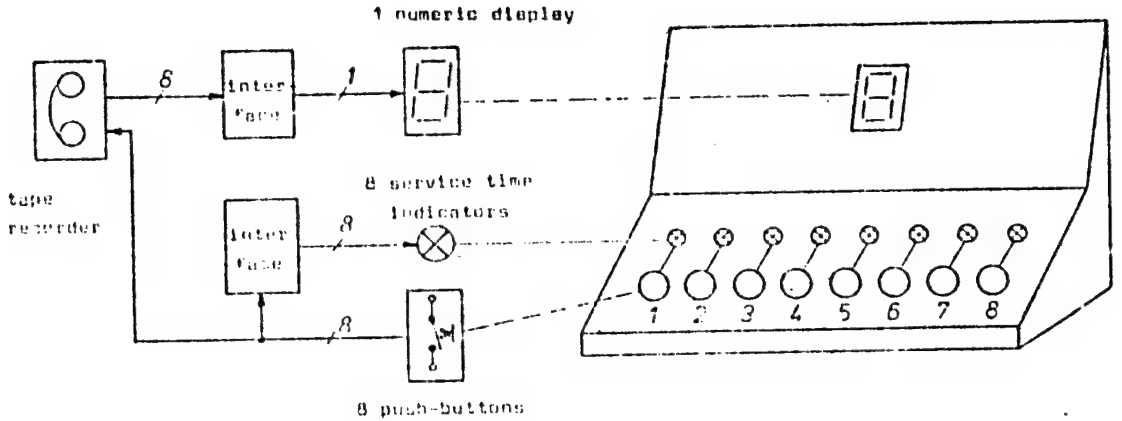

Fig. 6: Block diagram of the experimental set-up

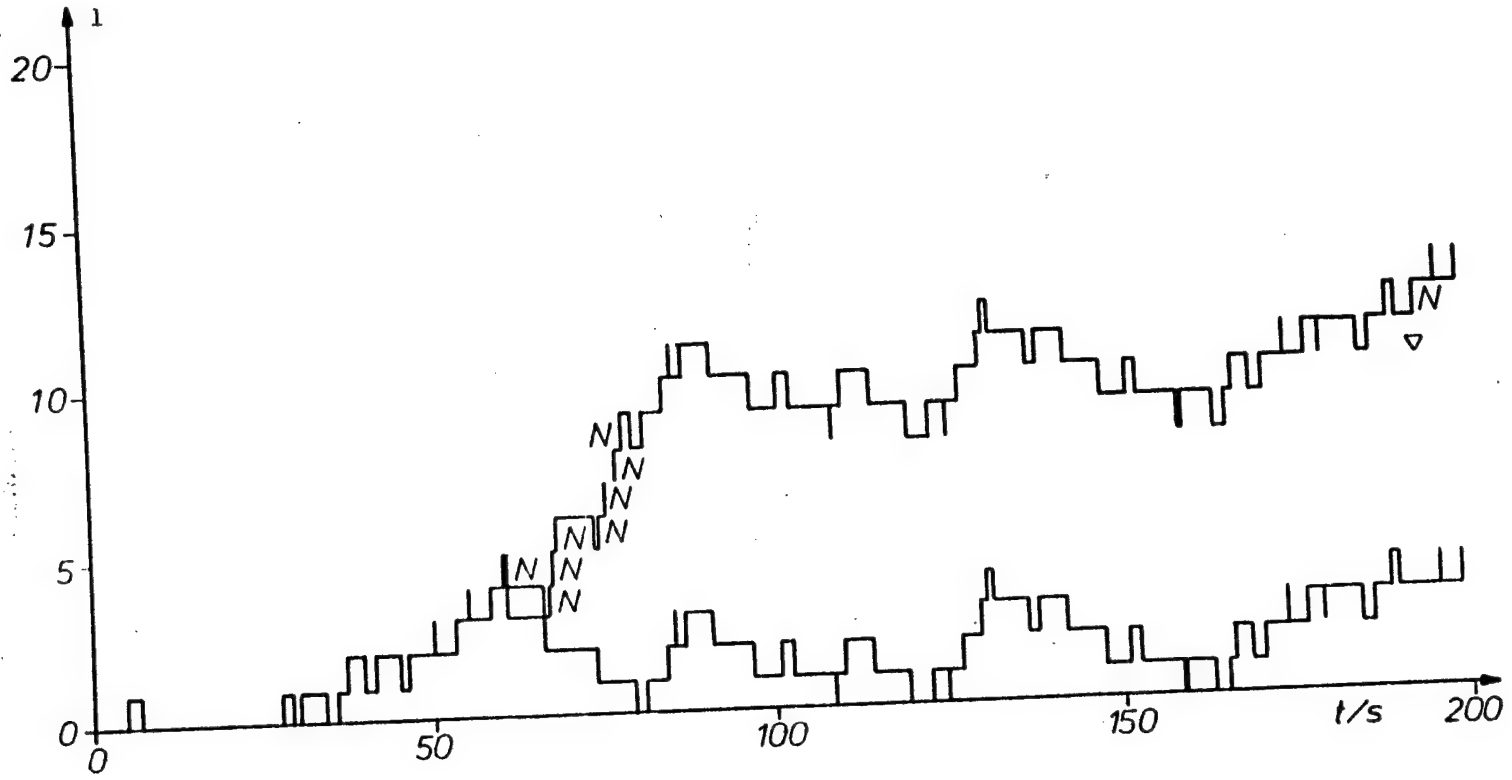

Fig. 7: Waiting-room diagram

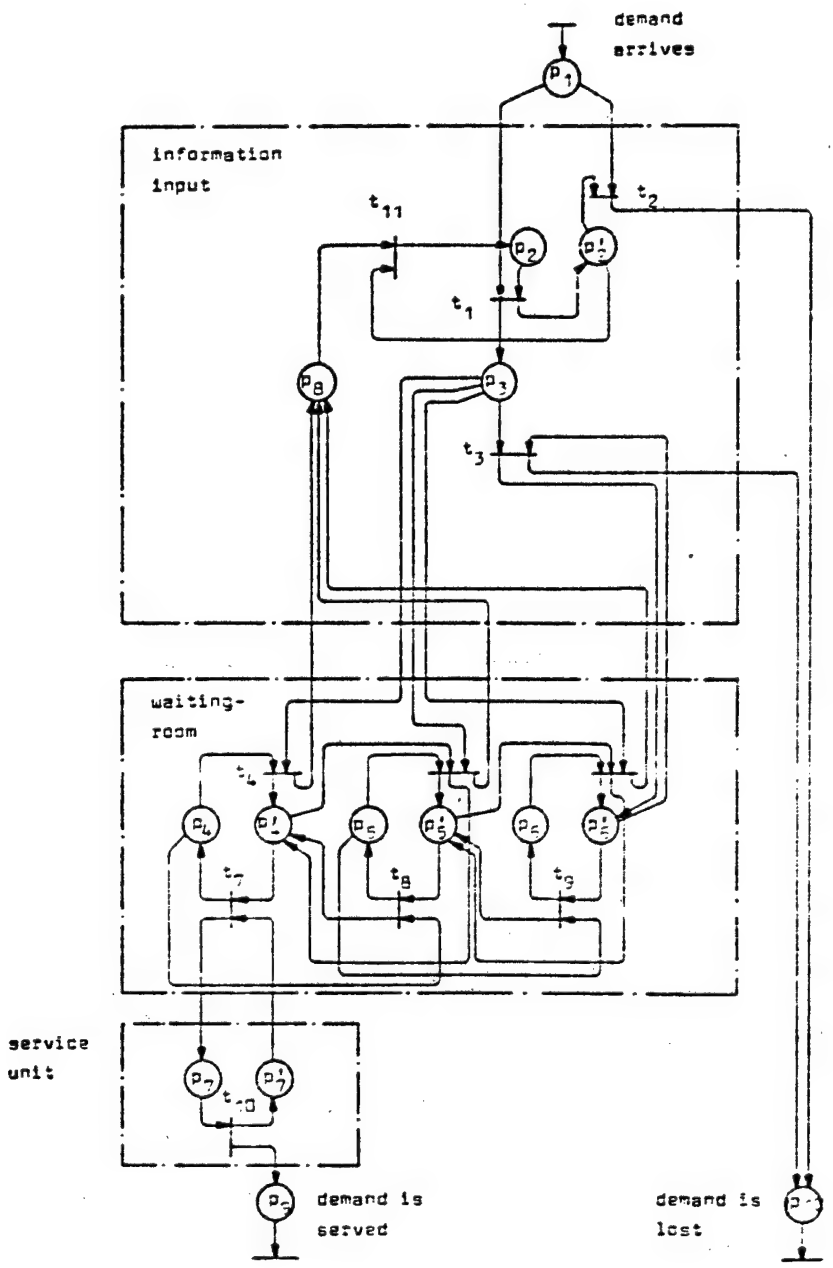

Fig. 8: Waiting-room with permanent access

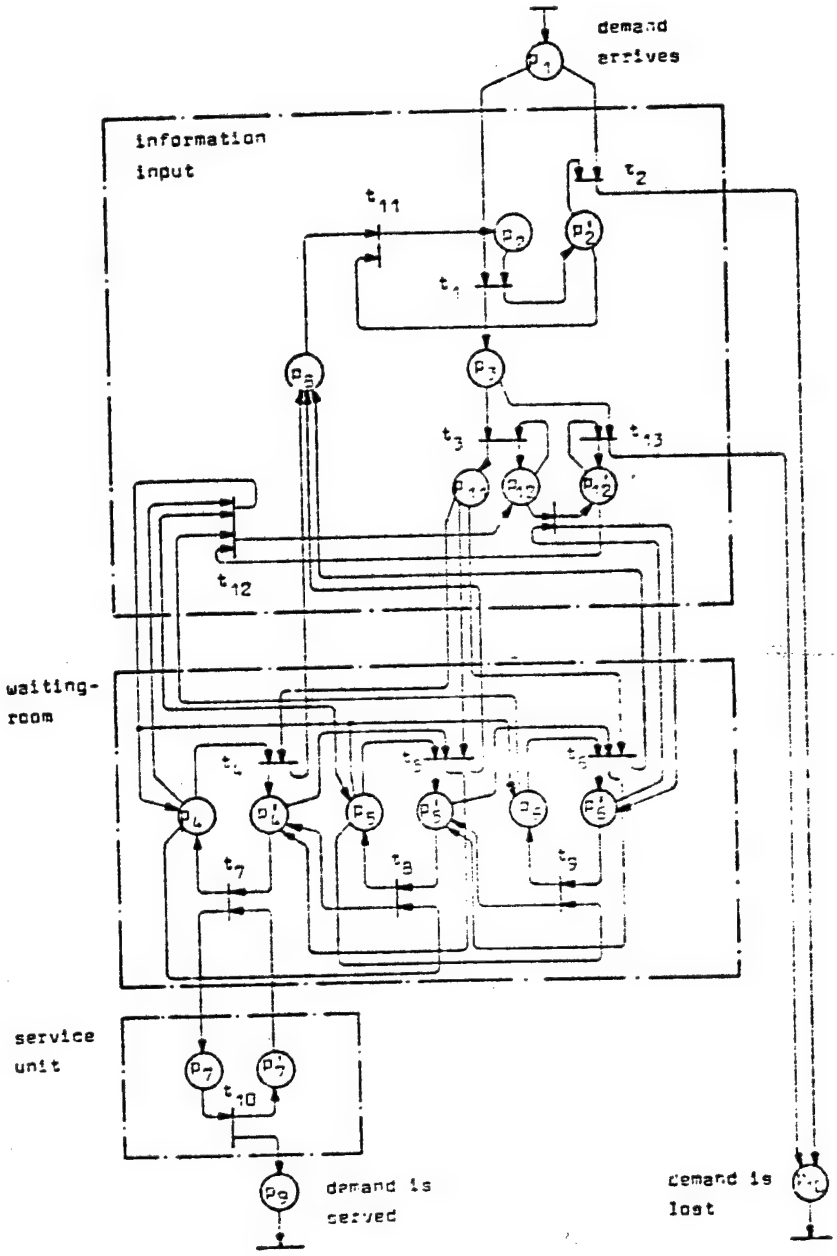

Fig. 9: Waiting-room with intermittent access

DISCRETE-TIME PILOT MODEL

by Daniel CAVALLI

Office National d'Etudes et de Recherches Aérospatiales (ONERA)
92320 Châtillon (France)

SUMMARY

The objective of this paper is to demonstrate the originality of our approach with regards to already existing pilot models and to present recently obtained results.

We consider the pilot's behavior as a discrete-time process where the decision making has a sequential nature. This model contrasts very clearly with previous approaches namely the quasi-linear model which follows from classical control theory and the optimal control model which considers the human operator as a Kalman estimator-predictor. We also consider that the pilot's objective may not be adequately formulated as a quadratic cost functional to be minimized, but rather as a more fuzzy measure of the closeness with which the aircraft follows a reference trajectory.

All model parameters, in the digital program simulating the pilot's behavior, have been successfully compared in terms of standard-deviation and performance with those of professionnal pilots in IFR configuration. The first practical application of our pilot model has been the study of its performance degradation when the aircraft model static margin decreases.

I. INTRODUCTION

Research on human operator models and especially on models of spacecraft, aircraft and helicopter operators has often been influenced by the current state-of-the-art. Before further investigation, the human operator appears as highly adaptative, versatile, complex and sufficiently creative so that we can always recognize in the diversity of all strategies he may use, one we know well and want to find.

The first approach to the problem was from the control specialists of the 1950's, attempting, at the beginning age of servomechanisms, to apply their basic tool, namely the linear transfer function of a phase lead regulator (ref. 1). These studies relied heavily on simulation techniques using analog computers.

One of the most-commonly accepted representations is the quasi-linear model of McRuer (ref. 2, 3, 4) so named because it represents the human operator by a linear transfer function, plus a remnant to describe that part of the human response that is not predicted by the linear approximation. The transfer function is essentially the result of an approximation to the first harmonic and the remnant accounts for higher-order effects and for other modeling errors. The most celebrated result from the above study is probably the "cross over model" which is based on the fact that the human operator adjusts the parameters of his own transfer function so that his open-loop response satisfies the closed-loop stability conditions with a reasonable error.

At the same time sampled-data models have been proposed (ref. 5). This type of models is suitable for numerical computation on digital computers. However, the assumption of fixed-rate sampling appears as a weakness of this representation.

An alternative to the quasi-linear model has been developed by Kleinman, Baron and

Levison (ref. 6, 7, 8). This approach is based on advanced optimal control and estimation theory with the assumption that the well-trained human controller behaves in an optimal manner subject to his inherent limitations and contraints and the requirement of his task. However, is the human operator only a Kalman estimator whose objective may be formulated as the minimization of a given criterion ?

These modeling studies have advanced a great step forward when becoming interdisciplinary through the involvement of psychologists in the research teams. These scientists can probably be credited for the introduction of the concept of operating image (ref. 9, 10, 11, 12) which is an internal model of the vehicle allowing the human operator to predict its short-term response. The conventional approach and the purely psychological one are currently merging (ref. 13). Without repudiating previous philosophies, our current approach tries to make a synthesis of them and develop the model of a human operator based on a new and more accurate analysis of the aircraft pilot's behavior (ref. 14, 15, 16, 17).

II. ANALYSIS OF THE PILOT'S BEHAVIOR

Consider the behavior of the human operator in the case of aircraft control.

The aircraft position as sensed by the pilot from his instrument dials or outer sight is compared to the attitude required to follow the nominal flight path. As an example, if the horizontal bar of the ILS indicator lies above the central mark, the pilot analyzes this situation and selects the appropriate correction maneuver to carry out. Once the maneuver has been selected, the pilot's brain (i.e. the decision center) request from the eyes through an internal loop (fig. 1), to collect information relating to the longitudinal attitude. The difference between the actual attitude and the desired one is analyzed and the pilot selects the right control to actuate and determines the force to apply to it. In this example, the pilot pulls on the control stick with a force he judges as correct while requesting his arm, through another loop, to sense the applied force. Stick motion is stopped when the pilot feels that the desired force has been applied.

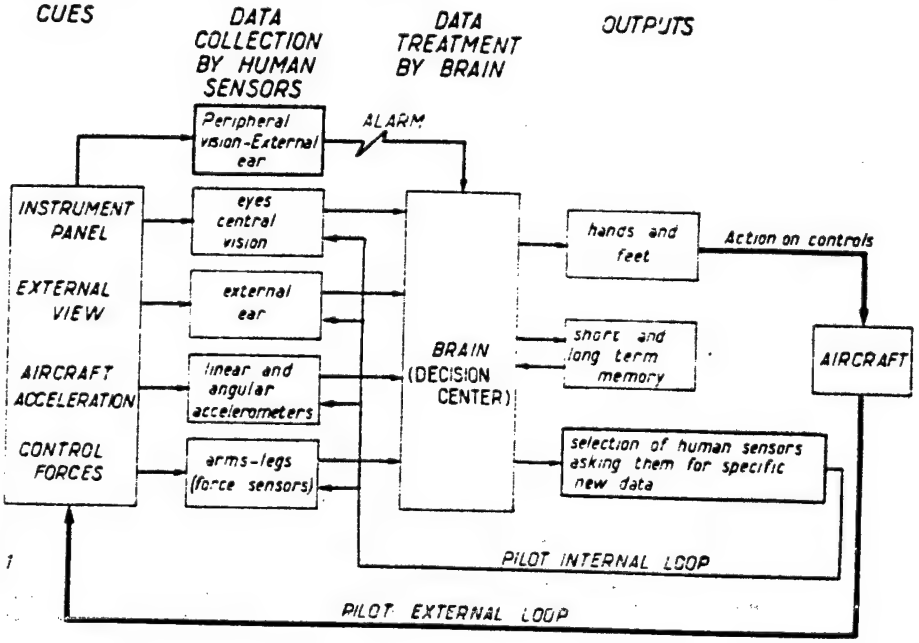

Fig. 1

Hence, the decision center (the brain) puts successively into action various loops while asking for further information from the human sensor. Three types of loops may be considered (fig. 2),

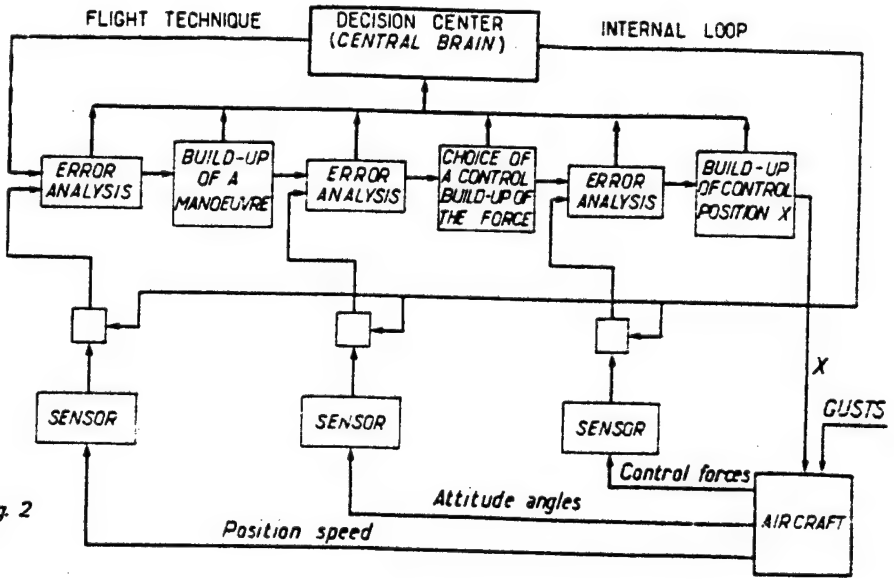

Fig. 2

— outer loops controlling the parameters related to the short-term safety, i.e. flight path, position and speed,

— loops controlling the parameters related to the immediate safety, i.e. the attitude angles, angle of attack, etc .... ,

— finally, the inner loops controlling the forces applied to the controls.

It should be noted that there is *only a single loop* in operation at a given time and this is one of the most fundamental differences between a human pilot and an autopilot. The selection of the currently operating loop is made by the decision center (brain) which designates the selected sensor to collect and transmit the necessary information through an internal loop (fig. 1).

An immediate consequence of this analysis is that it is impossible to determine directly the pilot's workload : at the present time, it seems virtually impossible to follow in detail the processing of data taking place within the brain.

Another consequence is that it is useless to determine experimentally a transfer function representing the pilot's behavior since there is not one, however complex, but a series of transfer functions used sequentially in an order determined by scanning of the various displays. This scanning itself depends on certain data, the environment, the pilot's training, etc... , that is partially on random phenomena. This random nature must be accounted for into some part of the pilot's behavior model.

III. RESPECT OF THE CONTROL LAW

The control law, which is the keeping of permissible deviations of the controlled parameters with respect to the nominal flight path, ensures the immediate safety as well as the short-term safety. This law is used by the pilot as a guideline, it depends on the objective

set by the pilot and on his ability to adapt himself to the conditions of the flight phase execution.

First, the objective set by the pilot may not be formulated in the form of a criterion to be minimized (as proposed by Kleinman, Baron and Levison (ref. 6, 7, 8)). The pilot is neither a perfect being, nor a well-trained monkey who as it is well known, does a better work than a human operator when his task is that of a robot. The human brain can collect a great number of quantitative and qualitative data, some of them being only sensations. The brain is able to built a model of the situation, to compare it with typical situations held in memory, and decide upon an action even if the case has not been foreseen. Then, the objective is much fuzzier : it consists on controlling the plane to reference flight path as close as possible to the nominal flight path. This reference corresponds to the pilot's learning and his know ledge of the plane.

The pilot possesses rather remarkable capabilities of adaptation which are evidenced by the nature of his control commands. An interpretation of this adaptability is the concept of operating image or internal model. The pilot possesses a probably very simplified model of the aircraft which permits him to predict its short-term response given his previous actions.

This concept of internal model permit us to account for the predictive nature of a human pilot's control, as opposed to conventional autopilots.

IV. CHOICE OF A MULTILOOP SEQUENTIAL MODEL

Taking into account the above considerations, a mathematical model must satisfy the following conditions to be as close as possible to the human pilot's behavior (ref. 15).

a) The elementary activities of data collection, development of correction procedures and actuation of controls occur sequencially and not simultaneously as in continuous type models.

b) The various control loops must be identified according to the type of aircraft as well as the nature and number of observed parameters. The type of each loop must be defined, namely as flight path loop relating to short-term safety, attitude loop relating to immediate safety, or loop relating to the control action (see fig. 2).

c) The instants of time when the various loops are activated are not defined in a deterministic manner but are partially random (Poisson process). *Only a single loop* can be in operation at a given time and the pilot applies rules based on his proficiency and personal experience from one loop to another or to monitor the instrument panel. These rules are not strict and depend on the pilot's judgment. Definition of a precise model for the process of selecting among the various loops is one of the most difficult problems to solve and is fully ignored in single loop models.

d) The model must be conceived in such a way that its various characteristic parameters be adjustable from one model of aircraft to another within a given type of aircraft. Obviously, the model for a Mach-2 fighter is necessarily different from that of a conventional subsonic aircraft.

e) Finally, the model must provide a good evaluation of the pilot's workload.

Research on such a multiloop model called "discrete-time model" because of its sequential nature, has been carried out in France, at ONERA (Office National d'Etudes et de Recherches Aérospatiales – French National Aerospace Agency) since 1973. These studies (ref. 16, 17) have led to the development of a computer program simulating the behavior of a pilot of a heavy transport plane (Airbus A300B) and capable to perform a particular flight path (final descent of an ILS approach). The model will soon be extended to make it adapt to various aircrafts of the same type (this version is currently being tested with a model of the Dassault Falcon 20).

V. DESCRIPTION OF THE DISCRETE-TIME PILOT MODEL

In this model, it is assumed that, at a given time, the pilot can either make a decision or carry out one of the following three elementary actions :

- actuate a control,
- read an information on the instrument panel,
- monitor a given parameter displayed on a dial.

It is assumed that the pilot's strategy, that is the process of selecting among the various procedures of parameter correction, has a sequential nature and is a function of the flight situation defined by the aircraft type and condition, the flight phase and atmospheric conditions.

Experimental data have led to distinguish between three levels of activity in the pilot's operating mode (fig. 3). This classification is only an assumption, but seems to be close to reality and corresponds to the three types of loops discussed above.

LEVEL	DEFINITION	OBJECTIVE	COST
STRATEGY	Choice of correction procedures	Short - term safety	Mental load (decision)
CORRECTION PROCEDURE	Algorithmic sequence of elementary actions	Immediate safety	Mental load (memorization)
ELEMENTARY ACTION	• Read indicator • Act on one control • Monitor one dial		Physical load

Fig. 3 – Levels in operating mode.

The model selects the correction procedure to be used as a function of the followed strategy. This procedure is further divided into a sequence of elementary actions (instrument reading, monitoring of a parameter, action on a control) which are successively taken.

A dual integration is performed at each time in the model, namely the integration of the equations of motion and the integration of the equations describing the operating image of the situation as memorized by the model.

In the proposed strategy, care has been exercised to make a clear distinction between the selection of dials monitoring (a strategy with Markovian readings is used) and the selection of parameter correction procedures (a strategy with short term evaluation is used). The differenciation between these two strategies is based on the concept of seriousness of the instantaneous situation as perceived by the pilot's model and defined by :

$$G(O) = \text{Max.}_{\text{on the main parameters}} \left| \frac{\text{estimated deviation}}{\text{permissible deviation}} \right|$$

This is the maximum ratio, over the flight path main parameters, between the estimated deviation (as memorized or predicted by the internal model) of a given parameter and its permissible deviation. The permissible deviations are determined experimentally. If $G(O)$ is under a given minimum threshold of seriousness, the situation is evaluated as safe and the model adopts the dial monitoring strategy ; if $G(O)$ is above his threshold, the situation is evaluated as serious and the model applies the strategy of parameter correction procedures (fig. 4).

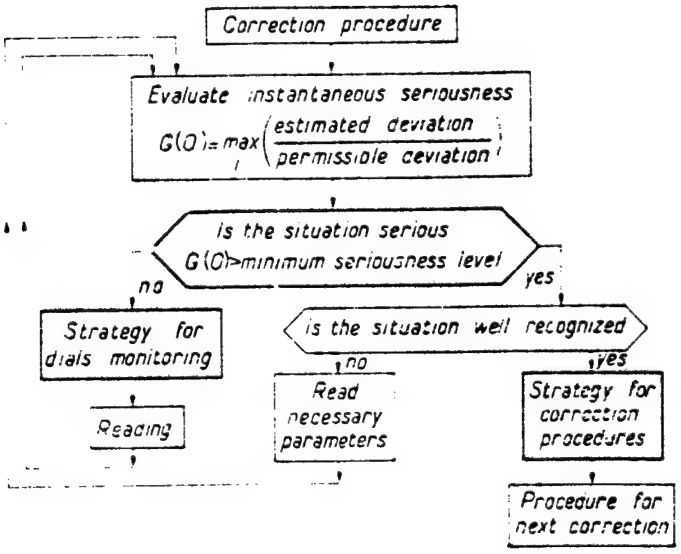

Fig. 4 — Overall strategy.

As far as the strategy of dials monitoring is concerned, the sequence of observed dials is governed by a matrix of conditional probabilities of reading each instrument after another one. This matrix is called "switching matrix". After each instrument reading, the value of a random variable determines which dial will be read next, depending on the switching matrix. The sequence of reading times is regarded as a Poisson process. Figure 5 gives an example of switching matrix in the case of the ILS approach phase of an Airbus A-300B. This matrix has been determined experimentally by means of an electro-oculometer. In retrospect, were observed in this matrix the features of elementary monitoring rules during IFR flight. For instance, the artificial horizon was mostly observed.

SWITCHING MATRIX

	ε_{GL}	ε_{LOC}	$\dot{z}$	Φ	Θ	Ψ	F	z	V
ε_{GL}	0.03	0.10	0.11	0.04	0.15	0.03	0.06	0.21	0.20
ε_{LOC}	0.28	0.15	0.05	0.21	0.06	0.23	0.05	0.05	0.08
$\dot{z}$	0	0.03	0.06	0.07	0.10	0.05	0.06	0.11	0
Φ	0.10	0.39	0.12	0.29	0.18	0.28	0.17	0.09	0.10
Θ	0.40	0.14	0.20	0.16	0.29	0.13	0.19	0.21	0.18
Ψ	0.08	0.12	0.16	0.13	0.13	0.10	0	0.16	0.07
F	0	0.01	0.10	0.01	0	0.05	0.11	0	0.09
z	0.03	0.04	0.13	0.07	0.07	0.11	0.12	0.12	0.08
V	0.08	0.02	0.07	0.02	0.02	0.02	0.24	0.05	0.20
Σ	=1	=1	=1	=1	=1	=1	=1	=1	=1

MATRIX OBTAINED WITH EOM EQUIPMENT

- ALL PARAMETERS $x_i < L_i$ → INSTRUMENT READINGS ARE GOVERNED BY THE SWITCHING MATRIX
- ONE PARAMETER $x_i \geq L_i$ → READING OF x_i
- SEVERAL PARAMETERS $x_i \geq L_i$ → READING OF x WHICH HAS THE GREATEST PROBABILITY IN THE SWITCHING MATRIX

L_i LEVEL GIVEN IN ADVANCE FOR EACH PARAMETER x_i

Fig. 5 — Strategy for dials monitoring.

C-3

The strategy of the correction procedures is based on the fact that the human pilot makes decisions depending on the short-term predicted evolution of the situation while taking into account all previous actions.

The model has no access to the equations governing the aircraft dynamics but, by using its operating image, it can predict approximately the short-term situation. This prediction capability is used by the model to select the best correction procedure to implement, each time it is necessary. This choice is made by developping a logical tree (fig. 6) in which,

- the root is the memorized situation (So) ;
- branches are the correction procedures whose implementation is considered ;
- nodes other than the root are situation predicted from the root by means of the operating image while taking into account the intented correction procedures.

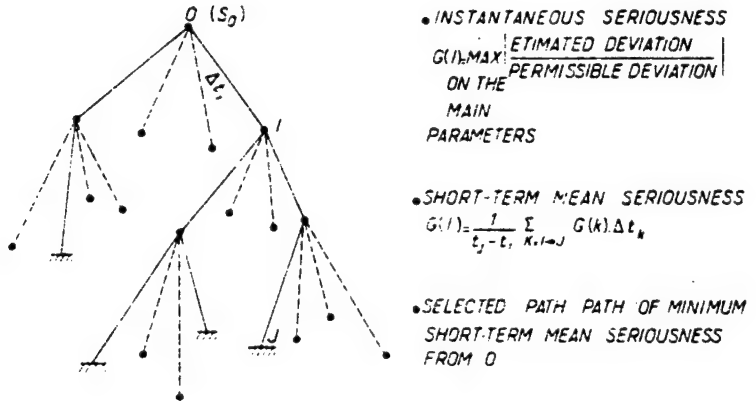

Fig. 6 – Strategy for correction procedures.

The instantaneous seriousness G(K) is computed at each node K. Considering that it remains constant during the time Δtl elapsed from the previous node to the node I, the model computes a short-term mean seriousness $G(I)$ on each path leading to a terminal node. To that end, the instantaneous seriousness is weighted by the time elapsed on each branch and the result is divided by the total time elapsed on the path. The short-term mean seriousness of a path (I, J) is then expressed by

$$G([I, J]) = \frac{1}{t_J - t_I} \sum_{K = I \rightarrow J} G(K) \cdot \Delta tk$$

The mean seriousness of the best path $G([I, J])$ chosen at I is denoted $G(I)$. This choice is simply made by taking among all possible paths from I the one with the minimum mean seriousness.

The path from the root with the minimum mean seriousness is then chosen and the implementation of the correction procedure corresponding to its first branch can be initiated.

VI. PROGRAM APPLICATIONS

Two applications have been made to validate this program. Both apply to the simu-

lation of the final descent of the ILS approach phase for an Airbus A-300B. First, a statistical comparison has been made between the performances of the model and those of professionnal pilots. Secondly, the performance loss of the model when the static margin of the simulated aircraft is decreased has been investigated.

VI,1. Comparison between the model and professionnal pilots

It is meaningless to compare the time responses obtained from the model and from human pilots. As good as it may be, the match between the curves cannot be perfect. A statistical comparison would be more meaningful. We have therefore chosen a comparison between the standard deviation and the performance, which are defined below for the various flight parameters.

$$\text{Standard deviation } \sigma x = \sqrt{\frac{\int_0^t x^2\,dt}{t}}$$

$$\text{Performance } Px = \sqrt{\frac{t}{\int_0^t |x|\,dt}}$$

where t is the duration of the final descent of the ILS approach phase.

The results from the model have been compared to those of five professionnal pilots performing final descents in IFR conditions on a flight simulator representing the heavy transport plane considered in this study. The comparison is illustrated in figure 7 ; it can be seen that the model exhibits a behavior close to the pilot's as far as the above defined standard deviations and performances are concerned.

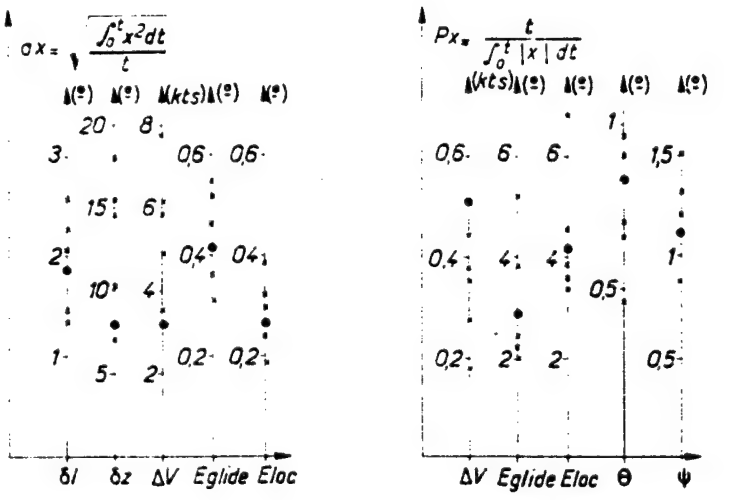

Model-pilot initial deviations at 1900 feet

x human pilot

● model

Localizer deviation : − 0,6°
Glide path deviation : 0,65°
ΔV = + 8 kts (Va = 137 kts)

Fig. 7 – Standard-deviations and performances.

VI,2. Application of the model to flight control with reduced static margin

One of the first practical applications of the model has been the study of its performance loss when the static margin of the simulated aircraft decreases, i.e. when the center of gravity moves backward, progressively destabilizing the plane. It appears that the performance of the model decreases when the static margin is reduced, which seems realistic. The loss of control occurs suddenly (fig. 8) when the workload resulting from a decrease in static margin becomes excessive. The most interesting result of this study is that, whenever control difficulties appear on the pitch axis, the overall aircraft control is impaired ; for most of the cases losses of control occur on the transversal axis.

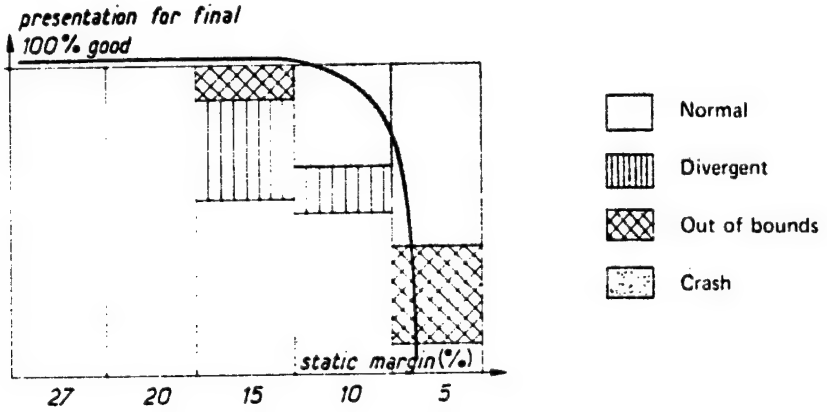

Fig. 8 – Basic ILS approaches with reduced static margins.

VII. CONCLUSION

The model described in this paper is expected to be more conform to the actual pilot's behavior than those of previous studies. It tries to make a synthesis between the mathematical approach and the psychological approach through the introduction of the aircraft internal model.

In the future, studies will attempt to introduce the concept of pilot adaptativity to a new type of aircraft as well as the concept of learning which could take into account the degree of professionnal development of individual pilots.

REFERENCES

1. Goodyear Aircraft Corporation – Final Report : Human Dynamics Study – Report GER-4750, April 1952.

2. McRuer D., Graham D., Krendel E., Reisener W. – Human pilot dynamics in compensatory systems. USAF Tech., Report AFFDL TR-65-15, July 1965.

3. McRuer D., Jex H. – A review of quasi linear pilot models. IEEE Transactions on Human Factors in Electronics, vol. 8, No. 3, pp. 231-249, September 1967.

4. McRuer D.T., Krendel E.S. – Mathematical Models of Human Pilot Behavior. AGARDograph No. 188, January 1974.

5. Bekey G.A., Meissinger H.F., Rose R.E. — Mathematical models of human operators in simple two-axis manual control systems. IEEE Transactions on Human Factors in Electronics, vol. 6, pp. 42-52, 1965.

6. Kleinman D.L., Baron S., Levison W.H. — An Optimal Control Model of Human Response — Part I, pp. 357-369, Part. 2, pp. 370-383, Automatica, vol. 6, No. 3, May 1970.

7. Kleinman D.L., Baron S. — Manned Vehicle Systems Analysis by Means of Modern Control Theory. NASA CR-1753, June 1971.

8. Kleinman D.L., Baron S., Levison W.H. — A Control Theoretic Approach to Manned-Vehicle Systems Analysis. IEEE Trans., vol. AC-16, No. 6, pp. 824-832, December 1971.

9. Piaget J., Inhelder B. — Mémoire et Intelligence. Col. BSI-PUF-1968.

10. Bisseret A. — Mémoire opérationnelle et structure du travail. Bulletin de Psychologie XXVI, 1972-1973.

11. Sperandio J.C. — Compléments à l'étude de la mémoire opérationnelle. Deux expériences sur les contrôleurs de la navigation aérienne. Le Travail Humain, vol. 38, 1975.

12. Veldhuyzen W., Stassen H.G. — The Internal Model - What does it mean in Human Control ? - International Symposium NATO "Monitoring Behavior and Supervisory Control", Published in NATO Conference Series III, vol. 1 by Plenum Press, 1976.

13. Phatak A.V. — Formulation and Validation of Optimal Control Theoretic Model for Human Operator. IEEE Systems Man and Cybernetics Newsletters, vol. 2, June 1976.

14. Wanner J.C. — General guideline for the design of manned aerospace vehicles - Automation on Manned Aerospace System. AGARD Conf. Proc. No. 114 (1973).

15. Wanner J.C. — The multiloop concept of the pilot workload as a basis of future experiments and studies. T.P. ONERA No. 1978-10.

16. Cavalli D., Soulatges D. — Discrete-time modelization of human pilot behavior. Proceedings of the 11th Annual Conference on Manual Control. NASA Ames Research Center, Ca. May 1975, NASA TM X-62, 464, pp. 119-129.

17. Cavalli D. — Discrete-time modeling of heavy transport plane pilot behavior. Proceedings of the 13th Annual Conference on Manual Control, MIT, Cambridge, Mass., June 1977, pp. 321-328.

SESSION D: FLIGHT CONTROL AND PILOT DYNAMICS

Chairman: I. Ashkenas

FLIGHT EXPERIENCE WITH MANUALLY CONTROLLED UNCONVENTIONAL AIRCRAFT MOTIONS

BY

A. FINLEY BARFIELD

AIR FORCE FLIGHT DYNAMICS LABORATORY

WRIGHT-PATTERSON AFB, OHIO

ABSTRACT

During 1976 and 1977, a modified YF-16 aircraft was used to flight demonstrate decoupled control modes under the USAF Fighter Control Configured Vehicle (CCV) Program. Higher levels of direct force control were achieved by the aircraft than had previously been flight tested. The direct force capabilities were used to implement seven manually controlled unconventional modes on the aircraft, allowing flat turns, decoupled normal acceleration control, independent longitudinal and lateral translations, uncoupled elevation and azimuth aiming, and blended direct lift. A miniature two-axis force controller was installed on top of the YF-16 sidestick controller for commanding the decoupled modes. At the pilot's discretion, the directional modes could also be commanded using rudder pedals.

The unconventional control modes were flight evaluated during simulated operational tasks, such as air-to-ground bombing and strafing, and air-to-air tracking and defensive maneuvering. The flight testing identified many actual and potential uses for these control modes, but also identified areas where refinements are needed to arrive at operationally suitable implementations. This paper describes the design, development, and flight testing of these new control modes. It includes lessons learned in the areas of unconventional control law implementation and controller design. The need for task-tailored mode authorities, gain-scheduling and selected closed-loop design is discussed.

INTRODUCTION

The Air Force Flight Dynamics Laboratory's Fighter CCV Advanced Development Program was conducted to develop and evaluate advanced control concepts for improving fighter aircraft mission effectiveness. Specific new control degrees of freedom were provided in an existing high-performance fighter. Control modes selected for implementation had been identified by previous research efforts as possessing the potential for significantly improving fighter aircraft performance. Use of these unconventional control modes provided the pilot with unique aircraft maneuvering capabilities. This program provided the first true test of

the utility of these new capabilities. Design, modification and flight testing were conducted under contract to General Dynamics/Fort Worth.

The YF-16 shown in Figure 1 was uniquely suited as a testbed for the program. It served as a state-of-the-art baseline configuration with its full authority quad redundant analog Fly-by-Wire control system, sidestick controller, and advanced aerodynamic design employing vortex lift and leading edge maneuvering flaps. The aircraft was designed to be statically unstable longitudinally in subsonic flight with artificial stability being provided by the control system. Angle of attack and "g" limiting allowed full maneuvering without reliance on stall warning or cockpit instruments and provided maximum use of the airframe load factor capability throughout the flight envelope. This advanced control system design facilitated implementation of the new CCV control modes.

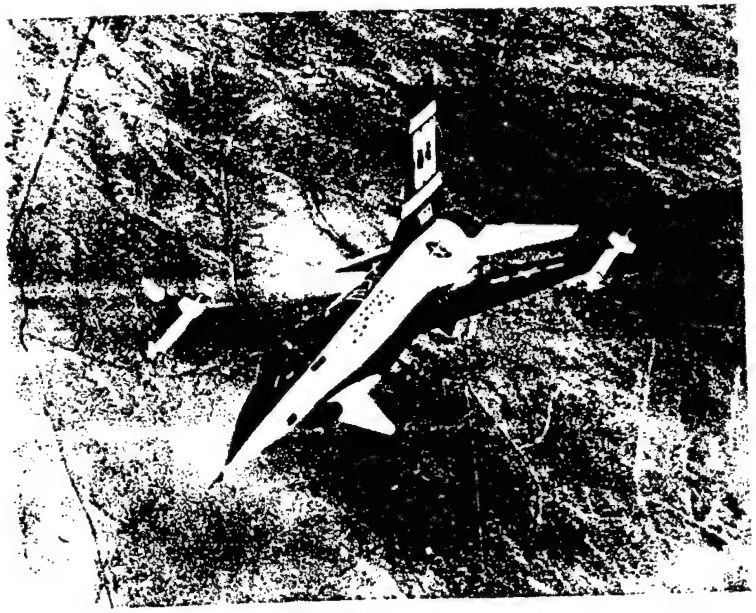

Fig 1 Fighter CCV Test Aircraft

DESIGN APPROACH

Cost effectiveness and safety considerations were major driving factors in the configuration selection and design. In this light only minor modifications were made to the YF-16 aircraft. Although providing a means of assessing the new control capability, this approach prevented overall control and aerodynamic design optimization. Exterior changes to the aircraft consisted of the addition of twin all-movable vertical canards. The new surfaces, canted outward 30 degrees from vertical, were

attached at the engine inlet. The installation was accomplished without altering the external or internal mold lines of the inlet. Although separately actuated, the canards are deflected together by the same pilot-generated command signal. Use of the canards in conjunction with the rudder enabled direct sideforce to be developed by the aircraft. The flaperons were modified to allow both up and down symmetric deflections. Operation of the flaperons with the horizontal tail provided a direct lift capability.

An auxiliary analog computer was added to allow implementation of the new control laws. A fail-safe design was required. Additionally, the CCV modifications were not to result in degradation of the operational reliability of the basic YF-16 control system. That system was retained intact to provide suitable control and stability augmentation. The conventional YF-16 control system formed the baseline configuration for the program. It also served as the reversion configuration should problems cause CCV system disengagement. The addition of CCV signal interfaces was the only change to that system. Control reconfiguration was achieved by injection of bias signals and crossfeeds to alter the normal pilot commands or system feedbacks. Operation throughout the aircraft's envelope was needed for a valid evaluation of the unconventional modes. Gain scheduling was extensively employed to provide proper response as flight conditions varied. Emphasis was placed on obtaining maximum CCV mode capability across the mach-altitude range without creating adverse transients.

Crew station changes involved the addition of instruments such as sideslip, side acceleration, canard and flaperon position indicators to allow evaluation of CCV responses by the pilot. A CCV control panel was installed to enable mode selection, and modifications were made to the trim button on the sidestick controller to provide a means of commanding the open-loop CCV modes.

UNCONVENTIONAL CONTROL MODES

At the pilot's command were six open-loop modes illustrated in Figures 2 and 3. Direct control of the aircraft's flight path in two axes was provided by the A_n and A_y modes. The aircraft rotated in pitch and yaw with the velocity vector. In pitch, α was held constant while direct lift was generated on the aircraft. Sideslip remained zero during use of the sideforce mode as side acceleration was generated allowing turning of the aircraft without banking. Attitude control at constant flight path angle was available with the α_1 and β_1 modes resulting in independent fuselage pointing in either axis. Vertical and lateral translations were provided by the α_2 and β_2 modes. In this case vertical velocity and side velocity were the controlled parameters at constant aircraft attitude. Thus the aircraft could effectively elevate or side step.

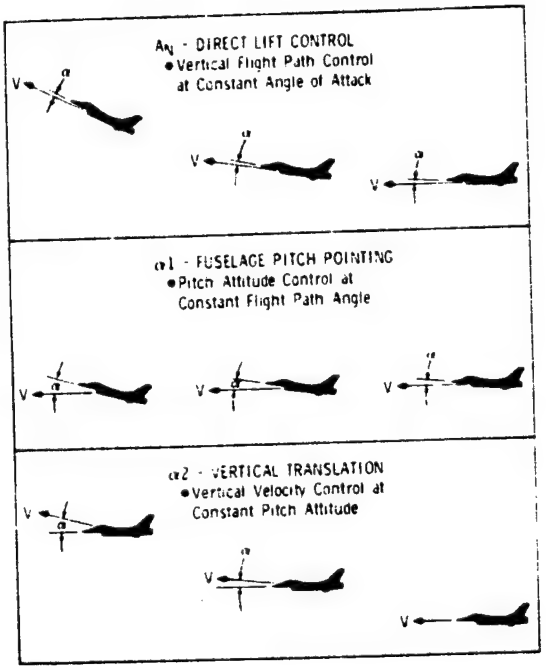

Fig 2 Open-Loop Longitudinal CCV Modes

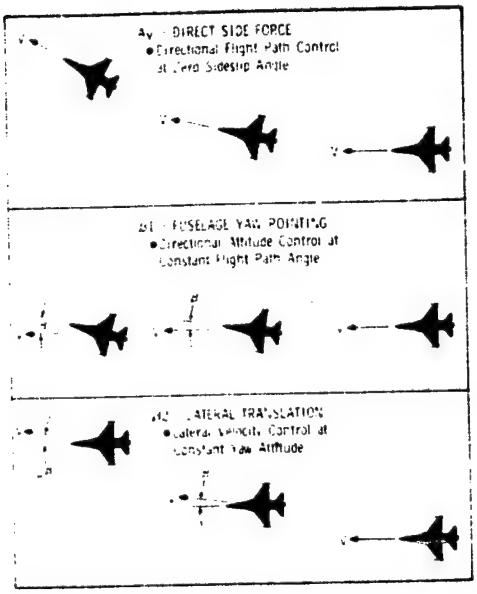

Fig 3 Open-Loop Directional CCV Modes

One closed-loop mode, Maneuver Enhancement (ME), was also available to the pilot. Direct lift was blended with basic aircraft pitch control in this mode. It provided an initial direct lift during a maneuver which was washed out as the commanded aircraft normal acceleration was obtained. Use of this capability resulted in maneuver quickening. Due to the use of normal acceleration feedback, a level of gust alleviation was also provided as illustrated in Figure 4.

Implementation in accordance with the approach of an "add on" design is illustrated with the simplified block diagrams in Figures 5, 6 and 7. The conventional YF-16 control system is shown in solid black in the figures. Dashed lines indicate the CCV modes. For the three open-loop longitudinal modes, the pilot commands flaperon deflection directly with the elevator being driven through a scheduled crossfeed gain. Biases to prevent opposition of the CCV commands are computed and introduced into the YF-16 control system. In the case of the A_n mode, Figure 5, stick command and pitch rate paths are modified by the bias signals. CCV system gains were determined using wind tunnel data and digitally predicted aircraft responses.

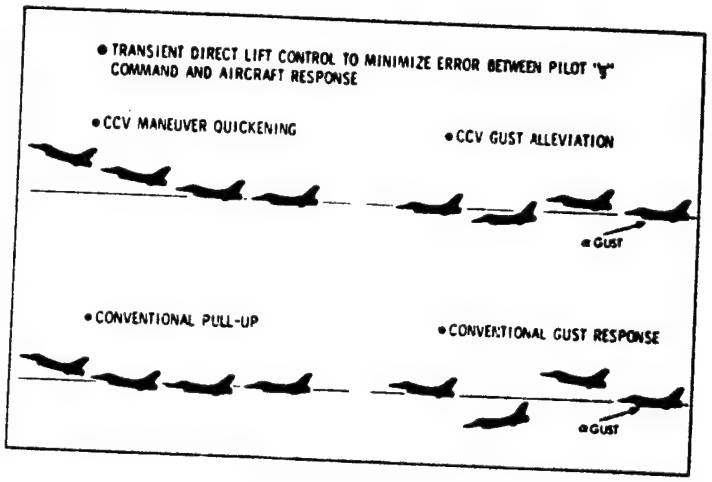

Fig 4 Maneuver Enhancement Mode

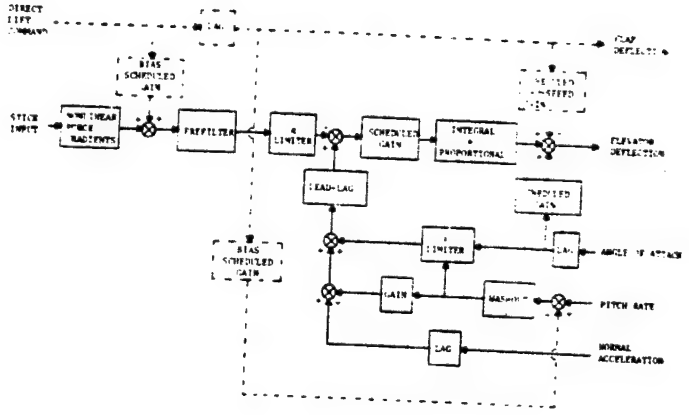

Fig 5 Simplified Functional Block Diagram of the A_n Mode

The directional modes are structured in much the same manner. The pilot commands a canard deflection with an appropriate crossfeed to the rudder as shown for the direct sideforce mode in Figure 6. In this case a gain scheduled crossfeed to the flaperons is needed to counter rolling moments from the canard-rudder deflections. Biases are also added to the yaw rate and lateral acceleration feedbacks of the basic control system.

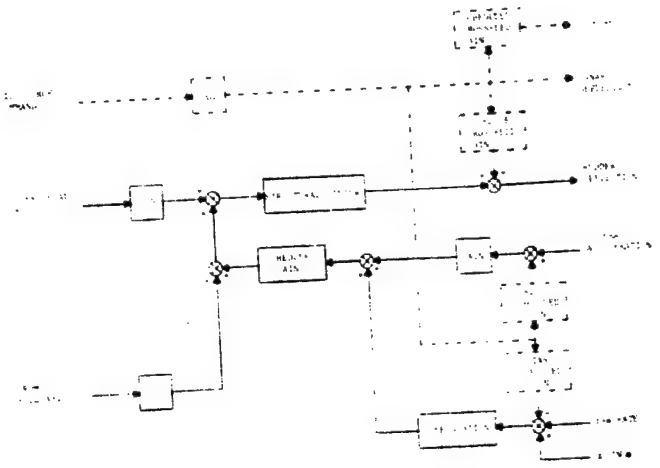

Fig 6 Simplified Function Block Diagram of the A_y Mode

The one exception to this type of implementation is Maneuver Enhancement. As shown in Figure 7, the error between pilot command and aircraft normal acceleration drives the flaperons and horizontal tail. A washout in the pitch rate feedback path, and integral plus proportional control in the forward path, provides a "g" command response in steady state. Thus as the aircraft attains the commanded "g" level, the direct lift flaperons return to zero deflection. The technique provides an instantaneous direct lift for maneuver quickening. Gust alleviation is obtained when the normal accelerometer feedback senses gust induced aircraft response and drives the flaperons to counter it.

Minor modifications to the YF-16 cockpit were made to allow use of the CCV modes. Specific modes are selected by the pilot using the CCV control panel shown in Figure 8. Any of the three open-loop longitudinal modes can be commanded by fore or aft force on the CCV controller installed on the YF-16 sidestick, Figure 9. The trim switch was replaced with the two-axis CCV force controller, and the normal "coolie hat" thumb button was retained. The three open-loop directional modes can be selected for operation through either rudder pedal inputs or left/right force on the CCV controller. Besides mode selection the control panel also provides the pilot with pitch and roll autopilot

functions as well as mode purification capability. Purification was designed to allow engineering evaluation of the modes by enabling various feedbacks to force "pure" steady state uncoupled aircraft motion. In this way the adequacy of interconnect and bias gain schedules based on predicted CCV responses could be ascertained. The control panel also provides a means of removing side acceleration, A_y, feedback to the rudder in the basic control system. Various self-test functions were also included for system checkout and diagnosis on the ground.

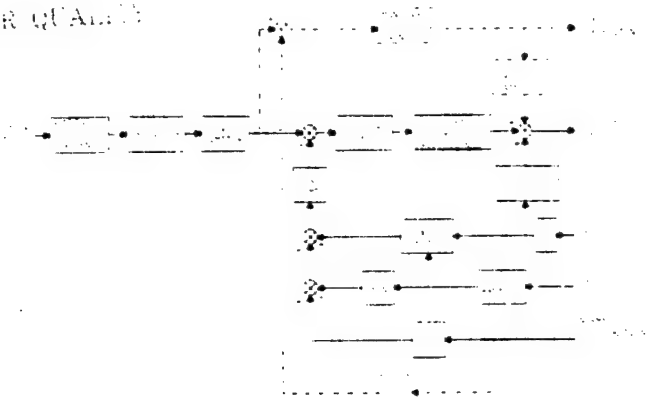

Fig 7 Simplified Functional Block Diagram of Maneuver Enhancement

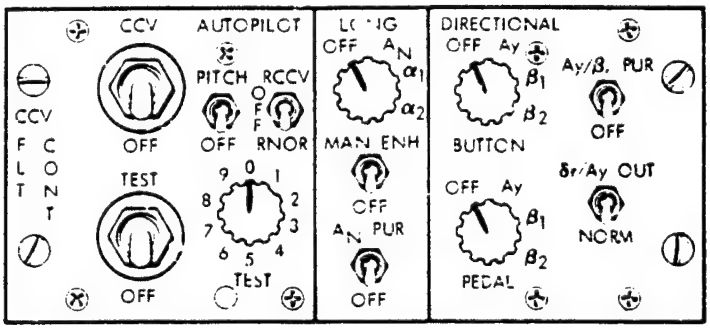

Fig 8 CCV Control Panel

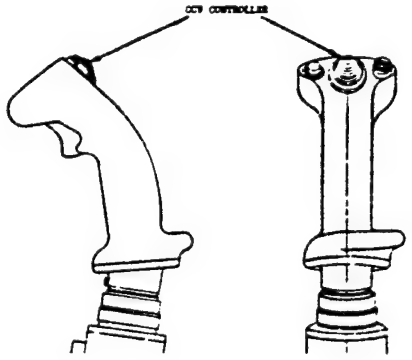

Fig 9 CCV Controller Installation on Sidestick

The basic airplane sidestick controller is essentially a force stick although the sensors employed are Linear Variable Differential Transformers which measure a very small displacement of the stick resulting from forces applied by the pilot. Maximum command in pitch requires 31 lbs.,and maximum roll requires a little more than 15 lbs. Both axes have parabolic stick force versus command gradients. The CCV button has a 0.1 lb. deadzone with a linear force versus command gradient up to a maximum of 3.1 lbs.

FLIGHT TESTING

The flight test program consisting of 87 flights and totalling over 125 flight hours was conducted at Edwards AFB in California. Figure 10 presents the range of flight conditions over which testing was performed. Initially the flight envelope was cleared in tests to identify flutter, aeroservoelastic instabilities, or stability and control problems. The effect of the canards addition on inlet/engine operation and the aerodynamic destabilizing effects were also evaluated during the initial tests. Preliminary checks were performed to verify proper functioning of the CCV control system. Engineering evaluations were then conducted to ascertain the functional adequacy of the CCV control system design and to obtain data for detailed evaluation of the various mode characteristics. Figure 10 also indicates test conditions for evaluating predicted performance improvements with Relaxed Static Stability (RSS). Although not covered in this paper, the aircraft's fuel system was modified to allow a wide range of center-of-gravity locations to be evaluated during the later portion of the test program. Finally quasi-operational tasks were conducted simulating air-to-air gunnery, formation, refueling, air-to-ground bombing and air-to-ground strafing.

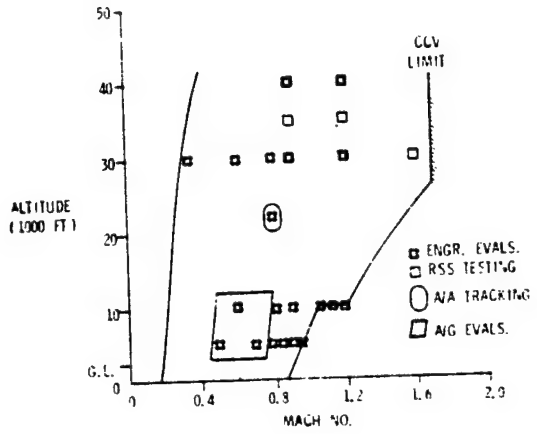

Fig 10 Primary Test Points

The CCV modes produced responses as predicted, and the modified aircraft was found to be free of instabilities. It also possessed adequate handling qualities throughout the flight envelope up to its angle of attack and sideslip limits. No adverse effects of the canards on inlet or propulsion system performance were detected. Although the canards were destabilizing both longitudinally and directionally, the YF-16 control system provided stability augmentation that effectively compensated for the change. The engineering evaluations provided data to allow refining of the CCV control system gain schedules which had been selected originally on the basis of wind tunnel information. The evaluations also verified the available CCV mode authorities. Direct lift levels of up to $\pm$ 1.5 g's and side force levels of 0.9 g were obtained. These capabilities varied considerably with flight conditions since the design was to obtain maximum capability, and not to provide uniform authority. Yaw pointing levels approaching $\pm$ 5 degrees and pitch pointing of approximately $\pm$ 2 degrees were realized. Translation authorities of 1500 fpm rate of climb for the α_2 mode and 40 kts side velocity for the β_2 mode were demonstrated.

The Handling Qualities During Tracking (HQDT) technique developed at the NASA Dryden Flight Research Center and the Air Force Flight Test Center was used for engineering analysis of the CCV modes during tracking. For this technique, scored gun camera film is used to obtain a quantitative measure of handling qualities, control system characteristics, and precision controllability during high-gain tracking tasks. A fixed depressed reticle is used in a preplanned tracking task employing in this case an F-4 or T-38 target aircraft. The air-to-air tracking maneuver

consisted of windup turns (WUT) to 4.5 g's and 3g constant turns. The technique was also applied to air-to-ground runs with limited success. Unfortunately, the technique does not resemble most air-to-ground delivery techniques. RMS, mean, and median tracking errors along with time histories of pipper position relative to the target are provided by the technique. This data was used in connection with pilot ratings and comments to evaluate the CCV modes' usefulness. Ordnance was not actually delivered because the YF-16 testbed did not have a weapon delivery capability.

Early in the evaluations, results from tracking with Maneuver Enhancement indicated the usefulness of this mode. Figure 11 is a longitudinal parameters comparison of the aircraft with and without ME during a windup turn tracking task. The reduction in magnitude of pitch rate perturbations and pilot inputs indicates a useful mode for precise tracking. Tighter "g" control was available to the pilot, and small corrections could be made without causing large rotational rates. This preliminary assessment proved to be correct when pilots from the F-16 Joint Test Force evaluated the modes in simulated air-to-air gunnery.

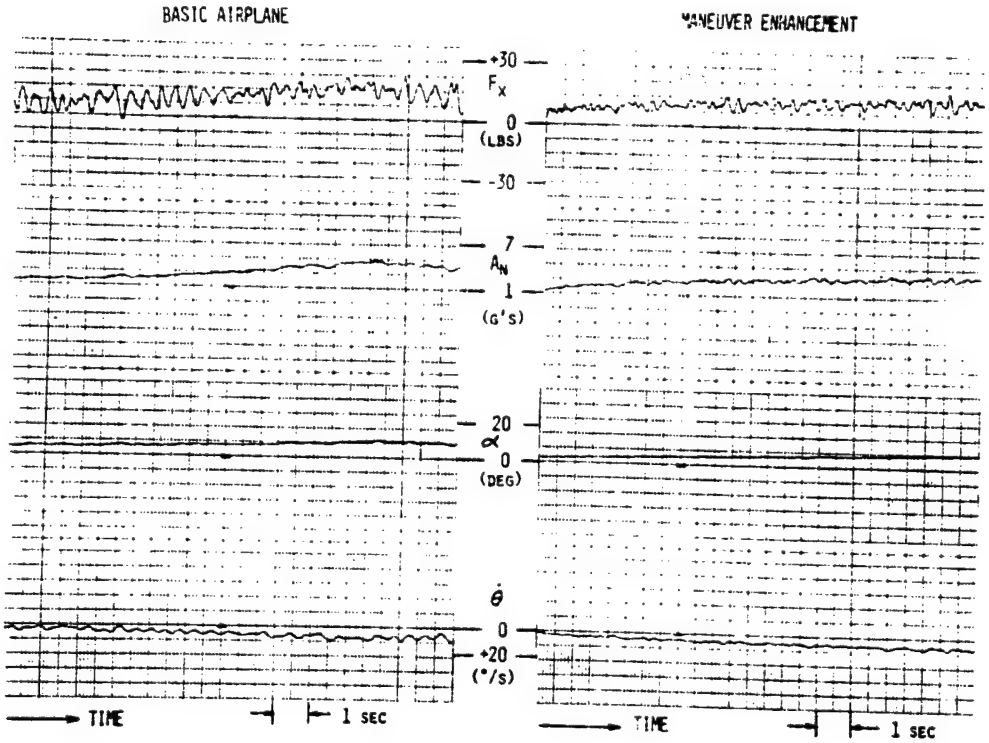

Fig 11 Windup Turn Tracking

Overall assessment of the CCV modes for various operational tasks are shown in Figure 12. This is a consensus of pilot opinion on the potential improvement these modes could provide. A "G" or green rating indicates that the mode is either preferred or has the potential for improvement over conventional controls. The "Y" or yellow rating is used to denote that the mode did not show a potential improvement over conventional controls or that pilot ratings and comments were inconclusive.

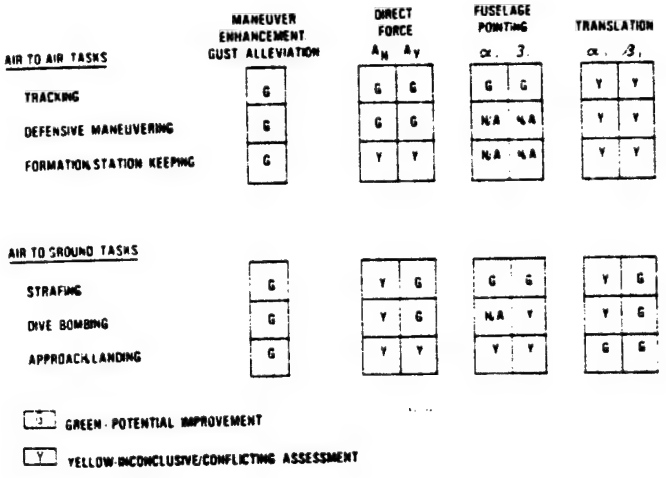

Fig 12 CCV Mode Assessment

Maneuver Enhancement was considered an improvement as it was implemented on the test aircraft in all air-to-air tasks. It provided tighter control in a tracking situation without the usual rotational perturbation. Pilot control was not complicated by an additional controller since this was a blended mode on the normal sidestick. Washout of flaperon deflections prevented saturation problems of the limited authority direct lift capability.

The direct force modes, A_n and A_y, were preferred over pointing or translation for precise tracking. The mechanization allowed pilots to "beep" CCV commands using the button controller in much the same manner as a trim switch. It provided an immediate precise change in flight path. Such a "beep" technique was realizable because command and release cause no objectionable pipper transients. The direct force modes were also considered to hold promise for some unusual and effective defensive maneuvering capabilities, but larger authority levels than obtainable on the CCV YF-16 were desired by most of the pilots.

The pointing modes were difficult for manual pilot control. Although providing reasonable authority and precise fuselage pointing, the command had to be held in continuously. Upon release of the CCV controller, the pipper moved sharply away from the target as the aircraft returned to align with the velocity vector. This proportional input on the CCV controller,while trying to keep the basic tracking solution through changing forces on the sidestick,resulted in what one pilot referred to as a hand conflict. A tendency existed to rapidly reach and hold full pointing capability as the maneuver changed. The pilot had to immediately realize when maximum capability had been reached and revert to basic aircraft control for further error reductions. This would result in maneuvering the aircraft with full pointing capability being commanded and at times introduced unwanted lags in tracking. Even with these drawbacks, the mode was rated highly as far as its potential for improvement. Most pilots commented that an automatic tie-in with the fire control system would make a very effective gunnery system.

The translation modes were implemented with slow onset rates and low steady state authorities which made them unsuitable for air-to-air combat maneuvering. Due to the open-loop design, the aircraft had a tendency to coast after a translation command had been removed. This was bothersome to the pilot as he tried to close on another aircraft since exact final position was not easily predicted. The translation modes could be used for formation/station keeping; however, the task was adequately handled with the basic aircraft controls. Thus, a clear need for improved means of accomplishing the task did not exist. The one exception was application in refueling operation. The CCV modes were believed to offer significant advantages in this case. Unfortunately, due to the limited redundancy in the mechanization and safety considerations, such applications could not be evaluated. Refueling with CCV modes engaged was prohibited.

For the air-to-ground work, Maneuver Enhancement again demonstrated an improvement as implemented on the test aircraft (Figure 12). This was primarily due to: 1) the gust alleviation capability it provided; and, 2) the increased response when pulling out of a dive. The manual control task was not significantly changed with the blended implementation on the sidestick. Normal piloting techniques could be used for task accomplishment.

Direct side force, A_y, received favorable pilot rating for both strafing and dive bombing. The primary advantage was elimination of having to roll-pull-roll back to make directional corrections. The effect of each correction could be immediately and easily determined since the basic sight picture remained unchanged. Rudder pedals for A_y commands were well liked,and the pilots easily adapted to their use. The authority provided appeared excessive for terminal tracking. The A_n mode found only sparing application in the air-to-ground tasks because longitudinal control posed no specific problem and was easily accomplished with the normal stick commands. Use of the force button was not natural

for the pilot in these tasks, and cross-talk between button and stick existed.

Pointing capability in both axes was found useful for strafing runs. Two techniques were used with pitch pointing. In the first method the pipper was allowed to walk up to the target and was then held on the target with the pointing capability to provide a longer firing opportunity. The second technique involved using full nose down pointing throughout the run. This allowed considerably more ground clearance during low-level passes. For bombing, the pointing modes were not appropriate since the velocity vector was not being changed. There was one exception. It was possible to use the mode to mimic the translation mode's crosswind cancelling capability with higher responsiveness. This was accomplished by establishing a crab in the normal manner to counter the crosswind and allow the flight path to cross the target. Then yaw pointing was used to align the nose with the resultant velocity vector giving the pilot a good HUD sight-target picture.

Longitudinal translation was useful in the power approach for maintaining a desired glide path. However, due to the limited authority and slow response, it was not satisfactory for strafing or bombing. In addition, the normal longitudinal command provided adequate control for these tasks. The lateral translation capability was useful for crosswind corrections during both landing approach and dive bombing. It could also be used to attack moving targets from an approach perpendicular to the target's motion. Slowness of response and the requirement to hold a constant button force during mode usage were considered drawbacks of these two modes.

SIMULATION INVESTIGATION

Results of the flight testing showed the need for additional unconventional control mode studies. Pilot comments clearly indicated the capability provided by the unconventional modes had the potential for improving the aircraft's effectiveness, but some aspects of the particular implementation on the test vehicle were unsatisfactory. The two-axis force button selected after evaluation of several types of controllers in a fixed-base simulation at General Dynamics provided adequate for engineering evaluations but lacking for operational usage. Various mode authorities, responses and mechanizations were found to be inadequate for tracking and weapon delivery tasks. The flight test effort had been extremely ambitious in terms of flight rate. This restricted modifications from being accomplished to the CCV hardware except to satisfy safety-of-flight requirements. As a result of these findings, the Flight Control Division of the Flight Dynamics Laboratory initiated an extensive simulation investigation to be conducted on the Large Amplitude Multi-mode Aerospace Research Simulator (LAMARS) shown in Figure 13. LAMARS comprises part of the Flight Dynamics Laboratory's Engineering Flight Simulation Facility at Wright-Patterson. The sphere, containing a single place cockpit, and the 30 ft. support beam are computer controlled to provide realistic cockpit motion cues. The pilot's visual display is

projected on the interior of the 20 ft. sphere. It can be either a simple sky/earth image or projection of terrain features from one of two 15 ft. by 48 ft. terrain boards. An air-to-air target aircraft projector is also included for combat simulations. The spherical contour provides a maximum 266 degree horizontal and 108 degree vertical field of view. Motion capability of the simulator is listed in Figure 14. A hybrid computing system forms the core of the simulation facility. Nonlinear aerodynamics and the complete YF-16 and auxiliary CCV control system have been modeled on the computers.

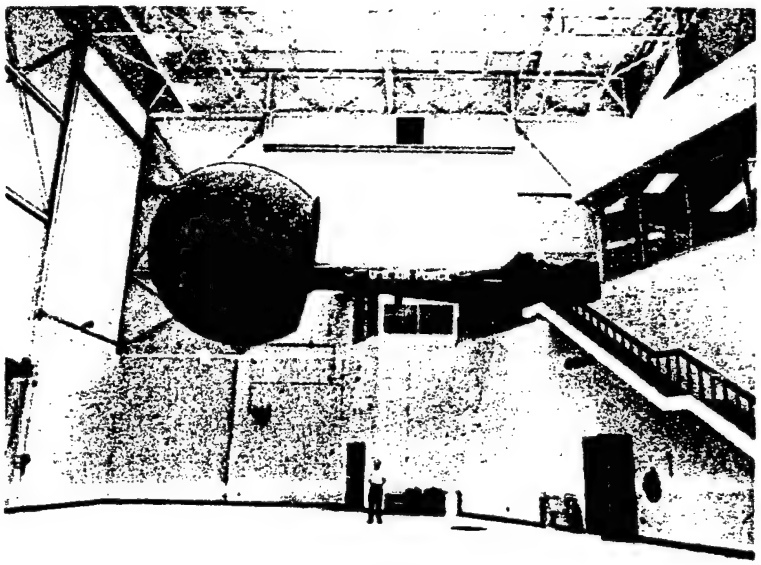

Fig 13 LAMARS Facility

Major emphasis of the simulation program will be the development of Task-Oriented CCV control modes. The LAMARS effort will pursue two different approaches in the investigation of unconventional aircraft maneuvering capabilities. The first will be concerned with minor modifications to the CCV modes as they were implemented on the YF-16. This approach is aimed at resolving basic problems/shortcomings highlighted during the flight test program. Candidate changes are listed below:

- CCV controller gradient variations
- Alternate gain scheduling
- Integral command of pointing and translation modes
- Elimination of operating restrictions

° Mode authority matching and tailoring

	DISPLACEMENT	[illegible] VELOCITY	STEADY ACCELERATION
BEAM-VERTICAL	[illegible] FT	[illegible]	[illegible]
BEAM-LATERAL	[illegible] FT	[illegible]	[illegible]
SPHERE-PITCH	[illegible]		[illegible] DEG/SEC^2
SPHERE-YAW	[illegible]	[illegible]	[illegible] DEG/SEC^2
SPHERE-ROLL	[illegible]	[illegible]	[illegible] DEG/SEC^2

Fig 14 LAMARS Motion Capability

The gradient variations and gain scheduling are both intended to reduce mode sensitivity evident in the air-to-ground tasks. An integral mechanization would allow "pulse" type inputs without requiring the pilot to hold CCV commands during a tracking task. Unfortunately, this quickly results in mode authority saturation. A trim type follow-up technique is needed in which adverse pipper motion does not result. In order to develop "pure" CCV modes and insure safety from failures with the limited redundancy employed in flight test, rather severe restrictions were placed on several modes. The emphasis will now be on obtaining "useful" modes by reducing these restrictions such as bank angle and α limits and accepting impure responses. In the interest of providing the pilot with a useful tool, authority of the modes will be tailored to the operational task and matched in both axes for control harmony. In addition, the CCV modes will be evaluated with several HUD gun-sight systems to ascertain the benefits and problems associated with such use.

The second approach involves alternate methods of providing the CCV capabilities to the pilot and new control law structures. It includes consideration of the following techniques:

° Blended modes using only the YF-16 sidestick

° Weapon-line stabilization and improved gust alleviation

° Closed-loop velocity command

Based on the acceptance by the pilot of the maneuver enhancement mechanization and the fact that pilot workload was actually increased with the addition of another controller in the cockpit, blending of CCV

modes with the basic aircraft controls is needed. Such blending must not result in adverse transients on initial command or when reaching maximum CCV authority. In addition, a means must be provided to washout CCV inputs to prevent combat maneuvering with residual canard or flaperon deflections. The mode to be blended will be selected based on its usefulness in the particular mission phase being flown. The techniques being considered included frequency selective separation of CCV versus conventional stick inputs using filter techniques and separation based on detected command magnitude and rate. In both cases gradual removal of the CCV mode in steady state is required. A recentering technique allowing placement of CCV command gradient within the basic control system stick force gradient is also being examined. Such a technique would provide the CCV capability as a vernier control for the pilot while allowing normal aircraft maneuvering for large inputs. Such a recentering scheme must allow full aircraft capability to be commanded and must not produce an unacceptable stick force per "g" relationship.

Work is being conducted to arrive at an optimum design of maneuver enhancement to provide weapon-line stabilization for improved gunnery. In this application the primary design objective is faster acquisition and better tracking as opposed to simply quickened maneuvering response. Changes to improve the gust alleviation capability are also being studied, but the focus is on reducing pipper disturbance rather than improving ride quality.

Closed-loop design providing a velocity command system for the translation modes is aimed at faster mode response and the elimination of coasting. With such a design, the pilot would command vertical or side velocity instead of flaperon or canard deflection. The control system positions the surfaces as needed to develop or cancel independent translations. This would improve mode usefulness in tasks requiring precise positioning and possibly allow application to combat maneuvering.

The flight test also accented the need for more operationally oriented evaluation techniques. The HQDT constant "g" and WUT tracking maneuvers for 20 to 30 seconds are not reasonable for representation of the air-to-air combat situation. Although providing useful information on basic control characteristics in a tracking task, it is not well suited for task-oriented design. In an effort to solve this problem, the LAMARS simulation will be using various weapon delivery scoring techniques based on aircraft position, target location and munition ballistics. However, HQDT type data will be taken for correlative purposes. Target aircraft combat algorithms to allow realistic operational task evaluation of the CCV modes have also been developed.

CONCLUSIONS

Flight testing of the Fighter CCV has provided valuable insight into the implications to manual control of uncoupled aircraft motions. A pronounced learning curve was encountered due to the very unusual maneuvers possible with the CCV modes in the flight evaluation. While

providing additional capability, the open-loop modes sometimes resulted in an increase in pilot workload with the addition of another controller. Use of rudder pedals for A_y command was natural for the pilot. The one blended closed-loop mode, Maneuver Enhancement, was found to be beneficial during all evaluation tasks. Although requiring optimization, the blending technique was readily accepted by the pilot. The flight test program demonstrated the feasibility of decoupled aircraft control and verified predicted performance levels. It also provided an indication of the usefulness of these new control modes in operational tasks.

The urgent need for task-oriented control mode investigations was clearly indicated during the test program. The CCV modes were implemented from an engineering standpoint of obtaining "pure" motion with well-behaved responses and maximum capability throughout the flight envelope. Emphasis must now be placed on designing to the specific task application. Through the use of AFFDL's large moving-base simulator and lessons learned from flight testing, engineering efforts are underway to provide CCV capabilities to the pilot in a manner that will significantly improve fighter aircraft effectiveness. Prior to adaptation in future designs, these capabilities must be provided in ways which do not complicate the manual control task. A multimode approach is indicated in which the pilot is provided with various predetermined combinations of conventional and CCV control tailored to the specific mission phase.

PILOT-OPTIMAL AUGMENTATION SYNTHESIS

by

David K. Schmidt

School of Aeronautics and Astronautics
Purdue University
West Lafayette, Indiana 47907

Abstract

Given adequate open-loop specifications, for example, aircraft handling qualities criteria, design techniques, particularly modern control approaches, are available to the system designer for synthesizing even the most complex flight control systems. Unfortunately, however, weaknesses exist in the handling qualities areas, particularly for "non-conventional" aircraft such as V/STOL and control configured vehicles (CCV's). In this paper, an augmentation synthesis method usable in the absence of quantitative handling qualities specifications, and yet explicitly including design objectives based on pilot-rating concepts, will be presented. The algorithm involves the unique approach of simultaneously solving for the stability augmentation system (SAS) gains, pilot equalization and pilot rating prediction via optimal control techniques. Simultaneous solution is required in this case since the pilot model (gains, etc.) depends upon the augmented plant dynamics, and the augmentation is obviously not a priori known. Another special feature is the use of the pilot's objective function (from which the pilot model evolves) to design the SAS.

Introduction

Given adequate design specifications, or aircraft handling qualities criteria, and a valid system model, design techniques, particularly modern control approaches, are available to the system designer for synthesizing even the most complex flight control systems. Unfortunately, however, weaknesses exist in the design specification area for non-conventional aircraft such as V/STOL and control configured vehicles (CCV's). The assertion here is that due to the "non-conventional," multi-variable nature of the vehicle (and the piloting task in the case of V/STOL), and due to the anticipated complexity of the systems involved, a "non-conventional" approach to the control design problem is worthy of investigation.

Since pilot acceptance is the ultimate criteria, in the absence of prior pilot opinion we must predict pilot rating. This is in contrast to design methods which attempt to a priori define "good" dynamics, and then use a model-following design technique[1], that is, design the augmentation so the augmented system will behave like the "good" model. One major drawback to this approach is that one is never sure that the pilot will agree with the

206

PAGE INTENTIONALLY BLANK

designers choice of "good" dynamics.

To predict pilot rating, some form of pilot model is required and two types of pilot models exist. Each have been used extensively; they include describing-function models[2] and optimal control models[3]. It is felt that for the problem at hand the optimal-control pilot model is ideal. It is more compatible with the multi-variable aspects of the problem and the advanced control design techniques already existing. Also, the form of the pilots equalization network is automatically determined, a very important property in this case.

Both pilot modeling approaches have been used primarily to study closed-loop system performance. Recent application areas for the optimal control model include low-visability landing of CTOL[4] and STOL aircraft[5] and the stability of the pilot aircraft system in maneuvering flight[6]. However, any stability augmentation systems in these studies were designed initially, from handling criteria for example, then the system performance evaluated as a separate step. That is, the SAS was designed first using the conventional approaches (e.g., pole placement), then the pilot model was added around the augmented system to evaluate "piloted" system performance.

Alternate approaches include the pilot as part of the plant[7], then the SAS design proceeds for the "pilot-augmented" plant. Buy the form of the pilot model must be assumed before beginning this design process, an undesirable situation for systems with non-conventional plant dynamics. The pilot is known to adapt his gain and form of equalization to the plant and task, but selecting the pilot model a priori would tend to imply knowledge of and invariance of the form of pilot model. Hence, the form of the pilot model should be determined as an integrated part of the system design. As stated previously, this is naturally accomplished with the optimal-control pilot model.

An analytical pilot model has also been used, although not as frequently, to predict pilot opinion. The most notable of these techniques, applied to the VTOL hover task, was the "paper pilot" developed by Anderson[8,9]. In this approach, parameters in the pilot describing function of assumed form are chosen such that a pilot-rating metric is minimized. This metric consists of a measure of performance (e.g., rms tracking error), and a measure of pilot workload (e.g., the amount of lead the pilot must introduce). In an assessment of this technique[10] it was found that a pilot rating functional based on easily measured motion quantities was adequate for pilot opinion prediction. However, the proposed pilot model was found to require some additions for better system performance predictions. Notably, these improvements included modification in form (describing function) and the addition of the pilot's remnant (or the "random" portion of the pilot's control input.) Hence, again we see the problems created by imposing an assumed form of the pilot's describing function.

This problem would appear to be alleviated by the use of the optimal pilot model. In fact, Hess[11] has found that the optimal control model can be used equally well for predicting pilot opinion, and has used this approach

in analytical display design for helicopters[12,13]. Use of the optimal pilot model for pilot rating allows for a natural pilot-rating metric via the pilot model objective function. Proper selection, based on the task, of the state and control weights in the objective function provides for the determination of the pilot gains, equalization, and pilot rating prediction simultaneously. As we have mentioned previously, this is a very important point in dealing with systems with non-conventional dynamics for which the pilot's describing function may not be known. If this approach is now integrated with the SAS design problem, a proposed design procedure results.

The Pilot Model

As presented in Reference 3, the optimal pilot model evolves from the assumption that the well-trained, well-motivated pilot selects his control input(s), $\bar{u}_p$, such that the following objective is minimized,

$$J_p = E\left\{\lim_{T\to\infty} \frac{1}{T} \int_0^T (\bar{y}'Q\bar{y} + \bar{u}_p'Ru_p + \dot{\bar{u}}_p'G\dot{\bar{u}}_p)dt\right\}$$

The dynamic system being controlled by the pilot is described by the familiar linear relation

$$\dot{\bar{x}} = A_p\bar{x} + B_p\bar{u}_p + \bar{w}$$

$$\bar{y} = C\bar{x} \qquad (1)$$

where $\bar{x}$ is the system state vector, $\bar{u}_p$ the pilot control vector, $\bar{y}$ the output vector, and $\bar{w}$ is the vector of zero-mean external disturbances with covariance

$$E[\bar{w}(t)\bar{w}'(t+\sigma)] = W\delta(\sigma)$$

Included as human limitations are observation delay, τ, and observation noise, $\bar{v}_y$. So the pilot actually perceives the noise-contaminated, delayed states, or

$$\bar{y}_p = C_p\bar{x}(t-\tau) + \bar{v}_y(t-\tau)$$

The covariance of the zero-mean observation noise may include the effects of perception thresholds and attention allocation, and is denoted

$$E[\bar{v}_y(t)\bar{v}_y'(t+\sigma)] = V_y\delta(\sigma)$$

Defining the augmented state vector, $\hat{\bar{x}} = \text{col}[\bar{x},\bar{u}_p]$, the solution to the problem, or the pilot's control is given as

$$\dot{\bar{u}}_p^* = -G^{-1}[0\,|\,I]K_p\bar{x}$$

where K_p is the positive definite solution to the Riccati equation

$$-\left[\begin{array}{c|c} A_p & B_p \\ \hline 0 & 0 \end{array}\right]' K_p - K_p \left[\begin{array}{c|c} A_p & B_p \\ \hline 0 & 0 \end{array}\right] - \left[\begin{array}{c|c} C_p' QC_p & 0 \\ \hline 0 & R \end{array}\right]$$

$$+ K_p B_o G^{-1} B_o' K_p = \dot{K}_p \qquad (2)$$

It will be convenient to partition K_p such that

$$K_p = \left[\begin{array}{c|c} K_{p_1} & K_{p_2} \\ \hline K_{p_3} & K_{p_4} \end{array}\right]$$

and note that now the equations for the optimal control $\bar{u}_p^*$ is

$$\dot{\bar{u}}_p^* = -G^{-1}K_{p_3}\hat{\bar{x}} - G^{-1}K_{p_4}\bar{u}_p^*$$

or a linear feedback of the best estimate of the state, $\hat{\bar{x}}$, and some control dynamics. (These control dynamics have been shown to be equivalent to the pilot's neuro-muscular lag.)

Now, the state estimator consists of a Kalman filter and a least-mean square predictor, or

$$\dot{\hat{\bar{x}}}(t-\tau) = A_p\hat{\bar{x}}(t-\tau) + \Sigma C_p' V_y^{-1}[\bar{Y}_p(t) - C_p\hat{\bar{x}}(t-\tau)] + B_p\bar{u}_p^*(t-\tau)$$

$$\hat{\bar{x}}(t) = \bar{\beta}(t) + \ell^{A_p\tau}[\hat{\bar{x}}(t-\tau) - \bar{\beta}(t-\tau)]$$

---

†To model the pilot's remnant, motor noise is usually added to the control equation. The final pilot's control is represented by

$$\dot{\bar{u}}_p^* = -G^{-1}K_{p_3}\hat{\bar{x}} - G^{-1}K_{p_4}\bar{u}_p^* + G^{-1}K_{p_4}\bar{v}_m$$

where

$$E[\bar{v}_m(t)\bar{v}_m'(t+\sigma)] = V_M\delta(\sigma)$$

with $\dot{\bar{\beta}} = A_p\bar{\beta} + B_p\bar{u}_p^*$

and the estimation error covariance matrix Σ is the solution of the Riccati equation

$$A_p\Sigma + \Sigma A_p' + W - \Sigma C_p' V_y^{-1} C_p \Sigma = [0]$$

This system of equations, when solved, determines the optimal-control pilot model.

Finally, as noted previously, Hess has found that when the weightings on the state and control (i.e., Q anf R) in the pilot's objective function are appropriately selected, the resulting magnitude of the pilots objective function, after solving for the pilot model, is strongly correlated with the pilot's rating of the vehicle and task. If the pilot rating is given in the Cooper-Harper system, the relation is

$$\text{Pilot Rating (PR)} = 2.53 \ln (10 J_p) + 0.2^{R}$$

Now, through this relation and the solution of the pilot model above, we now have not only a pilot-control model but a prediction of the pilot's rating of the dynamic system.

Augmentation Synthesis Method

In the determination of the pilot model parameters above, we have expressed the system dynamics in terms of the matrices A_p and B_p. However, since the augmentation has not been defined, the augmented plant, A_p and B_p is as yet unknown.

Consider the un-augmented plant dynamics to be described by

$$\dot{\bar{x}} = A\bar{x} + B\bar{u} + \bar{w}$$

where, as before, $\bar{x}$ is the system state vector and $\bar{w}$ is the same disturbance vector. However, A and B are now the un-augmented system matrices, and $\bar{u}$ is the control input vector. Now, the total control input to the plant will include pilot input, $\bar{u}_p$, plus augmentation input, $\bar{u}_{SAS}$, or

$$\bar{u} = \bar{u}_p + \bar{u}_{SAS}$$

Further, from the pilot model, we know that although the feedback gains (e.g., $G^{-1}K_{p_3}$, $G^{-1}K_{p_4}$) have not been determined, the pilot's control input in expressible as

$$\dot{\bar{u}}_p = -G^{-1}K_{p_3}\dot{\hat{\bar{x}}} - G^{-1}K_{p_4}\bar{u}_p \qquad (3)$$

Now, the estimate of the state, $\hat{\bar{x}}$, can be expressed in terms of the true state plus some estimation error, $\bar{\varepsilon}$, or

$$\hat{\bar{x}} = \bar{x} + \bar{\varepsilon}$$

By treating this error as another disturbance, $\bar{w}_p$, we can write the pilot's control equation as

$$\dot{\bar{u}}_p = -G^{-1}K_{p_3}\bar{x} - G^{-1}K_{p_4}\bar{u}_p + \bar{w}_p$$

(Note, the disturbance term, $\bar{w}_p$, can also include the pilot's remnant as well.) Combining this relation with the plant dynamic and pilot equations we have

$$\dot{\bar{\chi}} = \left[\begin{array}{c|c} A & B \\ \hline -G^{-1}K_{p_3} & -G^{-1}K_{p_4} \end{array}\right]\bar{\chi} + \left[\begin{array}{c} B \\ \hline 0 \end{array}\right]\bar{u}_{SAS} + \left[\begin{array}{c} \bar{w} \\ \hline \bar{w}_p \end{array}\right] \qquad (4)$$

where $\bar{\chi} = \mathrm{col}[\bar{x},\bar{u}_p]$.

We now may proceed to determine an objective function for determining $\bar{u}_{SAS}$.

From the correlation between pilot rating and the pilot's objective function we clearly see that the best (i.e., lowest) pilot rating implies the lowest pilot objective function. Therefore, for optimum pilot rating, the control $\bar{u}_{SAS}$ should be chosen to minimize J_p as defined in the pilot rating method. (This method defines the state and control weights, Q and R, as the inverse of the maximum allowable deviations in the variables as perceived by the pilot.) Finally, to preclude infinite augmentation gains, we must also penalize augmentation control energy. Therefore, the augmentation is chosen to minimize

$$J_{SAS} = J_p + E\left\{\lim_{T\to\infty}\frac{1}{T}\int_0^T \bar{u}'_{SAS}\,F\,\bar{u}_{SAS}\,dt\right\}$$

or

$$J_{SAS} = E\left\{\lim_{T\to\infty}\frac{1}{T}\int_0^T (\bar{y}'Q\bar{y} + \bar{u}_p'R\bar{u}_p + \dot{\bar{u}}_p'G\dot{\bar{u}}_p + \bar{u}'_{SAS}F\bar{u}_{SAS})dt\right\}$$

and Q, R, and G are as chosen in the pilot's objective function, J_p.

This may be written as

$$J_{SAS} = E\left\{\lim_{T\to\infty} \frac{1}{T}\int_0^T (\bar{x}'P\bar{x} + \bar{u}'_{SAS}F\bar{u}_{SAS})dt\right\}$$

where

$$P = \left[\begin{array}{c|c} C_p'QC_p + K_{P_3}'G^{-1}K_{P_3} & K_{P_3}'G^{-1}K_{P_4} \\ \hline K_{P_4}'G^{-1}K_{P_3} & R+K_{P_4}'G^{-1}K_{P_4} \end{array}\right]$$

and instead of Equation 3 being substituted for $\dot{\bar{u}}_p$ in the above J_{SAS}, we have invoked a sort of separation principle and substituted the relation

$$\dot{\bar{u}}_p = -G^{-1}K_{P_3}\bar{x} - G^{-1}K_{P_4}\bar{u}_p$$

The justification for this relation being used lies in the fact that we wish to synthesize the augmentation based on how the pilot is <u>trying</u> to perform the control function rather than on how the pilot is capable of doing so.

With this objective function and the system dynamics given in Equation 4, the problem is now stated in conventional form, except K_{P_3} and K_{P_4} are as yet undetermined of course. If we assume, for example, full state feedback, the solution of this problem is known to be

$$\bar{u}^*_{SAS} = -F^{-1}[B' \vdots 0]K_{SAS}\bar{x}$$

or

$$\bar{u}^*_{SAS} = -F^{-1}B'K_{SAS_1}\bar{x} - F^{-1}B'K_{SAS_2}\bar{u}_p$$

where

$$K_{SAS} = \left[\begin{array}{c|c} K_{SAS_1} & K_{SAS_2} \\ \hline K_{SAS_3} & K_{SAS_4} \end{array}\right]$$

is the solution to the Riccati equation

$$-\left[\begin{array}{c|c} A & B \\ \hline -G^{-1}K_{P_3} & -G^{-1}K_{P_4} \end{array}\right]' K_{SAS} - K_{SAS}\left[\begin{array}{c|c} A & B \\ \hline -G^{-1}K_{P_3} & -G^{-1}K_{P_4} \end{array}\right]$$

$$- P + K_{SAS}\left[\begin{array}{c} B \\ \hline 0 \end{array}\right]F^{-1}[B' \vdots 0]K_{SAS} = \dot{K}_{SAS} \qquad (5)$$

We see in this expression that the solution for K_{SAS} obviously depends on K_p (or K_{p_3} and K_{p_4}). Returning to the Riccati equation for the pilot gain (Equation 2), we also see that that equation depends in turn on the SAS gains (or K_{SAS}) since the pilot Riccati equation involves the augmented plant matrices A_p and B_p. As a result of the SAS design procedure just presented, we now know, however, the SAS structure. Returning to the pilot model, we may now include this SAS structure specifically, so that A_p and B_p (as in Equation 1) may in fact be expressed as

$$A_p = A - BF^{-1}B'K_{SAS_1}$$

and $$B_p = B(I - F^{-1}B'K_{SAS_2})$$

Substituting these expressions in the pilot Riccati equation yields two coupled Riccati equations, one for the pilot gains, Equation 2, and one for the SAS gains, Equation 5. These may be solved simultaneously for K_{SAS} and K_p by integrating both equations backward. Note that this solution does not involve a two-point-boundary-value problem. The system is represented in Figure 1.

A Simple Numerical Example

Consider a simple tracking task with the controlled element (plant) dynamics considered in Ref. 11,

$$\theta(s)/\delta(s) = K/s^2, \quad K = 11.7$$

The command signal, θ_c, is white noise, w, passed through the filter

$$\theta_c(s)/w(s) = 3.57/(s^2 + 3s + 2.25)$$

and $$E(w) = 0, \quad \sigma_w^2 = 1.0$$

If we define the state vector as $\bar{x} = \text{col}(\theta_c, \dot{\theta}_c, \theta, \dot{\theta})$, we have the plant

$$\dot{\bar{x}} = A\bar{x} + B\delta + 3.67\bar{w}$$

where

$$A = \begin{bmatrix} 0 & 1 & 0 & 0 \\ -2.25 & -3. & 0 & 0 \\ 0 & 0 & 0 & 1 \\ 0 & 0 & 0 & 0 \end{bmatrix}$$

$$B' = [0,0,0,11.7]$$

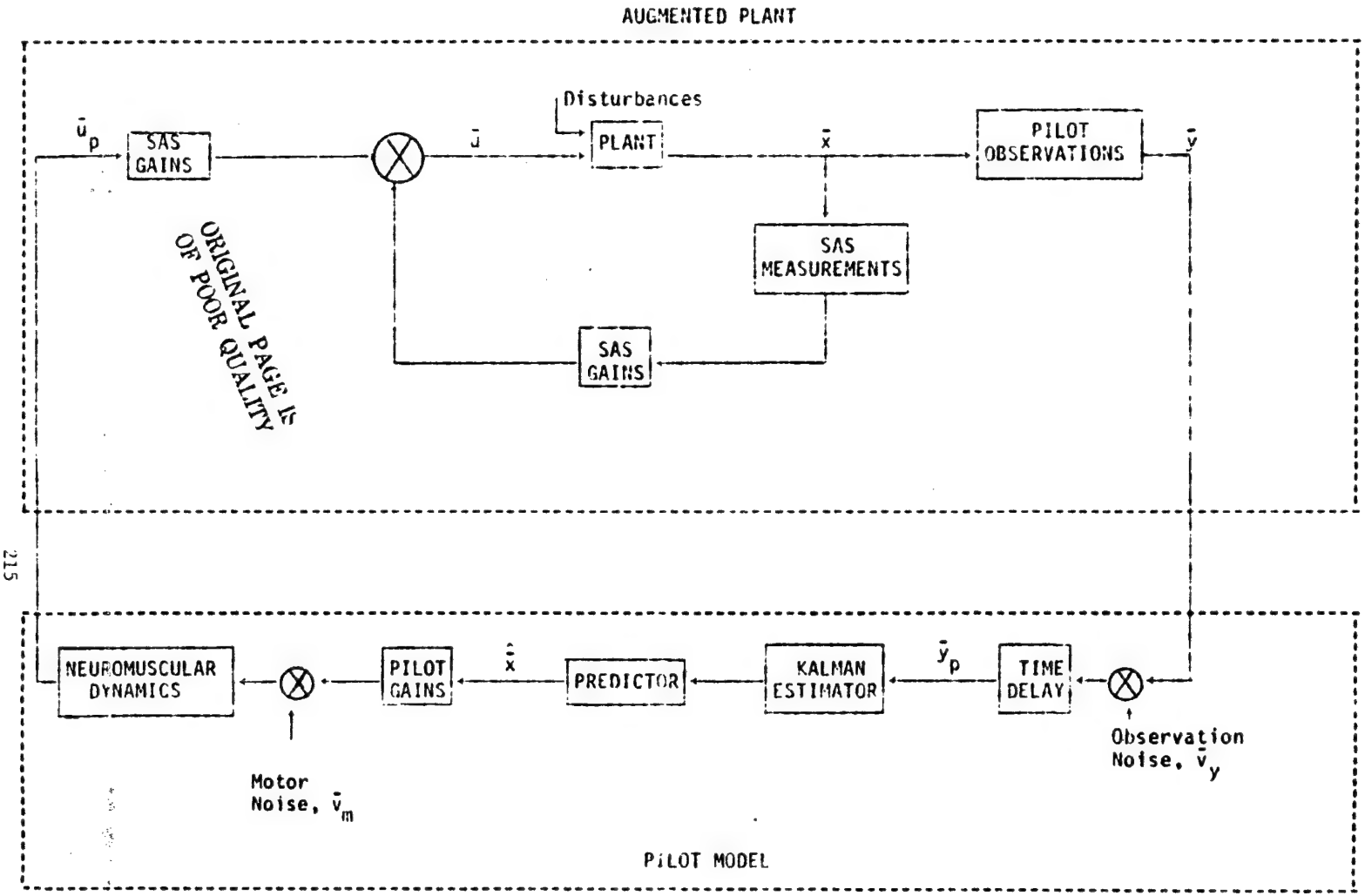

Figure 1 Piloted Vehicle Schematic

For this system, error and error rate are perceived by the pilot or

$$\bar{y}_p = \begin{bmatrix} \theta_c - \theta \\ \dot{\theta}_c - \dot{\theta} \end{bmatrix} = \begin{bmatrix} 1. & 0 & -1. & 0 \\ 0 & 1. & 0. & -1. \end{bmatrix} \bar{x}$$

The performance index, chosen consistent with Hess's rating hypothesis is

$$J_p = E\{\lim_{T\to\infty} \frac{1}{T} \int_0^T [(\theta_c - \theta)^2 + .01\delta_p^2 + g\dot{\delta}_p^2]dt\}$$

and g is chosen to yield a neuromuscular lag, $1/\tau_N = G^{-1}K_{p_4} = 10.$, or $\tau_N = 0.1$ seconds. Unagumented, the pilot Riccati equations are solved with the following noise statistics (human limitations)

1) Equal attention allocation between error and error rate.
2) Observation thresholds on error and error rate = 0.5(units of display displacement.)
3) Sensor noise, $(V_y)_{ii}/E(y_i^2) = -20dB \quad i=1,2$
4) Motor noise, $(Vu)/E(u_c^2) = -20db$, where $u_c = -G^{-1}K_{p_3}\hat{x}$
5) Observation delay, $\tau = 0.1$ seconds

The "piloted" system performance is given in the following table.

Table 1, Un-augmented System Performance

$(\theta_c - \theta)$ rms	δ_p rms	J_p	P.R.
1.17	1.00	1.39	6.9*

* This pilot rating has been verified by experiment

Assuming full-state feedback, the augmentation control law is

$$\delta_{SAS} = -K_1\theta_c - K_2\dot{\theta}_c - K_3\theta - K_4\dot{\theta} - K_\delta\delta_p$$

The SAS objective function is

$$J_{SAS} = J_p + E\{\lim_{T\to\infty} \frac{1}{T} \int_0^T f\delta_{SAS}^2 \, dt\}$$

so the piloted plant, including augmentation will be

$$\dot{\bar{x}} = A_p\bar{x} + B_p\delta_p + 3.67\bar{w}$$

where

$$A_p = \begin{bmatrix} 0 & 1. & 0 & 0 \\ -2.25 & -3. & 0 & 0 \\ 0 & 0 & 0 & 1. \\ -11.7K_1 & -11.7K_2 & -11.7K_3 & -11.7K_4 \end{bmatrix}$$

$$B_p' = [0,0,0,11.7(1-K_\delta)]$$

Solving the pilot and SAS Riccati equations simultaneously, and then determining piloted system performance as before yields the results given in the following table.

Table 2 Augmented System Performance

f	$(\theta_c - \theta)$ rms	δ_p rms	J_p *	P.R.**
100.0	1.10	0.89	1.21	6.6
10.0	0.79	0.61	0.62	4.9
1.0	0.38	0.35	0.15	1.3

* Note this is the numerical value of the pilot's objective function, J_p, not J_{SAS}.

** Predicted pilot rating based on J_p.

The augmentation gains, K_1 - K_4 and K_δ, for the three cases above are given in Table 3, along with the augmented plant eigenvalues.

Table 3 Augmentation Gains

f	K_1	K_2	K_3	K_4	K_5	Plant Eigenvalues*
100.0	-.009	-.002	.009	.003	.004	$-.017 \pm .331j$
10.	-.078	-.016	.084	.024	.036	$-.142 \pm .982j$
1.	-.513	-.090	.542	.130	.155	$-.758 \pm 2.40j$

* Not including noise filter eigenvalues of course.

Summary

In summary, we have cited the flight-dynamic and control problems of non-conventional flight vehicles (V/STOL and CCV) due to the complexity of augmentation required and the lack of handling qualities objectives. We have presented a methodology intended to be suitable for this type of problem. The method uses an optimal control pilot model, not only to predict

piloted performance but pilot rating as well. With the optimal-control model structure, we were able to formulate the augmentation synthesis problem as an optimal control problem with the parameters in plant matrices depending on the pilot model, and vice versa. This necessitates simultaneous solution of the two (pilot and augmentation) problems. We have included the form of the solution under the assumption of full-state variable feedback and no measurement noise, and a simple numerical example.

The first extension to be addressed will be the solution for the case of limited state feedback. This case is actually closer to pure plant augmentation than the case addressed here. In our solution, and in the example, we have closed the tracking loop, and pure plant augmentation would only feed back plant states. However, the primary purpose of our discussion here was to provide the problem structure which would be unchanged regardless of augmentation approach.

Further extensions will also include the cases with state estimation, with and without measurement noise. Also, the necessity of pre-tuning the pilot model will be investigated.

References

1. Kriechbaum, G., K.L. and R.W. Stineman, "Design of Desirable Airplane Handling Qualities via Optimal Control," Journ. of Aircraft, Vol. 9, No. 5, May, 1972.

2. McRuer, D.T. and E.S. Krendel, Mathematical Models of Human Pilot Behavior, AGARD-AG-188, AGARD, NATO, Jan., 1974.

3. Kleinman, D.L., S. Baron, and W.H. Levison, "An Optimal Control Model of Human Response, Part I: Theory and Validation," and Part II: Prediction of Human Performance in a Complex Task," Automatica, Vol. 6, 1970, pp. 357-383.

4. Harrington, W.W. Capt., "The Application of Pilot Modeling to the Study of Low Visibility Landing," NASA-TMX-73, 170, Proceedings of the Twelfth Annual Conf. on Manual Control, May, 1976.

5. Porter, M.B. Jr., "The Effects of Stability Augmentation on the Gust Response of a STOL Aircraft During a Curved Manual Approach" Ph.D. Dissertation, School of Aeronautics and Astronautics, Purdue University, West Lafayette, IND., May, 1975.

6. Broussard, J.R. and R.F. Stengel, "Stability of the Pilot-Aircraft System in Maneuvering Flight," NASA-TMX-73,170, Proc. of the Twelfth Annual Conf. on Manual Control, May, 1976.

7. Cunningham, T.B., "The Design of a Pilot Augmented Landing Approach Control System," Ph.D. Dissertation, School of Aeronautics and Astronautics, Purdue Univ., W. Lafayette, IND., May, 1973.

8. Anderson, R., "A New Approach to the Specification and Evaluation of Flying Qualities," AFFDL-TR-69-120, USAF Flight Dynamics Laboratory, 1969.

9. Dillow, J.D., Major, The "Paper Pilot" - A Digital Computer Program to Predict Pilot Rating for the Hover Task, AFFDL-TR-70-40, USAF Flight Dynamics Laboratory, March, 1971.

10. Teper, G.L. An Assessment of the "Paper Pilot" - An Analytical Approach to the Specification and Evaluation of Flying Qualities, AFFDL-TR-71-174, USAF Flight Dynamics Laboratory, June, 1972.

11. Hess, R.A., A Method for Generating Numerical Pilot Opinion Ratings Using the Optimal Pilot Model, NASA-TMX-73, 101, Feb., 1976.

12. Hess, R.A., "Analytical Display Design for Flight Tasks Conducted Under Instrument Meteorological Conditions," IEEE Trans. on Systems, Man and Cybernetics, Vol. SMC-7, No. 6, June, 1977.

13. Hess, R.A., "Application of a Model-Based Flight Director Design Technique to a Longitudinal Hover Task," Journ. of Aircraft, Vol. 14, No. 3, March, 1977.

PREDICTION, EVALUATION, AND SPECIFICATION OF FLYING QUALITIES BY MEANS OF STEP TARGET TRACKING

E. D. Onstott

W. H. Faulkner

Northrop Corporation
Aircraft Group
Hawthorne, California

ABSTRACT

A new approach to flying qualities specification and evaluation is presented which coordinates current research in the areas of pilot ratings, pilot-aircraft modeling techniques, and simulation and flight test procedures. A time-domain pilot model is described which can model discontinuous and nonlinear pilot behavior in conjunction with completely general time-varying nonlinear aircraft models to simulate discrete manuevers. This pilot-aircraft model is applied to an existing set of in-flight simulation data, and calculates tracking error and time-on-target statistics for step target tracking that directly relate to the reported pilot comments and ratings. Predicted step target tracking data for eighteen F-5E flight conditions are presented, and the use of the method for control system design is demonstrated using the YF-17.

INTRODUCTION

Pilot ratings and pilot comments often refer to two basic kinds of evaluation:

1) How well can the aircraft be made to perform?
2) How hard is the task to carry out?

Since these two questions are asked simultaneously by the Cooper-Harper decision tree employed by the pilot in assigning a rating, performance and pilot workload are combined into a single scalar quantity, the rating. Pilot rating prediction formulas have been developed that weight normalized statistical performance, usually an rms tracking error, along with an assumed correlate of pilot workload, such as the pilot lead compensation constant. Although these methods have correlated well with steady state tracking data, the predictive and practical aspects of this approach have yet to be demonstrated, especially in view of the simplifications required in task descriptions and system models. One basic problem with these approaches is that pilot model parameters of lead, reserve attention as defined by additional task

requirements on the pilot, or other identifiable pilot characteristics are difficult to relate quantitatively to pilot comments. Furthermore, the limitation of pilot model analysis to steady state statistics of a linearized pilot-aircraft model precludes analysis of discrete flight test maneuvers such as wind-up turns and step target tracking.

Furthermore, as the control characteristics of advanced tactical aircraft depend increasingly less on the dynamics of the bare unaugmented airframe, the existing relations of handling qualities evaluation parameters to airframe dynamics become less reliable. Since most flying qualities evaluation and specification methods depend upon this correlation between airframe parameters and pilot ratings, there are now serious deficiencies in existing design criteria. MIL-F-8785B, Military Specification, Flying Qualities of Piloted Airplanes, Reference 1, presents boundaries of acceptance in terms of such quantities as short period frequency and damping. These criteria have been obtained through operational experience with large numbers of past and current aircraft, and present values of airframe parameters that correlate with pilot ratings.

References 2 and 3 present a simple and direct method for evaluating the performance of a tactical aircraft performing a discrete step target tracking maneuver. This approach calculates tracking error and time-on-target statistics for step target tracking in a way that is directly related to both pilot ratings and comments. As an illustration of this technique, the definitive in-flight simulation study of longitudinal flying qualities, performed by Neal and Smith, Reference 4, was analyzed in terms of step target tracking.

The objective of this paper is to summarize References 2 and 3 and to present further details and applications of this flying qualities prediction and evaluation method by demonstrating YF-17 control system design improvement.

DISCRETE AND STEADY-STATE TRACKING

Much analysis of closed loop piloted tracking has been published for random steady-state tracking tasks. These studies, References 5 and 6, for example, have demonstrated that pilot models are useful in the prediction of tracking performance of continuous random tracking tasks, and success has been achieved in correlating model parameters with pilot opinion ratings obtained from flight simulations, Reference 7.

However, in actual flight situations, the pilot is also faced with the task of performing quick corrections to flight path or attitude errors. The ability of an aircraft

to respond well to such discrete corrections in a short tracking time is therefore of great importance to flying qualities analysis. This is particularly true in target tracking where the target must first be acquired and then precisely tracked.

It is clear that the objectives of quick initial response and precise tracking once the target is acquired are to some degree opposed. If the pilot pulls the airplane toward the target too rapidly, unwanted overshoot and oscillation about the target may result. On the other hand, pulling too slowly to the target may lead to steady tracking but with a penalty of unacceptably slow target acquisition. The ability to investigate this compromise and predict how well the overall task can be achieved for a given aircraft is the primary advantage of using time-domain pilot models to investigate step target tracking.

Consider a target that suddenly appears above steady-state trim pitch for the tracking aircraft. The pilot sees the target and initiates a pull-up. At some point, say D seconds into the maneuver, he will possibly change the nature of his control to initiate precision tracking and reduce steady-state errors. By repeatedly flying this maneuver, he will learn just how much he can force a quick initial response without producing overshoot and oscillation. The performance of this step target tracking task can then be measured by rms tracking error and time-on-target for a given pipper size and total tracking time.

The Northrop time-domain pilot model, Reference 3, is set up to perform this tracking task in just the way the pilot does it as described above. This is shown in Figure 1. There will be two forms for the pilot compensation elevator command δ_e: one which provides the initial target acquisition, and the other after time D has passed which controls final precision tracking and eliminates steady state errors. These are of the form:

ACQUISITION

$$\text{time} < D, \quad \delta e_I = (\text{Delay } \tau) \left\{ K_{p_I} \left(\theta_e(t) + T_{I_I} \dot{\theta}_e(t) \right) \right\}$$

TRACKING

$$\text{time} > D, \quad \delta e_F = (\text{Delay } \tau) \left\{ K_{p_F} \left(\theta_e(t) + T_{I_F} \dot{\theta}_e(t) + K_{IC} \int_0^t \theta_e(s)\, ds \right) \right\}$$

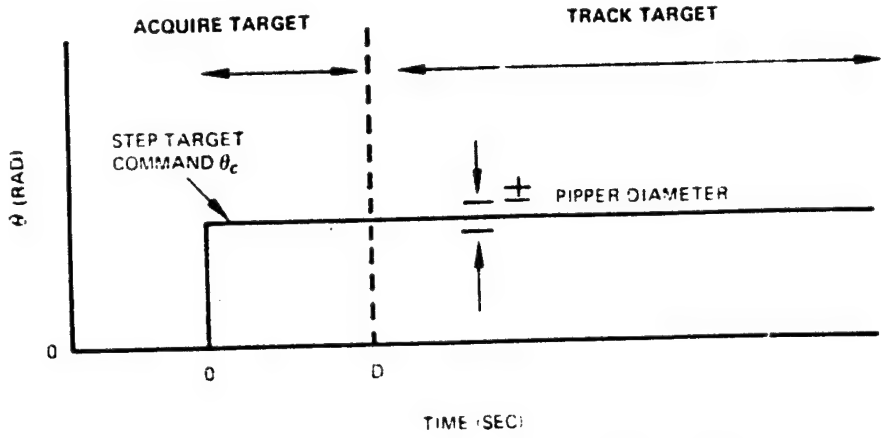

Figure 1. Definition of Step Target Tracking Task

where θ_e is pitch angle tracking error and the subscripts I and F refer to initial acquisition and final tracking, respectively. The K_{IC} term represents a pilot's avoidance of steady state error by means of integral control. A pilot delay of $\tau = 0.3$ sec will be used.

The following quantities must be adjusted in order to perform a simulation of this step tracking task for the evaluation of a given aircraft configuration:

$$K_{P_I},\ T_{L_I},\ D,\ K_{P_F},\ T_{L_F},\ K_{IC}$$

This adjustment is performed using an optimization principle. For the analysis of step target tracking, it will be assumed that the pilot optimizes time-on-target and that this leads to the best compromise of rapid target acquisition and steadiness of target tracking. The adjustment rule for the pilot model is thus: choose the parameters any way that leads to maximum time-on-target.

PILOT – AIRCRAFT ANALYSIS OF LONGITUDINAL STEP TARGET TRACKING

One of the most familiar and widely employed guides to longitudinal flying qualities is the data obtained by Neal and Smith of Cornell Aeronautical Laboratory during an in-flight simulation sponsored by the Air Force Flight Dynamics Laboratory in 1970. The test matrix included variations in short period frequency, damping, and control

system parameters. Flight test evaluation included pitch angle tracking of both random and step commands. The reported pilot ratings and pilot comments cover stick forces, predictability of response, attitude control/tracking capability, normal acceleration control, effects of random disturbances, and IFR problems. Most pilot comments deal with initial response ("predictability of response") or precision attitude tracking control ("attitude control/tracking capability").

Forty-two configurations, Series 1 through 7, were calculated and presented in Reference 3. A pipper diameter of 0.005 radian, a step size of 0.2 radian, and a total tracking time of 5 seconds were adopted. Since the system was linear, any choice of step and pipper size that preserves the 40 to 1 ratio will lead to the same time-on-target and normalized rms θ_e statistics.

Figure 2 shows the calculated step tracking response of one of the better configurations surveyed, 7C, which was given a rating of PR = 1.5. In this case, the rapid acquisition of the target leads to low rms θ_e, while the steadiness of the precision tracking results in large time-on-target. On the other hand, Figure 3 shows a poor configuration, 1F (PR = 8), that has sluggish response indicated by high rms θ_e. Even worse is the inability of this configuration to settle out on the target, so that time-on-target is mostly achieved during target crossings. Other configurations show a wide

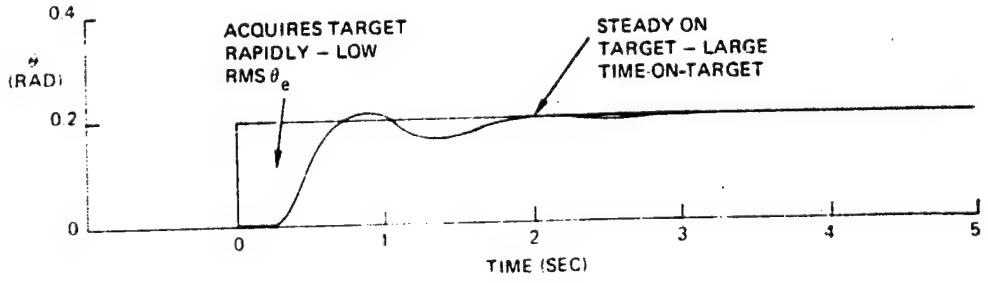

K_{PI}	70.0	K_{PF}	65.0	TOT	2.80
T_{LI}	.05	T_{LF}	0	RMSθ_e	.32
D	5	K_{IC}	0	PR	1.5

Figure 2. Configuration 7C Step Tracking Response

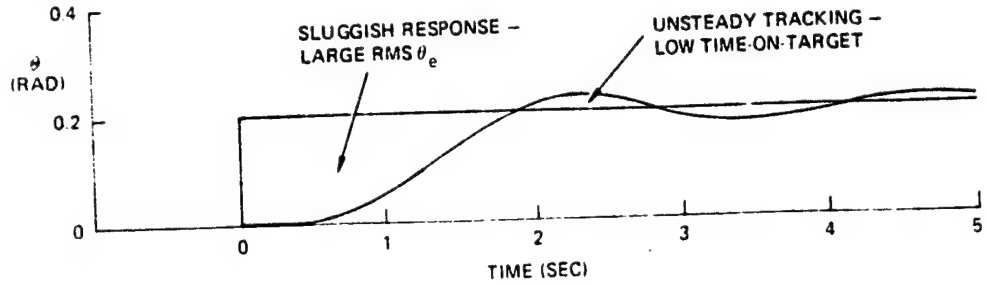

K_{PI}	= 4.6	K_{PF}	= 7.0	TOT	= .4
T_{LI}	= .2	T_{LF}	= .5	$RMS\theta_e$	= .47
D	= 1.5	K_{IC}	= 0	PR	= 8.0

Figure 3. Configuration 1F Step Tracking Response

range of specific handling qualities problems; aircraft that exhibit great overshoot and others whose steady-state error is difficult to overcome, even with the use of the integral control compensation.

The primary objective of the flying qualities specifications, called out in MIL-F-8785B, is to establish numerical criteria that define levels of performance in terms of pilot ratings: Level 1 — PR 1-3.5, Level 2 — PR 3.5-6.5, and Level 3 — PR 6.5-9.5.

It is useful to examine the correlations of the rms θ_e and time-on-target data calculated for the Neal and Smith configurations with pilot ratings. The rms θ_e data are presented in Figure 4. The expected result of increasing pilot rating number with increasing rms θ_e is clearly shown. However, if an attempt is made to draw a specification boundary as a vertical line at some rms θ_e value, in order to specify the performance in Level 1 or 2, the result is that no lines can be drawn that do not also include many points from the wrong levels. This failure of rms θ_e to correlate with pilot ratings sufficiently well for specification purposes has been frequently noted. From the description of the piloted task, it is clear that the rms θ_e statistic is incidental, time-on-target being the primary performance measure. If calculated time-on-target is plotted against pilot ratings, there is again a strong correlation, as shown in Figure 5. Unfortunately, this correlation is even less able to furnish specification boundaries than the rms θ_e vs pilot rating data.

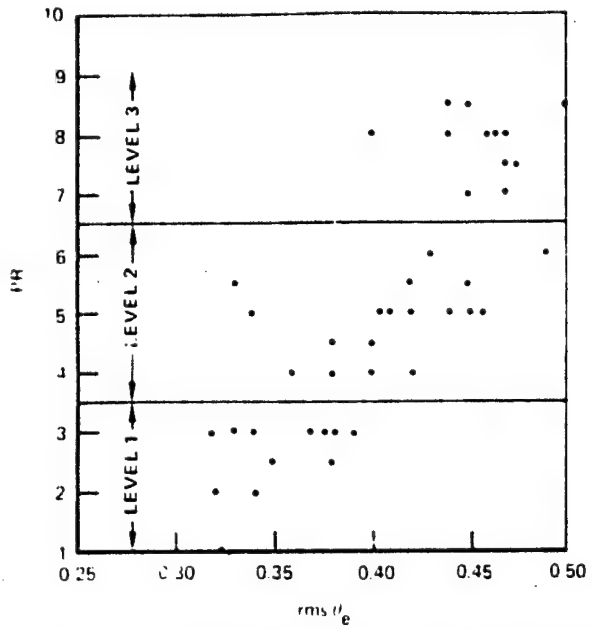

Figure 4. Correlation of rms θ_e with Pilot Ratings

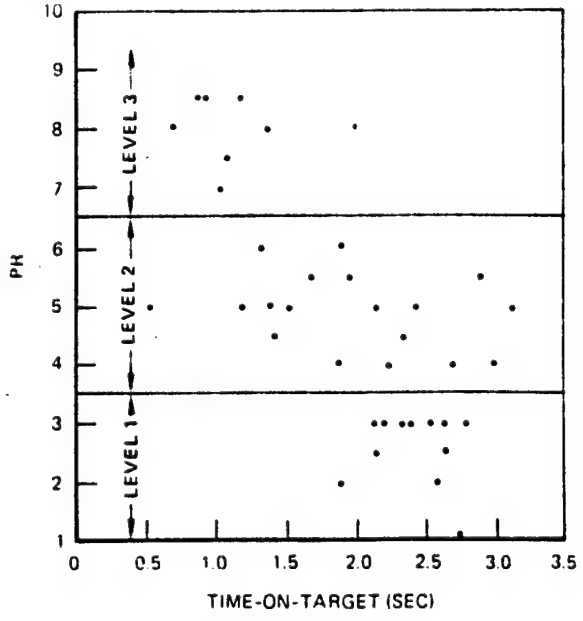

Figure 5. Correlation of Time-On-Target with Pilot Ratings

CORRELATION OF STEP TARGET DATA WITH NEAL-SMITH PILOT RATINGS

From the above it is clear that the single performance parameters rms θ_e or time-on-target are not sufficient to specify acceptable performance of the Neal and Smith configurations. If one considers that the pilot might trade rms θ_e and time-on-target against one another in generating his pilot rating, these statistics become more useful. To see how this trade-off may take place, normalized rms θ_e is plotted versus time-on-target with the point indicated by the minimum pilot rating given by a test pilot during the in-flight simulation. This is shown in Figure 6 along with apparent boundaries that neatly separate the regions of Levels 1, 2, and 3. With the exception of seven points out of forty-two, all configurations lie in regions bounded by apparent curves that illustrate the trade-off between the two performance measures. These curves show, for example, that a pilot will tolerate more sluggish response in a given

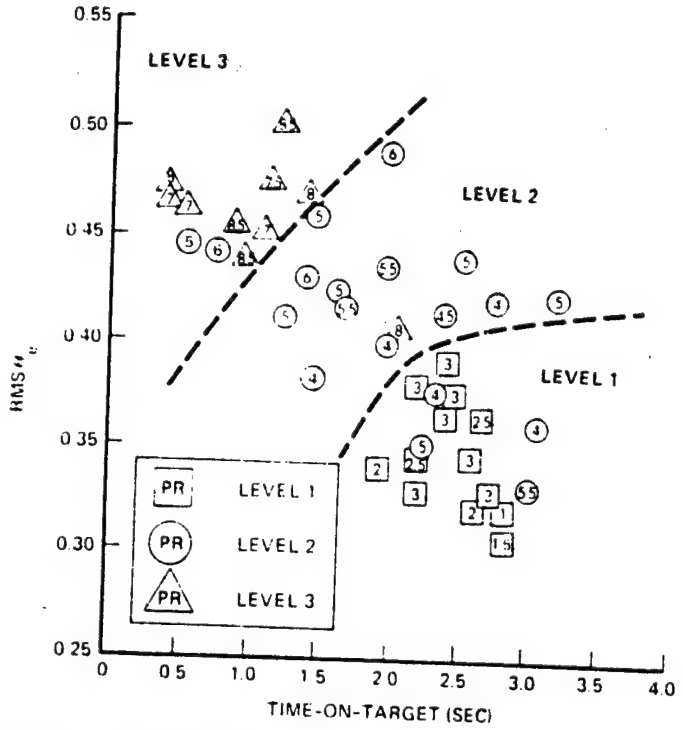

Figure 6. Pilot Ratings as Functions of rms θ_e and Time-On-Target

Level if the resulting time-on-target is especially good, and conversely. Since the parameters rms θ_e and time-on-target correlate with pilot ratings obtained during a flight test program that examined various tracking tasks, the representation of target tracking by the step target appears to be justified.

VALIDATION OF THE STEP TARGET METHOD USING THE F-5E AIRCRAFT

Further validation of the method was obtained by comparing F-5E aircraft with and without control augmentation at nine flight conditions representative of the primary maneuvering envelope. Full data is given in Reference 3 from which the examples shown in Figures 7 and 8 are drawn.

Comparison in Reference 3 of the step tracking responses for each flight condition with and without augmenter shows the importance of proper augmentation for good tracking response. In the augmented cases, the initial response is faster as reflected in the rms tracking error statistic, while the better damped dynamics lead to larger time-on-target values. To demonstrate the validity of the boundaries shown in Figure 6 based on the Neal-Smith data, the F-5E response data is plotted on these boundaries in Figure 9. Since the augmented F-5E has good Level 1 flying qualities, while the unaugmented aircraft may or may not meet Level 1 criteria, the Level 1-Level 2 boundary is consistent with the F-5E data. In this way, not only do the data of Figure 9 show the gradient direction of improving performance which characterized the Neal-Smith data, but the actual suggested boundary position is consistent as well.

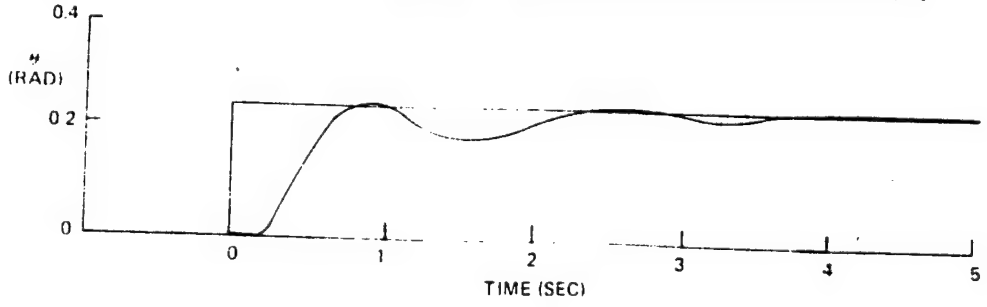

K_{PI}	- .49	K_{PF}	- .6	TOT	- 2.28
T_{LI}	.3	T_{LF}	.2	RMSσ_e	.31
D	8	K_{IC}	06	AUGMENTER	

Figure 7. F-5E Case 4 Step Target Tracking Response

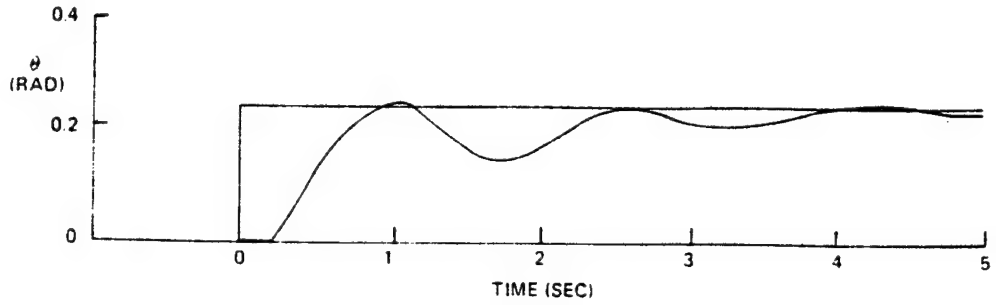

K_{PI}	= - .23	K_{PF}	= - .3	TO*	= 1.50
T_{LI}	= .5	T_{LF}	= .7	RMSθ_e	= .34
D	= .8	K_{IC}	= .09	NO AUGMENTER	

Figure 8. F-5E Case 4 Step Target Tracking Response

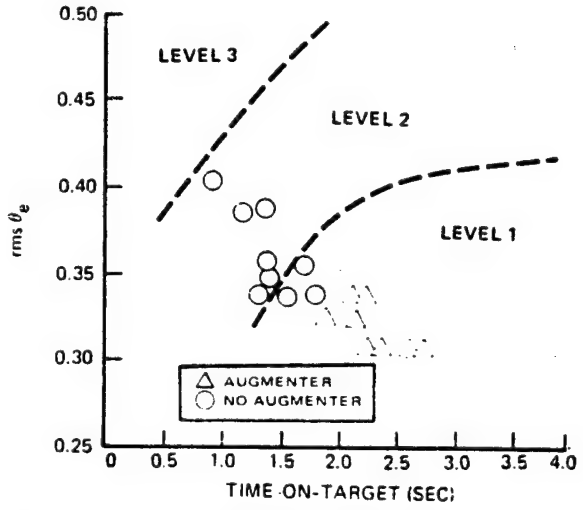

Figure 9. F-5E Validation of Step Target Prediction Method

YF-17 CONTROL IMPROVEMENT DESIGN EXAMPLE

Recently, the step target method was used to evaluate and study possible control configuration improvement of the YF-17 aircraft. The baseline aircraft was designed to meet the Neal-Smith flight control criteria, but a multi-parameter perturbation of control constants has led to improvements in predicted tracking performance. Flight simulations are now planned to verify these predictions, which involved only small changes in control parameters.

The predicted improvements are shown for a number of flight conditions in Figure 10. Time-on-target and rms tracking error are plotted against the boundaries shown in Figures 6 and 9. The tail of each arrow represents the baseline YF-17 as flight tested, and the head shows the predicted response of the aircraft with the modified control design. It is clear that these small changes in the control parameters have produced substantial improvements in the predicted tracking performance. It should also be pointed out that these calculations were performed using the full nonlinear YF-17 aircraft and control descriptions.

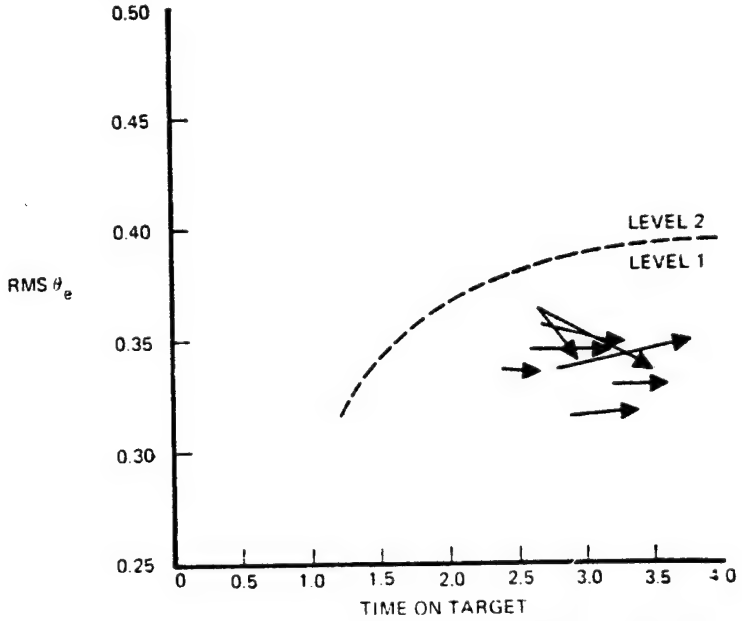

Figure 10. Predicted Improvement of Baseline YF-17 Step Target Tracking

The tracking improvements shown in Figure 10 were calculated using the same modified control parameters in each case. The most striking of the time-on-target improvements is seen by comparing the baseline step response shown in Figure 11 with the modified performance shown in Figure 12. The flight condition for this case is Mach 0.6 at sea level.

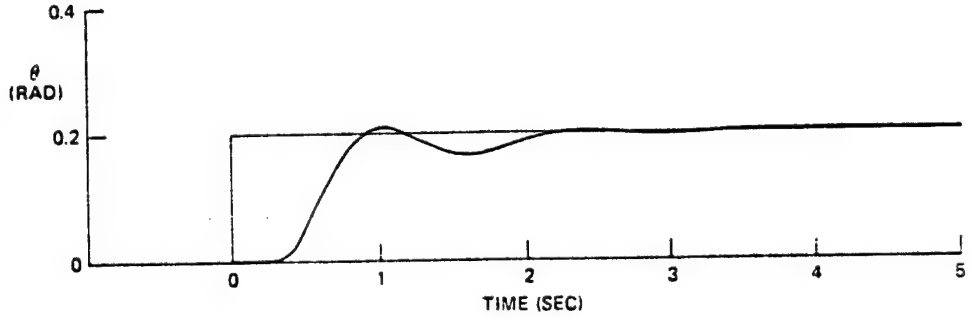

Figure 11. Step Target Tracking Response of Baseline YF-17

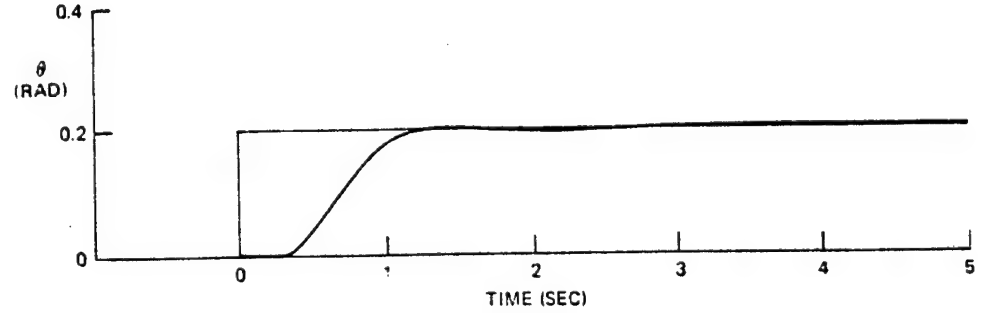

Figure 12. Step Target Tracking Response of Modified YF-17

SPECIFICATION OF AIR-TO-AIR TRACKING PERFORMANCE

The success of the step target tracking prediction method allows the following suggestions for tracking performance specification. For a specification to be a useful, discriminating, and fair criterion for tactical aircraft procurement, the following items must be satisfied:

1) The specification item must be numerical.

2) The specification item must correlate with pilot comments and pilot ratings.

3) The specification item must be easily measured in flight test or flight simulation.

4) The specification item must be reliably predictable by analytical means for use in early design and development evaluation.

5) The method that predicts the specification item must be applicable in a completely standardized form that evaluates the most general models of the candidate aircraft available.

6) The specification item must be valid for all current acceptable aircraft, and must exclude poor or unacceptable aircraft.

Unfortunately, these six requirements for military specification criteria have not all been met by any steady-state approach to the precision tracking problem. However, the transient method of step target tracking potentially satisfies these items. In particular, the step target method has the following characteristics that correspond to the requirements listed above:

1) The step target method is based on the numerical measures of rms tracking error and time-on-target as shown in Figure 6.

2) The two measures correspond with pilot comments in the following way:

rms tracking error:	Quickness of response and overshoot characteristics
time-on-target:	Steadiness on target and precision tracking characteristics

In addition, these two measures strongly correlate with pilot ratings obtained by Neal and Smith.

3) The use of step target tracking is already an established flight test procedure. It is completely standardized and easily tested.

4) The step target response is easily predicted for longitudinal step target tracking, and the extension to multiaxis target tracking is straightforward.

5) The method can be used with all representations of candidate aircraft from linear to full nonlinear equations.

6) The method clearly establishes performance boundaries for the Neal-Smith and F-5E aircraft. The only remaining requirement for MIL-F-8785B inclusion is further validation by current advanced tactical aircraft.

FINAL REMARKS

Pilot ratings have been successfully correlated with regions in the two-dimensional space having calculated rms tracking error and time-on-target coordinates for the in-flight simulation data obtained by Neal and Smith. This shows the generality, versatility, and practicality of time-domain pilot models. By demonstrating analytically the tradeoff between target acquisition and precise tracking for a short tracking period, the interrelationships of pilot ratings, the dynamics of pilot control compensation, and discrete maneuver flight test procedures are made clear. Validation by F-5E aircraft and a control improvement design study of the YF-17 further demonstrate the use and practicality of the method. It is expected that future research into multiaxis step target tracking will yield similar correlations with flight test data. In the meantime, the time-domain pilot model can be readily used to evaluate a wide variety of continuous and discrete tasks encountered in the flying qualities of modern high performance aircraft.

ACKNOWLEDGMENT

This work was partially performed under Contract 33615-77-C-3008 for the U.S. Air Force Flight Dynamics Laboratory, FGC, Wright-Patterson AFB, Ohio.

REFERENCES

1. "Military Specification, Flying Qualities of Piloted Airplanes," MIL-F-8785B, August 1969.

2. Onstott, E.D. and Faulkner, W.H., "Discrete Maneuver Pilot Models for Flying Qualities Evaluation," Journal of Guidance and Control, Vol. 1, No. 2, March-April 1978.

3. Onstott, E.D. and Faulkner, W.H., "Prediction, Evaluation, and Specification of Closed Loop and Multiaxis Flying Qualities," AFFDL-TR-78-3, Air Force Flight Dynamics Laboratory, February 1978.

4. Neal, T.P. and Smith, R.E., "An In-Flight Investigation to Develop Control System Design Criteria for Fighter Airplanes," Vols. I and II, AFFDL-TR-70-74, Air Force Flight Dynamics Laboratory, December 1970.

5. McRuer, D.T. and Krendel, E.S., "Mathematical Models of Human Pilot Behavior," AGARDograph No. 188, Advisory Group for Aerospace Research and Development, January 1974.

6. Faulkner, W.H. and Onstott, E.D., "Error Rate Information in Attention Allocation Pilot Models," Proceedings of the Thirteenth Annual Conference on Manual Control, June 1977.

7. Anderson, R.O., "A New Approach to the Specification and Evaluation of Flying Qualities," AFFDL-TR-69-120, Air Force Flight Dynamics Laboratory, May 1970.

N79-15605

ANALYSIS OF A VTOL HOVER TASK WITH PREDICTOR DISPLAYS USING AN OPTIMAL CONTROL MODEL OF THE HUMAN OPERATOR*

Gunnar Johannsen** and T. Govindaraj

Department of Mechanical and Industrial Engineering
Coordinated Science Laboratory
University of Illinois
Urbana Illinois 61801

SUMMARY

The influence of different types of predictor displays in a longitudinal VTOL hover task is analyzed in a theoretical study. It has been assumed that pitch angle and position will be presented to the pilot in separate displays namely the artificial horizon and a position display. The predictive information is calculated by means of a Taylor series. The future pitch angle is extrapolated 0.7s ahead and displayed as an additional bar, whereas the position is displayed as an extrapolated path element. This path element is approximated by three straight line segments, i.e., three future position values are calculated with the end point being 2.0s ahead.

From earlier experimental studies it is well known that predictor displays improve human and system performance and result in reduced human workload. In this study, the optimal control model is used to prove this effect theoretically. The status and predictive quantities are considered as separate observed variables. The Taylor series coefficients are incorporated in the observation matrix. Also, rate information included in the movement of the position and pitch angle indication is represented.

Several cases with differing amounts of predictive and rate information are compared. The results show the expected improvements in human and system performance in terms of RMS-values. The strongest influence is caused by the indication of the extrapolated path element, especially the end point. Computed cost gradients and fractions of attention show the relative importance of the individual pieces of displayed information. An optimization of the attention allocation shows a further improvement in system performance in all cases.

* This work was supported in part by the National Aeronautics and Space Administration under NASA-Ames Grant NSG-2119.

** Permanent Address: Research Institute for Human Engineering(FAT)
D-5309 Meckenheim, F. R. Germany

I Introduction

Predictor displays have been investigated intensively in laboratory simulations [1]-[5]. It has been found that they improve human and system performance and result in reduced human workload. More recently, predictor displays have been receiving increasing attention (see, e.g., [6]) because the technology of computer graphics has reached a high standard [7] which allows one to implement these displays more easily in real man-machine systems.

During the last few years, an optimal control model of the human operator (see e.g., [8], [9]) has been applied as a unified methodology for analytical display design and evaluation [10]-[13]. Attitude/director indicator and flight director displays have been considered as examples.

This paper is a contribution to such an analytical display design and evaluation procedure. Different types of predictor displays in a longitudinal VTOL hover task are analyzed theoretically by means of the optimal control model of the human operator. Rather than fitting experimental data, the purpose here is to calculate the expected human and system performance with different display designs. These results are validated by intuitive reasoning by considering earlier experimental results

In the next section, the VTOL hover task is described. The assumed predictor-display layout is explained in Section III. Section IV gives a brief overview of the optimal control model and emphasizes specific considerations for applying this model to the utilization of predictor displays. Finally, the results of a case study are discussed in Section V

II Description of the VTOL hover Task

The task chosen in this paper concerns the longitudinal motion of a hovering VTOL aircraft. For comparison purposes the task is the same as that in [14] which since then has also been considered in other papers, e.g ,[15], [16].

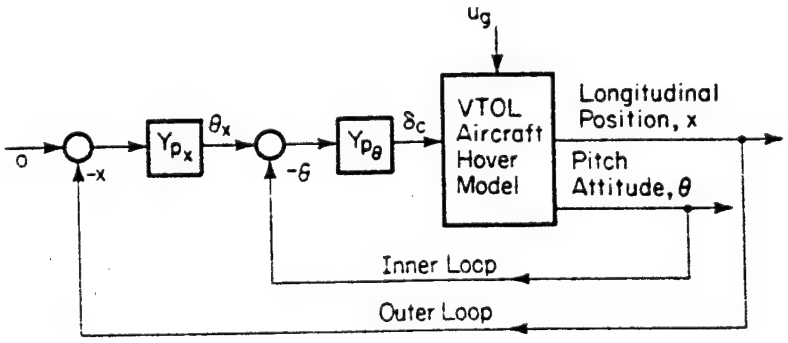

Figure 1: Series Loop Model for Pilot Longitudinal Control in Hover (after [15])

Figure 1 shows a possible structure of this man-machine system, assuming a series loop model for the pilot in which his behavior is represented by the two transfer functions Y_{p_x} and Y_{p_θ}.

The system dynamics of the aircraft are described by the following equation (see also Figure 2):

$$\begin{bmatrix} \dot{u}_g \\ \dot{x} \\ \dot{u} \\ \dot{\theta} \\ \dot{q} \\ \dot{\delta} \end{bmatrix} = \underbrace{\begin{bmatrix} -\omega_b & 0 & 0 & 0 & 0 & 0 \\ 0 & 0 & 1 & 0 & 0 & 0 \\ X_u & 0 & X_u & -g & 0 & 0 \\ 0 & 0 & 0 & 0 & 1 & 0 \\ M_u & 0 & M_u & 0 & M_q & M_\delta \\ 0 & 0 & 0 & 0 & 0 & -100 \end{bmatrix}}_{\underline{A}} \cdot \begin{bmatrix} u_g \\ x \\ u \\ \theta \\ q \\ \delta \end{bmatrix} + \begin{bmatrix} 0 \\ 0 \\ 0 \\ 0 \\ 0 \\ 100 \end{bmatrix} \delta_c + \begin{bmatrix} w_1 \\ 0 \\ 0 \\ 0 \\ 0 \\ 0 \end{bmatrix} \qquad (1)$$

$$\dot{\underline{x}} = \underline{A} \cdot \underline{x} + \underline{b} \cdot u + \underline{w}$$

Equation (1) includes a first order lag filter for deriving the longitudinal gust u_g from a white noise source w_1 as well as a first order lag with time constant $T_\delta = 0.01s$ limiting the control rate of the actuator. The main reason for the second lag is to extend the state vector in such a way that the second derivative of the pitch angle is also a component of the state vector. This is needed for the predictor display as will be shown later.

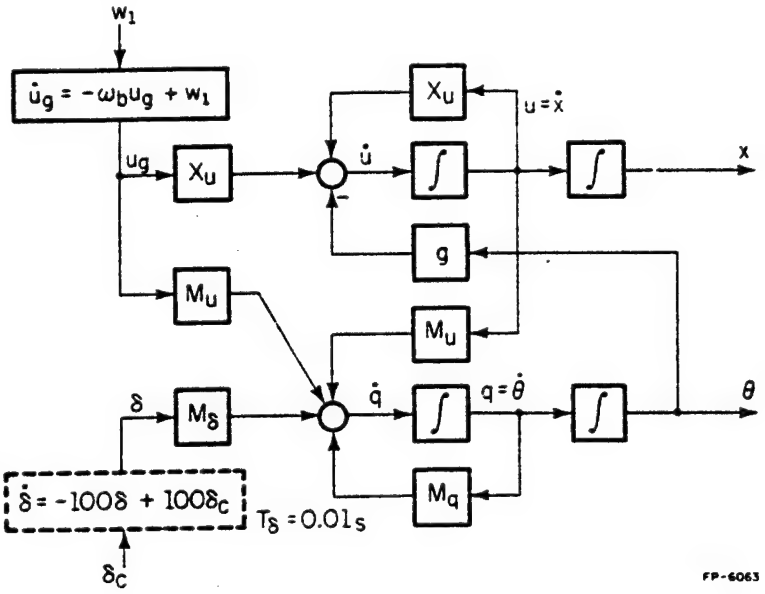

Figure 2: Block Diagram of the Aircraft Dynamics

In Equation (1) and Figure 2, g is the gravitational constant and X_u, M_u, M_q, M_δ are aircraft stability derivatives. Their values are chosen to be the same as in the nominal case in [15]. namely

$X_u = 0.1 s^{-1}$, $M_u = 0.0207\ ft^{-1}s^{-1}$, $M_q = -3.0 s^{-1}$, $M_\delta = 0.431 s^{-2}$.

Also the simulated gust is the same as in [15]. The bandwidth of the gust filter is $\omega_b = 0.314\ rad.s^{-1}$ and the rms-value of the gust is $u_{g_{rms}} = 5.14$ $ft.s^{-1}$, i.e., the variance of the driving white noise is $W_{11} = 16.59$.

III Layout of Assumed Predictor Displays

Two main techniques have been used for generating predictor displays. One is the fast-time model technique [3], [4]; the other one is the extrapolation technique [2], [5]. In this paper, the extrapolation technique is applied. Its advantage is that no model of the aircraft needs to be implemented and run repetitively, faster than real time, to generate predictions on the basis of expected control inputs. Instead, the predictions are calculated by means of a Taylor series on the basis of present measurable position, rate, and acceleration. The only disadvantage of this technique is that it might be difficult to generate noise-free acceleration information, if this is not measurable.

The extrapolation technique is used in the present study to predict extrapolated longitudinal position x as well as pitch angle θ. For position x the predicted value is calculated as follows:

$$x_{PD}(t) = x(t + \tau_x) = x(t) + \tau_x \dot{x}(t) + \frac{\tau_x^2}{2} \ddot{x}(t) \qquad (2)$$

The corresponding Taylor series expression for the pitch angle θ reads:

$$\theta_{PD}(t) = \theta(t + \tau_\theta) = \theta(t) + \tau_\theta \dot{\theta}(t) + \frac{\tau_\theta^2}{2} \ddot{\theta}(t) \qquad (3)$$

The Taylor series expressions of Equations (2) and (3) are truncated after the second derivative terms. This has been found in earlier experimental studies (see [5]) to be a reasonably good approximation.

It has been assumed, for the longitudinal hover task studied here, that the pilot would view displays with predictive information like those shown in Figure 3. The pitch angle and position information is separately indicated in two displays. The one for the pitch angle or inner loop of Figure 1 is like one dimension of an artificial horizon, whereas the one for the position or outer loop of Figure 1 is presented as a function of time. Similar displays have been studied experimentally in [5] with similar system dynamics, which allows for accepting the following data. A prediction span of

τ_θ = 0.7s seems to be appropriate for pitch. For the position, the indication of an extrapolated path element with a prediction span showing the range between the actual value and the end point (see Figure 3), i e., τ_x = 0...2s, has been chosen. The curved extrapolated path element can be approximated by, e.g., three straight lines as shown in Figure 3. This reduces the calculation of the path element to that of three points in the future i.e., (1/3, 2/3, and 1) τ_x ahead.

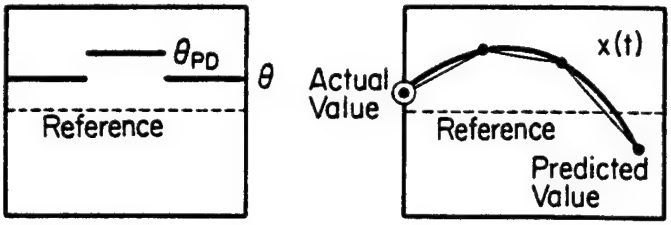

Figure 3: Displays with Predictive Information for Indications of Pitch Angle (left) and Position (right)

IV. Application of the Optimal Control Model

In this paper the same optimal control model for the human operator has been applied as in [15]. In the block diagram of Figure 4, a distinction has been made, however, between influences of display parameters and human perceptual abilities on the observation vector y(t). The human perceptual abilities include (1) estimation in the sense of extracting the first derivative of a displayed variable from its movement as well as (2) perceptual thresholds for the position and rate of displayed variables. For this study all thresholds have been assumed to be zero.

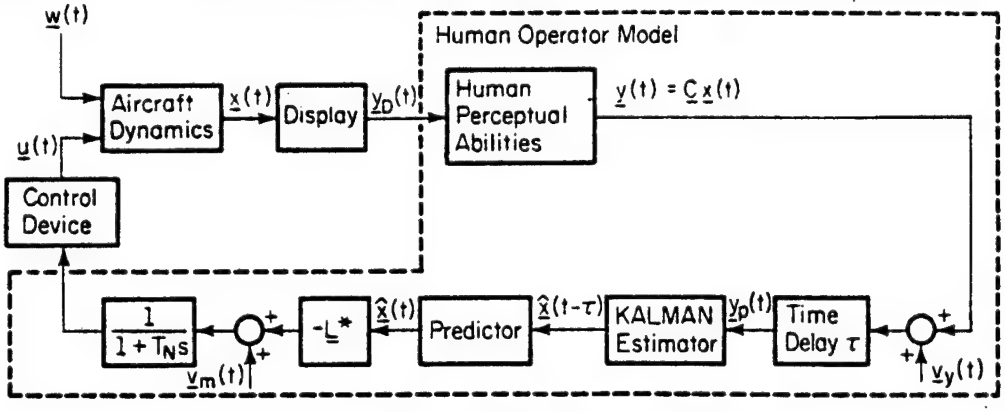

Figure 4: Optimal Control Model for the Human Operator (after [15] and [9])

For reasons of comparing the results of this paper with those of [15], the same parameters of the human operator model and the cost functional have been adopted, whereas the aircraft dynamics are those described by Equation

(1), i.e., having only the very slight change mentioned before. The cost functional for optimal control is

$$J = \overline{x^2} + 400\,\overline{q^2} + \tilde{g}\,\overline{\dot{\delta}_c^2} \qquad (4)$$

i.e., a weighted sum of the mean-square values of the position x, the pitch rate $q = \dot{\theta}$ and the control rate $\dot{\delta}_c$. The time delay of the human operator model is $\tau = 0.15$s, and the lag time constant of the neuromuscular system is adjusted to $T_N \approx 0.1$s by an appropriate choice of $\tilde{g}$ in Equation (4), i.e., $\tilde{g} = 0.03$. The noise-to-signal ratio of the motor noise is $\rho_m = -25$dB. The noise-to-signal ratios of the observation noises change in this study. However for the baseline display format with the same observation vector $\underline{y} = [x,u,\theta,q]^T$ as in [15], they are adopted as $\rho_1 = \rho_2 = \rho_3 = \rho_4 = -20$dB.

The described optimal control model should be able to explain the improvements of human and system performance which occur when predictor displays are used. Looking at Figure 3, one can see that all status and predictive information can be described by the following observation vector:

$$\underline{y} = \begin{bmatrix} x \\ u \\ x_{1/3PD} \\ x_{2/3PD} \\ x_{PD} \\ \theta \\ q \\ \sigma_{PD} \end{bmatrix} = \underbrace{\begin{bmatrix} 1 & 0 & 0 & 0 & 0 & 0 \\ 0 & 1 & 0 & 0 & 0 & 0 \\ 1 & 1/3\tau_x & 1/18\tau_x^2 & 0 & 0 & 0 \\ 1 & 2/3\tau_x & 2/9\tau_x^2 & 0 & 0 & 0 \\ 1 & \tau_x & 1/2\tau_x^2 & 0 & 0 & 0 \\ 0 & 0 & 0 & 1 & 0 & 0 \\ 0 & 0 & 0 & 0 & 1 & 0 \\ 0 & 0 & 0 & 1 & \tau_\theta & 1/2\tau_\theta^2 \end{bmatrix}}_{\underline{P}} \begin{bmatrix} x \\ \dot{x} \\ \ddot{x} \\ \sigma \\ \dot{\sigma} \\ \ddot{\sigma} \\ \vdots \end{bmatrix} \qquad (5)$$

which can be expressed in terms of position x and pitch angle θ as well as the first and second derivatives of both variables by applying Equations (2) and (3). The observation vector in Equation (5) considers also rate information, namely $u = \dot{x}$ and $q = \dot{\theta}$ as in the baseline display format, thereby combining the two influences of display parameters and human perceptual abilities of Figure 4.

As the observation vector is normally derived from the state vector, the vector on the right side of Equation (5) composed of position x, pitch angle θ and its first and second derivatives has to be expressed in terms of the state vector. All these components appear in the systems equation (1) and in Figure 2. The mathematical description is:

$$\begin{bmatrix} x \\ \dot{x} \\ \ddot{x} \\ \theta \\ \dot{\theta} \\ \ddot{\theta} \end{bmatrix} = \begin{bmatrix} x \\ \dot{x} \\ \dot{u} \\ \theta \\ \dot{\theta} \\ \dot{q} \end{bmatrix} = \underbrace{\begin{bmatrix} 0 & 1 & 0 & 0 & 0 & 0 \\ 0 & 0 & 1 & 0 & 0 & 0 \\ X_u & 0 & X_u & -g & 0 & 0 \\ 0 & 0 & 0 & 1 & 0 & 0 \\ 0 & 0 & 0 & 0 & 1 & 0 \\ M_u & 0 & M_u & 0 & M_q & M_\delta \end{bmatrix}}_{\underline{T}} \underbrace{\begin{bmatrix} u_g \\ x \\ u \\ \theta \\ q \\ \delta \end{bmatrix}}_{\underline{x}} \qquad (6)$$

Taking Equations (5) and (6) together results in the following equation for the observation vector:

$$\underline{y} = \underline{P} \cdot \underline{T} \cdot \underline{x} = \underline{C} \cdot \underline{x} \qquad (7)$$

Equation (7) shows that a matrix multiplication is necessary to find the observation matrix $\underline{C}$. One of the two matrices being multiplied, i.e., $\underline{P}$, reflects the display format and the human perceptual abilities, whereas the other one, i.e., $\underline{T}$ contains mainly components of the systems matrix $\underline{A}$.

In order to investigate the influence of different amount of predictive and rate information, a theoretical case study with the optimal control model has been run. The 13 cases studied differ only in their observation vectors which are chosen as shown in Table I. Available information is denoted by a "1" whereas a "0" means that this component of the observation vector is not present in the corresponding case.

Table I
Composition of the Observation Vectors for the Case Study

	A	B	C	D	E	F	G	H	I	J	K	L	M
x	1	1	1	1	1	1	1	1	1	1	1	1	1
u	1	0	0	1	1	0	0	1	0	0	1	1	0
$x_{1/3PD}$	0	0	0	0	0	0	0	0	0	1	1	1	1
$x_{2/3PD}$	0	0	0	0	0	0	0	0	0	1	1	1	1
x_{PD}	0	0	0	0	0	0	0	1	1	1	1	1	1
θ	1	1	1	1	1	1	1	1	1	1	1	1	1
q	1	1	0	0	1	1	0	1	0	0	1	1	0
θ_{PD}	0	0	0	0	1	1	1	0	0	0	0	1	1

Case L is identical with Equation (5). From this, all others have been derived by omitting a certain amount of information, i.e., deleting the corresponding rows in the observation vector and observation matrix.

Cases A, B, C, and D are concerned with the influence of rate information which has also been investigated in [17]. Case A is the baseline display format of this study and is the same as in [15]. Cases E, F, and G consider only predictive pitch information, whereas cases H, I, J, and K assume only predictive position information, being either only the end point (H,I) or the complete extrapolated path element (J,K). Finally, cases L, M include both predictive pitch and position information.

The case study is carried out using the version of the optimal control model which is described in [18].* This includes an optimization of the fractions of attention the pilot devotes to the individual pieces of displayed information. The optimization technique based on the cost gradients of all pieces of information is described in more detail in [19]. The observation noise-to-signal ratio P_i of the ith observed variable is related to its fraction of attention f_i by

$$P_i = P_o \frac{1}{f_i} \qquad (8)$$

$$\text{with} \quad \sum_i f_i = f_{\text{total}}$$

where P_0 is the full attention noise-to-signal ratio, normally -20 db [10]. Thus the above mentioned noise-to-signal ratios of -20dB for all four

* The authors are grateful to Aerospace Systems, Inc., Burlington, Mass., and William C. Hoffman in particular for furnishing the optimal control model software.

observed variables in the baseline display format correspond to a total attention of 4. The value of 4 is the baseline for full attention and should not be interpreted as the human operator devoting 4 times his full attention to the task.

V Results

Performance scores have been shown in Figures 5 and 6 for all 13 cases. These correspond to a total attention of 4. with attention allocation optimized. RMS-longitudinal and pitch errors have been plotted. They are discussed in some detail here. For both variables, position x and pitch angle θ certain trends are apparent. The error is reduced in all cases when prediction information is presented (cases E-M). There is an increase in RMS-errors when the rate information is not available (without prediction ; see cases A-D).

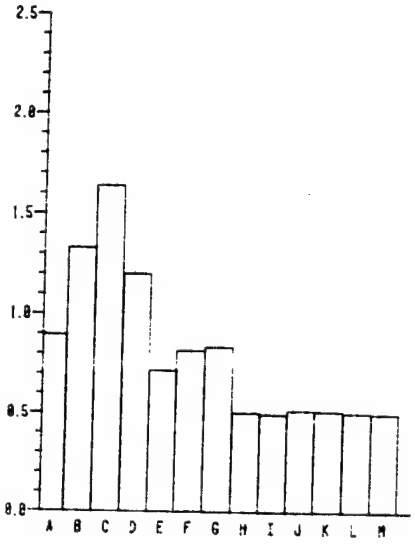

Figure 5: RMS-Longitudinal Errors

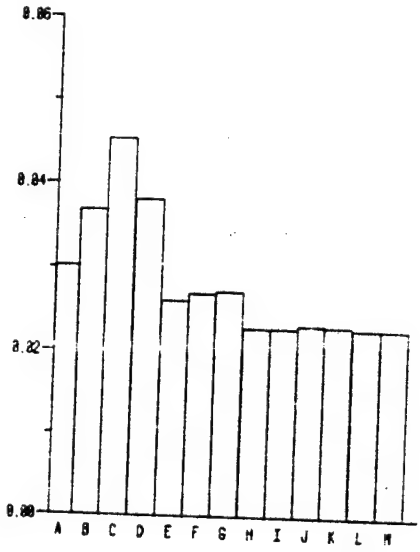

Figure 6: RMS-Pitch Errors

(for all 13 Cases with Optimized Attention Allocation)

For the longitudinal position, the absence of derivative information for position and pitch (C) results in about 80% increase in RMS-error. When only rate u is removed (B), the error increases by about 50%, whereas the increase is only about 33% when the pitch rate is absent (D). Therefore, it is very important that the displays are designed to easily allow the human operator to make good rate estimates.

Compared with the base line performance (A), the reduction in RMS-error is rather small when only the pitch angle predictor is available (E). The error is reduced by about 20%. With predictor information, lack of pitch

rate does not have much effect (see G vs. F), presumably due to the rate information contained implicitly. When rate u is not available (F,G), the RMS-error is reduced only slightly compared with A even when prediction is available for pitch. However when B and C are compared to F and G respectively, the error is reduced by 35 to 50% with the addition of predictor information.

It is significant to observe that the lack of rate information does not affect the results when the position predictor display is available. This is seen in H and I having nearly equal performance scores. From the baseline performance (A). a reduction in RMS-error of about 45% is observed. It is also important to note that compared to C, the addition of position prediction alone reduces the error to less than 1/3 of its original value. This is validated by intuitive reasoning based on earlier experimental results [5]. With the predictor for a two-dimensional map display, it was found that the lap time, i.e., for one circuit of the map. was reduced by 32%.

When the position predictor is available. all the cases (H-M) result in about the same RMS-errors. This happens irrespective of whether the position and pitch rates and the attitude predictor information are available. This confirms our belief that it is more important to employ predictor display aiding for the slower time constant outer loop. An unexpected result, however, is the fact that additional intermediate points of the extrapolated path element (J-M) do not further improve performance. The most important predictive information seems to be the indication of the end point of the extrapolated path element.

The trends for the pitch angle error are similar to the longitudinal position error. When all derivative information is removed (C), the error increases by about 50%. Absence of u (B) results in a 23% increase, whereas for the pitch rate (D) the corresponding increase is about 30%. The order of B and D is reversed with respect to position error, as could be expected. The pitch angle predictor reduces the error by about 10% (E). Loss of pitch rate information is not important when the predictor is available (G vs. F). These results are in qualitative agreement with earlier experimental results [5] , where RMS-errors have been improved by a factor of 2-4 with the addition of a predictor for an artificial horizon in a pure attitude control task. Further reduction in RMS-pitch error, by 23%, occurs when the position predictor display is added (H-M). This is a 50% reduction compared to the no-derivative case (C). As before, no substantial difference occurs if the rate information or intermediate points are removed when the position predictor display is available.

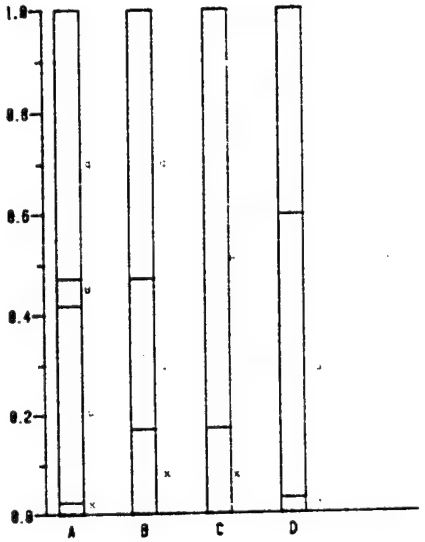

Figure 7: Optimized Fractions of Attention for Cases A B C D

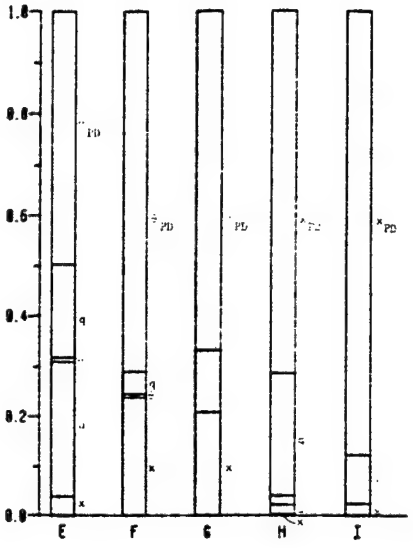

Figure 8: Optimized Fractions of Attention for Cases E F,G H,I

For all 13 cases, the optimized fractions of attention are plotted in Figures 7,8,and 9. The total attention is constant at 4 for all cases, normalized to 1 in the figure, assuming that the human operator will not increase his effort with additionally displayed information. For each displayed variable fractions of attention are shown which result in minimum total cost. When rate information is available, the optimum fraction of attention required is more (mostly by about 8 to 10 times) for the rate than for the corresponding displayed variable itself, i.e., position or pitch angle (Figure 7).

With no predictor, the inner loop (see Figure 1) demands more attention (by about 4 times more than the outer loop), when rate u is not available (cases B C). With the addition of the predictor, position or pitch or their derivatives require comparatively less attention than the predicted variables. The predictor requires 3 to 15 times more attention.

Total attention for the position predictor is about 2 to 3 times greater than that for the pitch predictor (Figure 9). From this and the discussions for RMS-errors, the importance of the position predictor information is obvious.

It should be pointed out that for constant total attention, the RMS-errors are still small even when the information available is limited (e g., only 3 variables in case I compared to 8 in case L), as long as the position predictor is available. This could be due to less noise in observing what is available and, hence the possibility for better state estimation. From the foregoing discussions it is clear that the rate

information is highly useful when a predictor is not available. Having a predictor for the low speed outer loop is more important for performance since it reduces the RMS-errors more effectively.

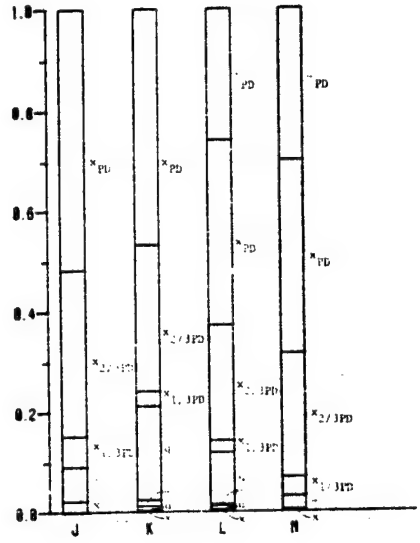

Figure 9: Optimized Fractions of Attention for Cases J,K,L.M

In Figure 10, the RMS-values of position, pitch angle, and control for different cases with and without rate and predictor information are plotted corresponding to optimized attention allocation. These cases have been chosen because the additional indication of the end point of the extrapolated path element (h) compared with the baseline display format (A) results in the simplest predictor display design with the maximum performance improvement. Compared with these two cases, C and I show the influence of the omitted rate information. The trends discussed earlier are seen again in Figure 10.

The effects of varying the total attention and optimizing the attention allocation are illustrated for RMS-longitudinal errors for the cases A,C,H, and I (Figure 11). The first bar in each case corresponds to variable total attention split equally among displays (1 for each observed variable). For the second bar, total attention is 4, split equally between the inner loop and the outer loop, and equally among displays in any particular loop. The remaining bar corresponds to a total attention of 4, split optimally. The errors are reduced by 18% for case A. For case C, a reduction of about 30% occurs when total attention changes from 2 to 4. Optimization reduces this further by only 8%. The slight increase of RMS-error in case H is due to a decrease in total attention from 5 to 4. However, in case I, the increase in total attention from 3 to 4 does not change the RMS-value. When attention is optimized, up to 30% reduction in error is obtained.

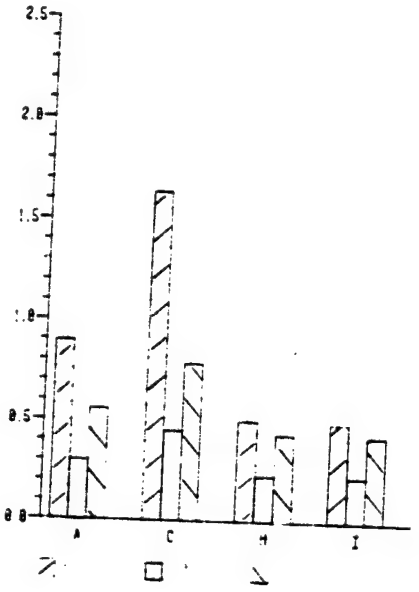

Figure 10: RMS-values of Position x, Pitch Angle θ, and Control δ_c for Cases A,C,H,I with Optimized Attention Allocation.

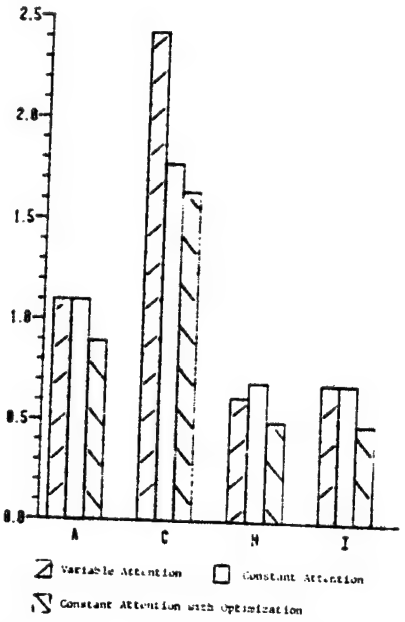

Figure 11: RMS-Longitudinal Errors For Cases A,C,H,I with Variable and Constant Total Attention.

It is necessary to point out that the fractions of attention obtained may not be the globally optimum values. Due to the coupling between inner and outer loop and the interdependence of prediction and rate information (see Figure 2 and Equations 2 and 3), different combinations of initial conditions lead to different optimal attention allocations with similar total cost values. This corresponds, however, to the freedom the human operator has also in choosing between equally appropriate combinations of interrelated information. The optimized fractions of attention shown in this paper seem to be typical values found with different initial conditions.

VI Conclusions

Predictors improve man-machine system performance as shown by the model results of this study. This is consistent with the results obtained e.g., in [5]. The position predictor display is more useful in reducing the RMS-errors. Especially, the end point of the extrapolated path element has the strongest influence. Due to slower dynamics, it is possible that the human finds it difficult to infer the longitudinal position rate compared to pitch rate.

The addition of a predictor might result in reduced workload as evidenced by the smaller RMS-control movements. The control actions by the pilot are guided by the predictor. This could also have an effect on the internal model because estimation of the states is aided by the predictor display. The accuracy requirements of the state predictor implicitly included in the optimal control model of the human operator might be relaxed. The improvement of state estimation with an even inaccurate internal model might also be important for monitoring and supervisory control tasks. Separate studies are needed to evaluate this effect.

The study shows that the optimal control model is suitable for analytical predictor display designs. Using this methodology it is possible to investigate the effects of certain display parameters, e.g., to find the optimal length of the prediction span. This may allow one to avoid expensive man-in-the-loop simulation studies.

VII References

1 Wierwille, W.W.: "Improvement of the Human Operator's Tracking Performance by Means of Optimum Filtering and Prediction," IEEE Trans. Human Factors in Electronics, Vol. HFE-5, 1964, pp. 20-24.

2 Bernotat, R.: "Das Prinzip der Voranzeige und seine Anwendung in der Flugführung Z. Flugwiss., Vol. 13, 1965, pp. 373-377.

3 Kelley, C.R ; Manual and Automatic Control, New York: Wiley, 1968.

4. Warner. J.D.S.; "A Fundamental Study of Predictive Display Systems," NASA CR-1274. 1969.

5 Dey, D.; and Johannsen, G.: "Anthropotechnische Untersuchung einer Übergrundanzeige und eines künstlichen Horizonts mit Voranzeige zur manuellen Regelung von VTOL-Flugzeugen," Z. Flugwiss., Vol. 21, 1973. pp. 140-145.

6. Roscoe. S.N.; and Eisele, J.E.: "Integrated Computer-Generated Cockpit Displays." In: Sheridan, T.B., Johannsen. G. (Eds.) Monitoring Behavior and Supervisory Control, New York: Plenum Press, 1976, pp. 39-49.

7 Machover. C ; Neighbors, M.; and Stuart, C.: "Graphics Displays," IEEE Spectrum, Vol. 14, 1977, pp. 24-32.

8 Kleinman, D.L.; Baron, S; and Levison, W.H.: "An Optimal Control Model of Human Response. Part I: Theory and Validation," Automatica, Vol. 6. 1970, pp. 357-369.

9 Johannsen, G.; Boller, R.E.; Donges. E.; and Stein, W: Der Mensch im Regelkreis - Lineare Modelle, München: Oldenbourg. 1977.

10 Baron, S.; and Levison W.H.; "An Optimal Control Methodology for Analyzing the Effects of Display Parameters on Peformance and Workload in Manual Flight Control", IEEE Trans. Syst. Man Cybern., Vol. SMC-5, 1975, pp. 423-430.

11 Baron. S.; and Levison, W.H.: "Display Analysis with the Optimal Control Model of the Human Operator." Human Factors, Vol. 19, 1977, pp. 437-457.

12 Hess, R.A.; "Analytical Display Design for Flight Tasks Conducted Under Instrument Meteorological Conditions." IEEE Trans. Syst. Man Cybern. Vol. SMC-7, 1977. pp. 453-462.

13 Curry, R.E.; Kleinman, D.L.; and Hoffman, W.C : "A Design Procedure for Control/Display Systems," Human Factors, Vol. 19, 1977, pp. 421-436.

14 Miller. D.P.; and Vinje, E.W.: "Fixed-Base Flight Simulator Studies of VTOL Aircraft Handling Qualities in Hovering and Low-Speed Flight," Wright-Patterson AFB, Ohio: AFFDL-TR-67-152, 1968.

15. Baron, S.; and Kleinman, D.L.: "Prediction and Analysis of Human Performance in a VTOL Hover Task," Proc. 7th Annual Conf. on Manual Control, NASA SP-281, 1972, pp. 247-256.

16 Hess R.A., "Prediction of Pilot Opinion Ratings Using an Optimal Pilot Model," Human Factors, Vol. 19, 1977. pp. 459-476.

17 Baron, S.; and Berliner, J.E.; "The Effects of Deviate Internal Representations in the Optimal Model of the Human Operator." U.S. Army Missile Research and Development Command, Alabama: Tech. Rept. TD-CR-77-3, 1977.

18 Curry, R.E.; Hoffman. W.C.; and Young. L.R.: "Pilot Modeling for Manned Simulation." Vol. I; Doyle K M and Hoffman W C ,...., Vol. II (Program User's Manual), Wright-Patterson AFB. Ohio: AFFDL-TR-76-124, 1976.

19. Hoffman, W.C.; Curry, R.E.; Kleinman, D.L.; Hollister. W.M.; and Young. L R.; "Display/Control Requirements for VTOL Aircraft." Aerospace Systems, Inc. Burlington, Mass : ASI-TR-75-25 (NASA CR-145026), 1975.

SESSION E: GROUND VEHICLE CONTROL AND DRIVER BEHAVIOR

Chairman: L. Summers

N79-15606

VEHICLE STEERING CONTROL: A MODEL OF LEARNING

Alison Smiley, Ph.D.*
Southern California Research Institute
Los Angeles, California
and
Lloyd Reid, Ph.D.
Institute of Aerospace Studies
University of Toronto
Ontario, Canada
and
Morris Fraser, M.D.
Department of Systems Design
University of Waterloo
Ontario, Canada

SUMMARY

A hierarchy of strategies were postulated to describe the process of learning steering control. Vehicle motion and steering control data were recorded for twelve novices who drove an instrumented car twice a week during and after a driver training course. Car-driver describing functions were calculated, the probable control structure determined, and the driver-alone transfer function modelled. The data suggested that the largest changes in steering control with learning were in the way the driver used the lateral position cue.

INTRODUCTION

Various aspects of driver behavior have been studied using manual control theory. To date, most, if not all, of this research has used experienced drivers. The research to be described in this paper used inexperienced drivers in order to study the changes in the driver describing function as a novice learns to steer a car.

The mathematical model used to describe the driver is the crossover model, described in Reference 1. Though the model was developed using single-loop, compensatory tracking tasks, it has been successfully used to describe car driving where two loops are involved. The basic tenet of the crossover model is that the human adapts to each controlled element so that the open loop man-machine transfer function always has the form:

$$Y_p(jw)Y_c(jw) = \frac{w_c e^{-jw\tau}}{jw} \qquad (1)$$

*Work sponsored by the National Research Council of Canada and drawn from principal author's Ph.D. dissertation completed at the U. of Waterloo, Canada.

where w_c is the system crossover frequency, and τ is the effective time delay (incorporating delays due both to the operator and the control device), Y_p is the operator describing function, Y_c is the transfer function describing the control device dynamics, and jw is the complex frequency variable.

Weir and McRuer (Reference 2) applied this model to automobile lane-keeping steering tasks in order to determine which of the available visual cues would yield good performance without great effort on the part of the driver. From previous studies with the crossover model it has been shown that the human operator selects from the possible cues or feedbacks those that minimize his/her equalization requirements. In other words, the operator prefers to act as a simple gain and time delay rather than as a single or double differentiator, and selects cues so that s/he can do this. The car dynamics in lateral position are such that the use of lateral error as a cue would require the operator to act as a differentiator. ($Y_p(jw) = jwKe^{-jw\tau}$ from the crossover model.) This eliminates lateral error as a dominant cue for the experienced driver. Heading angle and rate, path angle and rate, and time-advanced lateral deviation were studied (Reference 2) as possible cues. As heading rate control allows a fairly large lag and produces a high crossover frequency, it appears to be the best cue to use. As its use is associated with high frequency control movements, heading angle (an intermediate frequency cue) is a more probable cue in less demanding situations. Control is unlikely to be purely directional since drifts in lateral position will occur which, if uncorrected, may result in the car going out of the lane. Therefore, it was suggested that a probable structure for an experienced driver is an outer loop controlling lateral position and an inner loop controlling heading angle or rate. The heading angle inner loop provides the path damping necessary for a stable, well-behaved closed loop system - and thereby avoids the necessity of the operator differentiating the input (which would difficult because it must be done at low frequencies as well as high) which would be needed to stabilize the outer loop, if it were the only loop closed. Though a single loop structure of time advanced lateral deviation had also been suggested in Reference 2, the time advance (preview time) necessary for such a control loop to work was in the order of 5 to 10 seconds. Below these values the lead generated by using predicted future lateral deviation 'would not compensate sufficiently for the inherent lags in the driver/vehicle system'. In Reference 3 a survey is presented of the research on estimated preview times used by experienced drivers. Only when the driver viewed the road through a narrow slit were preview times in the range needed for good use of time advanced lateral deviation as a control loop. This suggests that such a control loop is an unlikely possibility under normal driving conditions. The reader must be cautioned at this point that statements about which cues are used in driving in no way imply that these cues are directly perceived by the driver. For example, the driver may perceive heading angle directly or may perceive some function of heading angle. The mathematical analysis cannot differentiate between two such dependent variables.

Hypotheses About Learning Steering Control

Perceptual-motor learning studies, eye movement studies of novice drivers and anecdotal information obtained from driver instructors were used to generate hypotheses about the stages in the learning of steering control. In the first stage it was postulated that the driver controls lateral position (y), the most obvious cue. In reference 4 it was shown through a study of the eye movements of novice drivers that novices tended to look closer in front of the vehicle than experienced drivers, suggesting they were looking for lateral position cues. As was pointed out earlier, lateral position is a difficult cue to control so this stage was not expected to last long (see Fig. 1).

With experience the novice begins to look further ahead of the car. This is necessary in order to better monitor the environment but also allows the driver to pick up heading angle (ψ) movements more easily. The car's dynamics in heading angle ($G^{\psi}_{\delta w}$) are rate dynamics, so that the driver's control may be modelled by a simple gain and time delay. Thus the second stage is that the driver will use heading angle as the dominant cue, but will still control lateral position directly (as in the first structure), with corrections being made when a significant lateral position error has accumulated. An analogous strategy was used by subjects in an experiment described in reference 5, where subjects using an oscilloscope centered a target on crosshairs by sequentially pressing two keys, one causing target acceleration to the right and the other, to the left. The response pattern suggested that some subjects modified their responses on the basis of feedback i.e. after drifting off target they made a single, long duration corrective movement, while other subjects, who maintained a higher rate of responding and were consistently better in overall performance, used a more efficient strategy. These latter subjects 'when the target drifted off center to the left...maintained a high rate of responding but at the same time gradually increased the length of time the right key was active relative to the left key, so that over a series of responses the target was made to drift back towards the center'. It was postulated that at an intermediate stage, learning drivers would be using a strategy similar to Pew's first group of subjects, which would be represented by an alternating operation on lateral position and heading angle as shown in Fig. 2.

In the final stage of learning, it was postulated that the driver would begin to use dual loop control, where heading angle is the dominant cue, controlled by an inner loop, and lateral position is controlled with an outer loop. In this way lateral position may be controlled by heading angle corrections i.e. using a simple gain ($Y'_y = K_y$) rather than having to estimate rate of change of lateral position. The operators control of heading angle was modelled by a gain, $K\psi$, a lead term ($1 + T'_r jw$), and a time delay ($e^{-jw\tau}$). (i.e. $Y_{\psi} = K_{\psi}(1 + T'_r\, jw)e^{-jw\tau}$). The lead term is needed to offset a lag in vehicle response at higher frequencies. For the experimental car the break frequency of this lag occurred at $T_r = 9.4$ rad./sec., therefore the same value was assumed for T'_r when the driver-alone transfer function was modelled. In reference 6 it was shown that this structure satisfied the crossover model

and appeared to provide a reasonable fit to experimental data. Such a form of control is analogous to that used by the subjects using the more efficient strategy in the experiment described in reference 5.

Theoretical Analysis

The driver-car transfer function for the control structures postulated as stages in the learning process will now be derived.

. Using Fig. 1, the following relationship may be obtained:

$$\delta_w=\delta_d+nG_s-\delta_w G^y_{\delta w} Y_y G_s-nG^y_{\delta w} Y_y G_s \quad (2)$$

Fig. 1. Single-loop control of lateral position (δswa-steering wheel angle, δw-front tire angle, Gs-steering gain, other definitions in text)

If each variable is cross-correlated (see reference 7 for a description of these techniques) with the input disturbance, δ_d, the following is obtained:

$$\phi_{\delta_d\delta_w} = \phi_{\delta_d\delta_d} + \phi_{\delta_d n}G_s - \phi_{\delta_d\delta_w}G^y_{\delta_w} Y_y G_s - \phi_{\delta_d n}G^y_{\delta_w} Y_y G_s \quad (3)$$

The remnant, n, is by definition that part of the drivers output which is uncorrelated with the input, so that $\phi_{\delta_d n}$ may be considered to be zero. Because δ_d is such designed so that it is much larger than n, $\phi_{\delta_d n}$ will be negligible in comparison with $\phi_{\delta_d\delta_w}$ and $\phi_{\delta_d\delta_d}$. Equation (3) is then reduced to:

$$\frac{\phi_{\delta_d\delta_d} - \phi_{\delta_d\delta_w}}{\phi_{\delta_d\delta_d}} = Y_y G_s G^y_{\delta_w} \quad (4)$$

For structure 2 this expression is equal to $Y_\psi G_s G^\psi_{\delta_w}$ or $Y_y G_s G^y_{\delta_w}$ depending on which loop is in use. For the dual-loop structure 3 this expression becomes:

$$\frac{\phi_{\delta_d\delta_d} - \phi_{\delta_d\delta_w}}{\phi_{\delta_d\delta_d}} = Y_\psi\left[1 + \frac{Y'_y G^y_{\delta_w}}{G^\psi_{\delta_w}}\right] G^\psi_{\delta_w} G_s \quad (5)$$

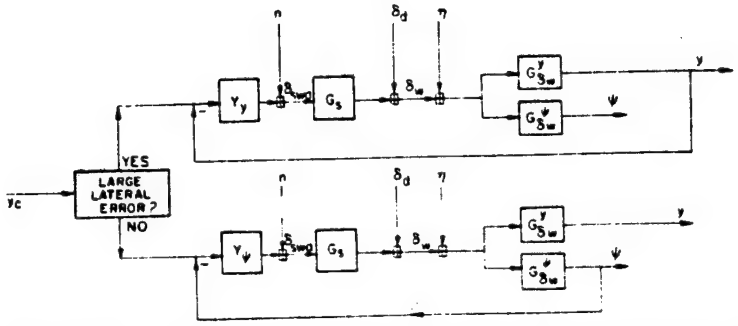

Fig. 2. Parallel loop control of heading angle and lateral position

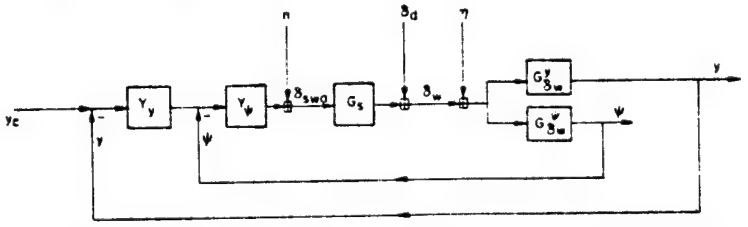

Fig. 3. Dual loop control of heading angle and lateral position

Thus, no matter which structure the driver is using, the same cross spectral expression is calculated to obtain the car-driver transfer function. However, as will now be shown, the form of the transfer function obtained differs depending on which structure is in use.

In the first two structures, either heading angle or lateral position is being controlled at any one time. Thus the first two structures are single control loops which, in the frequency range used in this study, may be expected to conform closely to the crossover model. Therefore, using equation (1), the car-driver transfer will have the form $w_c e^{-jw\tau}/jw$. When this function is plotted on a Bode plot (amplitude and phase vs. frequency) the amplitude slope is 20db per frequency decade (see Fig. 4).

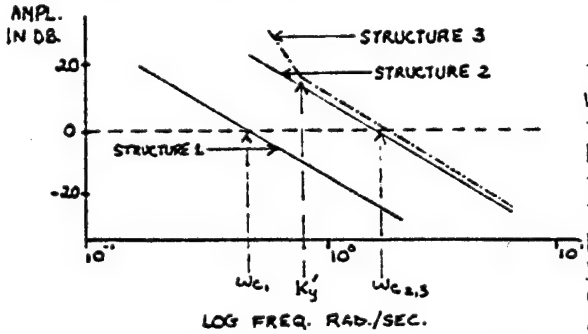

Fig. 4. Amplitude Bode plot of the car-driver transfer function for structures 1, 2, 3

The values assumed for the driver's transfer functions in the third structure were such that the car-driver transfer function could be modelled at mid- and high frequencies (i.e., near crossover frequency) by the crossover model, as in the first two structures. However, the presence of the outer loop operating on y, affects the expected amplitude slope of the Bode plot. Using equation (5), as frequency increases, the ratio $G^y_{\delta_w}/G^{\psi}_{\delta_w}$ decreases rapidly so that the main effect of the Y'_y term is at low

frequencies, where it causes an increase in the amplitude slope as seen in Figure 4. Thus structure 3 may be distinguished from structures 1 and 2 by the presence of an increased slope in the Bode amplitude plot of the car-driver transfer function. Structures 1 and 2 must be distinguished from each other by more subtle cues, however. Because of the change in operator requirements, a change from control of lateral position to dominant control of heading angle would result in a jump in crossover freqeuncy and an increased phase angle at low frequencies. (The difficulty of generating the low frequency lead needed for lateral position control results in a pronounced phase droop at low frequencies and a lower crossover frequency.)

The considerations discussed above were used to help determine the control structure used by the subjects.

EXPERIMENTAL PROCEDURE

Subjects

To test the hypothses about changes in steering control with learning, twelve novice drivers participated in an experiment using an instrumented car over a five week period. The subjects were all high school students who at the start of the experimental test period were beginning a three week intensive driver training program. They were selected on the basis of having had minimal experience of driving. Three subjects had never driven a car before being recorded driving the instrumented car and the other subjects had driven on at most five previous occasions. The subjects were tested on nine separate occasions over the five week period.

Equipment

The instrumented car driven by the subjects was capable of recording driver control measures, vehicle motion variables and vehicle lane position, and was built by Systems Technology Inc., Los Angeles, and lent to this author by the U.S. National Highway Traffic Safety Administration. The car is described in detail in an STI technical manual (Klein et al, 1976). Two features of particular interest, though, are the lateral position detector and the servo control.

The lateral position detector was developed by the Institute for Perception in the Netherlands. It consists of a position transducer and a control unit. The position tranducer uses a rotating prism to scan the intenstiy of reflected light in a lateral plan across the road and reflect the light in a photoamplifier. Any marker which sufficiently contrasts with its surroundings is taken as being part of the reference line by the lane tracker. For the experiment a 2.5 inch wide strip was laid down as the center lane marker to be picked up by the position detector.

The servo control allows for application of steering inputs to the front wheels independently of the driver's steering inputs. This is accomplished by

hooking up an analogue tape recorder containing a taped disturbance which is played back and passed by means of an electro-mechanical device through the steering linkage to the front wheels. This provides a means of measuring the closed loop dynamic behavior of the driver by insertion of a known input or disturbance function into the loop. The disturbance function used in the experiment was a sum of nine sinusoids - .377, .503, .754, 1.257, 1.634, 2.765, 4.271, 5.781 and 10.801 rad./sec. Each of these input frequencies has an integral number of cycles in a 50 second run length. The advantage of using a sum of sines input is that while the remnant is spread out over many frequencies, the input is concentrated at discrete frequencies. Thus, at these discete frequencies, where the driver car-driver transfer function is measured, the remnant is swamped by that part of the output signal which is correlated with the input, so that relatively clean estimates of the correlated output are obtained.

The variables recorded during the subject runs were: steering wheel angle, front tire angle, heading angle, lateral acceleration, lateral position, forward velocity and the disturbance signal input.

Procedure

Each of the twelve subjects came to the test site twice a week for five weeks. On the first test day it was determined from the first two subjects that the novices could manage a speed of 40 k.p.h. This determined the speed which was used for all the test runs. Runs were made up and down two marked lanes on a half mile stretch of an unused runway. In total 200 seconds of data were collected for each subject on each day.

RESULTS

Changes in the Car-Driver Transfer Function with Learning

Table 1 summarizes the one factor, repeated measures, analyses of variance which were carried out for the amplitude and phase angle values in the car-driver transfer function, using twelve subjects and nine (treatment) days. Analysis of the power spectrum of steering wheel angle showed that the driver's input at frequencies above 2.765 rad./sec. was negligible (< 1% of total input). Also, at these frequencies the signal to noise ratio is high and therefore the estimates are less reliable. Consequently changes at the first six frequency points (in the disturbance signal car-driver transfer function) are of greatest interest.

Table 1 and Figure 5 show that a significant increase in amplitude of the car-driver transfer function occurred over the test period at the first four freqeuncy points. However, the amplitude at the first frequency point showed the most dramatic change. While the means of the first two days were approximately equal, the mean increased by 40% on the third day and fluctuated about this value for the last six days. As this large increase did not occur at frequency points adjoining .377 rad./sec., a change in slope of the amplitude plot of the car-driver tansfer function is indicated. When individual subject

TABLE 1
Summary Anova Results: Amplitude and Phase of the Car Driver Transfer Function
Nine (treatment) Days: 12 Subjects

	Amplitude		Phase	
Frequency rad./sec.	$F_{8,88}$	Differences Between Days (.05 Level)	$F_{8,88}$	Differences Between Days (.05 level)
.377	2.242^{+}	Day 1 < 3-9	1.622	
.503	3.158^{++}	Day 1 < 5,6,9: Day 2 < 9	1.550	
.754	4.725^{+++}	Day 1 < 3-9; Day 2 < 4,9	0.930	
1.257	2.651^{++}	Day 1 < 3-9	4.216^{+++}	Day 2>5; Day 8>5; Day 9>5-7
1.634	0.845		8.646^{+++}	Day 1-6 < 8,9
2.765	1.607		21.234^{+++}	Day 1,2<4-9; Day 3-6<7-9

level of significance: + .05, ++ .01, +++ .001

plots were examined it was found that, for half of the subjects, the amplitude of the .377 rad./sec. point showed a sharper increase over the first three days than did the amplitudes at other frequencies, while, for the other half, the whole amplitude slope increased. As will be shown in the section on modelling, an increase in the amplitude slope, particularly at low frequencies, is a result of the way subjects used the lateral position cue.

When the phase angle (of the car-driver transfer function) drops below -180^{0}, the car-driver system becomes unstable so that an input generates an exponentially increasing output. Therefore, large phase angles ($> -180^{0}$) are to be desired around crossover. (Phase angles at frequencies further from crossover have little effect on system stability.) Figure 6 shows that at the frequencies surrounding the crossover the phase angle increases gradually, though a little erratically, between days one and nine, indicating that the subjects improved their stability of control.

The changes in amplitude and phase angle of the car-driver transfer function over the test period were reflected in improved tracking performance, with the largest improvements occurring during the first three days.

For all the variables studied, the changes that took place over the last six days were much less dramatic, and much more erratic, than those that occurred over the first three days. If measures on day 3 are compared with those for days 8 and 9, no changes are significant, but the following trends were noted: an increase in the amplitude of the car-driver transfer function at .503, .754, and 1.275 rad./sec., an increase in phase margin, and reduced heading angle deviation.

Modelling the Driver-Alone Describing Function

In the first two structures postulated, the driver adapts to each set of controlled mechanics in such a manner that the overall car-driver transfer function has the same form (see Fig. 4). However, as was noted previously,

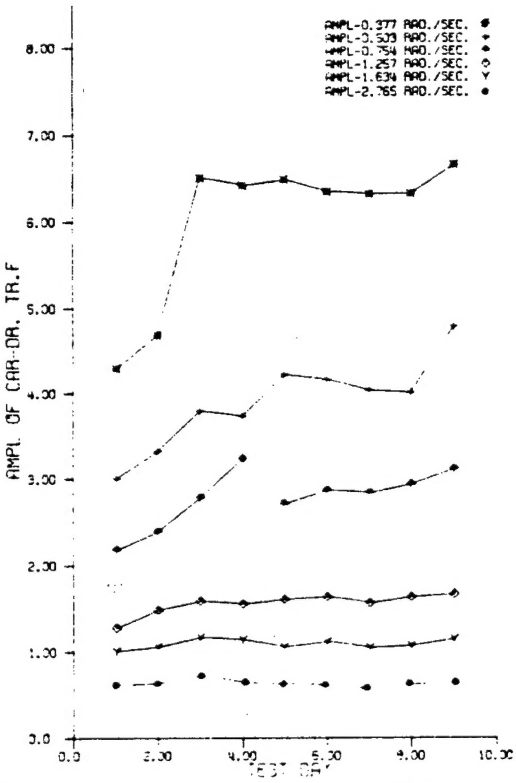

Fig. 5. Change in amplitude (12 subjects)

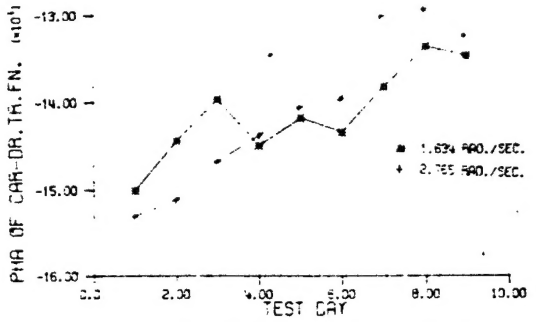

Fig. 6. Phase angle changes around crossover (12 subjects)

experimental data shows that a switch from proportional control (i.e., control of lateral position) to rate control (i.e., control of heading angle) results in a large improvement in crossover frequency. Although there was mean increase in crossover frequency in this study, from 1.696 to 1.929 rad./sec., the increase was small, occurred gradually, and was statistically insignificant. Only two of the twelve subjects showed large changes in crossover frequency. Further examination of the data suggested that reasons other than a change in control structure were responsible for the increase.

Another factor which aids in deciding upon the control structure in use is the percent of high frequency area (%HFA) in the power spectrum of the steering wheel angle. A car's dynamics are such that at the higher frequencies it shows a greater response in heading angle than it does in lateral position. Therefore, a driver who controls lateral position most use lower frequency inputs to get a reasonable response from the car. Consequently, one would expect that %HFA would be lower for a driver controlling lateral position than it would be for a driver controlling heading angle. The data showed that the %HFA was higher rather than lower, though not significantly so, in the first days of the experiment than in the last. This is another indication that the subjects were probably not using the first postulated structure where lateral position was the primary cue for control.

Though this assumption will be used in determining how the driver transfer functions will be modelled, it must be stressed that the structure of a system with only one input, with which identify two operator transfer functions, can only be inferred; it cannot be known with certainty.

If the first structure can be eliminated as a mode of control, the modelling of the driver-alone transfer function is simplified.

Let us consider the third control structure. As was discussed previously, the form used for Y_y, the driver's operation on functions of lateral position, was to be a simple gain K_y. If the data are fitted to this third structure, but have, in fact, been generated by the subject's using the second structure, the term K_y will be zero. Consequently, equation (5) will reduce to an equation which describes the second control structure. Consequently the value of K_y will indicate which structure was probably in use.

The effective driver-alone transfer function for the third structure was derived by removing $G^{\psi}_{\delta_w}$, the car's dynamics in heading, and modelled using:

$$Y_p = \underbrace{K_\psi(1 + T'_{rjw})e^{-jw\tau}}_{Y_\psi} \underbrace{\left[1 + K_y \frac{G^y_w(jw)}{G^{\psi}_{\delta_w}(jw)}\right]}_{Y_y} \qquad (5)$$

Table 2 shows the values derived for K_ψ, τ, T'_r, and K_y for selected test days, averaged over twelve novice drivers (see also Figure 7).

TABLE 2
Parameters for the Averaged
Effective Driver Transfer Function

Day	K_ψ deg./deg.	K'_y rad./sec.	τ sec.
1	0.590	0.20	.42
2	0.655	0.20	.42
3	0.595	0.44	.36
6	0.615	0.71	.37
9	0.630	0.82	.25

(since $T'_r \simeq T_r$ (= 9.4 rad./sec. for the test car), $T'_r = T_r$ was assumed), $K'_y = K_y U_o$ where U_o is the forward velocity

Discussion of Modelling Results

Data, from experienced drivers, that (in reference 8) was fitted to the third control structure show the amplitude fit to be good across all frequencies measured and the phase fit to be best nearest the crossover frequency. This same type of model fit was obtained with the experimental data. Goodness of fit parameters were calculated using the distance from the modelled to the actual data point, relative to the standard deviation at that point. For the experimental car, the response lag which is offset by the driver's use of heading rate (vs. heading angle) begins to have effect at 9.4 rad./sec. (the break frequency). Though $1/T'_r$ is expected to be approximately equal to 9.4 rad./sec., and because this value is far enough outside the measurement frequency range to have little effect on the model anyway, 9.4 rad./sec. was used for the value of $1/T'_r$ for all days. It is evident from the fit parameters

in Table 2 that the largest changes occured in the value of K'_y. The smaller changes in the K_ψ parameter indicate that heading angle was controlled in much the same way on the first day as on the last. In contrast, the value of K'_y doubled between days two and three, moving within the measurement frequency range (i.e., > .377 rad./sec.), and doubled again between days three and nine. This change reflects the large increase in the amplitude of the car driver transfer function at .377 rad./sec. between days two and three. The increases in the value of K'_y point to the increased control of lateral position as defined in the third structure. The phase fits were so poor that very little faith can be placed in the time delay values. However, they do conform to the findings of other reasearchers that the time delay decreases with learning (Reference 1). A large improvement in the model fit to the phase data occurred over the learning period as the low frequency phase droop became less noticeable (as illustrated in Fig. 7).

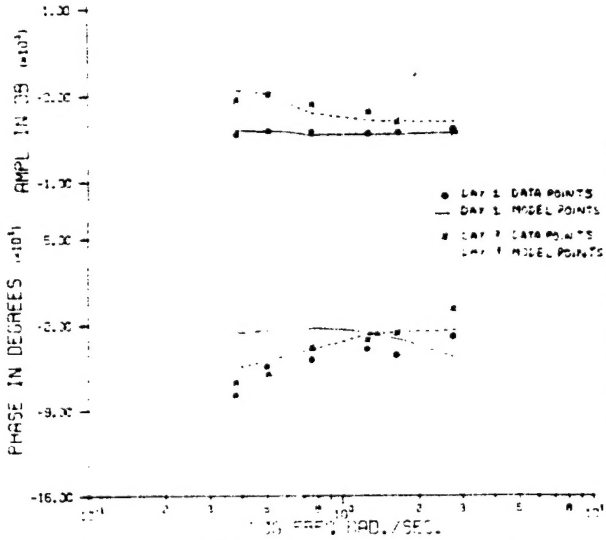

Fig. 7. Effective driver transfer function, averaged over 12 subjects, days 1 and 9

CONCLUSIONS

In summary, though the fit parameters do not indicate a sharp division between days one and two and day three, enough of a change in K'_y is indicated to suggest that on day three and thereafter the drivers' control structure bore more resemblance to structure three, where an outer loop controlled lateral position, than to structure two, while on days one and two, the reverse was true.

Other experimenters, using laboratory tracking tasks (Reference 9) have not found changes in strategy with the learning of tracking control but did note improvements in gain and crossover frequency. Using a more complex tracking task, steering a car, such a change in strategy was found to occur, as well as the previously noted change in gain. Phase margin rather than crossover frequency was found to improve with learning indicating that the subjects opted for an improvement in stability of control over improved system response.

REFERENCES

1. McRuer, D.T. and Krendel, E.S. Mathematical models of human pilot behavior. AGARD Report #Ag-188, 1974.

2. Weir, D.H. and McRuer, D.T. A theory for driver steering control of motor vehicles. Highway Research Record, No. 247, 1968.

3. McLean, J.R. and Hoffman, E.R. The effects of restricted preview on driver steering control and performance. Human Factors, 15(4), 1973.

4. Mourant, R.R. and Rockwell, T.H. Strategies of visual search by novice and experienced drivers. Human Factors, 14(4), 1972.

5. Pew, R.W. Acquisition of hierarchical control over the temporal organization of a skill. Journal of Exper. Psych., 71(5), 1966.

6. Weir, D.H. and McRuer, D.T. Measurement and interpretation of driver steering behavior and performance. SAE Paper No. 730098, 1973.

7. Bendat, J.S. and Piersol, A.G. Random data: Analysis and measurement procedures. Wiley-Interscience, 1971.

8. McRuer, D.T. and Klein, R.H. Automobile controllability - driver/vehicle response for steering control. Systems Technology Inc., Los Angeles, California, November, 1974.

9. Reid, L.D. An investigation into pursuit tracking in the presence of a disturbance signal. Procedures of the Fifth Annual NASA-University Conference on Manual Control, 1970.